RHODIUM(I) BETADIKETONE COMPLEXES AS MODEL CATALYSTS IN METHANOL CARBONYLATION

by

ALICE BRINK

A dissertation submitted to meet the requirements for the degree of

MAGISTER SCIENTIAE

in the

DEPARTMENT OF CHEMISTRY

FACULTY OF SCIENCE

at the

UNIVERSITY OF THE FREE STATE

SUPERVISOR: PROF. ANDREAS ROODT

CO-SUPERVISOR: DR. HENDRIK G. VISSER

NOVEMBER 2007

Acknowledgements

Firstly I would like to thank my God and Heavenly Father for the countless blessings that You have bestowed on me and for allowing me to see great and unsearchable things which I do not know. The honour and the glory of all belong to You for I am nothing without You.

Thank you to Prof. Andre Roodt for all the guidance, support and patience in answering numerous questions. Your enthusiasm for chemistry and life makes learning an adventure. It is a privilege to be known as your student.

To Dr. Deon Visser, thank you for your help, encouragement and unwavering support. Your encouragement to learn as much as I can and for always being available to give advice is greatly appreciated.

Thank you also to Prof. Roodt, Prof. Ola Wendt and the SIDA program for the opportunity to study abroad in Sweden. I am truly grateful for the opportunity.

Thank you to the Inorganic girls: Tania, Nicoline and Truidie for the continuous laughter, jokes and support, and to Johannes and Bernadette van Tonder for their precious friendship. Thank you to Lephallo Police Ntsaoana, a teacher of life!!! And to Anita Perrow, teacher and friend for selflessly sharing your knowledge with me.

To my parents, Andrew and Jeanita Brink, and my sister and brother without your love, continuous encouragement, support, faith and sacrifices none of this would have been possible.

The financial assistance from the University of the Free State, SASOL and the National Research Foundation (NRF) towards this research is hereby gratefully acknowledged. Opinions expressed and conclusions arrived at, are those of the author and are not necessarily to be attributed to the NRF.

TABLE OF CONTENTS

TABLE OF CONTENTS

TABLE OF CONTENTS

ABBREVIATIONS AND SYMBOLS

ABBREVIATION	MEANING
L,L'-Bid	Bidentate ligand
acac	Acetylacetonate
OX	8-Hydroxyquinolinato
Z	Number of molecules in a unit cell
Å	Angstrom
NMR	Nuclear magnetic resonance spectroscopy
KMR	Kern magnetiese resonance spektroskopie
ppm	(Unit of chemical shift) parts per million
IR	Infrared spectroscopy
υ	Stretching frequency on IR
t-Bu	Tertiary-butyl
MO	Molecular orbital
π	Pi
σ	Sigma
α	Alpha
β	Beta
γ	Gamma
σ*	Sigma anti-bonding
λ	Wavelength
θ	Sigma
°	Degrees
°C	Degrees Celsius
$X^{\neq}$	Activated state
TON	Turn over number
TOF	Turn over frequency
STY	Space time yield
wt%	Weight percentage
cm	Centimeter
g	Gram
M	($mol.dm^{-3}$)
mg	Milligram
$(OPh)_3$	Triphenylphosphite
ΔH	Enthalpy of activation
ΔS	Entropy of activation
CO	Carbonyl
h	Planck's constant
k_B	Boltzman's constant
k_{obs}	Observed pseudo-first-order rate constant
Me	Methyl
Ph	Phenyl
Cy	Cyclohexyl
T or temp.	Temperature
UV	Ultraviolet region in light specturm
Vis	Visible region in light spectrum
DCM	Dichloromethane
CH_3I	Iodomethane
$CDCl_3$	Deuterated chloroform
C_6D_6	Deuterated benzene
TMS	Tetramethylsilane
DMF	N,N-Dimethylformamide

ABSTRACT

The aim of this study was to synthesise simple *mono*-phosphine rhodium(I) complexes of the type [Rh(acac)(CO)($PR_1R_2R_3$)] (R_1, R_2, R_3 = different alicyclic and aryl compounds; *acac* = acetylacetonate) and to do a kinetic study of iodomethane oxidative addition to these square-planar complexes. The phosphine ligands were selected to provide a systematic range of electronic and sterically demanding ligand systems, as determined by their Tolman cone angles.

Characterization of the complexes was done by infrared (IR) and nuclear magnetic resonance (NMR) spectroscopy, as well as X-ray crystallographic structure determinations of [Rh(acac)(CO)(PPh_3)] **(1)**, [Rh(acac)(CO)($PCyPh_2$)] **(2)**, [Rh(acac)(CO)(PCy_2Ph)] **(3)** and [Rh(acac)(CO)(PCy_3)] **(4)** which were successfully completed. Selected crystallographic parameters are listed in the table below.

Table 1: Selected crystallographic parameters for [Rh(acac)(CO)($PR_1R_2R_3$)] complexes.

	[Rh(acac)(CO)($PR_1R_2R_3$)]			
	(1)	**(2)**	**(3)**	**(4)**
Space group	Triclinic	Orthorhombic	Monoclinic	Monoclinic
Z =	2	4	4	4
Rh-P distance (Å)	2.2418(9)	2.2327(6)	2.2425(9)	2.2537(4)
Rh-CO distance (Å)	1.807(2)	1.802(3)	1.798(2)	1.791(2)
Effective cone angle (°)	149.3	151.2	163.5	169.5

(1) = PPh_3; **(2)** = $PCyPh_2$; **(3)** = PCy_2Ph; **(4)** = PCy_3

A kinetic investigation was conducted to investigate the oxidative addition of iodomethane to the *mono*-phosphine rhodium(I) complexes. The reaction was studied by three spectroscopic techniques namely, IR, NMR and UV-Vis spectroscopy in order to characterize the intermediate and final products. All four complexes underwent first a rapid oxidative addition equilibrium which resulted in the formation of a first Rh(III)-alkyl species. Different behaviour was obtained for the different complexes after this first step was completed. The Rh(III)-alkyl species slowly converted to a Rh(III)-acyl and finally a second Rh(III) alkyl isomer for **(1)** and **(3)**. However,

ABSTRACT

Complex **(4)** proceeded *via* the first Rh(III)-alkyl species to a second Rh(III)-alkyl isomer before converting to the Rh(III)-acyl product. Complex **(2)** followed the above pathway but no conversion to the Rh(III)-acyl product was observed. Scheme 1 indicates the proposed reaction scheme.

The resultive values of the rate constants for the oxidative addition step (k_1) were found to increase in the following order:
[Rh(acac)(CO)(**PCy_2Ph**)], **(3)** < [Rh(acac)(CO)(**PCy_3**)], **(4)** < [Rh(acac)(CO)(**PPh_3**)], **(1)** < [Rh(acac)(CO)(**$PCyPh_2$**)], **(2).** The value of k_1 for **(3)** was approximately 8 times larger than that of **(2)**.

Table 2: Summary of the kinetic results obtained from the oxidative addition of iodomethane to the different *mono*-phosphine complexes. (All reactions were conducted in dichloromethane)

[Rh(acac)(CO)($PR_1R_2R_3$)]	Temperature (°C)	Rate Constant		K_{eq} (M^{-1})
		k_1 (x 10^{-3} $M^{-1}s^{-1}$)	k_{-1} (x 10^{-3} s^{-1})	
PPh_3	24.9	30.8(5)	1.1(2)	27(4)
	15.1	17.2(4)	0.5(1)	31(7)
	5.3	9.71(4)	0.30(1)	33(1)
$PCyPh_2$	26.0	55(1)	0.9(4)	59(26)
	14.0	27.2(4)	1.2(1)	22(2)
	6.0	18.6(2)	0.64(8)	29(4)
PCy_2Ph	25.6	6.98(6)	0.08(2)	90(24)
	14.5	3.38(4)	0.11(2)	31(4)
	5.5	1.88(4)	0.07(2)	27(6)
PCy_3	25.6	27.1(2)	0.29(9)	92(29)
	14.3	13.8(2)	0.45(6)	31(4)
	5.9	9.1(1)	0.15(5)	62(20)

The rates of the reactions seem to be both sterically and electronically dependent, while the activation parameters indicated an associative mechanism for the oxidative addition step. This is consistent with low, positive enthalpies and large, negative entropies which is typical for iodomethane oxidative addition to rhodium(I) square planar complexes.

The configurations of the final Rh(III)-alkyl products are difficult to assign; taking into consideration the IR and ^{31}P NMR signals and no defined result can be obtained to quantify the *cis* or *trans*-Rh(III) alkyl isomer configuration. Further investigation, which include more

detailed crystallographic investigation and theoretical computational calculations, is necessary to determine the absolute conformation.

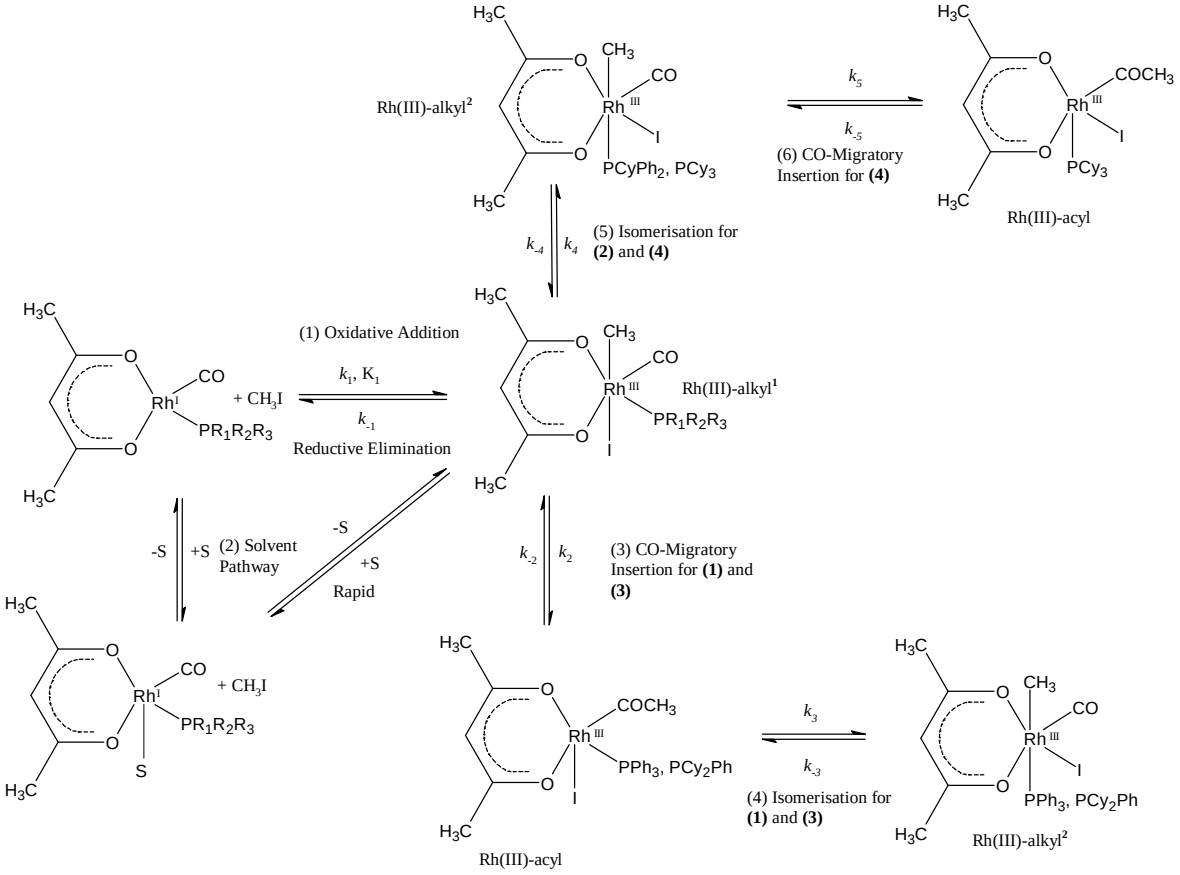

Scheme 1: **Proposed scheme for the oxidative addition of iodomethane to [Rh(acac)(CO)($PR_1R_2R_3$)] complexes.**

Keywords: Rhodium
Phosphine
Iodomethane
Oxidative Addition
Acetylacetonate
Alkyl
Acyl
Phenyl
Cyclohexyl
Tolman

OPSOMMING

Die doel van hierdie studie was eerstens die sintese van eenvoudige *mono*-fosfien rhodium(I) komplekse; [Rh(acac)(CO)($PR_1R_2R_3$)] (waar R_1, R_2, R_3 = verskillende asikliese en arielkomplekse en *acac* = asetielasetonaat) en tweedens om 'n kinetiese studie te doen van die oksidatiewe addisie reaksies van jodometaan met hierdie vierkantig-planêre komplekse. Die fosfienligande is só gekies dat daar ‘n sistematiese verskeidenheid is in terme van steries (Tolman hoeke) en elektroniese effekte tydens die ondersoek.

Die karakterisering van die komplekse is gedoen met behulp van infrarooi (IR) en kernmagnetiese resonansie (KMR) spektroskopie, asook X-straal-kristallografiese struktuurbepalings van [Rh(acac)(CO)(PPh_3)] **(1)**, [Rh(acac)(CO)($PCyPh_2$)] **(2)**, [Rh(acac)(CO)(PCy_2Ph)] **(3)** en [Rh(acac)(CO)(PCy_3)] **(4)** wat suksesvol voltooi is. Sommige kristallografiese parameters is in die tabel hieronder uiteengesit.

Tabel 1: Enkele uitgesoekte kristallografiese parameters van [Rh(acac)(CO)($PR_1R_2R_3$)] komplekse

	[Rh(acac)(CO)($PR_1R_2R_3$)]			
	(1)	**(2)**	**(3)**	**(4)**
Ruimtegroep	Triklinies	Ortorombies	Monoklinies	Monoklinies
Z =	2	4	4	4
Rh-P afstand (Å)	2.2418(9)	2.2327(6)	2.2425(9)	2.2537(4)
Rh-CO afstand (Å)	1.807(2)	1.802(3)	1.798(2)	1.791(2)
Effektiewe konus hoek (º)	149.3	151.2	163.5	169.5

(1) = PPh_3; **(2)** = $PCyPh_2$; **(3)** = PCy_2Ph; **(4)** = PCy_3

'n Kinetiese ondersoek van die oksidatiewe addisie van jodometaan met die *mono*-fosfien rhodium(I) komplekse is ook voltooi. Die reaksie is met behulp van drie spektroskopiese tegnieke naamlik, IR, KMR en UV-Vis spektroskopie ondesoek in 'n poging om die intermediêre en finale produkte te identifiseer. Al vier komplekse het eerstens 'n vinnige oksidatiewe addisie stap ondergaan om 'n Rh(III)-alkiel spesie te vorm. Verskillende gedrag is waargeneem vir die verskillende komplekse nadat hierdie eerste stap plaasgevind het. Vir **(1)** en **(3)** is die eerste Rh(III)-alkielspesie stadig omgeskakel na 'n Rh(III)-asiel kompleks en daarna na 'n tweede

Rh(III)-alkiel isomeer. Kompleks **(4)** het egter eerste 'n isomerisasie-stap ondergaan en daarna 'n Rh(III)-asiel produk gevorm. Kompleks **(2)** het ook eers geïsomeriseer, maar geen getuienis vir asielvorming is waargeneem nie. Skema 1 toon die voorgestelde reaksieverloop aan.

Die relatiewe waardes van die tempokonstantes van die oksidasie addisie (k_1) het die volgende tendens getoon:
[Rh(acac)(CO)(**PCy_2Ph**)], **(3)** < [Rh(acac)(CO)(**PCy_3**)], **(4)** < [Rh(acac)(CO)(**PPh_3**)], **(1)** < [Rh(acac)(CO)(**$PCyPh_2$**)], **(2).** Die waarde van k_1 van **(3)** was ongeveer 8 keer groter as die van **(2)**.

Tabel 2: **Opsomming van die kinetiese resultate verkry van die oksiderende addisiereaksies van jodometaan en die verskillende rhodium(I)-*mono*-fosfien komplekse. (Al die reaksies is uitgevoer in dichlorometaan)**

[Rh(acac)(CO)($PR_1R_2R_3$)]	Temperatuur (°C)	Tempokonstante		K_{eq} (M^{-1})
		k_1 (x 10^{-3} $M^{-1}s^{-1}$)	k_{-1} (x 10^{-3} s^{-1})	
PPh_3	24.9	30.8(5)	1.1(2)	27(4)
	15.1	17.2(4)	0.5(1)	31(7)
	5.3	9.71(4)	0.30(1)	33(1)
$PCyPh_2$	26.0	55(1)	0.9(4)	59(26)
	14.0	27.2(4)	1.2(1)	22(2)
	6.0	18.6(2)	0.64(8)	29(4)
PCy_2Ph	25.6	6.98(6)	0.08(2)	90(24)
	14.5	3.38(4)	0.11(2)	31(4)
	5.5	1.88(4)	0.07(2)	27(6)
PCy_3	25.6	27.1(2)	0.29(9)	92(29)
	14.3	13.8(2)	0.45(6)	31(4)
	5.9	9.1(1)	0.15(5)	62(20)

Die tempo's van die reaksies blyk beide steries en elektronies afhanklik te wees. Die aktiveringsparameters dui op 'n assosiatiewe meganisme, wat tiperend is van hierdie reaksies.

Die samestelling van die finale alkiel produkte is moeilik om te bepaal as in aanmerking geneem word dat die IR- en ^{31}P KMR-resultate nie tussen *cis* of *trans*-Rh(III) alkielisomere kan onderskei nie. Verdere studies, wat meer uitgebreide kristallografiese ondersoek en teoretiese berekenings insluit, word egter nog benodig om die absolute konformasie te bepaal.

OPSOMMING

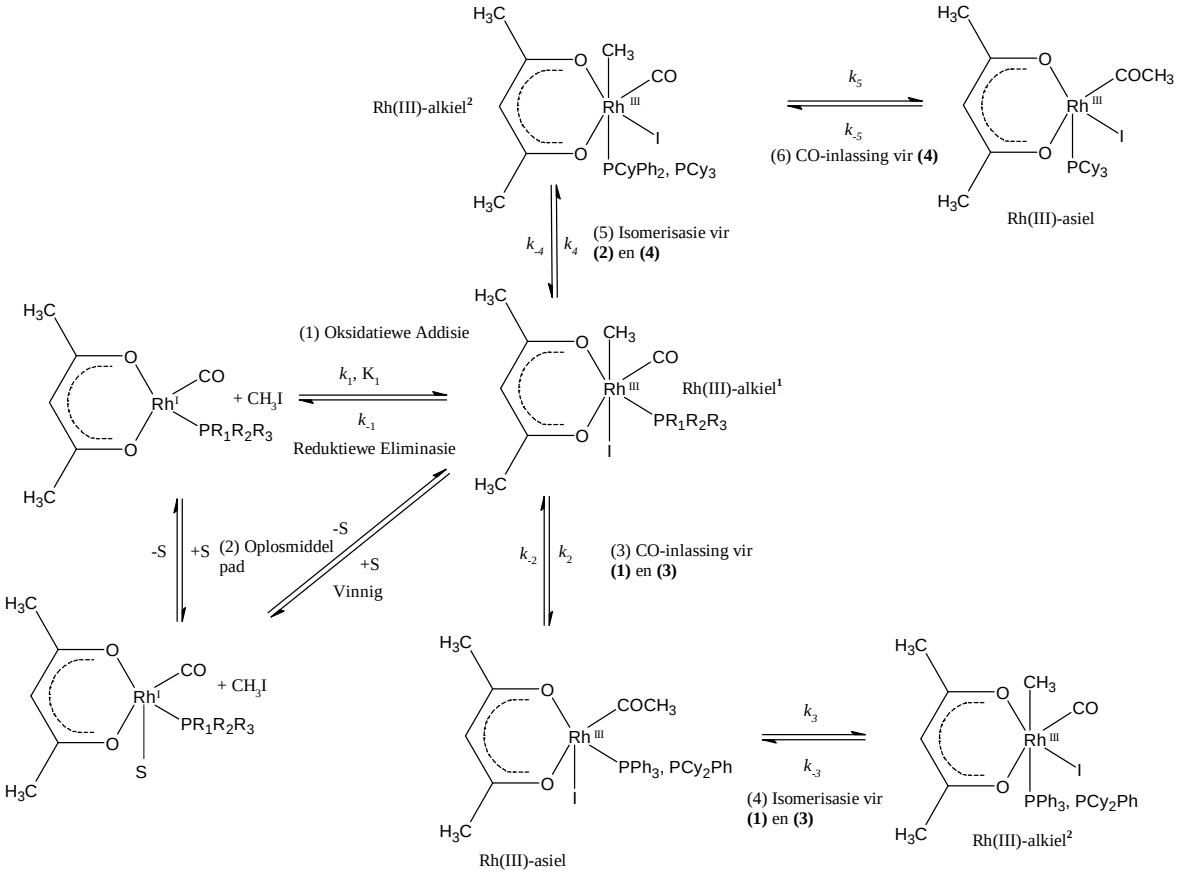

Skema 1: **Voorgestelde reaksieskema vir die oksidatiewe addisie van jodometaan aan [Rh(acac)(CO)($PR_1R_2R_3$)] komplekse.**

1 INTRODUCTION

1.1 GENERAL

Rhodium (Rh), a transition metal, which often has a red-pink colour,[1] was named after *rhodon*, the Greek term for *rose*. It is one of the least abundant metals in the earth's crust and was discovered by William Hyde Wollaston (1803-04) in crude platinum ore from South America. Rhodium is often used as an alloying agent to harden platinum and palladium. It is used in electrical contact material, due to its low electrical resistance, and in optical instruments and jewellery because of its high reflectance and hardness. It is extensively used in chemical synthesis as an important catalyst and to control car exhaust emissions.[2]

Rhodium can exist in a variety of oxidation states from +6 [RhF_6] to -1 [$Rh(CO)_4]^-$. The +6, +5 and +4 states are strongly oxidising, while the Rh(III) state is the most stable. The rhodium(I) oxidation state has a d^8 electron configuration and usually occurs in four-coordinate square planar structures e.g. [$Rh(CO)Cl(PCy_3)_2$] or five-coordinate trigonal bipyrimidal structures[3] e.g. [$HRh(PF_3)_4$]. Rhodium(III) has a d^6 electron configuration and mostly occurs in six-coordinate octahedral geometries. The oxidative addition and reductive elimination reactions from Rh(I) to Rh(III) and *vice versa*, has transformed the catalytic industry and has produced many fascinating reactions over the years.

The worldwide production of liquid fuels and bulk chemicals makes use of catalysis in many different aspects during production. Well-known catalytic transformations such as hydroformylation, hydrogenation and carbonylation have mostly used cobalt or rhodium as catalysts with a combination of various ligand systems.

The *first generation* of hydroformylation processes, such as those developed by BASF, Kuhlmann and Ruhrchemie, were exclusively based on cobalt as the catalyst metal which

[1] B. Carincross, *Field Guide to Rocks and Minerals in South Africa*, Cape Town: Struik Publishers, 2004
[2] J.D. Lee, *Concise Inorganic Chemistry*, 4th Ed., London: Chapman & Hall, 1991
[3] F.A. Cotton, G. Wilkinson, *Advanced Inorganic Chemistry*, 4th Ed., London: John Wiley & Sons, Inc., 1980

reacted under harsh reaction conditions. Significant development occurred in the 1960's with the Shell process and the use of cobalt-phosphine catalysts. S*econd generation* processes saw the advantageous combination of ligand modification with the transition from cobalt to rhodium as catalyst metal. This led to the development of processes which operate under milder reaction conditions and used highly active catalysts with excellent selectivity for the formation of the desired products.[4]

The rhodium Monsanto process, which is one of the main catalytic systems used to produce acetic acid, evolved from the cobalt catalyst system,[5] $[HCo(CO)_4]$, to the rhodium based system,[6,7] $[RhI_2(CO)_2]^-$. Further development resulted in the iridium Cativa process. The selective hydrogenation of alkenes and alkynes occurred with the Wilkinson's catalyst[8] $[Rh(Cl)(PPh_3)_3]$, where as $[RhH(PPh_3)_3(CO)]$ is an important hydroformylation catalyst.[9] These are just a few examples of catalysts which use rhodium and phosphorous ligands as an essential part of the catalytic system.

1.2 PHOSPHOROUS LIGAND SYSTEMS

Tertiary phosphine based ligands have played an important role in organometallic chemistry and in industrial applications of homogeneous catalysis. Phosphorous ligands and their coordination chemistry have been studied in great detail. The cone angle (θ_T) and electronic parameter (ν) was introduced by Tolman[10] to classify phosphine ligands according to their steric demand and coordination ability.

Electronically, phosphorous ligands can be either strong π-acceptors (e.g. fluoroalkoxide substituents) or strong σ-donor (e.g. t-Bu substituents). Organophosphites are strong π-acceptors and form stable complexes with electron rich transition metals. Nitrogen-containing ligands such as amides, amines or isonitriles showed lower reaction rates in the oxo reaction, due to their

[4] B. Cornils, W.A. Herrmann, *Applied Homogeneous Catalysis with Organometallic Chemistry*, New York: VCH Publishers, 1996
[5] D. Forster, M. Singleton, *J. Mol. Catal.*, 1982, 17, 299
[6] P.M. Maitlis, A. Haynes, G.J. Sunley, M.J. Howard, *J. Chem. Soc., Dalton Trans.*, 1996, 2187
[7] F.E. Paulik, J.F. Roth, *J. Chem. Soc., Chem. Commun.*, 1968, 1578
[8] J.F. Young, J.A. Osborn, F.H. Jardine, G. Wilkinson, *Chem. Commun.*, 1965, 131
[9] F.H. Jardine, J.A. Osborn, G. Wilkinson, J.F. Young, *Chem. Ind (London)*, 1965, 560; *J. Chem. Soc. (A)*, 1966, 1711
[10] C.A. Tolman, *Chemical Reviews*, 1977, 77, 313

stronger coordination to the metal centre.[4] Mixed oxygen and nitrogen substituents also lead to the formation of amidites.[11] Nitrogen groups which are connected with electron-withdrawing sulfone groups or acyl groups, can make these phosphorous amidites good π-acceptor ligands.[12] A very electron-poor phosphorous ligand can be formed by having pyrrole as a substituent at the phosphorous atom.[13] The advantage of nitrogen substituents compared to those of oxygen is that the steric hindrance near the metal centre is more easily modified due to the presence of an extra linkage. Generally, phosphites and phosphorous amidites are more easily synthesised than phosphines and they allow a greater variation in structure and properties.[11]

It is clear from the above that changing the substituents at the phosphorous atom can significantly alter the steric and electronic properties of the coordinating ligand. About 250 papers and patent applications appear annually in the field of hydroformylation, of which most deal with new phosphine structures and catalytic results obtained therewith.[4] There is no denying that phosphine ligands play an important role in understanding and constructing new catalytic systems. It was for this reason that we were prompted to look at rhodium systems with simple phosphine ligands in order to increase the understanding of the effect that steric and electronic parameters play on catalytic systems.

1.3 AIM OF STUDY

It is clear from available literature that rhodium(I) complexes play an important role in catalytic cycles, in particular those containing phosphorous ligands. One only needs to grasp the magnitude of several million tons of acetic acid which is produced by the Monsanto rhodium process per annum, in order to explain the importance of understanding the mechanism of rhodium(I) reactions.

Oxidative addition plays an integral role in the catalytic cycle of homogeneous catalysis with regards to rhodium(I) complexes. A study of the effects that influence the mechanistic pathway and rate constants of oxidative addition is therefore of prime importance in designing improved future catalysts.

---

[11] P.W.N.M. van Leeuwen, *Homogeneous Catalysis: Understanding the Art*, Dordrecht, Kluwer Academic Publishers, 2004

[12] S.C. van der Slot, P.C.J. Kamer, P.W.N.M. van Leeuwen, J. Fraanjie, K. Goubitz, M. Lutz, A.L. Spek, *Organometallics*, 2000, 19, 2504

[13] K.G. Moloy, J.L. Petersen, *J. Am. Chem. Soc*., 1995, 117, 7696

CHAPTER 1

In this study, a model complex of general formula [Rh(acac)(CO)($PR_1R_2R_3$)] ($PR_1R_2R_3$ = PPh_3, $PCyPh_2$, PCy_2Ph, PCy_3) with possible catalytic properties was selected. The use of the simple acetylacetonate moiety prevented any isomers from forming due to the symmetrical nature of the bidentate ligand. A better understanding into the exact properties of phenyl and cyclohexyl rings was one of the main aims of this study as the use of triphenylphosphine and tricyclohexylphosphine, are two commonly cited examples when comparing steric and electronic parameters of phosphine ligands.

With the above in mind, the following stepwise aims were set for this study.

- Synthesis of model complexes such as [Rh(acac)(CO)($PR_1R_2R_3$)] ($PR_1R_2R_3$ = PPh_3, $PCyPh_2$, PCy_2Ph, PCy_3) that contain the acetylacetonate bidentate ligand and to study the solid state and solution properties thereof, also with respect to the effects of electronic and steric interactions.

- The crystallographic characterization of selected four and six coordinated complexes [Rh(acac)(CO)($PR_1R_2R_3$)] and [Rh(acac)I(CH_3)(CO)($PR_1R_2R_3$)] to study the coordination mode, bond lengths and distortion of the phosphine moieties.

- Kinetic mechanistic investigation of the oxidative addition of iodomethane to the four-coordinated [Rh(acac)(CO)($PR_1R_2R_3$)] complexes.

- Analysis of results with respect to phosphine reactivity and coordinating ability and comparison to other phosphine and phosphite systems available in literature.

2 THEORETICAL ASPECTS OF CATALYSIS

2.1 INTRODUCTION

Research and development into transition metal complexes have gained momentum over the past years due to its unique properties and widespread use in the industrial and economical setting. It plays a very important role as transition metal catalysts in industrial processes such as polymerisation, hydrogenation, hydroformylation and carbonylation reactions.

The properties, effectiveness and selectivity of transition metal catalysts are individual to each catalyst and determined by the inherent characteristics of the metal centre. The effect of the ligands and substituents bonded to the metal centre is profound and very near to limitless. All these possibilities spur researchers on to continually seek and, hopefully, discover that one, perfect catalyst.

The field of transition metal catalysts is very broad, therefore only the relevant aspects of catalysis, to this study will be discussed. The aim of this study was to investigate the effect of tertiary phosphines on the oxidative addition of CH_3I to a rhodium metal complex, a precursor step to the actual carbonylation reaction. General aspects of homogeneous catalysis focusing on the influence of rhodium, carbonylation and oxidative addition will be discussed in this chapter.

2.2 RHODIUM IN ORGANOMETALLIC CHEMISTRY

2.2.1 Rhodium Metal

The platinum group metals (PGMs) – *platinum, iridium, osmium, palladium, rhodium and ruthenium* – possess exceptional properties, such as high melting points, high lustre, resistance to corrosion and catalytic tendencies, which are used in the chemical, electrical and petroleum-refining industries, as well as in the jewellery trade. South Africa is a premier source of PGMs and in 1996 produced 56% (62 800 tonnes) of the World's identified reserves,[1] most of which were mined from the Bushveld Igneous Complex. After mining, the ore is concentrated by gravitation and flotation processes, and then smelted. The resulting Ni-Cu sulphide "matte" is cast into anodes. By means of electrolysis, copper is deposited at the cathode and nickel remains in solution. Further electrolytic refining of nickel creates anode slime which consists of a mixture of PGMs with silver and gold. Pd, Pt, Ag and Au are dissolved in aqua regia while the residue, containing Ru, Os, Rh and Ir, are further processed *via* a complex separation which yields Rh and Ir as powders.

Rhodium is a hard, but brittle, silvery, white metal. It is an extremely rare metal with a relative abundance of 10^{-7}% in the earth's crust. It is resistant to acids including aqua regia, but reacts with O_2 and the halogens at high temperatures. At red heat in air, the metal becomes coated with a dark layer of rhodium (III) oxide, Rh_2O_3. The metal may be dissolved in mineral acids after alloying with Zn metal by heating it at 450-500˚C, under a layer of zinc chloride as flux.[2]

Governmental institutions are placing more and more emphasis on 'green planet' systems. They are tightening laws on vehicle emissions, causing an increase in the global demand for catalytic converters in cars. Since rhodium is used in these catalytic converters, to reduce nitrogen oxide emissions, and since it cannot be substituted in diesel versions, its price is continually rising. To

[1] H.V. Eales, *A First Introduction to the Geology of the Bushveld Complex*, Pretoria: Council of GeoScience, 2001, 73
[2] D.T. Burns, A. Townshend, A.H. Carter, *Inorganic Reaction Chemistry*, Vol. 2, England: John Wiley & Sons Ltd., 1981, 355-358

date, the price has risen 11% this year (Jan – April 2007) and is selling at an average price of US $5 900 per ounce.[3]

2.2.2 Oxidation States of Rhodium

Rhodium and iridium differ from ruthenium and osmium in the sense that they do not form oxo anions or volatile oxides. Rhodium chemistry is mainly centred around the oxidation states of O, + I, II and III. The most common oxidation state is (III).

Rhodium(III) complexes are typically octahedral, stable, low spin and diamagnetic, e.g. $[RhCl_6]^{3-}$, $[Rh(H_2O)_6]^{3+}$ and $[Rh(NH_3)_6]^{3+}$. The chloride complex is synthesised by heating the finely divided Rh metal with chlorine or a Group I metal chloride.[4] Unlike Co^{III} which readily reduces to Co^{II}, the reduction of Rh^{III} normally yields the metal – usually with halogens, water or amine ligands present – or to hydridic species of Rh^{III} or to Rh^{I} complexes when π-bonding ligands are involved.

Rh^{III} readily gives octahedral complexes with halides, e.g. $[RhCl_5H_2O]^{2-}$, and with oxygen ligands such as oxalate and EDTA. The cationic and neutral complexes are generally kinetically inert, but the anionic complexes of Rh^{III} are usually labile.[5] Rhodium complex cations are very useful in studying *trans* effects in octahedral complexes.

One of the most important Rh^{III} compounds is the dark red, crystalline, trichloro complex, $[RhCl_3.xH_2O]$. It is the usual starting material for the preparation of many rhodium complexes and is made by dissolving hydrous Rh_2O_3 in aqueous hydrochloric acid and evaporating the hot solution.[4] It is soluble in water and alcohols, giving red-brown solutions. Solutions of $[RhCl_3.xH_2O]$ in water (Eq. 2.1) are extensively hydrolyzed,

$$RhCl_3(H_2O)_3 \overset{H_2O}{\rightleftharpoons} RhCl_2(OH)(H_2O)_3 + H^+ + Cl^- \qquad \textbf{... 2.1}$$

By boiling aqueous solutions of $[RhCl_3.xH_2O]$, $[Rh(H_2O)_6]^{3+}$ is formed and with excess HCl, the rose-pink $[RhCl_6]^{3-}$ ion is produced. Hexahalogenorhodates can be obtained by heating Rh metal

[3] J. Riseborough, X. Yu, *Business Report*, The STAR newspaper, 29 March 2007
[4] J.D. Lee, *Concise Inorganic Chemistry*, 4th Ed., London: Chapman & Hall, 1991
[5] F.A. Cotton, G. Wilkinson, *Advanced Inorganic Chemistry*, 4th Ed., London: John Wiley & Sons, Inc., 1980

and alkali metal halides in Cl_2, extracting the melt and crystallising. Halogen-bridged dimers[6] such as $[Rh_2Cl_9]^{3-}$, $[Rh_2Cl_6(PEt_3)_3]$ and $[Rh_2Cl_7(PR_3)_2]^-$ can be obtained with very large cations such as $[NEt_4]^+$ and $[PPh_4]^+$. The white, air-stable, crystalline salt $[RhH(NH_3)_5]SO_4$ can be produced by the reduction of $[RhCl_3.xH_2O]$ in NH_4OH by Zn in the presence of SO_4^{2-}. Some reactions of $[RhCl_3.xH_2O]$ are illustrated in Figure 2.1.

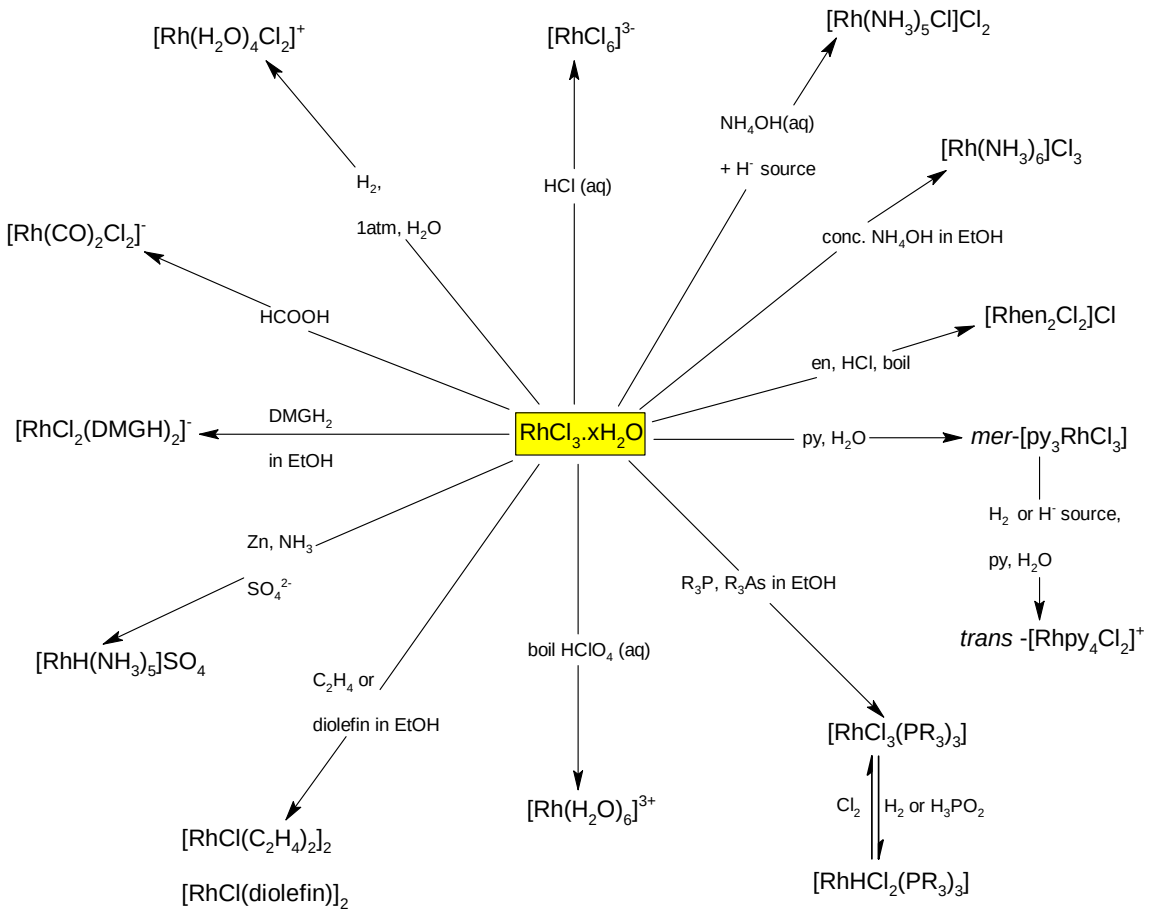

Figure 2.1: Some reactions of $[RhCl_3.xH_2O]$.[5]

The reaction of Rh^I to Rh^{III} complexes and *vice versa* are extensively used in industrial processes, especially with regards to catalysis. Rhodium(I) complexes exist in square, tetrahedral and five-coordinate diamagnetic species, generally bonded to π-bonding ligands such as CO, PR_3, RNC, cyclopentadienyls, arenes and alkenes. Rh^I complexes are generally prepared from reduction of similar Rh^{III} complexes or of halide complexes such as $[RhCl_3.xH_2O]$ in the presence of the complexing ligand. The majority of Rh^I complexes undergo oxidative addition which is used in catalytic reactions. Some reactions of Rh^I complexes are seen in Figure 2.2.

[6] F.A. Cotton, S.J. Kang, S.K. Mandal, *Inorg. Chim. Acta*, 1993, 206, 29; F.A. Cotton, S.J. Kang, *Inorg. Chem.*, 1993, 32, 2336

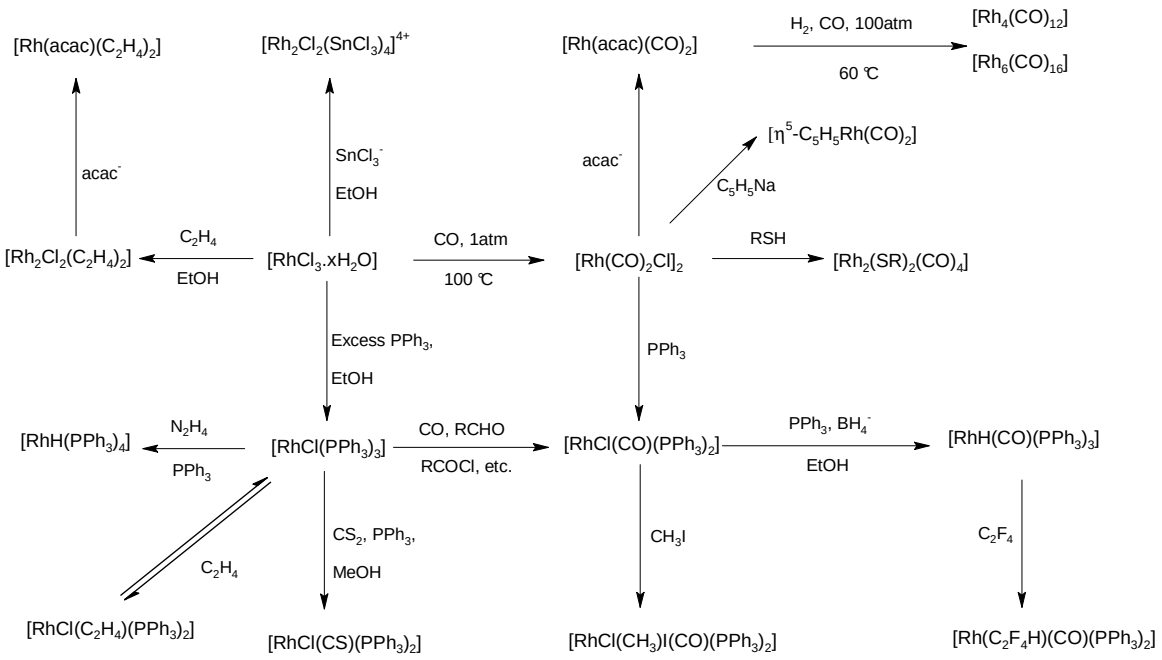

Figure 2.2: Some reactions and preparations of rhodium(I) compounds.[7]

A major part of Rh^{I} chemistry is the formation of tertiary phosphine complexes. Triphenylphosphine is used in catalytic hydroformylations of alkenes, while water soluble phosphines, such as $P(C_6H_4SO_3H)_3$, are used in two-phase systems. $[RhCl_3.xH_2O]$ is the starting reagent to make the rhodium counterpart of the original Vaska compound, $[IrCl(CO)(PPh_3)_2]$. Due to the lower basicity, the Rh Vaska complex, $[RhCl(CO)(PPh_3)_2]$, is less prone to oxidative addition than the Ir^{I} Vaska compound, which is indicated by the equilibria lying to the left in oxidative addition reactions such as:

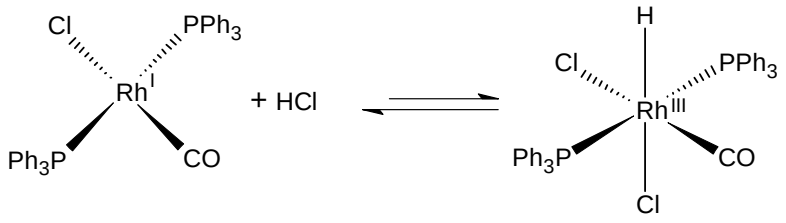

... 2.2

The above Rh^{I} Vaska complex is used to synthesize $[RhH(CO)(PPh_3)_3]$, a key intermediate in hydroformylation reactions. Wilkinson's catalyst, $[RhCl(PPh_3)_3]$, is also prepared from $[RhCl_3.xH_2O]$. It is one of the most studied compounds of all the Rh^{I} phosphine species because of the wide range of its stoichiometric and catalytic reactions. It was the first compound to be

[7] F.A. Cotton, G. Wilkinson, *Advanced Inorganic Chemistry*, 4th Ed., London: John Wiley & Sons, Inc., 1980

discovered that allowed the catalytic hydrogenation of alkenes and other unsaturated substances in homogeneous solutions at room temperature and pressure.[8]

2.2.3 Rhodium in Catalysis

Rhodium is used in a variety of ways in catalysis. Processes such as hydrogenation, polymerisation, hydroformylation, carbonylation (Fig. 2.3) and many others have all investigated rhodium(I) as a possible key ingredient in the catalytic cycle, at some time or another. Oxidative addition is a key step in many catalytic systems and four-coordinated complexes of rhodium(I), which are coordinatively unsaturated, are ideal for studying such reactions.

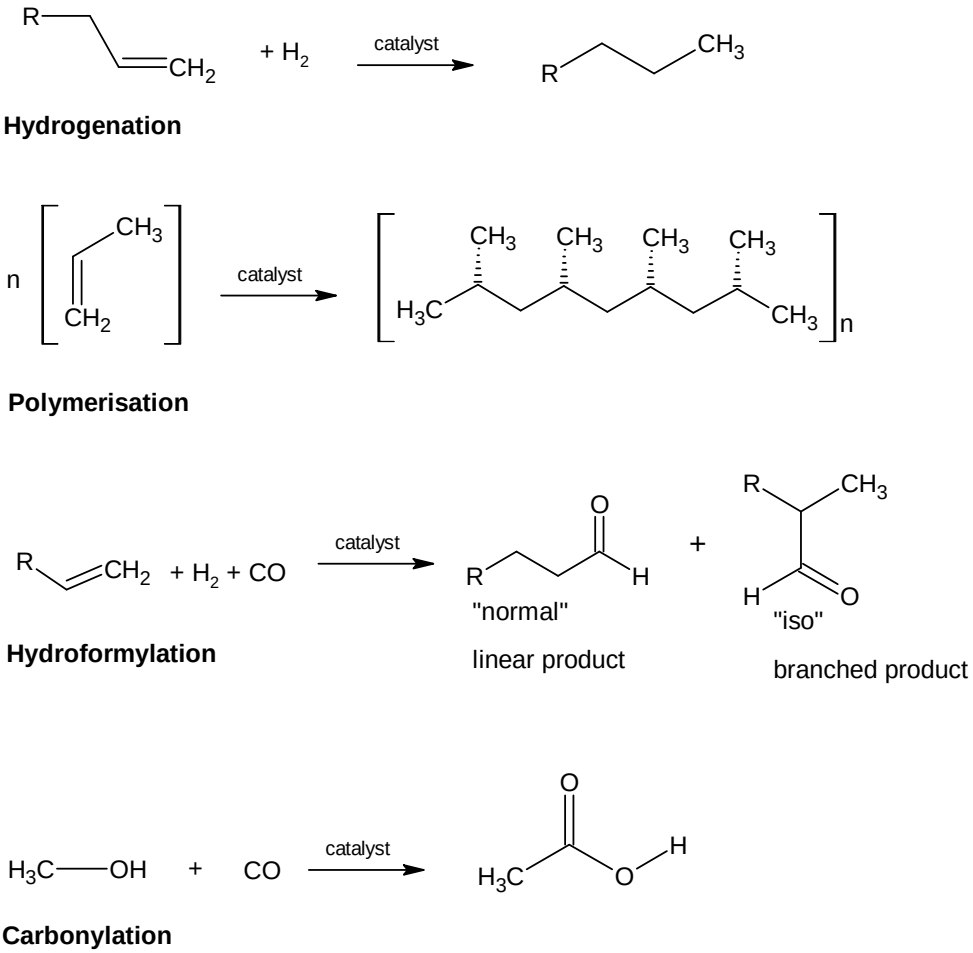

Figure 2.3: General reactions of hydrogenation, polymerisation, hydroformylation and carbonylation.

[8] F.H. Jardine, J.A. Osborn, J.F. Young, *J. Chem. Soc.*, *A*, 1966, 1711; *Progr. Inorg. Chem.*, 1981, 28, 63

2.3 OXIDATIVE ADDITION

2.3.1 Introduction

Oxidative addition / reductive elimination processes are universally important to a vast array of synthetically useful organometallic reactions. The *oxidative addition* (O.A.) reaction can be written generally as:

$$L_y M^n + XY \underset{\text{R. E.}}{\overset{\text{O.A.}}{\rightleftharpoons}} L_y M^{n+2}(X)(Y)$$

The reaction causes the formal oxidation state of the metal to increase by two units.[9] The reverse reaction is termed as *reductive elimination* (R.E.). These terms only describe a specific type of reaction and have no mechanistic implication. In the above equation, L_yM represents a stable organometallic complex, and XY is a substrate molecule that adds to the metal with a complete dissociation of the X-Y bond and formation of two new bonds, M-X and M-Y. The organometallic complex may be neutral, anionic or cationic. The substrate molecule usually contains a highly polarised X-Y bond, or a very reactive, low-energy bond between highly electronegative atoms.[10]

In general for an oxidative addition reaction to proceed, there must be:

- Nonbonding electron density on the metal.
- Two vacant coordination sites on the reacting complex L_yM to allow for the formation of two new bonds.
- Stable oxidation states of the metal separated by two oxidation numbers.

Metal complexes with the d^8 and d^{10} electron configuration, are the most intensively studied reactions for transition metals, notably, Fe^0, Ru^0, Os^0, Rh^I, Ir^I, Ni^0, Pd^0, Pt^0, Pd^{II} and Pt^{II}. One of the most studied complexes is of the square-planar, *trans*-$[IrX(CO)(PR_3)_2]$ type, because the equilibria lies well to the oxidised side and the oxidised compounds are usually stable octahedral species.

---

[9] F.A. Cotton, G. Wilkinson, P.L. Gaus, *Basic Inorganic Chemistry*, 3rd Ed., New York: John Wiley & Sons, Inc., 1995

[10] C.M. Lukehart, *Fundamental Transition Metal Organometallic Chemistry*, California: Brooks/Cole Publishing Company, 1985

Oxidative addition is frequently reversible, especially for addition to sixteen-electron complexes where no ligand loss is involved. The factors which determine whether oxidative addition or reductive elimination occur, depend critically on:

- The nature of the metal and its ligands.
- The nature of the added molecule XY and of the M-X and M-Y bonds that are formed.
- The medium/solvent in which the reaction is conducted.

The complexes with higher oxidation states are usually more stable for the heavier metals, e.g. Ir^{III} species are generally more stable than Rh^{III} species. Oxidative addition is favoured for ligands that increase the electron density of the metal. The steric properties of the ligands are also important. Very bulky ligands, e.g. PEt(*t*-Bu)$_2$ tend to favour the forward reaction, but the substitution of an *o*-methoxy group on a phenylphosphine increases the nucleophilicity of the metal by donation.[11]

2.3.2 Mechanisms of Oxidative Addition

There are a great variety of mechanisms for the oxidative addition to four-coordinate d^8-complexes and no simple generalisations can be made.[12] A particular reaction between a metal complex and a substrate can, depending on the reaction conditions (e.g. solvent polarity, temperature and presence of trace amounts of oxidising impurities), proceed by numerous pathways. A particular substrate may also react with different metal complexes in different ways. The following mechanisms are the most commonly proposed:

- Three-centre concerted processes.
- S_N2-type mechanism.
- Free radical mechanism.
- Ionic mechanism.

[11] E.M. Miller, B.L. Shaw, *J. Chem. Soc., Dalton*, 1974, 480
[12] P. Meakan, R.A. Schunn, J.P. Jesson, *J. Am. Chem. Soc.*, 1974, 96, 277; A.D. English, P. Meaken, J.P. Jeason, *J. Am. Chem. Soc.*, 1976, 98, 422

2.3.2.1 Three-Centre Concerted Process

The oxidative addition of non-polar molecules e.g. H_2, Cl_2 etc., tend to react according to the three-centre concerted mechanism whereby the *cis* isomer is formed.[13] The classic example is the addition of H_2 to a 16é square-planar d^8 species such as a Vaska complex,[14] [IrCl(CO)L_2].

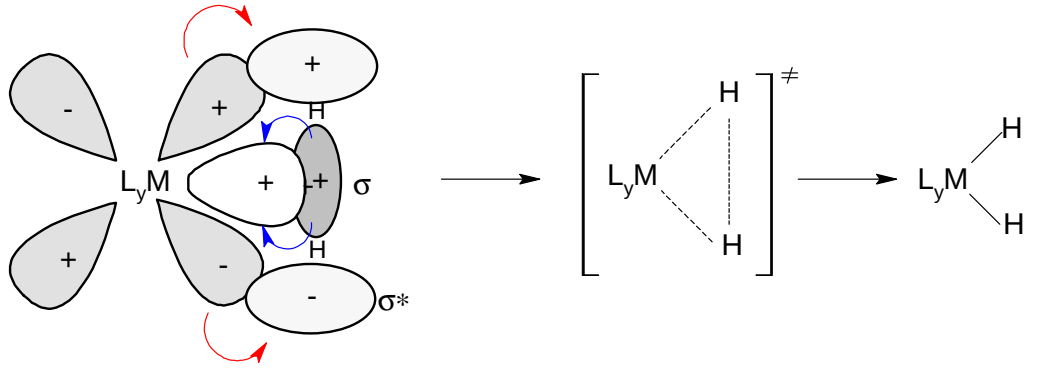

Figure 2.4: Concerted three-centre addition of H_2 to give a *cis*-dihydrido product.[10]

According to this mechanism, electron density in a filled *d* valence orbital on the metal, flow into the empty σ* molecular orbital (MO) of H_2 (red arrows in Fig. 2.4). Two M-H bond interactions form while weakening the H-H bond in the transition state.[15, 16] Electron density in the occupied σ MO of H_2, flow into an empty valence orbital on the metal atom (blue arrows). Two M-H single bonds are formed and the H-H bond is cleaved.

2.3.2.2 S_N2-type Mechanism

The addition of methyl, allyl, acyl and benzyl halides to species such as Vaska's complex is often achieved *via* a S_N2-type mechanism. These are second-order reactions, first order in metal and first order in substrate, and show a large negative activation entropy.[17] Typical S_N2-type mechanisms in organometallic catalysis are similar to the S_N2-type mechanisms found in organic chemistry. This is due to the similarity of the ordered, polar transition states achieved in both types. An example of a S_N2 mechanism is illustrated in Figure 2.5.

---

[13] R.J. Cross, *Chem. Soc. Rev.*, 1985, 14, 197
[14] L. Vaska, *Acc. Chem. Res.*, 1968, 1, 335
[15] C.E. Johnson, B.J. Fisher, R. Eisenberg, *J. Am. Chem. Soc.*, 1983, 105, 7772; C.E. Johnson, R. Eisenberg, *J. Am. Chem. Soc.*, 1985, 107, 3148
[16] R.H. Crabtree, R.J. Uriarte, *Inorg. Chem.*, 1983, 22, 4152
[17] P.B. Chock, J. Halpern, *J. Am. Chem. Soc.*, 1966, 88 3511

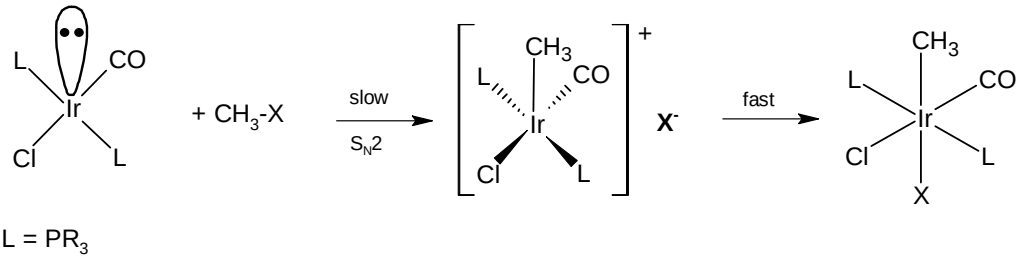

Figure 2.5: The S_N2 mechanism for the oxidative addition of CH_3X to *trans*-[IrCl(CO)PR_3].

Oxidative addition reactions that follow the S_N2 mechanism are characterised by electronic, steric and solvent effects such as polar solvents which accelerate the rate of the reaction.[18] The reactivity in the S_N2 additions are increased as the nucleophilicity of the metal increases, as illustrated by the reactivity order for Ni(0) complexes: $Ni(PR_3)_4 > Ni(PAr_3)_4 > Ni(PR_3)_2$(alkene) $> Ni(PAr_3)_2$(alkene) $> Ni(cod)_2$ (R = alkyl; Ar = aryl).[19]

2.3.2.3 Free Radical Mechanism

There are two subtypes of radical processes which can be distinguished, namely: non-chain and chain radical mechanisms.[20]

The non-chain radical mechanism is thought to operate by the additions of certain alkyl halides, RX, to $Pt(PPh_3)_3$ (R = Me, Et; X = I); (R = $PhCH_2$; X = Br).[21]

$$PtL_3 \xrightarrow{\text{fast}} PtL_2$$

$$PtL_2 + RX \xrightarrow{\text{slow}} {}^{\bullet}PtXL_2 + R^{\bullet} \xrightarrow{\text{fast}} RPtXL_2$$

As X is transferred from RX to the metal, there is a 1é oxidation of the metal by the alkyl halide. This produces the pair of electrons, as seen above, which combine rapidly to form the product. The more readily the substrate can be oxidised and the more basic the metal, the greater the reactivity of the radical reaction. The reaction rates also increase as the stability of the radical, R· increases.

---

[18] R.H. Crabtree, *The Organometallic Chemistry of the Transition Metals*, New York: John Wiley & Sons, Inc., 1988
[19] E. Uhlig, D. Walther, *Coord. Chem. Rev.*,1980, 33, 3
[20] J.A. Osborne, J.A. Labinger, *Inorg. Chem.*, 1980, 19, 3230, J.A. Osborne, J.A. Labinger, N.J. Coville, *Inorg. Chem.*, 1980, 19, 3236
[21] (a) M.F. Lappert, P.W. Lednor, *Chem. Comm.*, 1973, 948; (b) *J. Chem. Soc., Dalton*, 1980, 1448; (c) *Adv. Organomet. Chem.*, 1976, 14, 345

Alkyl halides, vinyl and aryl halides, and α-halo esters undergo oxidative addition to Vaska complexes *via* a radical chain mechanism. The reactions occur as one-electron (radical) transfer instead of the two-electron transfer which is found in S_N2 reactions. A radical chain reaction mechanism is illustrated in Figure 2.6, where [M] = *trans*-[IrX(CO)L_2]. A radical chain reaction can be initiated by trace amounts of Ir(II) species or by molecular oxygen.

Initiation steps:

$$[M^{I}] + Q\bullet \text{ (trace radical)} \longrightarrow [M^{II}]\text{-}Q\bullet$$

$$[M^{II}]\text{-}Q\bullet + \text{R-X} \longrightarrow \text{X-}[M^{III}]\text{-Q} + \text{R}\bullet$$

Propagation steps:

$$[M^{I}] + \text{R}\bullet \longrightarrow \text{R-}[M^{III}]\bullet$$

$$\text{R-}[M^{II}]\bullet + \text{R-X} \longrightarrow \text{R-}[M^{III}]\text{-X} + \text{R}\bullet$$

Termination step:

$$\text{Two radicals} \longrightarrow \text{Non-radical products}$$

Net reaction:

$$[M^{I}] + \text{R-X} \longrightarrow \text{R-}[M^{III}]\text{-X}$$

Figure 2.6: The free radical chain reaction in metal complexes.[10]

Radical initiators and inhibitors have a large effect on the reaction rate. The reactions slow down or stop in the presence of hindered phenols, a radical inhibitor. These inhibitors quench the chain-carrier radical R· to give R-H and the stable, unreactive, aryloxy radical, ArO·. Termination of the radical reaction occurs by radical coupling or disproportionation.[10]

2.3.2.4 Ionic Mechanism

The ionic mechanism is favoured in a polar medium. In a polar medium, hydrogen halides (e.g. HCl or HBr) would be dissociated. Protonation of a square complex would first produce a five-coordinate intermediate. Intramolecular isomerisation followed by coordination of Cl^- would then give the final product.

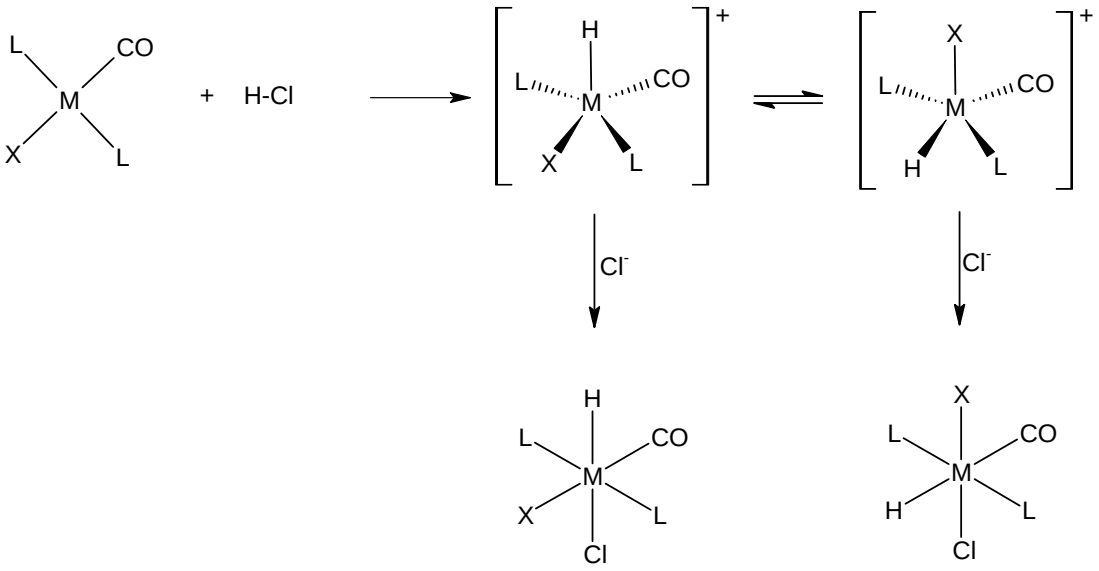

Figure 2.7: Ionic mechanism for the oxidative addition of HCl to $[MXL_2CO]$.[10]

2.3.3 Factors influencing Oxidative Addition

The metal centre can be considered as a nucleophile during an oxidative addition reaction. Hence any changes which affect the nucleophilic character of the metal centre, will also affect the reaction path, products and rate. A few of these factors will be mentioned briefly.

In general, oxidative addition is facilitated by ligands such as PR_3, R-, and H-, which are good σ-donors and increase the electron density at the metal centre, whereas ligands which are good π-acceptors, such as CO, CN^- and olefins, decrease the electron density at the metal and suppress oxidative addition.

Steric factors also play a role. It is important to consider the steric inhibition of oxidative addition especially with bulky phosphines such as tricyclohexylphosphine PCy_3.[22]

Coordinative unsaturated complexes are more reactive than its saturated counterparts. The nature of the metal also influences the reactivity. The ease of oxidation of a metal centre does provide an indication of its reactivity. In general the larger metals in lower oxidation states are more reactive towards oxidative addition, however there are exceptions. Figure 2.8 indicates the tendency of transition metals to undergo oxidative addition.[23]

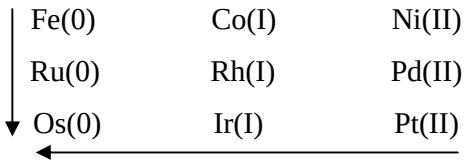

Figure 2.8: **Tendency of d^8 metals to undergo oxidative addition. The arrows indicate increased reactivity towards oxidative addition.**

2.3.4 Ligand Parameters

Steric and electronic parameters of ligands have a direct and large influential effect on the character and reactivity of a transition metal catalyst. It is important to understand and characterize these influences and parameters in order to tailor-make a catalytic system which will yield the desired products. Although steric and electronic parameters are often intimately related, a useful separation can be made through the parameters of ***v*** and **θ**; as described below.

2.3.4.1 The Electronic Parameter (*v*)

The electronic properties of a molecule can be altered by different electronic effects which are transmitted along the chemicals bonds, for example $P(p\text{-}C_6H_4OCH_3)_3$ will increase the electron-donor capacity of the ligand compared to $P(p\text{-}C_6H_4Cl)_3$.[24] Infrared (IR) frequencies are useful and reliable yardsticks, by which the electronic properties of a series of phosphorous ligands during co-ordination to a particular metal, can be determined. As many homogeneous rhodium

[22] A. Roodt, G.J.J. Steyn, *Recent Res. Inorganic Chem.*, 2000, 2, 1
[23] R.S. Nyholm, K. Vrieze, *J. Chem. Soc.*, 1965, 5337

catalysts have CO bonded to the metal center, and as CO is easily identified on an IR spectrum, it is a convenient method to determine the σ-basicity and π-acidity of phosphorous ligands. Strong σ-donor ligands increase the electron density on the metal and hence a substantial back-donation to the CO ligands occurs, which lowers the IR frequency. Strong π-acceptor ligands will compete with CO for the electron back-donation, and the CO stretch frequencies will remain high.

Tolman[24] based the electronic parameter *v* on the CO stretching frequency, A_1, of a $[Ni(CO)_3L]$ complex in CH_2Cl_2 where L = PR_3 or $P(OR)_3$. The reference ligand was *tri*-*tert*-butylphosphine, $P(t\text{-Bu})_3$. The electronic parameter *v* for a variety of ligands can be estimated by using the equation:[25]

$$\text{For } PX_1X_2X_3 \qquad v = 2056.1 + \sum_{i=1}^{3} \chi_i \qquad \textbf{... 2.3}$$

where χ_i (chi) is the individual substituent contribution that was calculated by a large number of substituents, X_1, X_2 and X_3.

2.3.4.2 The Steric Parameter (θ)

Steric effects are the result of forces, usually nonbonding, between parts of a molecule. For example changing $P(Me)_3$ to $P(t\text{-Bu})_3$ increases the bulkiness of the ligand which causes steric strain.[24] The steric parameter, θ, indicates the amount of space that a bulky phosphorous ligand occupies. The steric parameter, θ, for symmetric ligands is the apex angle of a cylindrical cone, centered 2.28 Å from the center of the P atom, which just touches the van der Waals radii of the outermost atoms of the model (Figure 2.9 (a)). The cone angle for an unsymmetrical ligand $PX_1X_2X_3$, (Figure 2.9 (b)), can be determined by using a model which minimizes the sum of the cone half angles as indicated by the following equation:

$$\theta = (2/3) \sum_{i=1}^{3} \theta_i/2 \qquad \textbf{... 2.4}$$

[24] C.A. Tolman, *Chem. Rev.*, 1977, 77, 313
[25] C.A. Tolman, *J. Am. Chem. Soc.*, 1970, 92, 2953

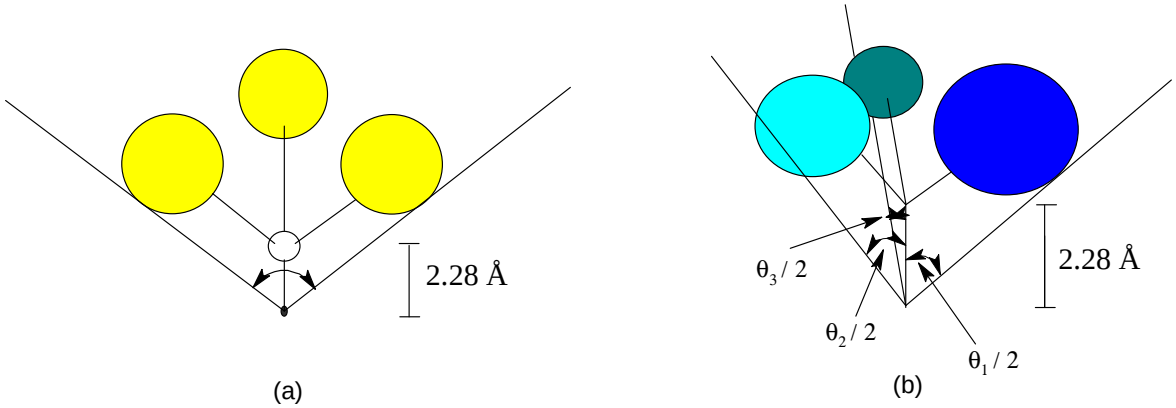

Figure 2.9: **(a) - Cone angle measurement for symmetrical ligands. (b) – Cone angle measurement for unsymmetrical ligands.[24]**

2.4 HOMOGENEOUS CATALYTIC SYSTEMS

2.4.1 Introduction

Catalytic reactions play an important role in the industrial production of liquid fuels and bulk chemicals. Many organic chemicals which are produced in bulk quantities are derived from natural gas or petroleum, usually by converting these hydrocarbons into olefins. A catalyst is defined as: *A substance that increases the rate of a chemical reaction without itself undergoing any permanent chemical change.*[26] A catalyst works by lowering the activation energy of the chemical reaction because it provides an alternative pathway by which the reaction can proceed. It increases the rate at which a reaction comes to equilibrium, but it does not alter the position of the equilibrium. Although a catalyst takes part in the reaction, formally it does not experience any permanent chemical change and therefore should be recovered chemically unchanged at the end of the reaction. It can however be physically changed, e.g. converted to a powder.

Heterogeneous catalysts, where the catalyst exists in a different phase from the reacting species e.g. a solid catalyst in contact with a gaseous or liquid solution of reactants,[26] are advantageous from a practical industrial point of view because the products can be easily separated from the excess reactants and from the catalyst.[7] Homogeneous catalysts, where the catalyst is in the same

[26] Oxford University Press, *Dictionary of Science,* London: Market House Books Ltd., 1999

phase as the reacting species, have been of great interest to industry because of higher selectivity in reactions, operation under milder conditions of temperature and pressure to name just a few advantages. A comparison of homogeneous and heterogeneous catalysis is listed in Table 2.1

Table 2.1: Advantages and disadvantages of homogeneous and heterogeneous catalysis.[27]

	Homogeneous	Heterogeneous
Efficiency of catalyst use	All metal centres active	Only surface site active
Experimental conditions	Generally mild	Often high temperatures and/or high pressures
Separation of catalyst from product	Difficult	Generally easy
Catalyst recovery	Difficult	Easy
Establishment of reaction mechanism	Kinetic studies and rate laws usually informative	Often difficult

The rest of this chapter will be focused on homogenous catalysts as this is the focus of the study. Some well-known homogenous catalytic systems are listed below, a few of which will be discussed in detail.

- The old catalytic process of making sulfuric acid *via* the "lead chamber process".[28]
- The Wacker synthesis of acetaldehyde from petroleum-based ethylene using a $PdCl_2$ catalyst and air.[29]
- DuPont's use of nickel phosphite complexes for hydrocyanation of alkenes.[9]
- The BASF cobalt catalysed carbonylation of methanol.[10]
- The Monsanto rhodium catalysed carbonylation of methanol.[30]
- The hydrogenation of unsaturated compounds using Wilkinson's catalyst $RhCl(PPh_3)_3$, $RhCl_3(py_3)$ etc.[18]
- Metathesis of alkenes e.g. Schrock's and Grubbs' catalysts.[31, 32, 33]

[27] M.L. Tobe, J. Burgess, *Inorganic Reaction Mechanisms*, England: Addison Wesley Longman Ltd., 1999
[28] P.W.N.M. van Leeuwen, *Homogeneous Catalysis: Understanding the Art*, Dordrecht: Kluwer Academic Publishers, 2004
[29] F.C. Philips, *J. Am. Chem.*, 1984, 16, 255; J. Smidt *et al.*, *Angew. Chem.*, 1959, 71, 176; *Angew. Chem.*, 1962, 74, 93; J.E. Backvall, B. Åkermark, *et al., J. Am. Chem. Soc.*, 1979, 101, 2411.
[30] P.M. Maitlis, A. Haynes, G.J. Sunley, M.J. Howard, *J. Chem. Soc., Dalton Trans.*, 1996, 2187
[31] R.R. Schrock, J.S. Murdzek, G.C. Bazan, J. Robbins, M. DiMare, M. O'Regan, *J. Am. Chem. Soc.*, 1990, 112, 3875
[32] R.H. Grubbs, *Tetrahedron*, 2004, 60, 7117
[33] R.H. Grubbs, S. Chang, *Tetrahedron*, 1998, 54, 4413

2.4.2 Hydroformylation

The introduction of oxygen into a molecule is one of the main aims in functionalising hydrocarbons from petroleum sources. Generally this can be done by two methods, namely oxidation and carbonylation. The preferred route for aromatic acids, acrolein, maleic anhydride, ethane oxide, propene oxide and acetaldehyde is via oxidation. Hydroformylation, which is also referred to as the "oxo" reaction, is used for the large scale preparation of butanal, butanol, 2-ethylhexanol, and detergent alcohols.

The reaction consists of the addition of synthesis gas (H_2 + CO) to an alkene under pressure in the presence of a catalyst[34] (Figure 2.10). An interesting issue in hydroformylation is the ratio of linear and branched product formation. The factors which control the linearity and selectivity, whether it is kinetics or ligands for instance, are of great scientific interest.

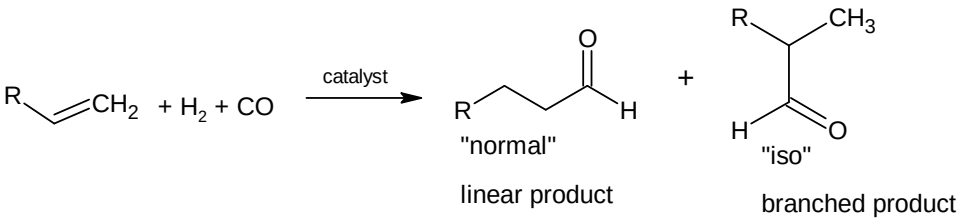

Figure 2.10: The hydroformylation reaction

Hydroformylation was discovered in 1938 by O. Roelen, who prepared propionaldehyde from ethylene and synthesis gas by means of a cobalt catalyst [$Co_2(CO)_8$] under extreme reaction conditions (90-150˚C, 100-400 bar).[35] The catalytic cycle for the linear aldehyde is shown in Scheme 2.1 on the next page. The [$Co_2(CO)_8$] first reacts with H_2 to give [$HCo(CO)_4$], the activate catalyst.

[34] D.W.A. Sharpe, *The Penguin Dictionary of Chemistry*, 3rd Ed., England: Penguin Books Ltd., 2003
[35] C. Elschenbroich, A. Salzer, *Organometallics: A Concise Introduction*, New York: VCH Publishers, 1989

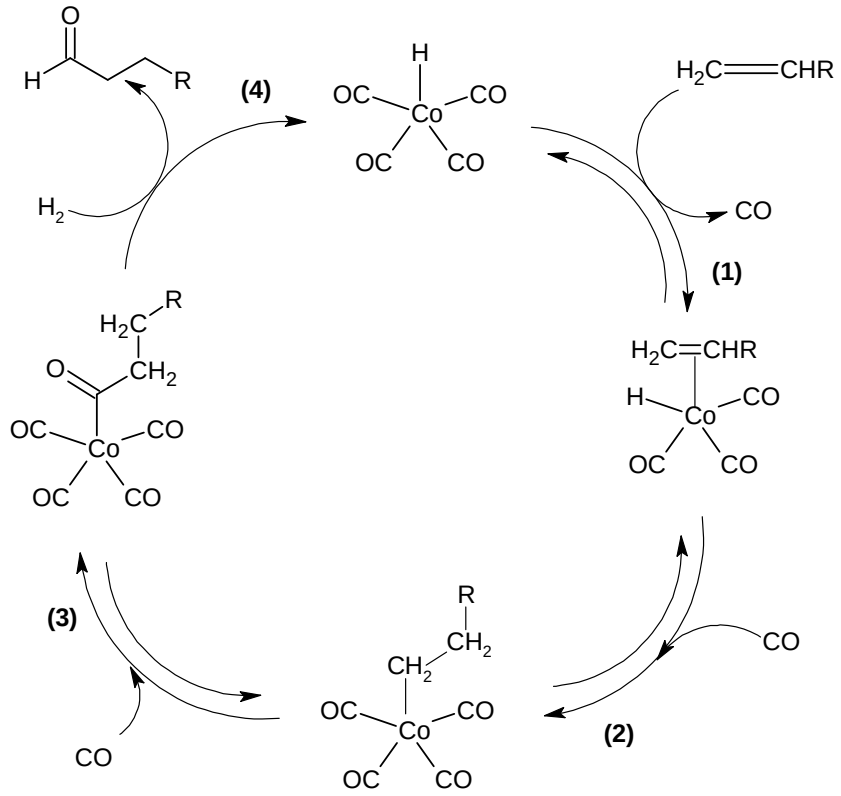

Scheme 2.1: Mechanism of the cobalt catalysed hydroformylation.[28]

The first step (**1**) consists of the replacement of a carbon monoxide with the alkene. There is a negative order in CO pressure and the rate is proportional to the alkene concentration. Migration of the hydride ion gives the alkyl cobalt complex (**2**), which may be either linear (as indicated in the reaction mechanism) or branched (Markovnikov or anti-Markovnikov addition). The vacant site is then occupied with an incoming carbon monoxide. Next, the acetyl complex is formed by the migration of the alkyl to a co-ordinated carbon monoxide (**3**). Up to this point, all the reactions are written as potential equilibria. The last step consists of dihydrogen reacting with the acyl complex to form the aldehyde product and to regenerate the starting hydrido cobalt carbonyl complex (**4**). This last step is often the rate-determining step.[28] Slaugh and Mullineaux[36] discovered that the addition of phosphines, such as P(*n*-Bu)$_3$, gives a more active catalyst (5-10 atm pressure compared to 100-300 atm for the unmodified catalyst), but it also favours the linear over the branched product to a greater extent (8:1 versus 4:1). It is thought that the steric bulk of the phosphine encourages the formation of the less hindered linear alkyl and speeds up the migratory insertion.

[36] L.H. Slaugh, R.D. Millineaux, *J. Organomet. Chem.*, 1968, 13, 169

There are, however, a few disadvantages[35] associated with the cobalt carbonyl hydroformylation process:

- catalyst losses, as the activated catalyst, $[HCo(CO)_4]$, is labile and highly volatile
- as much as 15% of the alkene is lost due to the competing hydrogenation reaction
- there are inherent difficulties in mechanistic studies.

The higher phosphine-substituted rhodium carbonyl hydride species $[RhH(CO)(PPh_3)_3]$, is an even more active catalyst, which reacts under milder conditions (70-120˚C, 10-30 bar) and is more selective to the linear product.[37] Thus many disadvantages of the cobalt catalyst are circumvented. The reaction mechanism is fairly similar to the cobalt catalysed process. In practice excess PPh_3 is added to the reaction mixture to prevent the formation of the less selective $[HRh(CO)_4]$ and $[HRhL(CO)_3]$ species by phosphine dissociation.[38] The highest selectivity for the linear product is obtained at high concentrations of PPh_3, or even liquid PPh_3, and low pressures of CO. The bulkiness and number of phosphines coordinated to the rhodium, as well as the stereochemistry at the rhodium, determines the regioselectivity.[28]

Tertiary bicyclic phosphine ligands derived from *cis, cis*-1,5,-cyclooctadiene (Phoban family) renders exceptional qualities to the cobalt hydroformylation system. The Phoban family of ligands is superior to ligands such as PBu_3 as indicated by increased reaction rates, higher selectivity towards linear alcohols and higher yields. The different manner in which PBu_3 and Phoban behave chemically is amazing considering that they are electronically similar with cone angles differing from 132º to ~165º for PBu_3 and the Phoban derivatives respectively.[39] Equilibrium constant determinations and catalytic behaviour were found to be very similar for all Phoban derivatives. A study of corresponding Phoban selenides have shown that changes in the Q-substituent on the Phoban backbone have a minor effect on the overall steric and electronic properties of the various Phoban derivatives and can be used to manipulate physical properties without significantly changing the chemical properties.[40]

The influence of phosphite ligands[41,42] in Co-catalysed hydroformylation has also been investigated. Phosphites are expected to yield fewer hydrogenation products because their

[37] J.A. Osborn, J.F. Young, G. Wilkinson, *Chem. Comm.*, 1965, 17
[38] R.H. Crabtree, *The Organometallic Chemistry of the Transition Metals*, New York: John Wiley & Sons, Inc., 1988
[39] P.N. Bungu, S. Otto, *J. Chem. Soc., Dalton Trans.*, 2007, 2876
[40] P.N. Bungu, S. Otto, *J. Organomet. Chem.*, 2007, 692, 3370
[41] M. Haumann, R. Meijboom, J.R. Moss, A. Roodt, *J. Chem. Soc., Dalton Trans.*, 2004, 1679
[42] R. Meijboom, M. Haumann, A. Roodt, L. Damoense, *Helvetica Chimica Acta*, 2005, 88, 676

presence decreases the electron density on the cobalt centre, relative to phosphines. The formation of bis(phosphito)cobalt hydride species occurs at high ligand-to-metal ratios with less bulky ligands, such as triphenylphosphite. These hydride complexes are less-active hydroformylation catalysts than monophosphite complexes and enhance the isomerisation of the alk-1-enes to less-reactive internal alkenes.[41] Sterically demanding phosphite ligands with large cone angles, such as tris(2,4-di-*tert*-butylphenyl)phosphite suppresses the formation of the catalytically inactive bis(phosphito)cobalt hydride.[42] The reaction rate of this modified cobalt catalyst was too low for industrial hydroformylation but the presence of internal alkenes were not observed.

2.4.3 Hydrogenation

Hydrogenation is a specific method of reduction whereby the hydrogen is added to the substrate, generally with gaseous H_2 and using a catalyst at high pressure. The most popular homogenous catalyst for hydrogenation, discovered in the sixties, is Wilkinson's catalyst,[43] $[RhCl(PPh_3)_3]$. The simplified general reaction mechanism is given in Scheme 2.2.

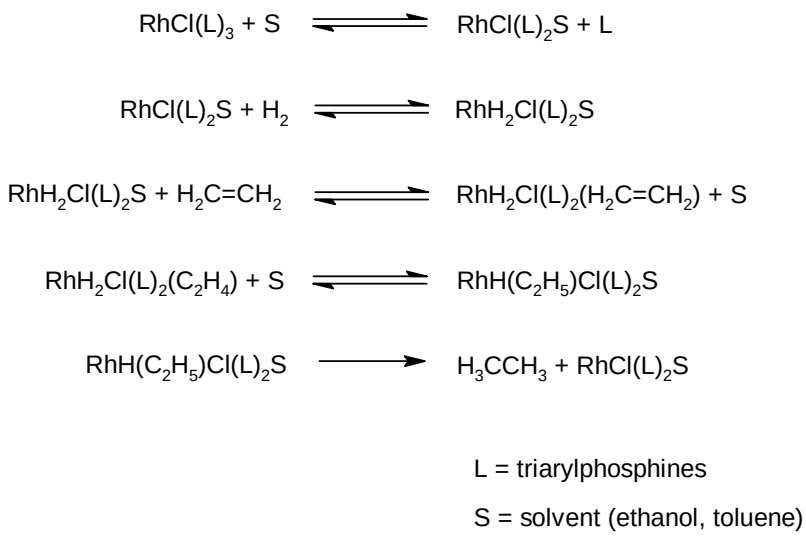

Scheme 2.2: Simplified reaction mechanism for Wilkinson's hydrogenation.

[43] F.H. Jardine, J.A. Osborn, G. Wilkinson, J.F. Young, *Chem. Ind (London)*, 1965, 560; *J. Chem. Soc. (A)*, 1966, 1711

The first step consists of the dissociation of one ligand, L, which is replaced by a solvent molecule, S. Oxidative addition of the dihydrogen then occurs. This usually occurs in *cis* fashion and can be promoted by the substitution of more electron-rich phosphines on the rhodium complex. However, very strong donor ligands can stabilise the trivalent rhodium(III) chloro-dihydride to such an extent that the complexes are no longer active. Next the migration of the hydride occurs to form the ethyl group. Finally reductive elimination of the ethane completes the cycle. By using electron-withdrawing ligands, the rate of this final step can be increased.[28] The ligand effects have been reported[44] but are unfortunately rather limited. Table 2.2 lists a range of reactivities, relative to $P(4\text{-}CH_3OC_6H_4)_3$, which have been reported for the hydrogenation of cyclohexene.

Table 2.2: Ligand effects for the hydrogenation of cyclohexene.

Ligand	Relative reactivity
$P(4\text{-}ClC_6H_4)_3$	1.7
PPh_3	41
$P(4\text{-}CH_3C_6H_4)_3$	86
$P(4\text{-}CH_3OC_6H_4)_3$	100

Hydrogenation with the Wilkinson catalyst are experimentally simple reactions. It is usually done at ambient temperature and in many cases a 'blanket' of hydrogen (1 bar) is sufficient and no hydrogen pressure is necessary. Solvents generally used are methanol, ethanol, acetone, THF or benzene.[45] Chloroform and carbon tetrachloride should be avoided because both solvents may undergo H/Cl exchange.[46]

Terminal olefins are easily hydrogenated. Their hydrogenation is faster than the hydrogenation of double bonds in cyclic systems or internal double bonds. *cis*-Olefins are hydrogenated faster than *trans*-olefins. Generally the higher the degree of substitution at the double bond, the lower the reactivity toward hydrogenation with Wilkinson-type catalysts. Carbonyl compounds are not compatible with Wilkinson-type catalysts. Aldehydes are decarbonylated during hydrogenation reactions[47] and the hydrogenation of ketones is slow compared with olefins. Functional groups, e.g. arene, carboxylic acid, ester, amide, nitrile, ether, chloro, hydroxy and nitro groups, are

[44] C. O'Connor, G. Wilkinson, *Tetrahedron Lett.*, 1969, 18, 1375
[45] B.R. James, *Comprehensive Organometallic Chemistry*, Editors: G. Wilkinson, F.G.A. Stone, E.W. Abel, Oxford: Pergamon, 1982
[46] H.D. Kaesz, R.B. Saillant, *Chem. Rev.*, 1972, 72, 231
[47] K. Ohno, J. Tsuji, *J. Am. Chem. Soc.*, 1968, 90, 99

tolerated during hydrogenation with Wilkinson-type catalysts. These reactivity differences can be utilized for selective reactions in the synthesis of natural products containing a variety of unsaturated functionalities. A further advantage of homogenous Wilkinson catalysts is its stability towards sulphur compounds which tend to poison heterogeneous catalysts.[48]

2.4.4 Carbonylation

Carbonylation is generally the reaction of an organic or intermediate organometallic compound with carbon monoxide,[34] CO. It is a variation of hydroformylation (oxo reaction) which is the reaction of synthesis gas (H_2 + CO) with alkenes under pressure in the presence of a catalyst.

The carbonylation of alkenes is of interest to both the academic and industrialists. Ethene can be converted to propionic acid or its anhydride with the use of $[Mo(CO)_6]$.[49] The carbonylation of methyl isocyanide can be achieved by reductive coupling to niobium.[50] The synthesis of lactones and lactams can be produced by palladium-catalysed carbonylation of halide containing alcohols.[27] These are just a few examples of what has been done with catalytic insertion of carbon monoxide.

However the most important homogeneously catalysed carbonylation reaction is that of methanol to form acetic acid (ethanoic acid):

$$CH_3OH + CO \longrightarrow CH_3CO_2H \qquad \textbf{... 2.5}$$

Acetic acid has been an important industrial product with a world annual production of 7 million metric tons. One of the largest and fastest growing uses of acetic acid is in the production of vinyl acetate, an important industrial monomer. It is prepared from acetic acid by the $Zn(OAc)_2$/carbon catalysed acetoxylation of acetylene, or by Pd/Cu^{II} catalyzed acetoxylation of ethylene.[51] It accounts for 40% of the total global acetic acid consumption. The majority of the remaining worldwide acetic acid production is used to manufacture other acetate esters. Methyl, ethyl, *n*- and *iso*-butylacetates are important industrial solvents and methyl acetate could

[48] H. Brunner, *Applied Homogeneous Catalysis with Organometallic Compounds,* Editors: B. Cornils, W.A. Herrmann, Vol. 1, New York: VCH Publishers, 1996
[49] J.R. Zoeller, E.M. Blakely, R.M. Moncier, T.J. Dickson, *Catal. Today*, 1997, 36, 227
[50] E.M. Carnahan, S.J. Lippard, *J. Am. Chem. Soc.*, 1990, 112, 3230
[51] R.P.A. Sneeden, *Comprehensive Organometallic Chemistry*, Editors: G. Wilkinson, F.G.A. Stone, E.W. Abel, Vol. 8, Oxford: Pergamon Press, 1982

constitute a starting material in the catalytic synthesis of acetic anhydride. Cellulose acetate is used extensively in the preparation of fibres and photographic films. Inorganic acetates (e.g. Na, Pb, Al and Zn) are used in the textile, leather and paint industries. Acetic acid is also used in the manufacture of chloroacetic acid and terephthalic acid,[52] to name just a few examples.

The synthesis of acetic acid has changed over the years with changing technologies (Figure 2.11) and gives an indication of the impact that homogeneous catalysis has had in industrial chemistry. The objective of the development of new acetic acid manufacturing processes has been to reduce raw material consumption, energy requirements and investment costs. The early synthesis of acetic acid was done by 'distillation' of woods or fermentation of agricultural products. The resulting product normally contained large quantities of water and side-products. The first large-scale industrial production was based on the oxidation of acetaldehyde prepared by the mercuric ion catalysed hydration of petroleum-derived acetylene.[51] However the loss and entrapment of mercury in the product lead to further development. It was replaced by the Wacker synthesis of acetaldehyde from petroleum-based ethylene. The existence of left-over light hydrocarbons (C_3, C_4, C_5) from petroleum refining, lead to the development of short-chain hydrocarbon oxidation process for the preparation of acetaldehyde and acetic acid. These oxidations used $[Co(OAc)_2]$ and $[Mn(OAc)_2]$ as catalysts and were often radical processes.[53] Problems occurred due to their lack of selectivity and formation of many side-products.

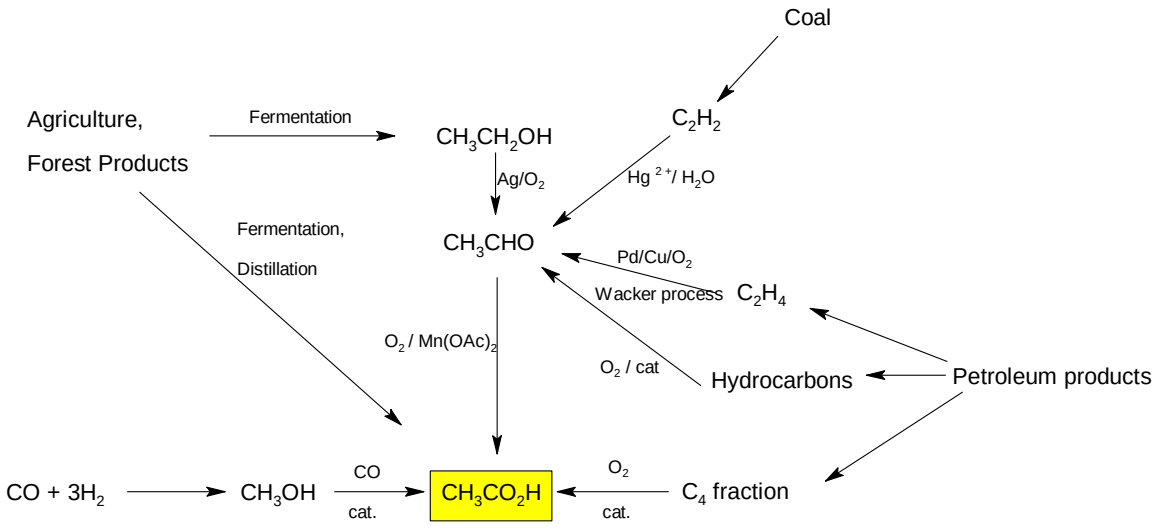

Figure 2.11: Industrial synthesis of acetic acid.[53]

[52] M. Gauβ, A. Seidel, P. Torrence, P. Heymanns, *Applied Homogeneous Catalysis with Organometallic Compounds*, Editors: B. Cornils, W.A. Herrman, Vol.1, New York: VCH Publishers, 1996
[53] G. Wilkinson, F.G.A. Stone, E.W. Abel, *Comprehensive Organometallic Chemistry*, Vol. 8, Oxford: Pergamon Press, 1982

These earlier methods are now economically obsolete and focus has been switched to the Group VIII metals Co, Ni, Ru, Rh, Pd, Ir and Pt to form effective carbonylation catalysts. Significant cost advantages resulted from the use of carbon monoxide (derived from natural gas) and of low-priced methanol (from synthesis gas) as feedstocks. Rh and Ir are the preferred and most active catalyst for carbonylation reactions to produce acetic acid or acetic anhydride. Cobalt is mentioned only for historical interest. An overview of Monsanto's catalyst system in comparison with other processes using rhodium[54] is given in Table 2.3.

Table 2.3: Catalyst systems for carbonylations of methanol and methyl acetate.

Company	Product	Central Atom	Complex	Co-catalyst
Monsanto	AcOH	Rh	$[Rh(CO)_2I_2]^-H^+$	MeI / HI
HCC	AcOH	Rh	$[Rh(CO)_2I_2]^-Li^+$	MeI / LiI
Eastman	Ac_2O	Rh	$[Rh(CO)_2I_2]^-Li^+$	MeI / LiI
Hoechst	Ac_2O	Rh	$[Rh(CO)_2I_2]^-P(R)_4^+$	MeI / P salts
BP	Ac_2O/AcOH	Rh	$[Rh(CO)_2I_2]^-N(R)_4^+$	MeI / N salts, (Zr compound)

The carbonylation of methanol to form acetic acid has been extremely successful and is a focus of this study. Although many transition metal compounds can be used in acetic acid synthesis, only the 3 main important industrial processes will be discussed in detail, namely the Cobalt BASF process, the Rhodium Monsanto process and the Iridium Cativa process.[28] Particular detail will be paid to the Monsanto process as it is the basis which inspired this study.

2.4.4.1 Cobalt BASF Process

BASF commercialized the cobalt based acetic acid synthesis in the 1960's. The starting reagent is CoI_2 which is transformed in the reaction to HI and $Co_2(CO)_8$ and then finally to the activated catalyst $[HCo(CO)_4]$. The assumption that the hydrido cobalt carbonyl is the active species stems from the observation that small amounts of H_2 enhance the catalytic activity.[55] Since methanol would insert CO into the O-H bond (to give methyl formate) and not into the C-O bond (to give acetic acid), the presence of iodide is necessary in order to convert methanol into methyl iodide

[54] B.L. Smith, G.P. Torrence, A. Aguilo, J.S. Alder, Hoechst Celanese Corp., US Patent, US 5.001.259, 1991; H. Papp, M. Baerns, *New Trends in CO Activation*, Editor: L. Guczi, Amsterdam: Elsevier Science, 1991
[55] C.M. Thomas, G. Süss-Fink, *Coord. Chem. Rev.* 2003, 243, 125

prior to carbonylation. Therefore, the actual substrate of carbonylation is methyl iodide.[56] The reaction is first order in MeOH, CO, halide (I^-) and Co. The reaction mechanism in Scheme 2.3 has been suggested.[53]

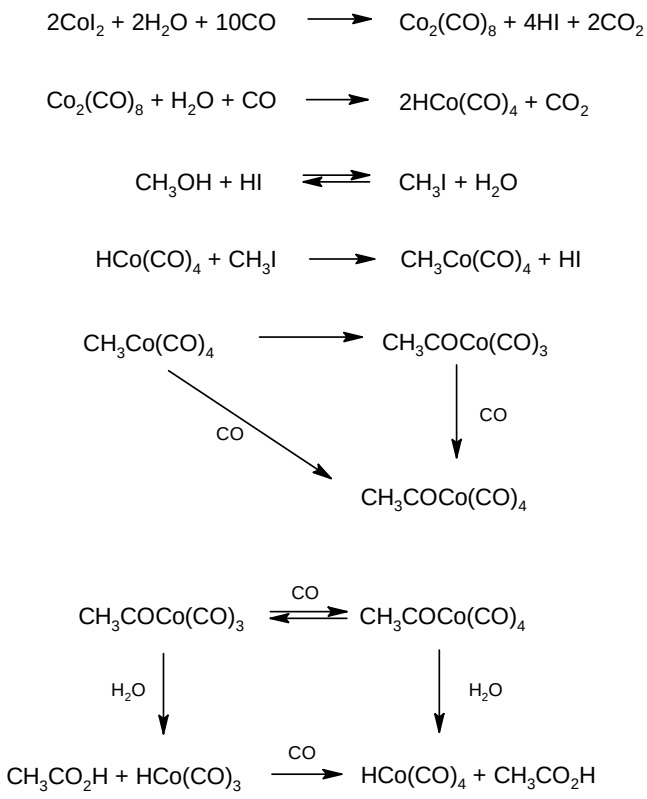

Scheme 2.3: **BASF cobalt catalysed reaction for acetic acid formation.**

In order to have good reaction rates, high reaction temperatures are needed because of the low reactivity of the cobalt catalyst. This in turn needs high CO partial pressures to stabilise the cobalt carbonyl catalyst. The end result is that the catalytic cycle requires very high temperatures and pressures (200-250˚C and 500-700 bar). The quantity of methyl acetate formed is controlled by introducing water into the methanol feedstock. The presence of hot HI/HOAc mixtures makes the cycle very corrosive. The selectivity to acetic acid is of the order 90% based on methanol and 70% based on CO. The side products consist of CO_2 and 4-5% of organic products, namely methane, acetaldehyde, ethanol and ethers. The presence of hydrogen has a large influence on the catalytic cycle as it decreases selectivity to acetic acid formation and increases the amount of organic side products formed.[57] As shall be seen in the Section 2.4.4.2, the presence of hydrogen has little effect on the rhodium catalysed Monsanto process.

[56] D. Forster, M. Singleton, *J. Mol. Catal.*, 1982, 17, 299
[57] C. Masters, *Homogeneous Transition-Metal Catalysis*, New York: Chapman & Hall, 1981

2.4.4.2 Rhodium Monsanto Process

The rhodium- and iodide-catalysed process for the carbonylation of methanol to produce acetic acid was developed in the late sixties by Monsanto. To date, it is one of the most successful industrial applications of homogeneous catalysis and produces several million tons of acetic acid per year.[30] Over 90% of all new acetic acid capacity worldwide is produced by this process. Currently, more than 50% of the annual world acetic acid capacity of 7 million metric tons is derived from the methanol carbonylation process.[52] The low-pressure reaction conditions, the high catalyst activity and exceptional product selectivity are key factors for the success of this process in the acetic acid industry.[58]

The process reacts under significantly milder conditions (30–60 atm pressure and 150-200˚C) than the cobalt-catalysed process. This reduces construction costs and leads to substantial savings. The selectivity is greater than 99% leading to easier purification which further saves on running costs. The disadvantage of the process is the corrosive nature of the reaction medium and the use of rhodium, a rare and very expensive metal.

The process is a classic example of a homogeneous catalytic process, made up of six separate stoichiometric reactions, which link to form a cycle. The first step is the reaction of methanol with HI to give methyl iodide and generates water, Scheme 2.4.

[58] F.E. Paulik, J.F. Roth, *J. Chem. Soc., Chem. Commun.*, 1968, 1578

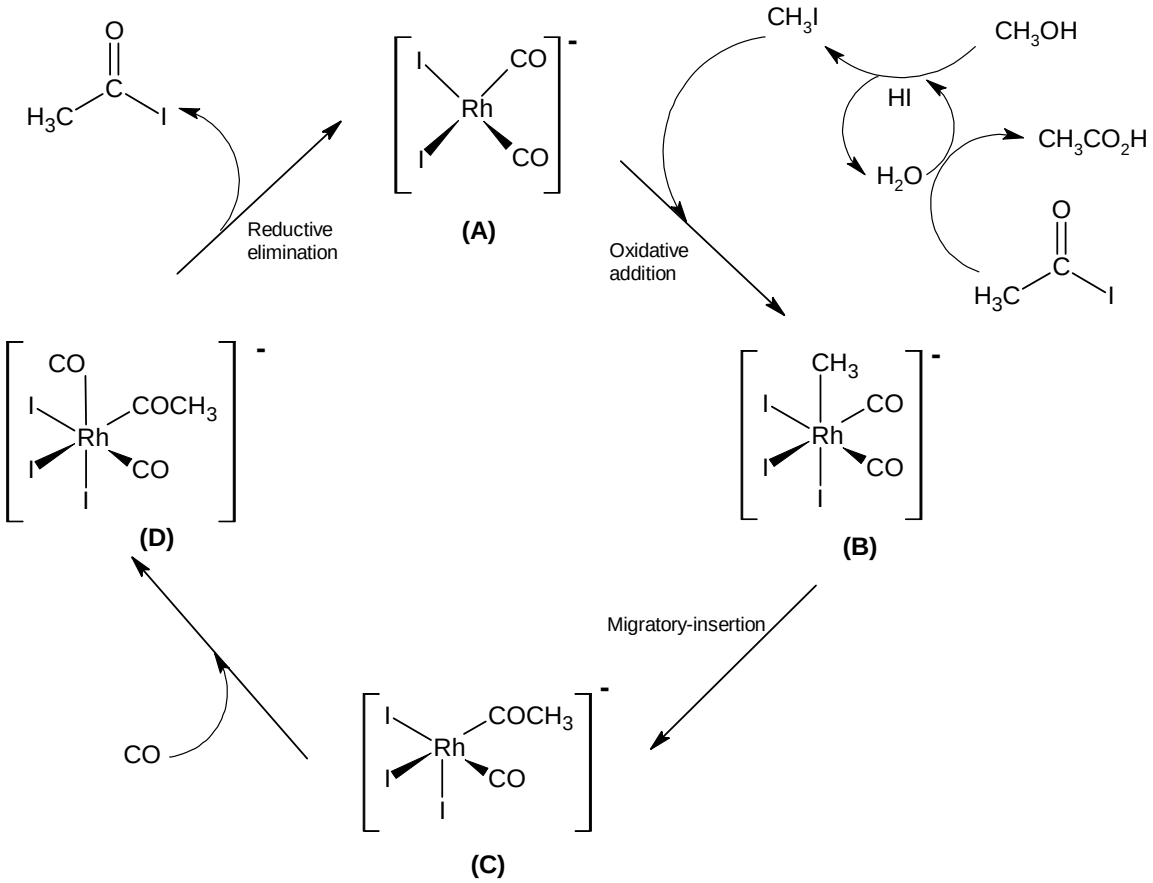

Scheme 2.4: Rhodium Monsanto Process.[28]

In situ and pressure related infrared spectroscopic studies indicate that the major rhodium species present under catalytic conditions is $[Rh(CO)_2I_2]^-$ (**A**). The rate of the overall reaction, determined by kinetic measurements, was first order in [Rh] and [MeI] but zero order in [CO] and [MeOH]. Therefore the oxidative addition of MeI to (**A**) to form the hexacoordinated alkyl rhodium(III) intermediate, $[MeRh(CO)_2I_3]^-$ (**B**) was found to be the rate-determining step of the cycle. The alkyl Rh^{III} intermediate (**B**) is kinetically unstable. Methyl migratory-insertion then occurs rapidly to form the acyl complex, $[(MeCO)Rh(CO)I_3]^-$ (**C**). Insertion of CO converts this complex to a six-coordinated dicarbonyl, $[(MeCO)Rh(CO)_2I_3]^-$ (**D**). Finally, reductive elimination of acetyl iodide regenerates (**A**) and the cycle begins again. Acetyl iodide reacts with water to give acetic acid and HI.

Both the first step (reaction of methanol with HI to give methyl iodide, Eq. 2.6) and the last (the reaction of acetyl iodide with water to give acetic acid and regenerate HI, Eq. 2.7) are simple organic reactions.

$$CH_3OH + HI \longrightarrow H_2O + CH_3I \quad \text{... 2.6}$$

$$CH_3COI + H_2O \longrightarrow CH_3CO_2H + HI \quad \text{... 2.7}$$

All the iodide in the system occurs as methyl iodide and from the above equations, the rate of the catalytic process is independent of the methanol concentration (and CO pressure). A large amount of water (14-15 wt.%) is needed for the above two reactions to achieve high catalyst activity and also to maintain good catalyst stability. If the water content is less than 14-15 wt.%, the rate-determining step becomes the reductive elimination of the acyl species from the catalyst species (**D**).[55] However, high concentrations of water cause a loss of carbon monoxide due to the water-gas shift reaction:

$$CO + H_2O \longrightarrow H_2 + CO_2 \quad \text{... 2.8}$$

Therefore, although the selectivity in methanol is in the high 90s, the selectivity in the carbon monoxide may be as low as 90%. *In situ* generation of water and methyl acetate can occur from the reaction of methanol with acetic acid. Not only water, but also HI can cause side-product formation,

$$[CH_3RhI_3(CO)_2]^- + HI \longrightarrow CH_4 + [RhI_4(CO)_2]^-$$

$$[RhI_2(CO)_2]^- + 2HI \rightleftharpoons H_2 + [RhI_4(CO)_2]^- \quad \text{... 2.9}$$

The above two reactions involve the oxidation of Rh(I) to Rh(III). Rh(III) iodide complexes may precipitate from the reaction medium which results in a loss of activated catalyst. They have to be converted back to Rh(I) by water and carbon monoxide.

Other companies[59] (e.g. Hoechst) have developed a different process whereby the water content is low in order to save CO feedstock. In the absence of water, the catalyst precipitates. At low water concentrations the reduction of Rh(III) to Rh(I) is much slower, but the formation of the Rh(III) species is reduced in the first place, because the HI content decreases with the water concentration. Therefore, they have suppressed the water-gas shift by keeping the water content

[59] P.W.N.M. van Leeuwen, C. Claver, *Comprehensive Coordination Chemistry II*, Editors: J.A. McCleverty, T.J. Meyer, Vol. 9, Oxford: Pergamon Press, 2004

low by adding part of the methanol in the form of methyl acetate. Stabilisation of the rhodium species and lowering of the HI content can be achieved by the addition of iodide salts (Li, ammonium, phosphonium, etc). Low catalyst usage and high reaction rates can be achieved at low reactor water concentrations by the introduction of tertiary phosphine oxide additives.[60]

A detailed kinetic, spectroscopic and analysis study into the rhodium catalysed carbonylation of ROH (R = Me, Et and Pr) has been reported.[61, 62] The reaction rates are first order in both [Rh] and added [HI] and independent of CO pressure in all three cases. $[Rh(CO)_2I_2]^-$ was the only rhodium species observed under catalytic conditions. The rates of carbonylation decreased in the stated order of R, with relative rates of 21:1:0.47, respectively at 170˚C. All the data are consistent with the rate-determining nucleophilic attack by the Rh complex anion on the corresponding alkyl iodide.

(a) Oxidative Addition of MeI to $[Rh(CO)_2I_2]^-$

Although extensive research had indicated that the rate-determining step was the oxidative addition of MeI to (**A**) (Scheme 2.4), the alkyl rhodium intermediate (**B**) had never been detected. Intermediate (**B**) was first detected by Haynes *et al.* at low concentrations, in neat MeI solvent using FTIR and FTNMR spectroscopy.[63, 64] The efficiency of the Monsanto process is largely due to the rapid conversion of (**B**) into (**C**) leading to a low standing concentration of (**B**) and minimising side reactions such as methane formation.

The oxidative addition of MeI to (**A**) (Scheme 2.4) obeys second-order kinetics, first order in (**A**) and [MeI]. The reaction rate is very dependent on solvent, added salts and counter ions. Protic solvents such as methanol accelerated the oxidative addition compared to aprotic solvents (e.g. Methyl acetate or CH_2Cl_2). The rates can be enhanced by the addition of iodide salts (LiI or Bu_4NI), an effect which may be due to the formation of a highly nucleophilic dianion, $[Rh(CO)_2I_3]^{2-}$. However the addition of counter ions containing NH groups (e.g. $C_{12}H_{25}NH_3^+$) inhibits oxidative addition. This is thought to be due to an interaction between the rhodium centre of (**A**) and NH which reduces the nucleophilicity of the rhodium complex.[30]

[60] N. Hallinan, J. Hinnenkamp, *J. Chem. Ind*., 2001, 82, 545.
[61] T.W. Dekleva, D. Foster, *J. Am. Chem. Soc*.,1985, 107, 3565
[62] D. Foster, T.W. Dekleva, *J. Chem. Educ*., 1986, 63, 204
[63] A. Haynes, B.E. Mann, D.J. Gulliver, G.E. Morris, P.M. Maitlis, *J. Am. Chem. Soc*., 1991, 113, 8567
[64] A. Haynes, B.E. Mann, G.E. Morris, P.M. Maitlis, *J. Am. Chem. Soc*., 1993, 115, 4093

As methanol is not sufficiently electrophilic to carry out the oxidative addition step to form the methyl rhodium complex (**A**), the presence of MeI is essential. The reaction is slower with other nucleophiles (e.g. methyl bromide or methyl chloride) as the catalyst component.[28]

(b) Reductive Elimination

The reductive elimination of acetyl iodide has received less attention than the oxidative addition of MeI. The monocarbonyl acyl complex (**C**) (Scheme 2.4), decomposes by the loss of methyl iodide instead of acetyl iodide. But if carbon monoxide is added, then formation of the dicarbonyl (**D**), occurs which reductively eliminates acetyl iodide to reform (**A**). Maitlis *et al.*[30] found that the reaction occurs slowly under ambient conditions ($t_{½}$ = 12 h at 25˚C in CH_2Cl_2). Howe *et al.*[65] found that the reductive elimination (Eq. 2.10) of acetyl iodide is reversible:

$$[(MeCO)Rh(CO)_2I_3]^- \rightleftharpoons [Rh(CO)_2I_2]^- + MeCOI \quad \text{... 2.10}$$

The addition of 1 molar equivalent of tetrabutylammonium acetate (Eq. 2.11) to a solution of (**D**) causes the quantitative formation of (**A**) and acetic anhydride.[30]

$$[(MeCO)Rh(CO)_2I_3]^- + MeCO_2^- \longrightarrow [Rh(CO)_2I_2]^- + (MeCO)_2O + I^- \quad \text{... 2.11}$$

Secondary amines can also react with (**D**) to form (**A**), this time with the formation of the corresponding amide (Eq. 2.12).

$$[(MeCO)Rh(CO)_2I_3]^- + R^1R^2NH \longrightarrow [Rh(CO)_2I_2]^- + R^1R^2NCOMe + HI \quad \text{... 2.12}$$

For dialkylamines (R^1 = R^2 = Et or Bu^n) the reactions were rapid at room temperature, but for less nucleophilic N-methylaniline (R^1 = Ph, R^2 = Me), the reactions were slower. Kinetic studies on the reaction with N-methylaniline suggest parallel first- and second-order pathways for reductive elimination, which Maitlis *et al.*[30] interpret as evidence for direct nucleophilic attack on the rhodium acyl competing with unassisted reductive elimination. It suggests that direct attack by external nucleophiles at the bound acyl ligand can play an important role in the reductive elimination process.

[65] L.A. Howe, E.E. Bunel, *Polyhedron*, 1995, 14, 167

(c) Phosphine Modified Rhodium Catalysts

The reactivity of metal complexes can be altered by selecting ligands with different properties (e.g. electron donating or withdrawing; sterically hindered or unhindered). This can be used to control the rate, stereoselectivity and products that are yielded by the catalytic reaction. Since the oxidative addition of MeI is the slow rate-determining step of the catalytic cycle, increasing the electron density of the Rh centre would increase the reaction rate. Numerous studies have concentrated on increasing the rate of oxidative addition by focusing on the ligands attached to the rhodium metal centre. Electron donating ligands such as phosphines have led to many interesting results. However, although some variants are faster, none have found industrial application yet, mainly due to instability of the complexes formed under the harsh reaction conditions.[55]

A few ligands, which have been studied in order to improve the Monsanto rhodium process, will be discussed and compared to the original $[Rh(CO)_2I_2]^-$ (**A**) complex found in Scheme 2.4. Complexes of the form $[RhX(CO)(PEt_3)_2]$ (X = Cl, Br or I) have ν(CO) at ± 1960 cm^{-1} compared with 1988 and 2059 cm^{-1} for (**A**), suggesting that the rhodium centre is more electron rich in the triethylphosphine complexes. $[RhI(CO)(PEt_3)_2]$[66, 67] **1** (Figure 2.12) catalyses the carbonylation of methanol 1.8 times faster than (**A**) under mild conditions in the presence of CH_3I and 17.1% m/m water at 150˚C. The water acts to maintain the catalyst in its active form, as a rhodium(I) complex and decreases the formation of inactive rhodium(III) complexes such as $[Rh(CO)_2I_4]^-$ or $[RhI_3(CO)(PEt_3)_2]$. Thus the rate of carbonylation was enhanced by a large concentration of water. No appreciable benefit was obtained under lower water concentrations (3.2% m/m water), by using $[RhCl(CO)(PEt_3)_2]$ over $[Rh(CO)_2Cl]_2$ as catalyst precursors.

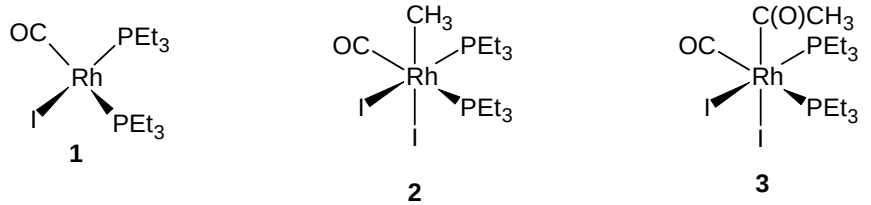

Figure 2.12: Triethylphosphine rhodium complexes.

The reaction of **1** is first order in $[CH_3I]$ and zero order in CO pressure. The phosphine complex degrades to (**A**) during the course of the reaction. Stoichiometric studies indicate that the rate of

[66] J. Rankin, A.D. Poole, A.C. Benyei, D.J. Cole-Hamilton, *Chem. Commun.*, 1997, 19, 1835
[67] J. Rankin, A.C. Benyei, A.D. Poole, D.J. Cole-Hamilton, *J. Chem. Soc., Dalton Trans.*, 1999, 3771

oxidative addition of CH_3I to **1** is 57 times faster than to (**A**) at 25˚C. Complex **2** was isolated and characterised. Complex **3** reductively eliminates CH_3COI in CH_2Cl_2. Complex **1** reacts with CO to give $[RhI(CO)_2(PEt_3)_2]$. Oxidative addition of HI to **1** cause catalyst degradation via $[RhHI_2(CO)(PEt_3)_2]$, which reacts further with HI to give $[RhI_3(CO)(PEt_3)_2]$ from which $[Et_3PI]^+$ reductively eliminates and is hydrolysed to give Et_3PO. The rate-determining step of the catalytic reaction in the presence of water is the oxidative addition of CH_3I to **1**.

Bidentate phosphines are generally more stable because less free phosphine is present due to higher complex binding constants. The use of [Rh(acac)(CO)(*dppp*)] (*dppp* = $Ph_2P(CH_2)_3PPh_2$) catalyst gives high rates (100-200 turnovers h^{-1}) and selectivities approaching 90% in the reductive carbonylation of methanol to acetaldehyde.[68, 69] The reaction occurs at much lower temperature (140˚C) and pressure (70 bar). *In situ* hydrogenation of acetaldehyde produced ethanol with the same high selectivity if ruthenium was used as a co-catalyst. The unsaturated intermediate **4** (Figure 2.13) has been reported, and possesses a distorted five-coordinated geometry that is intermediate between square pyramid and trigonal bipyramidal structures.

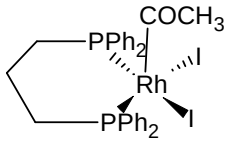

4

Figure 2.13: Symmetrical bidentate phosphine ligands.

Rhodium complexes of unsymmetrical ethylene diphosphines ligands[70] (e.g. $Ph_2PCH_2CH_2PAr_2$, Ar = F substituted Ph groups) are more efficient catalysts than the symmetrical *dppp* analogues for methanol carbonylation. They are also longer-living catalysts under industrial conditions. In all the variants the conversion of methanol was greater than 98% and the selectivity for acetic acid was greater than 99%. All the ligands are coordinated to the metal during catalysis as shown by *in situ* IR studies. A "ligand accelerated" process occurs, because the major species observed contain the diphosphine ligand and they perform better than the ligand free species. However the reason for the better performance of the unsymmetrical ligands compared to symmetrical ligands is still unclear.

[68] K.G. Moloy, R.W. Wegman, *Organometallics*, 1989, 8, 2883
[69] K.G. Moloy, R.W. Wegman, *Adv. Chem. Ser.*, 1992, 230, 323
[70] CA Carraz, E.J. Ditzel, A.G. Orpen, D.D. Ellis, P.G. Pringle, G.J. Sunley, *Chem. Commun.*, 2000, 1277

Square-planar rhodium complexes containing two monophosphine ligands in *trans* positions such as *trans*-[RhCl(CO)(PEt_3)$_2$], are highly active for methanol carbonylation, but less stable than unsymmetrical diphosphine complexes such as *cis*-[RhCl(CO)($Ph_2PCH_2CH_2PAr_2$)] but which are less active catalysts. The possibility of synthesising ligands which are bidentate and can coordinate in a *trans* fashion was investigated by Thomas and Süss-Fink.[55, 71] This led to the development of new diphosphines which were synthesised by condensation from 2-diphenyl-phosphinobenzoic acid with the corresponding aminoalcohols or diols. The catalyst, **5,** (Figure 2.14) formed with the best ligand, was about twice as fast as the original phosphine-free system (**A**) (Scheme 2.4). Thomas and Süss-Fink showed, by comparing the rhodium complexes of **6** with **7**, that changing the distance between the two esters by modifying the length of the chain showed little variation in catalytic activity.

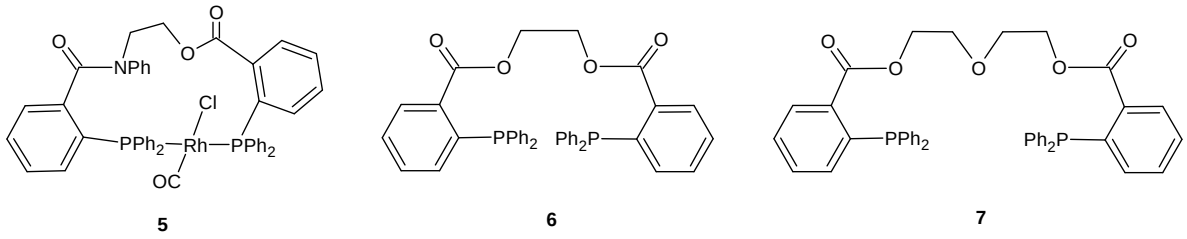

Figure 2.14: ***Trans*-coordinating bidentate phosphine ligands.**

Hemi-labile phosphine ligands carrying an ether function, ester function or thioether as the second, labile donor-group have shown to be very effective ligands for the rhodium-catalysed carbonylation of methanol.[69,72] Wegman *et al*. have found that *cis*-[RhCl(CO)($Ph_2P(CH_2)_2P(O)Ph_2$)] is a precursor to a very active catalyst for the carbonylation of methanol at unusually low temperature and pressure.[72] The reaction of *cis*-[RhCl(CO)($Ph_2P(CH_2)_2P(O)Ph_2$)] **8**, with CO results in the displacement of the rhodium-oxygen bond and the formation of the complex **9** as shown in Figure 2.15 below. The catalytic activity was ascribed to the complex in which the ligand acts as a monodenate.

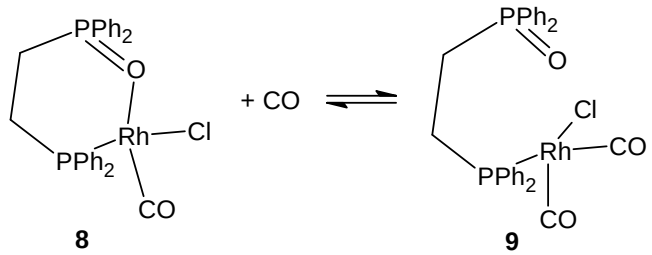

Figure 2.15: **Hemi-labile phosphine ligands.**

[71] C.M. Thomas, R. Mafua, B. Therrien, E. Rusanov, H. Stoeckli-Evans, G. Süss-Fink, *Chem. Eur. J.*, 2002, 8, 3343
[72] R.W. Wegman, A.G. Abatjoglou, A.M. Harrison, *Chem. Soc., Chem. Commun.*, 1987, 1891

Complex **10** is an example of a phosphino-ether ligand (Figure 2.16), which undergoes methyl migration after oxidative addition of CH_3I to afford the acyl complex **11** containing two Rh-O bonds. Heating **11** in the presence of CO results in the reductive elimination of AcI, which upon hydrolysis is converted to AcOH.[73]

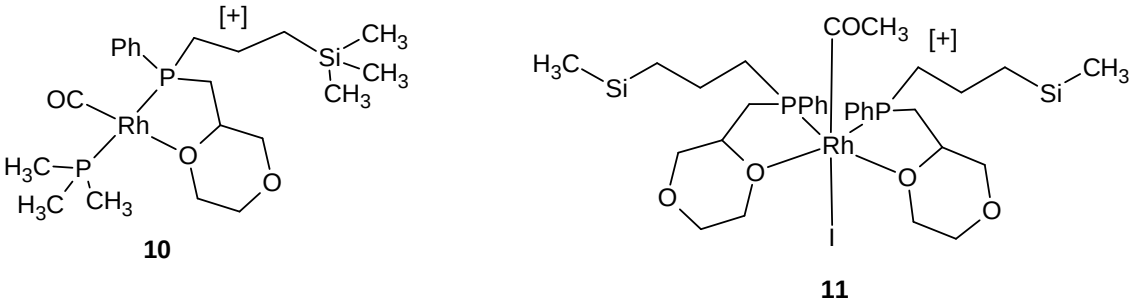

Figure 2.16: Phosphino-ether rhodium complexes.

The reaction of 2-(chloroethyl)phosphonic acid dimethylester with diphenylphosphine yields 2-(diphenylphosphino)ethylphosphonic acid dimethylester **12** (Figure 2.17), which can be used as a hemilabile ligand. Rhodium complexes of the type $[(MeO)_2P(O)CH_2CH_2P(Ph)_2RhL_3]$ exhibit very good catalytic properties in the carbonylation of methanol to acetic acid.[74]

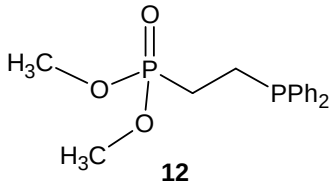

Figure 2.17: 2-(Diphenylphosphino)ethylphosphonic acid dimethylester.

Homogenous catalysts consisting of phosphino-thiolate and –thioether ligands bonded to rhodium(I) carbonyl complexes, such as complex **13**[75] (Figure 2.18), are four times more active in catalysing the carbonylation of methanol to acetic acid compared to the original Monsanto complex (**A**). The *cis*-$[RhI(CO)(Ph_2PCH_2P(S)Ph_2)]$, **14** complex's activity for the carbonylation of methanol is eight times greater than (**A**) at 185˚C. A detailed study of this complex showed that both the oxidative addition and CO insertion steps were accelerated, which was quite unexpected. It was assumed that the steric requirements of the ligand, destabilise the octahedral intermediate which would undergo migratory insertion to release the steric strain.[76]

[73] E. Lindner, E. Glaser, *J. Organomet. Chem.*, 1990, 391, C37
[74] J. Freiberg, A. Weight, H. Dilcher, *J. Prakt. Chem.*, 1993, 335, 337
[75] J.R. Dilworth, J.R. Miller, N. Wheatley, M.J. Baker, J.G. Sunley, *J. Chem. Soc. Commun.*, 1995, 1579
[76] L. Gonsalvi, H. Adams, G.J. Sunley, E. Ditzel, A. Haynes, *J. Am. Chem. Soc.*,1999, 121, 11233

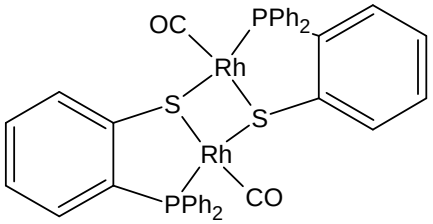

13

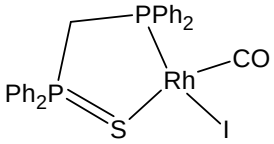

14

Figure 2.18: Phosphino-sulphide ligands.

P-S, P-P, and P-O ligands bonded to rhodium and iridium complexes have been studied with regards to their steric and electronic effects. These donor ligands have shown favourable effects on the rhodium systems,[77] however there is a concern on the stability and long term effects of the phosphine complexes.

2.4.4.3 Iridium Cativa Process

In 1996, BP introduced a new carbonylation process to produce acetic acid using iridium/iodide-based catalyst. This catalytic system has high rates at low water concentrations and exhibits high stability which allows for a wide range of process conditions.

The iridium-catalysed methanol carbonylation has many similarities to the rhodium system, but is more complex because of the participation of both neutral and anionic species[30] as well as the influence of promoters. The Cativa catalytic process is illustrated in Scheme 2.5. The oxidative addition of MeI to the activated iridium complex is faster than for similar rhodium complexes. The equilibrium of this oxidative addition favours the Ir(III) state. Therefore the oxidative addition is not the rate-determining step of the Cativa process. Instead the migratory-insertion of the methyl group to the co-ordinated CO has been found to be the slow rate-determining step. This is a tendency for third row metals. Migratory reactions for platinum complexes, is also slower than for palladium. The metal-to-carbon σ-bonds of third row metals are stronger, more localised and more covalent than those in second-row metal complexes. Hence the more diffuse, electron-rich, σ-bonded hydrocarbyl will migrate more easily.

[77] L. Gonsalvi, H. Adams, G.J. Sunley, E. Ditzel, A. Haynes, *J. Am. Chem. Soc.*, 2002, 124, 13597

A larger amount of iridium is required to achieve an activity comparable to the rhodium catalyst-based processes, however the catalyst system is able to operate at lower water levels (less than 8 wt.%). Hence there is lower side-product formation and improved carbon monoxide efficiency is achieved while the steam consumption is also decreased. The high stability of the iridium catalyst is one of its major advantages. It is robust at low water concentrations (0.5 wt.%), which is significant and ideal for the optimisation of the methanol carbonylation process. The catalyst remains stable under a wide range of experimental conditions that would cause similar rhodium analogues to decompose completely to inactive and largely unrecoverable rhodium salts. Iridium is much more soluble than rhodium in the reaction medium which allows the use of greater catalyst concentrations, making much higher reaction rates obtainable.[55]

There are two groups of promotors which affect the reaction, namely simple iodide complexes of zinc, cadmium, mercury, indium, and gallium, and carbonyl complexes of tungsten, rhenium, ruthenium, and osmium. The promotors are highly successful when combined with iodide salts, such as lithium iodide, under low water conditions.[59] The best rate is found at low water conditions. The selectivity to acetic acid is greater than 99% based on methanol and there are fewer side-products than the Monsanto process. In general the Cativa process is 25% faster than the Monsanto rhodium catalyst.

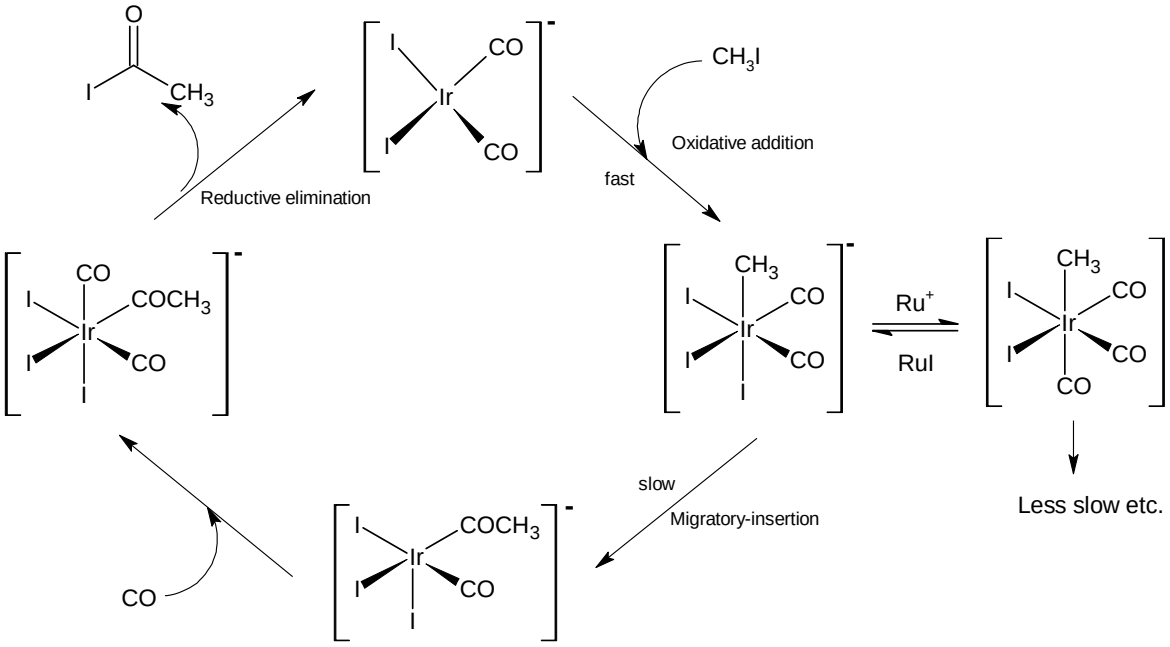

Scheme 2.5: Iridium Cativa Process.[28]

2.5 CONCLUSION

In this chapter, various aspects of rhodium chemistry were discussed in terms of general rhodium(I) and rhodium(III) reactions, factors affecting oxidative addition and various homogeneous catalytic processes. The industrial significance of rhodium was compared with regards to different important catalytic cycles.

It is important to understand the details of a catalytic cycle in order for progress to be made. Advances in homogeneous catalysis can occur by alternating and understanding the effects that various metal centers can have on a specific catalytic system. Furthermore, the choice of an appropriate ligand can significantly alter the final result. Ligand modification is an important part of industrial process design. Manipulation of the electronic and steric properties of a specific ligand will affect factors such as rate, selectivity, stability, lifetime, etc. all of which must be considered and understood.

In order to achieve specific objectives, it is important to characterize the catalyst and understand the reactivity of the complex in light of a catalytic reaction. With this objective in mind, the following chapters deal with the characterization of a chosen rhodium complex and investigation of its catalytic properties.

3 SYNTHESIS AND CHARACTERISATION OF RHODIUM COMPLEXES

3.1 INTRODUCTION

The synthesis and characterisation of a range of Rh(I) and Rh(III) phosphine complexes are discussed in this chapter. Complex characterisation was performed by using various techniques, including nuclear magnetic resonance (NMR) spectroscopy, infrared spectroscopy (IR) and ultraviolet-visible (UV-Vis) spectroscopy. A brief overview of the theory of these characterisation techniques is included.

Rhodium acetylacetonato carbonyl phosphine complexes were synthesised in order to study the effect of steric bulkiness on the reaction mechanism. Four phosphine ligands from triphenylphosphine to tricyclohexylphosphine (Fig. 3.1) with different steric demands, as indicated by their Tolman angles, were used. All complexes were characterised and identified by the above mentioned techniques.

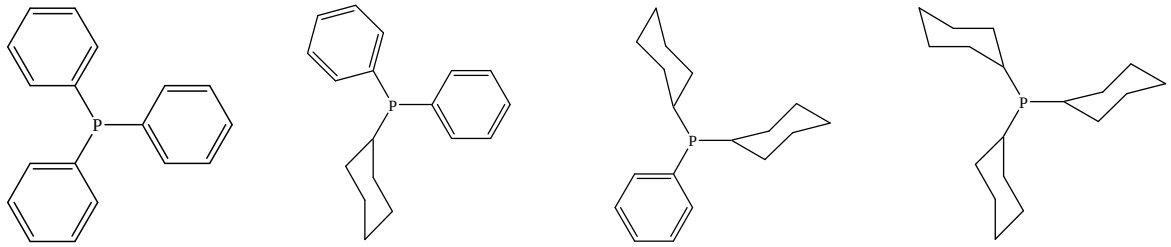

Figure 3.1: Structures of the four phosphorous ligands, triphenylphosphine (PPh_3), cyclohexyldiphenylphosphine ($PCyPh_2$), dicyclohexylphenylphosphine (PCy_2Ph), and tricyclohexylphosphine (PCy_3).

All the synthesised complexes were also characterised by X-ray crystallography. As X-ray crystallography is such a powerful identification tool for the characterisation of complexes in the solid state, the theoretical aspects of this technique as well as a detailed discussion of each crystal structure is included.

3.2 SPECTROSCOPIC TECHNIQUES

3.2.1 Infrared Spectroscopy

Infrared (IR) spectroscopy is a powerful analytical tool which can be used by chemists to qualitatively and quantitatively identify a complex. Almost all organic or inorganic compounds containing covalent bonds, with the exception of a few homonuclear molecules such as H_2, N_2 and Cl_2, absorb infrared radiation. Each molecular species, with the exception of chiral molecules in the crystalline state, has a unique infrared spectrum.

The infrared region on the electromagnetic spectrum consists of a wavelength range that varies from approximately 100 μm to 1000 nm. The near-IR wavelength range is from 0.78-2.5 μm while the mid-IR wavelength range is from 2.5-50 μm.[1] The energy of IR radiation can excite vibrational and rotational transitions but has insufficient energy to induce electronic transitions. Changes in rotational energy can split the peak for each vibrational state. In liquid and solid state, this rotation is often hindered or prevented, so the effects of these small energy differences are not detected. Therefore typical IR spectra originate in transitions between two vibrational levels of the molecule in the electronic ground state, and are usually observed as absorption spectra.

As with other types of energy absorption, molecules are excited to a higher energy state when they absorb quantized infrared radiation. The absorption of IR radiation corresponds to energy changes of the value of 8-40 kJ/mole. Molecules can only absorb the energy of infrared radiation if it corresponds to the molecule's natural, stretching and bending, vibrational frequencies. The absorbed energy serves to increase the amplitude of the vibrational motions of the bonds in the molecule.[2] Only bonds that have a dipole moment that changes as a function of time are capable of absorbing infrared radiation. Symmetrical bonds, such as H_2 or Cl_2, do not absorb infrared radiation. A bond must have an electrical dipole that changes at the same frequency as the entering radiation in order for energy to be transferred. Only then can the changing electrical dipole of the bond couple with the sinusoidally electromagnetic field of the incoming radiation.

---

[1] D.A. Skoog, D.M. West, F.J. Holler, S.R. Crouch, *Fundamentals of Analytical Chemistry*, 8th Ed., California: Thomson Brooks/Cole, 2004

[2] K. Nakamoto, *Infrared Spectra of Inorganic and Coordination Compounds*, 2nd Ed., New York: John Wiley & Sons, Inc., 1970

Since every type of bond has a different natural frequency of vibration, and although two different compounds may have the same type of bond, the bonds will experience two slightly different environments, therefore they cannot give the same infrared absorption pattern. Hence an infrared spectrum of each different molecule is unique and can be used to identify different compounds.

Another important use of IR spectra is to determine structural information about molecules. The absorptions of each type of bond (N-H, C-O, C=O, O-H, C≡N etc.) are regularly found only in certain sections of the vibrational infrared region. For each bond type, a small range of absorption can be defined. Outside of this range, absorptions are generally due to different types of bonds.

The carbonyl group is permanently polarized due to the difference in electronegativity between the carbon and oxygen atom, therefore any vibrational stretching of this bond will affect the dipole moment. For these reasons, the carbonyl group is often used for complex characterisation because the carbonyl stretching produces a distinct absorption peak.[3]

General CO stretching and bending frequencies have a range from 2360 to 1080 cm^{-1}. However characteristic stretching frequencies[2] of metal carbonyl complexes (M-CO) have a range from 2200 to 1700 cm^{-1}. Abel *et al.*[4] have found that the CO stretching frequency of the $M(CO)_3L_3$ type compounds (M = Cr, Mo or W; L = pyridine, PPh_3, $AsPh_3$, etc.) are in the region from 2100 to 1700 cm^{-1}. The carbonyl stretching frequency, *v*(CO), is very sensitive to the groups bonded to the C atom. The effect of the Group 15 donor ligands can be used as an example. As the electron-donating capability of the Group 15 donor ligands decreases (from Sb to P), the electron density on the metal will also decrease. Therefore less electron density is available to the C≡O moiety *via* π-back-bonding into the carbon anti-bonding orbitals[5] (Fig. 3.2). This results in a weaker M-CO bond, a stronger C≡O bond and hence an increase in *v*(CO), for example 1971, 1975 and 1979 cm^{-1} for *trans*-$[Rh(CO)(Cl)(SbPh_3)_2]$, *trans*-$[Rh(CO)(Cl)(AsPh_3)_2]$ and *trans*-$[Rh(CO)(Cl)(PPh_3)_2]$.[6]

[3] B. Stuart, *Modern Infrared Spectroscopy*, Editor: D.J. Ando, England: John Wiley & Sons, Ltd., 1996
[4] E.W. Abel, M.A. Bennet, G. Wilkinson, *J. Chem. Soc.*, 1959, 2323
[5] C. Elschenbroich, A. Salzer, *Organometallics: A Concise Introduction*, New York: VCH Publishers, 1989
[6] A. Roodt, S. Otto, G. Steyl, *Coord. Chem. Rev.*, 2003, 245, 121

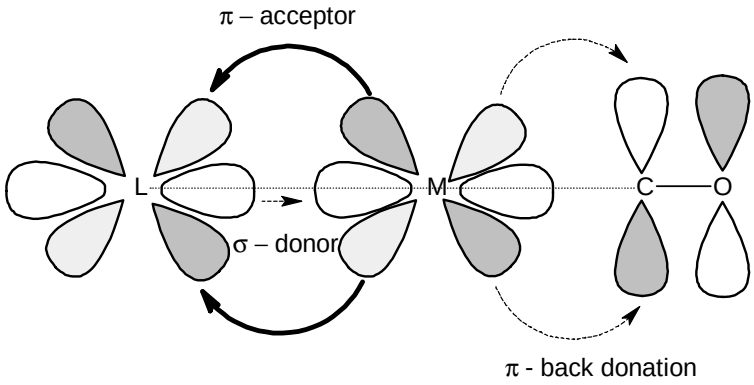

Figure 3.2: Strong π-acceptor ligands are weak σ-donors, which decrease electron density on metal and weakens the M-CO bond.[7]

The use of carbonyl stretching frequency is extensively used in this study since it provides valuable information about the structure and bonding of metal carbonyl complexes. It is not obscured by the presence of other vibrations and its distinct absorption peak makes this technique a very valuable tool to evaluate the relative electron density on metal centres tuned with subtle differences by the tertiary phosphine ligands.

3.2.2 Ultraviolet – Visible Spectroscopy

Ultraviolet (UV) and visible (Vis) light forms part of the electromagnetic spectrum with wavelengths that range from 190 to 800 nm. The technique of UV-Vis spectroscopy is based on the absorption of energy. As a result of energy absorption, atoms or molecules pass from a state of low energy (**ground state**) to a state of higher energy (**the excited state**). The electromagnetic radiation that is absorbed has energy exactly equal to the energy difference between the excited and ground states (Fig. 3.3).[8]

[7] P.W.N.M. van Leeuwen, *Homogeneous Catalysis: Understanding the Art*, Dordrecht: Kluwer Academic Publishers, 2004

[8] D.L. Pavia, G.M. Lampman, G.S. Kriz, *Introduction to Spectroscopy*, 3rd Ed., USA: Thomson Learning, Inc., 2001

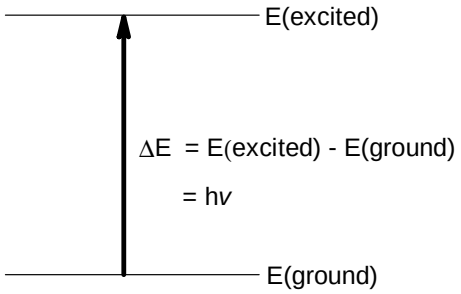

Figure 3.3: The excitation process.

In ultraviolet and visible spectroscopy, the absorption of electromagnetic radiation causes the transitions between electronic energy levels. As a molecule absorbs energy, an electron is promoted from a **highest occupied molecular orbital** (**HOMO**) to the **lowest unoccupied molecular orbital** (**LUMO**).

The absorption of energy by molecules in the UV-Vis region results from interactions between photons and electrons that either participate directly in bond formation or are localised about atoms such as oxygen, sulphur and the halogens. The wavelength that the molecules absorb depends on how tightly its electrons are bound. Electrons involved in double and triple bonds are not strongly held, are easily excited by radiation and therefore generally exhibit useful absorption peaks. Unsaturated organic functional groups that absorb in the ultraviolet and visible regions are known as chromophores. In general the ions and complexes of inorganic elements in the first two transition series absorb broad bands of visible radiation in at least one of their oxidation states. The absorption involves transitions between filled and unfilled *d*-orbitals with energies that depend on the ligands bonded to the metal ions. The energy differences between the *d*-orbitals depend on the position of the element in the periodic table, its oxidation state, and the nature of the ligands bonded to it.[1]

Ultraviolet and visible spectroscopy has many uses but is used primarily for quantitative analysis such as following reaction profiles corresponding to the formation or disappearance of different coloured reaction complexes.[9] UV-Vis spectra, however, do not always provide sufficient fine structure to permit unambiguous identification of a molecule. Therefore other analytical techniques, such as infrared and nuclear magnetic resonance spectroscopy as well as X-ray crystal diffraction, are required to support the information that UV-Vis spectroscopy produces.

[9] C.N.R. Rao, *Ultra-Violet & Visible Spectroscopy: Chemical Applications*, 2nd Ed., England: Butterworth & Co. (Publishers) Ltd., 1967

3.2.3 Nuclear Magnetic Resonance Spectroscopy

Nuclear Magnetic Resonance (NMR) spectroscopy is one of the most powerful tools available to modern science. The use of NMR has spread to encompass a wide range of fields such as chemistry, physics, and even to living biological material for medical diagnosis (magnetic resonance imaging, MRI). Unlike IR spectroscopy which reveals the type of functional groups present in a molecule, NMR gives information about the number of magnetically distinct atoms of the type that is being studied.

NMR makes use of the intrinsic magnetic character of an atom's nucleus. Magnetic nuclei have an intrinsic angular momentum known as *spin*. The *spin quantum number, I,* can have one of the following values:

$$I = 0, 1/2, 1, 3/2, 2,\ldots.$$

where quantum numbers greater than 4 are not that abundant.

In order for a nucleus to be observed by NMR, the spin, *I*, must have a non-zero value. The most common spin quantum number is $I = ½$ with common nuclides such as ^{1}H, ^{13}C, ^{15}N, ^{19}F, ^{29}Si and ^{31}P. Nuclei with spin quantum numbers greater than ½ generally give broad NMR lines.[10]

As a magnetic nucleus is placed in a magnetic field, it can adopt a few allowed orientations of different energy. A hydrogen nucleus only has two permitted orientations: a clockwise spin (+ ½) with the magnetic moment aligned with the magnetic field or a counter clockwise spin (- ½) with the magnetic moment pointing opposite to the magnetic field (Fig. 3.4).

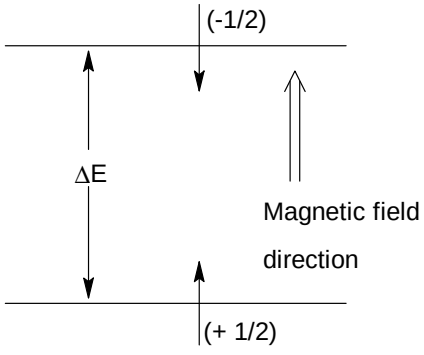

Figure 3.4: Energy levels of a hydrogen nucleus in a magnetic field.[10]

[10] P.J. Hore, *Nuclear Magnetic Resonance*, New York: Oxford University Press, Inc., 1995

The spin state + ½ has the lowest energy because it is aligned with the applied field, the other spin state – ½ has higher energy because it is opposed to the applied field. The two states are separated by an energy difference, ΔE, which depends on the size of the nuclear magnetic moment and the strength of the magnetic field. ΔE may be measured by applying electromagnetic radiation of frequency *v*, which causes the nuclei to flip from the lower energy level to the higher level (the resonance condition $\Delta E = h\nu$ must be satisfied). This interaction is termed NMR spectroscopy.[8]

The NMR spectrum is produced by the fact that the protons in a molecule exist in slightly different chemical and hence electronic environments from one another and therefore absorb different frequencies. The protons are shielded by the surrounding valence-shell electrons which vary from proton to proton, and causes the effective magnetic field that is felt by the proton to be less than the applied magnetic field. These varying resonance frequencies results in different signals known as chemical shifts, *δ*. Factors such as hydrogen bonding, polar functionality groups, stereochemistry and geometry can affect the shielding of the proton and alter the chemical shift.

A proton can be affected by the magnetic field of a nearby proton. This results in magnetic interactions between nuclei called *spin-spin coupling*, whereby the resonance frequency of the first proton is split by the presence of the second proton. The difference between the peaks of the split frequency is indicated by the *coupling constant J*, and is a measure of how strongly a nucleus is affected by the spin states of its neighbour.[8]

The values of chemical shift and spin-spin coupling can provide valuable information on the position, environment and forces which are experienced by atoms in different chemical species.

3.3 THEORECTICAL ASPECTS OF X-RAY CRYSTALLOGRAPHY

3.3.1 Introduction

Mineralogy, the study of naturally occurring chemical compounds, gave birth to the scientific field of crystallography. Crystals with their clean, regular morphology have fascinated people from times of old. The name *crystal* originated from the Greek term *krystallos*, meaning ice. This term was applied to quartz as it was believed the mineral was water that had crystallized at high pressure deep inside the earth.[11]

3.3.2 X-Ray Diffraction

Although X-rays had been discovered in 1895 by C.W. Röntgen, it was only in 1912 that Max von Laue discovered the diffraction of X-rays by crystals. This discovery allows the relative configuration of a previously unknown chemical compound to be determined. The general procedure[12] for determining the crystal structure of a chemical compound is summarized below:

1. Select a suitable crystal and mount it for X-ray study
2. Obtain unit cell geometry and preliminary symmetry information
3. Measure intensity data
4. Data reduction
5. Solve the structure by:
    a. Patterson methods
    b. Direct methods
    c. Other methods
6. Complete the structure – find all the atoms: Fourier and difference Fourier synthesis
7. Refine the structure model
8. Interpret the results

[11] H.R. Wenk, A. Bulakh, *Minerals: Their Constitution and Origin*, UK: Cambridge University Press, 2004
[12] W. Clegg, *Crystal Structure Determination*, New York: Oxford University Press, Inc., 1998

CHAPTER 3

Analytical instruments, such as NMR and IR spectroscopy, give information on the structure of a molecule by the manner which it absorbs or emits radiation. X-ray crystallography measures the variation of intensity with direction, in other words the scattering of monochromatic radiation. The scattered electromagnetic radiation waves can add constructively or deconstructively depending on the direction of the diffracted beam and the atomic positions because each atom is able to scatter X-rays.[13] *Diffraction*, or interference effects cause these intensity variations. This creates a complex scattering pattern which can be analysed. From measurements of the diffraction pattern, it is possible to determine the positions of the atoms in the sample.[12]

A crystal structure can be simplified by representing each molecule by a single point. This results in a regular array of points. The *lattice* of the structure is known as the array of identical points which are equivalent to each other by translation symmetry. A *unit cell* is the characteristic portion of the crystal, from which the whole part of the crystal can be reproduced, if it is repeated indefinitely in the directions of the crystal axes.[14] The lattice is built up from many unit cells. A unit cell consists of three sides (*a, b, c)* and three angles (α, β, γ). By placing certain restrictions on the unit cell, crystal symmetry can loosely be divided into the seven *crystal systems*. It has been shown that there are 230 possible three-dimensional patterns or *space groups* which arise when lattices are combined with the appropriate point and translational symmetry elements. These space groups are described in the *International Tables for Crystallography.*[15] A shorthand notation is used to describe the directions and planes in a crystal lattice, known as the plane index or *Miller index* (*hkl*).

X-rays are scattered by each atom in a crystal to contribute to an overall scattering pattern. A complete pattern can only be recorded by rotating the crystal in the X-ray beam. The diffraction pattern consists of a pattern of spots of varied intensity and has three properties which correspond to three properties of the crystal structure. The three properties are:

- The pattern has a particular geometry which is related to the lattice and unit cell geometry of the crystal structure.
- The pattern has symmetry which is related to the symmetry of the unit cell of the crystal structure.
- The pattern has varied intensities. The intensities reveal information about the position of the atoms in the unit cell.[12]

---

[13] M.F.C. Ladd, R.A. Palmer, *Structure Determination by X-ray Crystallography*, New York: Plenum Press, 1977
[14] D.W.A. Sharpe, *The Penguin Dictionary of Chemistry*, 3rd Ed., London: Penguin Books Ltd., 2003
[15] *International Tables of Crystallography*, *Volume A*, 5th Ed., The Netherlands: Kluwer Academic Publishers, 2002

Max von Laue envisaged crystals in terms of a three-dimensional network of rows of atoms and based his analysis on the idea that a crystal behaved as a three-dimensional diffraction grating. This led to the development of the first of the three Laue equations:[16]

$$a(\cos \alpha_n - \cos \alpha_0) = \mathbf{a}\bullet(\mathbf{s} - \mathbf{s}_0) = n_x\lambda$$

where a is the one-dimensional lattice spacing along the x-axis; α_n and α_0 are the angles between the diffracted and incident beams to the x-axis; n_x is an integer, $\mathbf{s}$ and $\mathbf{s}_0$ are the unit vectors along the directions of the diffracted and incident beams; $\mathbf{a}$ is the translation vector from one lattice point to the next.

The other two Laue equations are for atoms along the y-axis and z-axis:

$$b(\cos \beta_n - \cos \beta_0) = \mathbf{b}\bullet(\mathbf{s} - \mathbf{s}_0) = n_y\lambda$$
$$c(\cos \gamma_n - \cos \gamma_0) = \mathbf{c}\bullet(\mathbf{s} - \mathbf{s}_0) = n_z\lambda$$

Although Laue's equations are accurate, they are complicated to calculate. In order for constructive interference to occur simultaneously from all three atom rows, all three Laue equations must be satisfied simultaneously. An alternative and much simpler equation was derived by W.L. Bragg and is known as Bragg's Law.

3.3.3 Bragg's Law

Bragg assumed that when X-rays are diffracted by crystals, they act as though they are reflected by "atomic mirror planes" within the crystal. However a part of the X-ray beam may not be reflected at the given crystal plane, but can pass on to be subjected to a similar process at a next level deeper into the crystal. All X-rays that are reflected from a given plane remain in phase after reflection. The two X-rays that are reflected from neighboring planes are in general out of phase after reflection, because they have traveled different path lengths. Bragg's law is used to correct this difference in phase.[13]

[16] C. Hammond, *The Basics of Crystallography and Diffraction*, 2nd Ed., New York: Oxford University Press, Inc., 2001

Bragg's law defined for rays reflected by two adjacent planes is:

$$n\lambda = 2d_{hkl} \sin \theta \quad \text{... 3.1}$$

Where n is an integer, λ is the wavelength, d_{hkl} is the distance between the successive parallel crystal planes and θ is the angle of incidence and reflection of the reflected X-ray beam.

In Figure 3.5, the Bragg reflection of two parallel rays reflected at A and C, is illustrated.

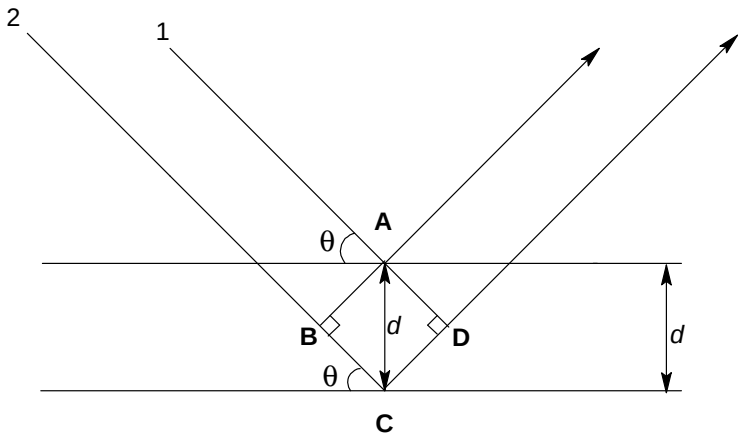

Figure 3.5: X-ray scattering according to Bragg's Law.

Where: $$BC + CD = 2d_{hkl} \sin \theta \quad \text{... 3.2}$$

Bragg's law is the basis of all methods for obtaining unit cell geometry from the measured geometry of the diffraction pattern. The exact application depends on the experimental setup used to obtain the diffraction pattern.

3.3.4 Structure Factor

Two numerical values can be associated with each reflection in a crystal diffraction pattern, namely the *amplitude* |F(*hkl*)| and the *phase* ϕ of the diffracted wave. The amplitude |F(*hkl*)| is represented by the height of the wave and is measured in electrons and the phase ϕ by the horizontal shift relative to some chosen origin.

The structure factor, **F**(*hkl*), expresses the combined scattering of all atoms (*j*) in the unit cell compared to that of a single electron:

The resultant wave for the unit cell is therefore[13]

$$F(hkl) = \sum_{j=1}^{N} g_j \exp(i\phi_j) = \sum_{j=1}^{N} g_j \exp[i2\pi(hx_j + ky_j + lz_j)] \quad \textbf{... 3.3}$$

Where g_j is the temperature-corrected atomic scattering factor ($g_j = f_{j,}T_{j,}$; $f_{j,}$ = atomic scattering factor and $T_{j,}$ = temperature).

Equation 3.3 indicates that the structure factor magnitude depends only on the relative disposition of the N atoms in the unit cell and on the atomic scattering factors. Each term in Equation 3.3 represents a wavelet with an amplitude g_j and a phase $\phi_j = 2\pi(hx_j + ky_j + lz_j)$ which expresses the path length for each scattered wavelet. The structure factor **F**(*hkl*) is then simply the resultant of the wavelets scattered by the *N* atoms in a unit cell.[17]

Equation 3.3 can also be written in the following form:

$$F(hkl) = \sum_{j=1}^{N} g_j [\cos 2\pi(hx_j + ky_j + lz_j) + i \sin 2\pi(hx_j + ky_j + lz_j)] \quad \textbf{... 3.4}$$

The energy associated with a cosine wave is proportional to the square of the amplitude of the wave. In X-ray diffraction it is expressed in terms of the intensity of the scattered wave from the unit, $I_o(hkl)$ where subscript *o* signifies an experimentally observed quantity. Since the amplitude

[17] L.V. Azároff, *Elements of X-ray Crystallography*, New York: McGraw-Hill, Inc., 1968

of the structure factor is |F(*hkl*)|, the symbol I(*hkl*) can be used to represent |F(*hkl*)|^2 which is sometimes called the ideal intensity. Therefore:

$$I_o(hkl) \propto |F_o(hkl)|^2 \quad \textbf{... 3.5}$$

Equation 3.5 forms the basis of X-ray structure analysis, which allows the experimental quantities of $I_o(hkl)$ to be directly related to the structure through |F(*hkl*)|.

The image or X-ray diffraction pattern created when X-rays are scattered by the electrons associated with the atoms in a crystal, can be used to determine the crystal structure. Atoms with high atomic numbers provide a greater concentration of electrons than do atoms of low atomic numbers. This concentration of electrons and its distribution around the atom is called the electron density, ρ. The units of electron density are measured in electrons per cubic angstrom, éA^{-3}. In general, since it is a function of position, it can be specified at a point *X, Y, Z* as ρ(*X, Y, Z).*

The electron density can be expressed in terms of the structure factor **F**(*hkl*):

$$\rho(x, y, z) = \frac{1}{Vc} \sum_h \sum_k \sum_l F(hkl)e^{-i2\pi(hx + ky + lz)} \quad \textbf{... 3.6}$$

Where *V*c is the unit cell volume.[18]

3.3.5 The 'Phase Problem'

The determination of a crystal structure cannot proceed directly from the observed intensity data. Analysis of the crystal structure is severely hampered in a X-ray diffraction experiment by its inability to determine the complete vectorial structure factor. The modulus |F(*hkl*)| can be obtained from the intensity data (Eq 3.5), but the corresponding phase $\phi(hkl)$ is not directly measurable. However to determine the structure, both amplitude and phase must be known. This inability to determine the phase is known as the 'Phase Problem', however it can be overcome

[18] G.H. Stout, L.H. Jensen, *X-ray Structure Determination: A Practical Guide*, London: The Macmillan Company, 1968

by using a number of means. The most common methods are the Patterson function or direct methods.

3.3.5.1 Direct Methods

Direct methods attempt to determine the approximate reflection phases from the measured X-ray intensities using mathematical formulae. Direct methods are particularly useful in determining good phase information for structures consisting only of light atoms. The Patterson function is best used for molecules which contain only one atom or a small number of atoms with significantly more electrons than the rest.[13]

3.3.5.2 The Patterson Function

The Fourier transform of the observed diffracted beam amplitudes $|F_o(hkl)|$ gives the correct electron density but requires the position of the phases to determine the structure factor **F**(*hkl*). However the Fourier transform of the squared amplitudes $|F_o(hkl)|^2$ with all the phases set equal to zero produces the Patterson Function or Patterson Map.

$$P(x, y, z) = \frac{1}{Vc} \sum_h \sum_k \sum_l |F_o(hkl)|^2 \, e^{-i2\pi(hx + ky + lz)} \quad \textbf{... 3.7}$$

The Patterson Function looks like an electron density map with peaks of positive electron density in various positions. These are not the positions of atoms in the structure. The Patterson Function is a map of vectors between pairs of atoms in the structure. For each peak seen in the map, found at point (*u, v, w*), there are two atoms in the structure whose *x* coordinates differ by *u*, *y* coordinates differ by *v* and *z* coordinates differ by *w*. The Patterson peaks show where atoms lie relative to each other but not where they lie relative to the unit cell origin. The Patterson peaks are also proportional in size to the product of the atomic numbers of the two atoms involved.[12]

3.3.6 Least-Squares Refinement

Once it is believed that the correct crystal structure has been found, a calculated diffraction pattern can be made. If the atoms of the model structure are in the approximate correct positions, then there should be a degree of resemblance between the calculated diffraction pattern and the observed one. The least squares refinement compares the calculated structure factor $|F_c|$ to the experimental data, the observed structure factor $|F_o|$. This comparison is described in terms of the *residual index* of *R-factor*,[18] defined as

$$R = \frac{\sum || F_0 | - | F_c ||}{\sum | F_0 |} \quad \text{... 3.8}$$

The value of the *R-factor* for a correct and complete crystal structure determined from well measured experimental data is around 0.02-0.07.

A variation on Equation 3.8 uses F^2 values instead of |F| values, squaring the differences, and/or incorporating different weighting factors multiplying different reflections, based on their standard uncertainties, and therefore incorporating information on the relative reliability of different measurements. A residual factor which is widely used for crystal structure determination is:

$$wR2 = \sqrt{\frac{\sum w(F_0^2 - F_c^2)^2}{\sum w(F_0^2)^2}} \quad \text{... 3.9}$$

where each reflection has its own weight *w*. Equation 3.9 is more meaningful from a statistical viewpoint than the basic *R* factor.[12]

3.4 SYNTHESIS AND SPECTROSCOPIC CHARACTERISATION

3.4.1 Chemicals and Instrumentation

All reagents used for synthesis and characterisation were of analytical grade. If nothing else is stated, all commercially available reagents were used as received from Sigma-Aldrich. All organic solvents were dried and distilled before use. Rhodium trichloride hydrate ($RhCl_3.xH_2O$) was purchased from Next Chimica, South Africa, and used without further purification.

All infrared spectra were recorded from neat samples on a Digilab FTS 2000 Fourier transform spectrometer (ATR) utilizing a He-Ne laser at 632.6 nm, in the range of 3000 – 600 cm^{-1}. Solution infrared spectra were collected, in the same range, in dry organic solvents, in a NaCl cell. The IR spectrometer was equipped with a temperature cell regulator (accurate within 0.3˚C). The UV-Vis spectra were collected on a Varian Carey 50 Conc. spectrometer, equipped with a Julabo F12-mV temperature cell regulator (accurate within 0.1 ˚C) in a 1.00 cm quartz cuvette cell. The ^{1}H and ^{31}P NMR spectra were obtained in $CDCl_3$ and CH_2Cl_2 solutions on a 300 MHz Bruker spectrometer. ^{1}H chemical shifts are reported relative to TMS using the $CHCl_3$ peak (7.24 ppm) and the ^{31}P shifts are reported relative to 85% H_3PO_4 (0 ppm) external standard; positive shifts are downfield. All chemical shifts are reported in ppm and coupling constants in Hz.

3.4.2 Synthesis of Compounds

3.4.2.1 Synthesis of $[Rh(\mu\text{-}Cl)(CO)_2]_2$

Tetracarbonyldichloridodirhodium, $[Rh(\mu\text{-}Cl)(CO)_2]_2$, was synthesised according to the method developed by McCleverty and Wilkinson.[19]

[19] J.A. McCleverty, G. Wilkinson, *Inorg. Synth.*, 1990, 28, 84

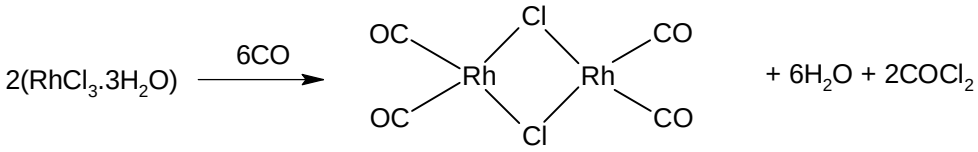

Scheme 3.1: Reaction scheme for rhodium dimer formation.

Rhodium(III) trichloride hydrate (1.048 g, 3.980×10^{-3} mol) was pulverised and placed on top of a porous disk sealed at the one end of a 20 x 2 cm tube. The apparatus was flushed with carbon monoxide and lowered into an oil bath maintained at 98˚C. Temperatures above 100˚C were avoided to prevent the formation of anhydrous rhodium(III) chloride, which is inert to carbon monoxide. Carbon monoxide was flushed through the apparatus for 8.5 hours, while long orange-red needle-like crystals of tetracarbonyldichloridodirhodium (Scheme 3.1) sublimed at the top of the tube. Condensed reaction water, at the top of the tube, was periodically removed with a cotton swab. The crystals were purified by recrystallization from dry hexane.

Yield: 0.514 g, 66.4 %

IR ν(CO): 1991 and 1967 cm^{-1}

3.4.2.2 Synthesis of $[Rh(acac)(CO)_2]$

Tetracarbonyldichloridodirhodium, $[Rh(\mu\text{-}Cl)(CO)_2]_2$, (0.109 g, 2.801×10^{-4} mol) was dissolved in minimal DMF. While stirring this solution at room temperature, another solution of acetylacetone, (acac) (0.067 g, 6.662×10^{-4} mol, 2.4 eq) in minimal DMF was slowly added. The mixture turned light pink and was stirred for 15 minutes before a large excess of ice-water was slowly added. A pink precipitate with a green tinge formed. The precipitate was filtered, washed with ice-water, dried and stored in a vacuum desiccator with phosphorous pentoxide.[20]

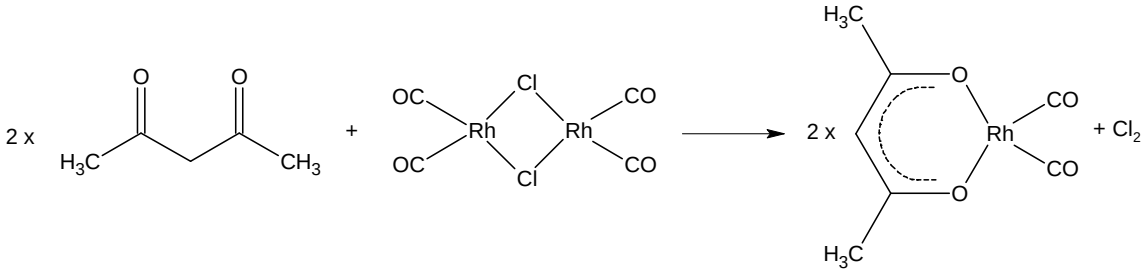

Scheme 3.2: Reaction scheme of $[Rh(acac)(CO)_2]$ formation

Yield: 0.145 g, 80.0 %

IR ν(CO): 1995 and 2062 cm^{-1}

[20] F. Bonati, G. Wilkinson, *J. Chem. Soc.*, 1964, 3156

3.4.2.3 Synthesis of [Rh(acac)(CO)($PR_1R_2R_3$)]

The different *mono*-phosphine rhodium(I) complexes were all prepared in the same manner. [Rh(acac)$(CO)_2$] was dissolved in octane (20 ml). The appropriate phosphine (1.1 eq) was slowly added and the reaction mixture gently heated and stirred for 20 min. The reaction mixture was allowed to cool and stand for 2 hrs. The yellow precipitate was filtered and dried. Crystals appropriate for X-ray diffraction analysis were obtained by recrystallization from acetone.[20, 21]

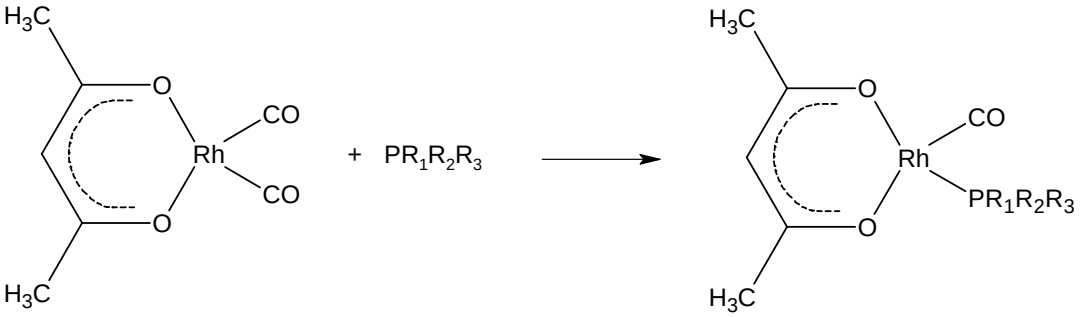

Scheme 3.3: A general reaction scheme for the preparation of different [Rh(acac)(CO)($PR_1R_2R_3$)] complexes. R_1 ; R_2 ; R_3 = phenyl and/or cyclohexyl rings.

(A) [Rh(acac)(CO)(PPh_3)]

A triphenylphosphine solution (56 mg, $2.129x10^{-4}$ mol) was added to the specified [Rh(acac)$(CO)_2$] solution (50 mg, $1.884x10^{-4}$ mol) to yield the product [Rh(acac)(CO)(PPh_3)].

Yield: 71.5 mg, 76.9%

IR ν(CO): 1977.6 cm^{-1}; ν(CO) (CH_2Cl_2): 1977.0 cm^{-1}

^{31}P NMR (CH_2Cl_2): δ (ppm) 48.6 (d, $^1J_{Rh\text{-}P}$ = 176.95 Hz)

(B) [Rh(acac)(CO)($PCyPh_2$)]

A cyclohexyldiphenylphosphine solution (95.5 mg, $3.560x10^{-4}$ mol) was added to the specified [Rh(acac)$(CO)_2$] solution (80 mg, $3.096x10^{-4}$ mol) to yield the product [Rh(acac)(CO)($PCyPh_2$)].

Yield: 102 mg, 66.0%

IR ν(CO): 1959.3 cm^{-1}; ν(CO) (CH_2Cl_2): 1971.2 cm^{-1}

^{31}P NMR (CH_2Cl_2): δ (ppm) 53.3 (d, $^1J_{Rh\text{-}P}$ = 171.25 Hz)

[21] J.G. Leipoldt, S.S. Basson, L.D.C. Bok, T.I.A. Gerber, *Inorg. Chim. Acta*, 1978, 26, L35

(C) [Rh(acac)(CO)(PCy_2Ph)]

A dicyclohexylphenylphosphine solution (72.7 mg, $2.650x10^{-4}$ mol) was added to the specified [Rh(acac)$(CO)_2$] solution (62.4 mg, $2.409x10^{-4}$ mol) to yield the product [Rh(acac)(CO)(PCy_2Ph)].

Yield: 96.9 mg, 79.6%

IR ν(CO): 1948.8 cm^{-1}; ν(CO) (CH_2Cl_2): 1967.4 cm^{-1}

^{31}P NMR (CH_2Cl_2): δ (ppm) 58.8 (d, $^1J_{Rh\text{-}P}$ = 168.3 Hz)

(D) [Rh(acac)(CO)(PCy_3)]

A tricyclohexylphosphine solution (61.7 mg, $2.20x10^{-4}$ mol) was added to the specified [Rh(acac)$(CO)_2$] solution (51.8 mg, $2.00x10^{-4}$ mol) to yield the product [Rh(acac)(CO)(PCy_3)].

Yield: 90.5 mg, 88.5%

IR ν(CO): 1945.3 cm^{-1}; ν(CO) (CH_2Cl_2): 1959.7 cm^{-1}

^{31}P NMR (CH_2Cl_2): δ (ppm) 59.3 (d, $^1J_{Rh\text{-}P}$ = 164.3 Hz)

3.4.3 Summary of Spectroscopic Data

The [Rh(acac)(CO)($PR_1R_2R_3$)] complexes were successfully synthesized and characterized with IR and ^{31}P NMR spectroscopy. Full characterization with X-ray crystallography was successfully completed and is discussed in detail in Section 3.5. High yields were obtained with the synthesis of the [Rh(acac)(CO)($PR_1R_2R_3$)] complexes, using octane as a solvent. The use of acetone as a solvent, with regards to [Rh(acac)(CO)($PCyPh_2$)] and [Rh(acac)(CO)(PCy_2Ph)], resulted in decomposition to an oil except when synthesized under Schlenk conditions. Crystals, suitable for X-ray diffraction analysis, were obtained from recrystallization from acetone. However this resulted in very low yields with oil formation. For future analysis it is recommended that crystals be harvested from the octane solution without recrystallization.

Table 3.1 summarizes the spectroscopic data for [Rh(acac)(CO)($PR_1R_2R_3$)] complexes. One of the interests of this study is to determine the steric effect on the rhodium complexes when a phenyl ring is systematically substituted by a more bulky and electron-rich cyclohexyl ring in a phosphine ligand. The steric and electronic properties of the [Rh(acac)(CO)($PR_1R_2R_3$)] complexes should gradually vary with the systematic change of ligands from PPh_3 to PCy_3. All

data of the previously published PPh_3 and PCy_3 complexes have been redetermined for the purpose of this study.[21, 22, 23]

It is clear from Table 3.1 and Figure 3.6, that as a phenyl ring is substituted by a cyclohexyl ring [complexes **(1) → (4)**], the carbonyl stretching frequency, *v*(CO), decreases in value in both the solid and solution state. This observation is best explained in terms of electron density. As the electron density on the metal centre increases, the electron back-donation from the metal to the anti-bonding orbital on the C atom increases. This strengthens the Rh-C bond and thus weakens the C≡O bond which results in a decrease in the CO-stretching frequency.[6] Thus from Table 3.1 it can be seen that the electron-donating ability of [Rh(acac)(CO)($PR_1R_2R_3$)] complexes increase from **(1) → (4)**.

Table 3.1: Summary of spectroscopic data for [Rh(acac)(CO)($PR_1R_2R_3$)] complexes.

		[Rh(acac)(CO)($PR_1R_2R_3$)]			
	$PR_1R_2R_3$	**(1)** - PPh_3	**(2)** - $PCyPh_2$	**(3)** - PCy_2Ph	**(4)** - PCy_3
IR	*v*(CO) (cm^{-1})*	1977.6	1959.3	1948.8	1945.3
	v(CO) (CH_2Cl_2) (cm^{-1})	1977.0	1971.2	1967.4	1959.7
^{31}P NMR	δ (ppm)	48.6	53.3	58.8	59.3
	$^1J_{Rh\text{-}P}$ (Hz)	177.0	171.3	168.3	164.3

*Neat samples, ATR.

[22] A.M. Trzeciak, J.J. Ziółkowski, *Inorg. Chim. Acta*, 1985, 96, 15
[23] A.M. Trzeciak, B. Borak, Z. Ciunik, J.J. Ziółkowski, M.F.C. Guedes da Silva, A.J.L. Pombeiro, *Eur. J. Inorg. Chem.*, 2004, 1411.

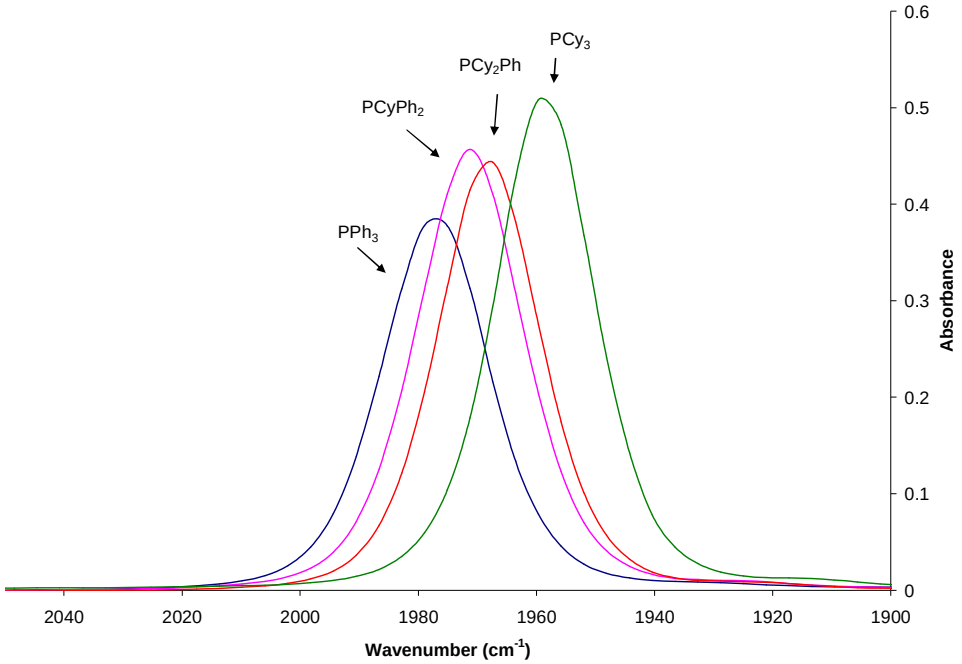

Figure 3.6: **Systematic variation in the IR carbonyl stretching frequency of [Rh(acac)(CO)($PR_1R_2R_3$)] complexes ($3x10^{-3}$ M) in CH_2Cl_2.**

^{31}Phosphorous NMR spectroscopy can provide a rich source of information about phosphorous ligands coordinated in compounds. The chemical shifts, δ, and especially the $^{1}J_{Rh\text{-}P}$ coupling constants are very sensitive to the electron density variations on rhodium atoms. From Table 3.1 the value of the coupling constant, δ, increases from complex **(1)** → **(4)**, whereas the $^{1}J_{Rh\text{-}P}$ decreases in value. The value of $^{1}J_{Rh\text{-}P}$, according to the Fermi contact term, is very sensitive to changes in the overlap between the 5s(Rh)-3s(P) orbitals.[24] The decreasing $^{1}J_{Rh\text{-}P}$ value suggests that the overlap between the orbitals decrease and the Rh-P bond distance will increase with the gradual substitution of the spatial demanding cyclohexyl ring.

With regards to this study, with particular reference to Table 3.1, the substitution of phenyl rings by cyclohexyl groups increases both the electron-density on the metal centre and the spatial demand of the ligand for the systematic progression from [Rh(acac)(CO)(**PPh_3**)] to [Rh(acac)(CO)(**PCy_3**)].

Similarly, infrared spectroscopy is very useful in determining the electron-donor ability of the phosphorous ligands. Phosphite ligands, such as $P(OPh)_3$ are known as better π-acceptors and

[24] A. Roodt, G.J.J. Steyn, *Recent. Res. Devel. Inorganic Chem.*, 2000, 2, 1

poorer σ-donators compared to PPh_3.[22, 25] The *ν*(CO) value of [Rh(β-diketone)(CO)($P(OPh)_3$)] is located around 2000 cm^{-1}, while analogous phosphine complexes[22] are found at about 1970 cm^{-1}. The use of even stronger π-acceptors ligands,[26, 27] such as $P(NC_4H_4)_3$, increases the *ν*(CO) frequency even further to 2012 cm^{-1}. The weaker σ-donor and better π-acceptor properties of $P(OPh)_3$ may be further illustrated by the formation of [Rh(β-diketone)($P(OPh)_3)_2$] complexes. Both CO groups of [Rh(β-diketone)$(CO)_2$] complexes may be substituted by $P(OPh)_3$ due to the weakened Rh-C bond in the [Rh(β-diketone)(CO)($P(OPh)_3$)] complexes[22, 27] and since $P(OPh)_3$ has much less steric demand than PPh_3, it allows the Rh(I) metal centre to more easily accommodate two $P(OPh)_3$ ligands in this fashion. Similarly, the stronger π-acceptor $P(NC_4H_4)_3$ readily forms the disubstituted [Rh(acac)$(PR_1R_2R_3)_2$] complex, whereas the stronger σ-donor $PPh_2(NC_4H_4)$ ligand (*ν*(CO) = 1990 cm^{-1}) only forms the monosubstituted [Rh(acac)(CO)$(PR_1R_2R_3)$] complex.[27] In general, the *ν*(CO) frequencies in [Rh(acac)(CO)$(PR_1R_2R_3)$], [Rh{$CF_3C(O)CHC(NH)Me$}(CO)(PR_3)] and in bis(pyrazolylborato) complexes[23] decrease with an increase in σ/π-donor properties of the P-ligands in the order $P(NC_4H_4)_3 > PPh_3 > P(C_6H_4OMe\text{-}4)_3 > PCy_3$.

[25] C.A. Tolman, *Chem. Rev.*, 1977, 77, 313
[26] A.M. Trzeciak, T. Głowiak, R. Grzybek, J.J. Ziółkowski, *J. Chem. Soc., Dalton Trans.*, 1997, 1831
[27] W. Simanko, K. Mereiter, R. Schmid, K. Kirchner, A.M. Trzeciak, J.J. Ziółkowski, *J. Organomet. Chem.*, 2000, 602, 59

3.5 CRYSTAL STRUCTURE DETERMINATION OF SELECTED COMPLEXES

The complexes investigated in this study, [Rh(acac)(CO)(PPh_3)], [Rh(acac)(CO)($PCyPh_2$)], [Rh(acac)(CO)(PCy_2Ph)] and [Rh(acac)(CO)(PCy_3)], were characterized by means of X-ray crystallography and are described below.

3.5.1 Experimental

The reflection data was collected on a Bruker X8 ApexII 4K diffractometer[28] using graphite monochromated Mo *K*α radiation with ω-and-φ-scans at 100 K. COSMO[29] was utilized for optimum collection of more than a hemisphere of reciprocal space. After a completed collection, the first 50 frames were repeated to check for any decomposition, all the crystals remained stable throughout the collection. The frames were integrated using a narrow-frame integration algorithm and reduced with the Bruker SAINT-Plus[30] and XPREP[30] software packages, respectively. Data was corrected for absorption effects using the multi-scan technique SADABS.[31] The structures were solved by direct methods package SIR97[32] and refined using the software package WinGX,[33] incorporating SHELXL.[34] The program DIAMOND[35] was used for all graphical representation of the crystal structures. All structures are shown with thermal ellipsoid drawn at 50% probability level.

All non-hydrogen atoms were refined anisotropically, while the methyl, methane and aromatic H atoms were placed in geometrically idealized positions and constrained to ride on their parent atoms, with (C-H = 0.95-0.98 Å and U_{iso}(H) = 1.5U_{eq}(C) and 1.2U_{eq}(C)), respectively. The methyl protons were located in a difference Fourier map and the group was refined as a rigid motor.

---

[28] Bruker, APEX2 (Version 1.0-27), Bruker AXS Inc., Madison, Wisconsin, USA, 2005
[29] Bruker, COSMO, Version 1.48, Bruker AXS Inc., Madison, Wisconsin, USA, 2003.
[30] Bruker, SAINT-Plus (Version 7.12) (including XPREP), Bruker AXS Inc., Madison, Wisconsin, USA, 2004
[31] Bruker, SADABS, Version 2004/1, Bruker AXS Inc., Madison, Wisconsin, USA,1998.
[32] A. Altomare, M.C. Burla, M. Camalli, G.L. Cascarano, C. Giacovazzo, A. Guagliardi, A.G.G. Moliterni, G. Polidori, R. Spagna, *J. Appl. Cryst.* 1999, 32, 115.
[33] L.J. Farrugia, *J. Appl. Cryst.*, 1999, 32, 837
[34] G.M. Sheldrick, SHELXL97, *Program for Solving Crystal Structures*, University of Göttingen, Germany, 1997
[35] K. Brandenburg, H. Putz, DIAMOND, Release 3.0c, Crystal Impact GbR, Bonn, Germany, 2005

A summary of the general crystal data and refinement parameters is given in Table 3.2 for all four Rh(I) complexes. Supplementary data for the atomic coordinates, bond distances and angles and anisotropic displacement parameters are given in the Appendix Table A, B, C and D, for [Rh(acac)(CO)(PPh_3)], [Rh(acac)(CO)($PCyPh_2$)], [Rh(acac)(CO)(PCy_2Ph)] and [Rh(acac)(CO)(PCy_3)] respectively.

Table 3.2: General X-ray crystallographic data and refinement parameters for [Rh(acac)(CO)($PR_1R_2R_3$)].

Compound	**PPh_3**	**$PCyPh_2$**	**PCy_2Ph**	**PCy_3**
Empirical Formula	$C_{24}H_{22}O_3PRh$	$C_{24}H_{28}O_3PRh$	$C_{24}H_{34}O_3PRh$	$C_{24}H_{40}O_3PRh$
Formula weight	492.30	498.34	504.39	510.44
Temperature (K)	100(2)	100(2)	100(2)	100(2)
Wavelength (Å)	0.71069	0.71073	0.71069	0.71073
Crystal System	Triclinic	Orthorhombic	Monoclinic	Monoclinic
Space Group	$P\bar{1}$	$P2_12_12_1$	$P2_1/n$	$P2_1/n$
Unit Cell Dimensions				
a (Å)	8.856(5)	9.4682(5)	10.076(5)	10.3418(5)
b (Å)	10.314(5)	12.7534(6)	12.990(5)	13.0644(6)
c (Å)	12.844(5)	18.4602(9)	17.937(5)	17.9301(8)
α (°)	71.298(5)	90	90	90
β (°)	70.143(5)	90	90.576(5)	90.612(2)
γ (°)	82.775(5)	90	90	90
Volume (Å^3)	1045.0(9)	2229.10(19)	2347.6(16)	2422.39(19)
Z	2	4	4	4
Density$_{calc.}$ (g.cm^{-1})	1.565	1.485	1.427	1.400
μ (mm^{-1})	0.916	0.860	0.817	0.792
F(000)	500	1024	1048	1072
Crystal Colour	Yellow	Yellow	Yellow	Yellow
Crystal Morphology	Plate	Plate	Cuboid	Cuboid
Crystal Size (mm)	0.20x0.11x0.04	0.42x0.27x0.06	0.18x0.09x0.05	0.22x0.18x0.17
Theta Range (°)	2.45 - 27.00	2.21 - 27.00	2.31 - 26.75	2.26 - 27.00
Completeness	99.7 %	100.0 %	98.0 %	100.0 %
Index Ranges	h = -11 to 11 k = -13 to 13 l = -16 to 16	h = -11 to 12 k = -16 to 16 l = -23 to 12	h = -12 to 9 k = -16 to 16 l = -22 to 22	h = -13 to 10 k = -16 to 16 l = -22 to 22
Reflections Collected	23869	12624	25476	27734
Independent Reflections	4564	4825	4885	5288
R_{int}	0.0400	0.0233	0.0370	0.0304
Refinement method	Full-matrix least-squares on F^2	Full-matrix least-squares on F^2	Semi-empirical from equivalents	Full-matrix least-squares on F^2
Data / restraints / parameters	4564 / 0 / 264	4825 / 3 / 264	4885 / 0 / 264	5288 / 0 / 264
Goodness-of-fit on F^2	1.041	1.061	1.049	1.043
Final R indices [I>2sigma(I)]	R1 = 0.0243, wR2 = 0.0541	R1 = 0.0226, wR2 = 0.0567	R1 = 0.0273, wR2 = 0.0656	R1 = 0.0202, wR2 = 0.0503
R indices (all data)	R1 = 0.0287, wR2 = 0.0562	R1 = 0.0239, wR2 = 0.0573	R1 = 0.0355, wR2 = 0.0698	R1 = 0.0236, wR2 = 0.0523
ρ_{max} and ρ_{min} (e.Å^{-3})	0.546 and -0.429	0.543 and -0.332	0.469 and -0.315	0.454 and -0.297

3.5.2 Crystal structure of [Rh(acac)(CO)(PPh_3)]

The crystal structure of [Rh(acac)(CO)(PPh_3)], **(1)**, was first investigated by Leipoldt *et al.*[21] in 1978 who prepared the [$Rh_2Cl_2(CO)_4$] reagent in a solution of dimethylformamide according to the procedure of Varshavskii and Cherkasova[36] and the [Rh(acac)(CO)(PPh_3)] product according to Bonati and Wilkinson.[20] For the purpose of this study, the complex was resynthesised and analysed at low temperature in order to increase the accuracy relative to the previous data collection and to accurately determine the position of the hydrogen atoms. The redetermination of the crystal structure was successful and no significant deviations were found (Table 3.15).

[Rh(acac)(CO)(PPh_3)], **(1)**, was prepared according to the procedure described in Section 3.4.2.3 (A). Yellow crystals suitable for X-ray diffraction were obtained. The complex crystallized in the triclinic space group, $P\bar{1}$, with two molecules in the unit cell. The molecular structure of **(1)** is represented in Figure 3.7 along with the atom numbering system. Positional and thermal parameters for the atoms are given in Table A of the Appendix.

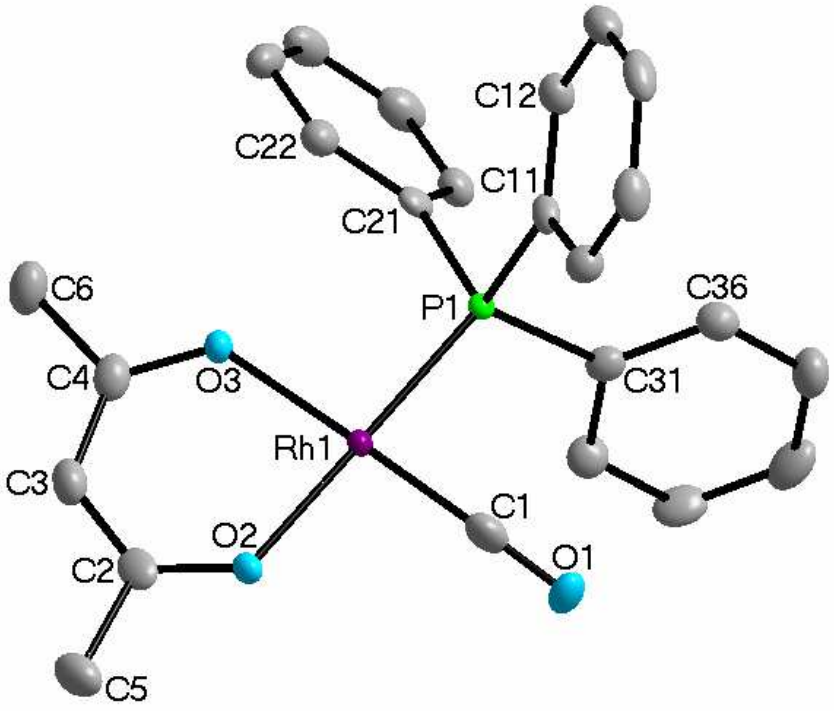

Figure 3.7: **Molecular structure of [Rh(acac)(CO)(PPh_3)] showing the atom numbering system. For the phenyl rings, the first digit refers to the ring number, while the second digit refers to the C-atom in the ring. H atoms have been omitted for clarity.**

[36] Yu. S. Varshavskii, T.G. Cherkasova, *Russ. J. Inorg. Chem.*, 1967, 12, 1709

The molecular structure of **(1)** consists of a Rh(I) metal centre bonded to two O atoms of the acetylacetonato ligand, one carbonyl carbon and a phosphorous atom. The complex has a slightly distorted square-planar geometry. The PPh_3 is *trans* to one oxygen atom of the acetylacetonato bidentate ligand, and *cis* to the carbonyl ligand.

Selected interatomic bond distances and angles are presented in Table 3.3.

Table 3.3: Selected bond lengths and angles for [Rh(acac)(CO)(PPh_3)].

Bond	Distance (Å)	Bond Angle	Angle (°)
Rh(1)-C(1)	1.807(2)	C(1)-Rh(1)-O(2)	93.01(8)
Rh(1)-O(3)	2.0332(15)	O(3)-Rh(1)-O(2)	88.02(7)
Rh(1)-O(2)	2.0748(16)	O(1)-C(1)-Rh(1)	175.9(2)
Rh(1)-P(1)	2.2418(9)	C(2)-C(3)-C(4)	125.1(2)
P(1)-C(21)	1.823(2)	C(1)-Rh(1)-P(1)	87.17(7)
P(1)-C(31)	1.823(2)	O(3)-Rh(1)-P(1)	91.88(5)
P(1)-C(11)	1.827(2)	O(2)-Rh(1)-P(1)	179.01(5)
O(3)-C(4)	1.275(3)	C(21)-P(1)-C(31)	104.21(9)
O(2)-C(2)	1.273(3)	C(21)-P(1)-C(11)	103.39(9)
O(1)-C(1)	1.153(3)	C(31)-P(1)-C(11)	104.23(9)
C(3)-C(2)	1.394(3)	C(31)-P(1)-Rh(1)	114.12(7)
C(3)-C(4)	1.396(3)	C(21)-P(1)-Rh(1)	114.81(7)
C(5)-C(2)	1.513(3)	C(11)-P(1)-Rh(1)	114.74(7)
C(6)-C(4)	1.507(3)	C(4)-O(3)-Rh(1)	127.75(13)
C(11)-C(16)	1.396(3)	C(2)-O(2)-Rh(1)	126.46(13)
C(11)-C(12)	1.397(3)	C(16)-C(11)-C(12)	118.92(19)
C(36)-C(31)	1.391(3)	C(26)-C(21)-C(22)	119.21(19)
C(26)-C(21)	1.390(3)	O(2)-C(2)-C(3)	126.1(2)
C(22)-C(21)	1.398(3)	O(2)-C(2)-C(5)	114.82(19)
C(32)-C(31)	1.400(3)	O(3)-C(4)-C(3)	125.83(19)
		O(3)-C(4)-C(6)	114.48(19)

A plane was constructed through C1, P1, O3, O2 and Rh1 as indicated in Figure 3.8 (a). Important distances from the plane are listed in Table 3.4. The acac bidentate ring, PPh_3 and CO ligands are bent away from the plane in a upside-down boat position. The carbonyl ligand is bent below the plane (Fig. 3.8 (a)) with a C1 atom distance of -0.129(3) Å from the plane and a O3-Rh-C1 angle of 174.45(8)º. The oxygen atom of the carbonyl ligand indicates even greater deviation with a Rh-C1-O1 angle of 175.9(2)º and a O1 – plane distance of -0.293(2) Å. The

phosphine ligand has an almost horizontal geometry with a O2-Rh-P1 angle of 179.01(5)º and a P1 – plane distance of 0.0051(7) Å.

The central atom in the acac ring has a C3 – plane distance of -0.254(3) Å, while the proton (H3) bonded to this carbon atom indicates the greatest deviation with a distance of -0.3950(3) Å from the plane (Figure 3.8 (b)) The oxygen atoms of the acac ring indicate that the bidentate ligand is not only bent down but also twisted. The O2 atom is found above the plane (O2 – plane distance = 0.034(2) Å) while the O3 atom is below the plane (O3 – plane distance = -0.046(2) Å).

Table 3.4: Selected distances between specific atoms and the horizontal plane through atoms C1, P1, O3, O2 and Rh1

Atom	Distance (Å)	Atom	Distance (Å)
C1	-0.129(3)	C6	-0.283(3)
O1	-0.293(2)	C4	-0.195(2)
P1	0.0051(7)	C2	-0.119(2)
Rh1	0.0016(4)	C5	-0.123(3)
C3	-0.254(3)	O2	0.034(2)
H3	-0.3950(3)	O3	-0.046(2)

The C1 phenyl ring (Figure 3.8 (c)), bonded to the phosphorous atom, lies above the horizontal plane with an angle of 114.74(7)º through Rh-P1-C11. The C3 phenyl ring lies completely below the plane with an angle of 114.12(7)º, only the H36 proton lies above the horizontal plane. The C2 phenyl ring is tilted so that it lies partly above and below the plane with an angle of 114.81(7)º through Rh-P1-C21 atoms. The C22, H22 and H21 atoms all lie above the plane (Figure 3.8 (c)). Planes were constructed through the carbon atoms of the phenyl rings. The plane through the C2 phenyl ring partially bisects the C3 ring (Figure 3.8 (d)), the dihedral angle between Plane C2 (purple) and Plane C3 (blue) is 80.99(8)º.

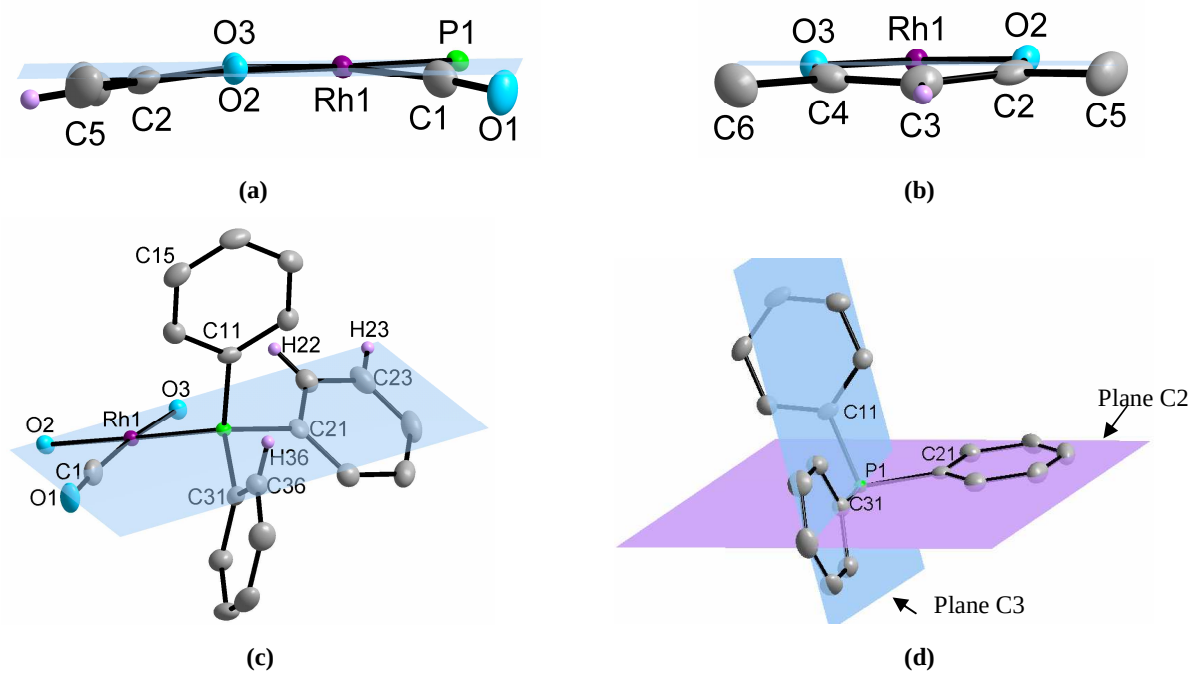

Figure 3.8: **Partial structure of [Rh(acac)(CO)(PPh_3)]. (a) – Side view of ligands bonded to Rh(I) metal center. (b) – Front view of acac bidentate ligand. (c) – Position of the phosphine ligand with regards to the horizontal plane. (d) – Figure of C2 plane (purple) partially bisecting the C3 phenyl ring.**

All the phenyl rings of the PPh_3 ligand are planar, within experimental error. The average C-C bond distances of 1.388 Å and bond angles of 120.0º are within the expected range for phenyl rings.[37]

The larger *trans* influence of the PPh_3 ligand with respect to the carbonyl ligand, is indicated by the longer Rh-O2 (2.0748(16) Å) bond compared to Rh-O3 (2.0332(15) Å) bond which is *trans* to the carbonyl ligand. The Rh-O bond distances compare favorably with the bond distances reported by Leipoldt *et al.*[21] of 2.087 Å and 2.029 Å respectively. The Rh-P1 and Rh-C1 bond distances are 2.2418(9) Å and 1.807(2) Å respectively.

An enolate type delocalization behaviour is found in the acac bidentate ring. The O2-C2 and O3-C4 bond distances are of similar order (1.273(3) and 1.275(3) Å) but are longer than the average C=O bond distance of 1.23 Å and shorter than a single C-O bond distance of 1.43 Å. The three carbon atoms in the acac backbone also have longer bonds (C2-C3, C3-C4 = 1.394(3), 1.395(3) Å) than expected for an average carbon-carbon double bond (1.32 Å)[38] but shorter than a single C-C bond of 1.53 Å. The triple bond character of the carbonyl functionality has a longer distance

[37] G.J. Lamprecht, J.G. Leipoldt, C.P. van Biljon, *Inorg. Chim. Acta*, 1984, 88, 55
[38] J. March, *Advanced Organic Chemisty: Reactions, Mechanisms and Structures*, 4th Ed., New York: John Wiley & Sons, Inc., 1992

(C1-O1 = 1.153(3) Å) than the expected value of 1.13 Å which indicates π back-donation from an electron-rich Rh metal centre which will shorten the Rh-C1 bond distance.

The O2-Rh-O3 and C1-Rh-P1 bite angles of 88.02(7) and 87.18(7)º are similar indicating that PPh_3 has little steric effect. The torsion angle of C2-O2-O3-C4 has a value of -0.31(16)º with the C2 atom slightly more elevated above the horizontal plane (Figure 3.8).

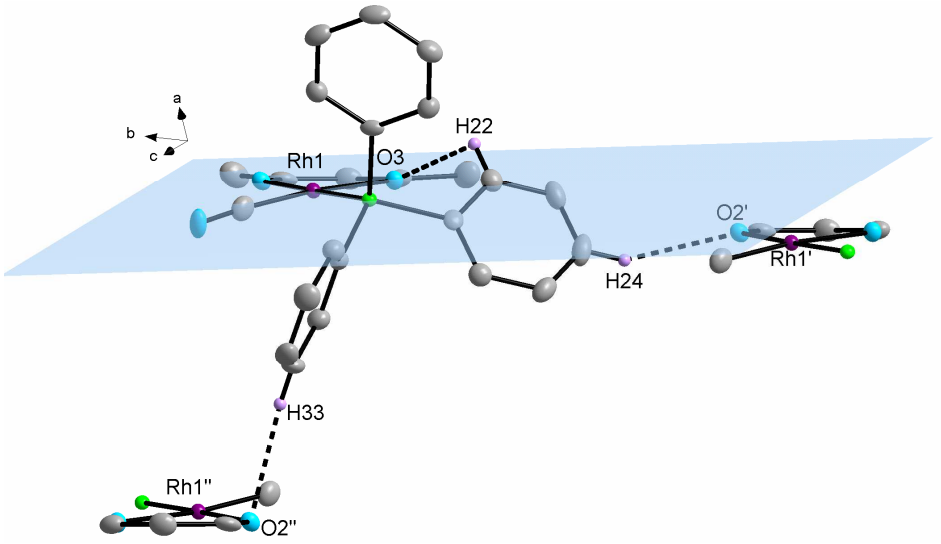

Figure 3.9: **Inter- and intramolecular H-bond interactions for [Rh(acac)(CO)(PPh_3)] complexes as viewed along the a-axis. Only applicable H atoms with relevance to H-bond interactions are indicated.**

Inter- and intramolecular hydrogen bonding is indicated in Figure 3.9. Intramolecular bonding occurs between O3 and H22 with a donor-acceptor (**D-A**) bond distance of 2.849 Å. Intermolecular bonding exists between H33 and O2" of the Rh1" molecule (-x, -y+1, -z+2; **D-A** = 3.373 Å) and between H24 and O2' of the Rh1' molecule (x, y-1, z; **D-A** = 3.386 Å). A complete list of H-bond interactions is given in Table 3.5.

Table 3.5: **Hydrogen bonds for [Rh(acac)(CO)(PPh_3)] [Å and °].**

D-H...A	d(D-H)	d(H...A)	d(D...A)	<(DHA)
C(24)-H(24)...O(2)#2	0.95	2.51	3.386(3)	153.5
C(33)-H(33)...O(2)#3	0.95	2.53	3.373(3)	147.7
C(22)-H(22)...O(3)#1	0.95	2.45	2.849(3)	105.1

Symmetry transformations used to generate equivalent atoms:
#1 x,y,z #2 x,y-1,z #3 -x,-y+1,-z+2

The hydrogen bond interaction may cause some of the geometrical strain of the [Rh(acac)(CO)(PPh_3)] complex as illustrated in Figures 3.8. The partial upward twisting of the C2 phenyl ring may be due to the intramolecular bond interaction between H22 and O3 of the same complex, and the intermolecular interaction of H24 and O2' of the Rh1' molecule (Figure 3.9). The C3 phenyl ring is twisted almost vertically with regards to the horizontal Rh-acac plane (Figure 3.8 (d)) which may be due to the intermolecular interaction of H33 with O2 of the Rh1" molecule (Figure 3.9). The C1 phenyl ring which lies above the Rh-acac plane is situated in a position of least steric hindrance and fits in the vacant site between the C1 phenyl rings of the adjacent molecules. There does not appear to be any significant intermolecular repulsion between these phenyl rings. All these factors result in a horizontal "sheet-like packing" of the [Rh(acac)(CO)(PPh_3)] complexes along the b-axis (Figure 3.10) and a "head to head" staggered packing along the a-axis (Figure 3.11). There does not appear to be any significant intermolecular repulsion between the C3 phenyl groups (Figure 3.10).

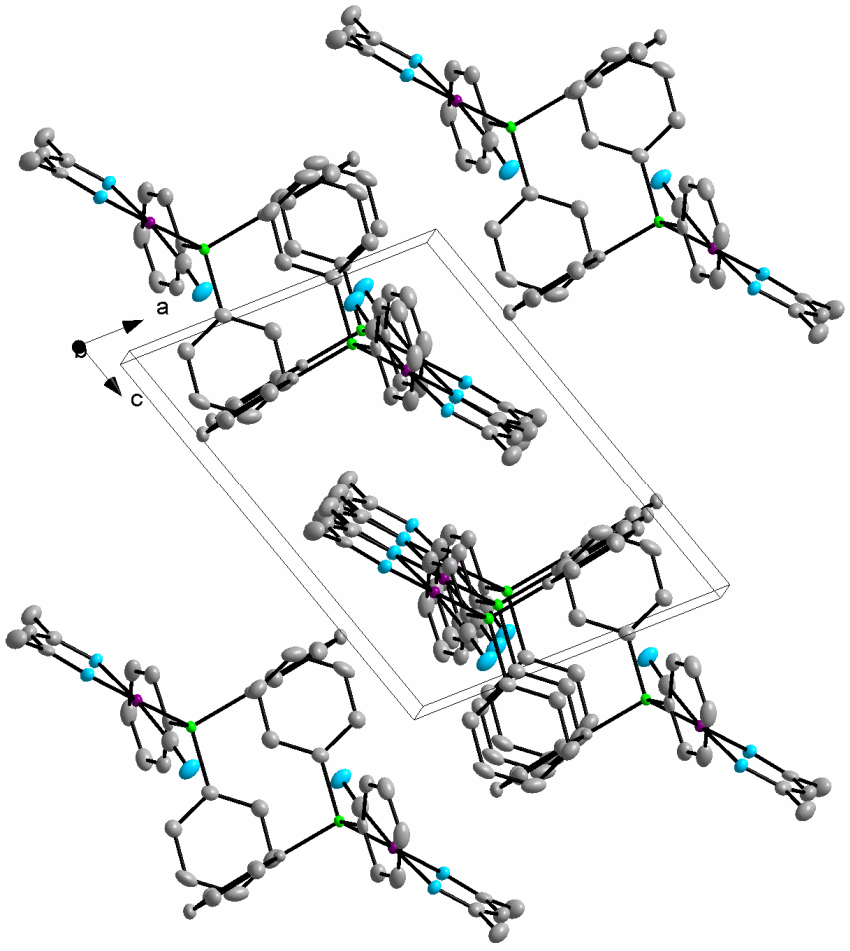

Figure 3.10: **Complexes of [Rh(acac)(CO)(PPh_3)] showing the "sheet like packing" crystal packing along the b-axis. H atoms have been omitted for clarity.**

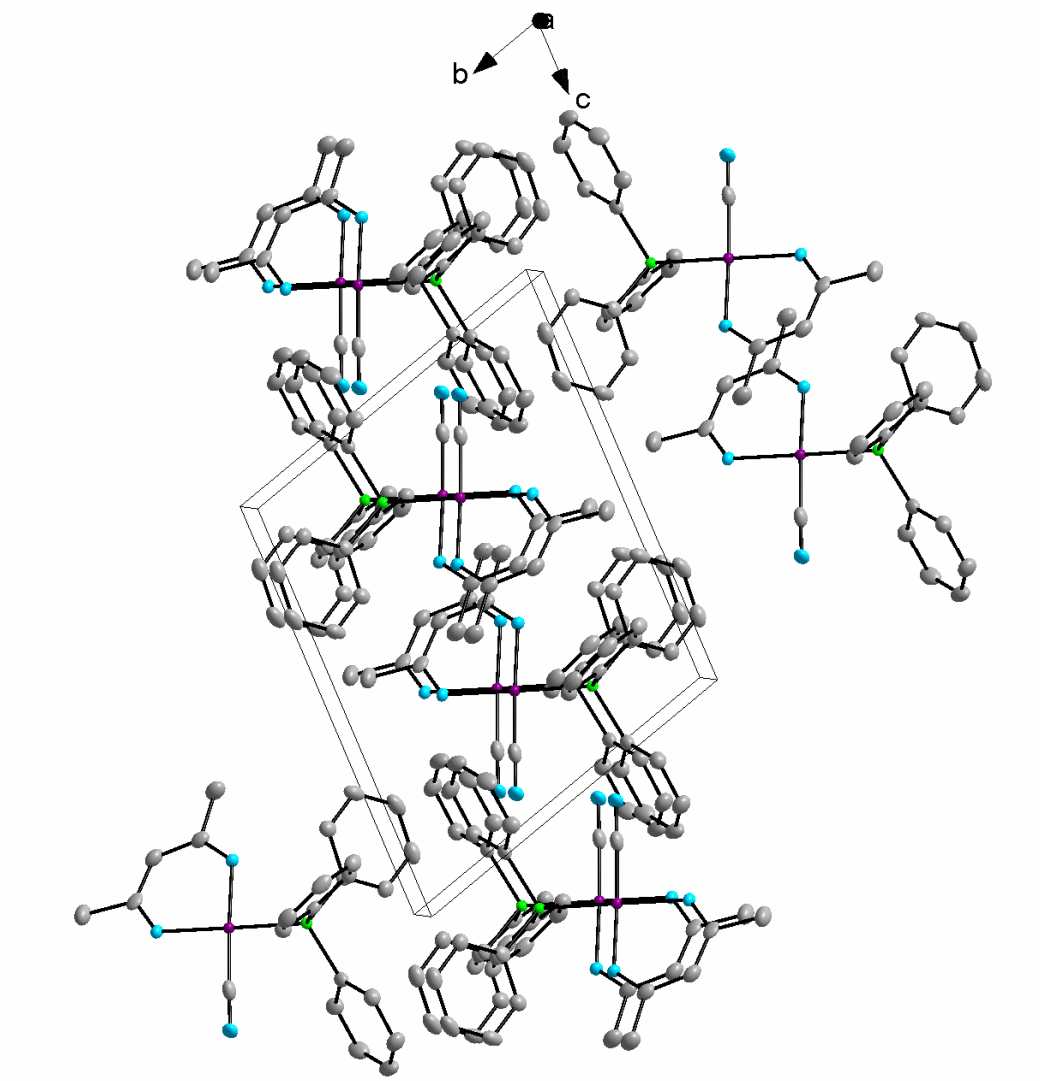

Figure 3.11: **[Rh(acac)(CO)(PPh_3)] complexes showing the "head to head" crystal packing along the a-axis. H atoms have been omitted for clarity.**

3.5.3 Crystal Structure of [Rh(acac)(CO)(PCyPh$_2$)]

Yellow crystals of the title compound, were synthesized as described in Section 3.4.2.3 (B). The [Rh(acac)(CO)(PCyPh$_2$)] **(2)**, complex crystallised in a non-centrosymmetric, orthorhombic space group, $P2_12_12_1$, with four molecules per unit cell.[39] The structure and numbering scheme of **(2)** is illustrated in Figure 3.12, while the most important bond distances and angles are reported in Table 3.6. The positional and thermal parameters are given in Table B.1 and a complete list of bond distances and angles are given in Table B.2 of the Appendix.

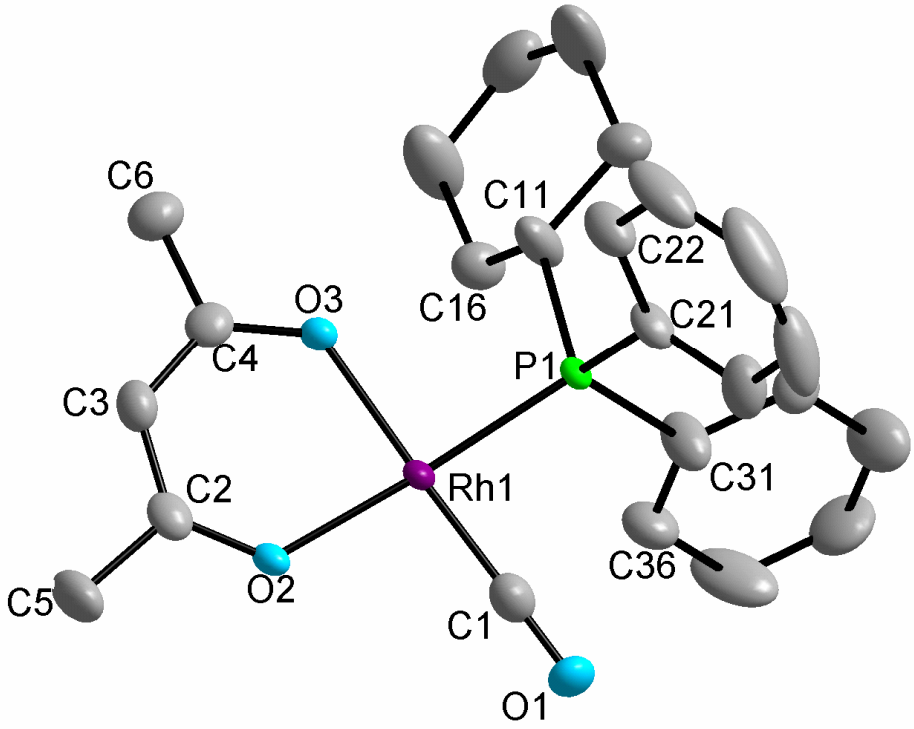

Figure 3.12: **Molecular structure of [Rh(acac)(CO)(PCyPh$_2$)] showing atom numbering system. For the phenyl/cyclohexyl rings, the first digit refers to the ring number, while the second digit refers to the C-atom in the ring. H atoms have been omitted for clarity.**

The molecular structure of [Rh(acac)(CO)(PCyPh$_2$)], **(2)**, consists of a Rh(I) metal centre which is bonded to two equivalent oxygen atoms of the acetylacetonato bidentate ligand, one carbonyl ligand and one phosphorous atom. The phosphine ligand, cyclohexyldiphenylphosphine (PCyPh$_2$), consists of one cyclohexyl ring (C1 ring), one planar phenyl ring (C2 ring) and one phenyl ring which show slight distortion (C3 ring).

[39] A. Brink, A. Roodt, H.G. Visser, *Acta Cryst.*, E**63**, 2007, m2831

Table 3.6: Selected bond lengths and angles for [Rh(acac)(CO)($PCyPh_2$)].

Bond	Distance (Å)	Bond Angle	Angle (°)
C(1)-O(1)	1.149(4)	O(1)-C(1)-Rh(1)	179.1(3)
C(1)-Rh(1)	1.802(3)	C(1)-Rh(1)-O(3)	177.27(9)
P(1)-Rh(1)	2.2328(6)	C(1)-Rh(1)-O(2)	93.70(10)
O(2)-Rh(1)	2.0763(17)	O(3)-Rh(1)-O(2)	88.72(7)
O(3)-Rh(1)	2.0428(19)	C(1)-Rh(1)-P(1)	88.51(8)
O(2)-C(2)	1.270(3)	O(3)-Rh(1)-P(1)	89.17(5)
O(3)-C(4)	1.276(3)	O(2)-Rh(1)-P(1)	174.96(5)
C(2)-C(3)	1.388(4)	C(2)-C(3)-C(4)	125.6(3)
C(2)-C(5)	1.513(3)	O(2)-C(2)-C(3)	126.4(2)
C(4)-C(3)	1.393(4)	O(3)-C(4)-C(3)	126.2(3)
C(4)-C(6)	1.502(4)	C(31)-P(1)-Rh(1)	119.18(9)
P(1)-C(31)	1.819(3)	C(21)-P(1)-Rh(1)	109.85(8)
P(1)-C(21)	1.821(3)	C(11)-P(1)-Rh(1)	112.37(9)
P(1)-C(11)	1.835(3)	C(31)-P(1)-C(21)	105.43(13)
		C(31)-P(1)-C(11)	103.55(15)
		C(21)-P(1)-C(11)	105.38(13)

The molecular structure of **(2)** has a square-planar geometry with slight deviation, 5.044(38)º, from the horizontal plane. A horizontal plane constructed through atoms C1, P1, O3, O2 and Rh1 is indicated in Figures 3.13. Important distances between selected atoms and the plane are indicated in Table 3.7. One side of the acac backbone is twisted upwards with a significantly larger torsion angle (C2-O2-O3-C4 = -3.123(191)º) compared to complex **(1)** . The C2 and O2 atoms have a distance of -0.233(2) and -0.144(2) Å respectively from the plane (Figure 3.13 (b)). The C5 methyl carbon deviates the most from the plane, -0.350(3) Å. The carbonyl ligand is less deviated from the plane than for the [Rh(acac)(CO)(PPh_3)] complex with a O3-Rh-C1 angle of 177.27(9)º. The phosphine ligand is bent slightly above the plane with the O2-Rh-P1 angle of 174.95(5)º. Both the C1 cyclohexyl and C3 phenyl rings lie below the plane (Rh-P1-C11 = 112.38(9)º and Rh-P1-C31 = 119.18(9)º) as indicated in Figure 3.13 (c). On the C1 ring only H11, H13B, H12A, H13A, C13 and C12 atoms are completely or partially displaced above the plane. The H32 atom on the C3 ring lies partially above the plane. The C2 phenyl ring lies above the plane and is bent closer to the Rh centre than the other two rings (Rh-P1-C21 = 109.85(8)º). The distance of the C11 atom (0.429(3) Å) from the plane is significantly shorter than for C21 (-1.701(3) Å) and C31 (1.062(3) Å) respectively. The protons bonded to the methyl carbons, C5

and C6, are positioned staggered to each other with an average dihedral angle of 29.16 º between corresponding protons (Figure 3.13 (d)).

Table 3.7: **Selected distances between specific atoms and the horizontal plane through atoms C1, P1, O3, O2 and Rh1**

Atom	Distance (Å)	Atom	Distance (Å)
C1	0.032(3)	C6	0.175(3)
O1	0.068(2)	C4	-0.025(3)
P1	-0.0174(6)	C2	-0.233(2)
Rh1	0.0027(2)	C5	-0.350(3)
C3	-0.203(3)	O2	-0.144(2)
H3	-0.3104(0)	O3	0.020(2)

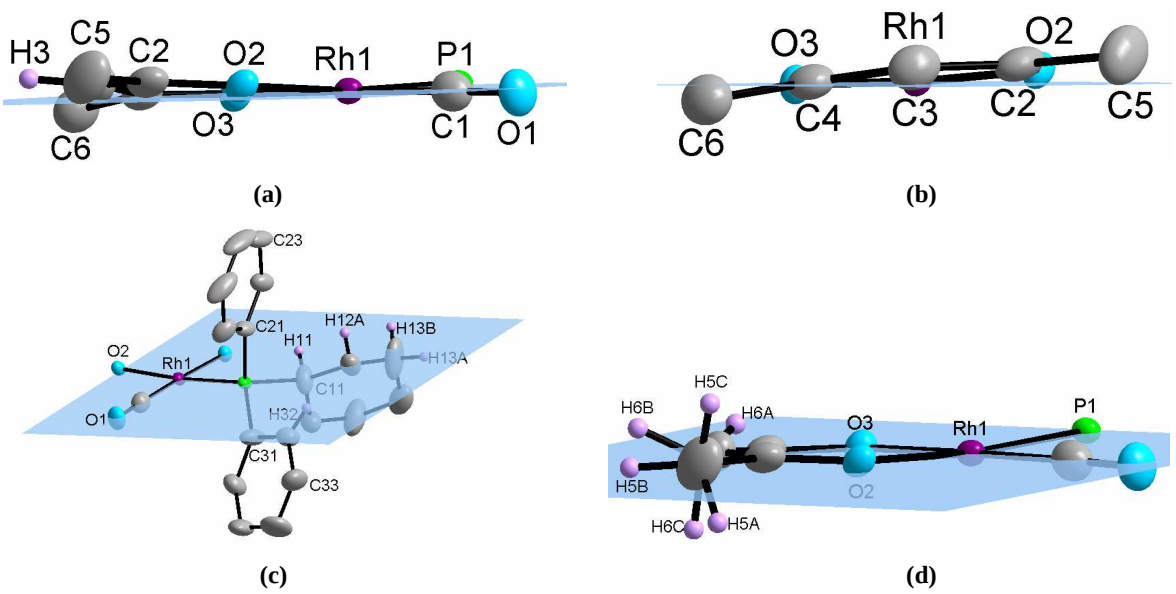

Figure 3.13: **Partial structure of [Rh(acac)(CO)($PCyPh_2$)]. (a) – Side view of ligands bonded to Rh(I) metal center. (b) – Front view of acac bidentate ligand. (c) – Position of the phosphine ligand with regards to the horizontal plane. (d) – Position of methyl protons of C6 and C5.**

The twisting of the C1 cyclohexyl ring with regards to the horizontal plane (Figure 3.13 (a), (b)) may be due to H-bond interactions. Intramolecular hydrogen bonds occur between atoms O3 and H11, with a donor-acceptor (**D-A**) bond distance of 2.962(3) Å, and between O3 and H16B (**D-A** = 3.095(3) Å) as indicated in Figure 3.14. A complete list of H-bond interactions is given in Table 3.8.

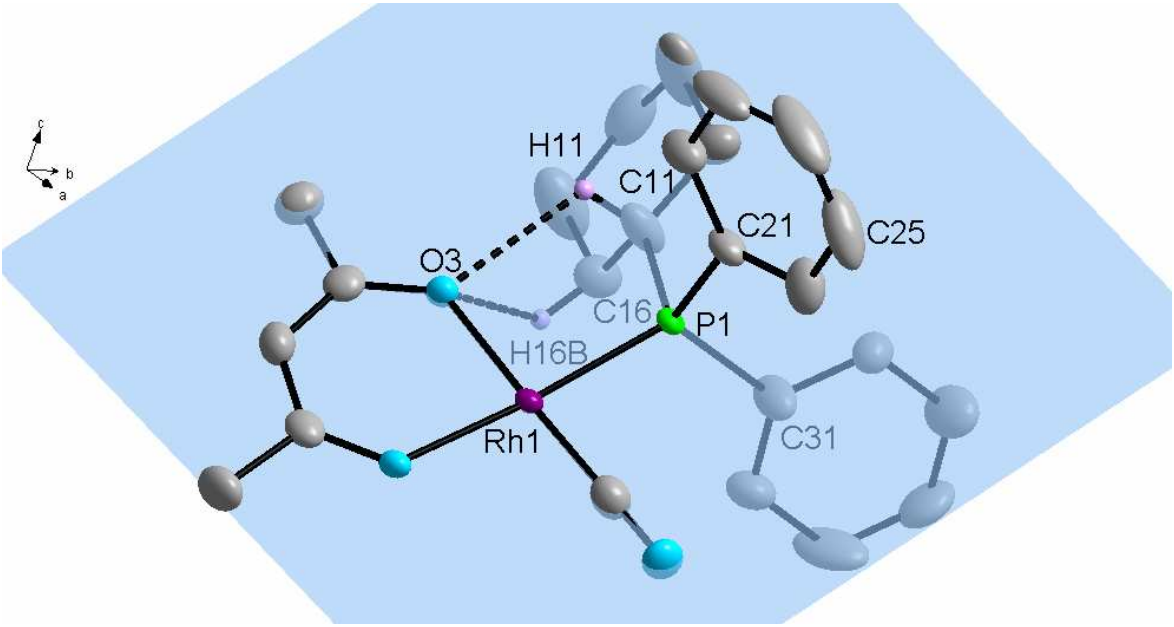

Figure 3.14: **Figure of the [Rh(acac)(CO)(PCyPh$_2$)] complex indicating the short intramolecular H-bond interactions. Only applicable H atoms with relevance to H-bond interactions are indicated.**

Table 3.8: **Hydrogen bonds for [Rh(acac)(CO)(PCyPh$_2$)] [Å and °].**

D-H...A	d(D-H)	d(H...A)	d(D...A)	<(DHA)
C(11)-H(11)...O(3)#1	1.00	2.39	2.962(3)	115.9
C(16)-H(16B)...O(3)#1	0.99	2.44	3.095(3)	123.3

Symmetry transformations used to generate equivalent atoms:
#1 x,y,z

The *trans* influence of the PCyPh$_2$ ligand is only slightly stronger than for the PPh$_3$ ligand as indicated by the Rh-O2 bond distance; 2.0764(17) Å vs. 2.0738(16) Å. As expected the *trans* influence of the carbonyl is much less (Rh-O3 = 2.0427(19) Å). The Rh-P1 and Rh-C1 bond distances are 2.2327(6) and 1.802(3) Å respectively. The O2-Rh-O3 and C1-Rh-P1 bite angles of 88.72(7)º and 88.51(8)º are equivalent within experimental error.

Unlike **(1),** the [Rh(acac)(CO)(PCyPh$_2$)] molecules do not have any "sheet-like" packing and are packed in positions of least steric hindrance with the phosphine ligands positioned above and below the Rh-acac backbone as seen in Figure 3.15. No intermolecular hydrogen bonding occurs between molecules.

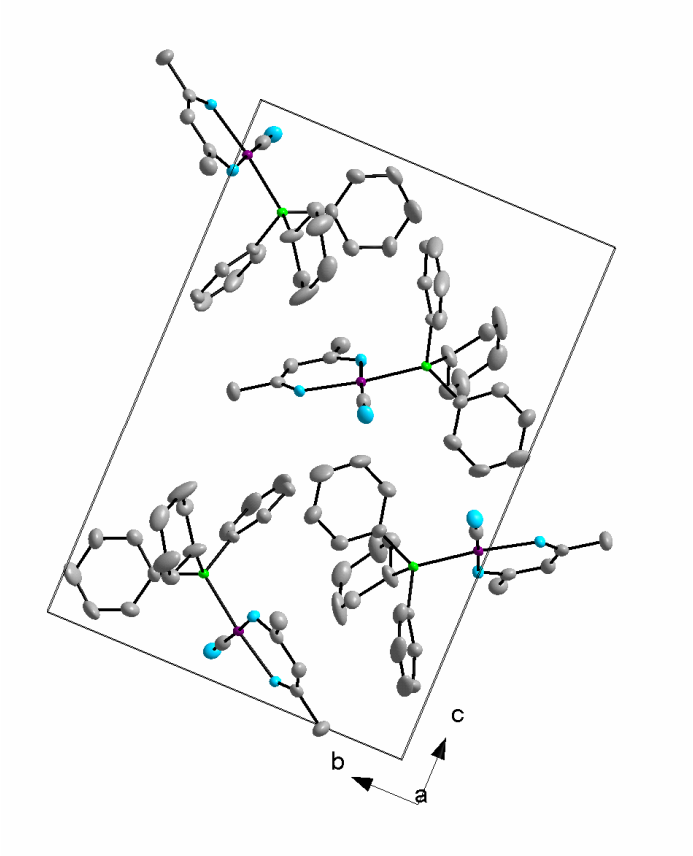

Figure 3.15: **The crystal packing of the [Rh(acac)(CO)($PCyPh_2$)] molecules. Unit cell is viewed along the a-axis. H atoms have been omitted for clarity.**

3.5.4 Crystal Structure of [Rh(acac)(CO)(PCy_2Ph)]

Yellow crystals of the title compound were synthesized as mentioned in Section 3.4.2.3 (C). [Rh(acac)(CO)(PCy_2Ph)] **(3)**, crystallised in the monoclinic space group, $P2_1/n$, with four molecules per unit cell.[40] The structure and numbering scheme of **(3)** is illustrated in Figure 3.16, while the most important bond distances and angles are reported in Table 3.10. The positional and thermal parameters are given in Table C.1 and a complete list of bond distances and angles can be found in Table C.2 of the Appendix.

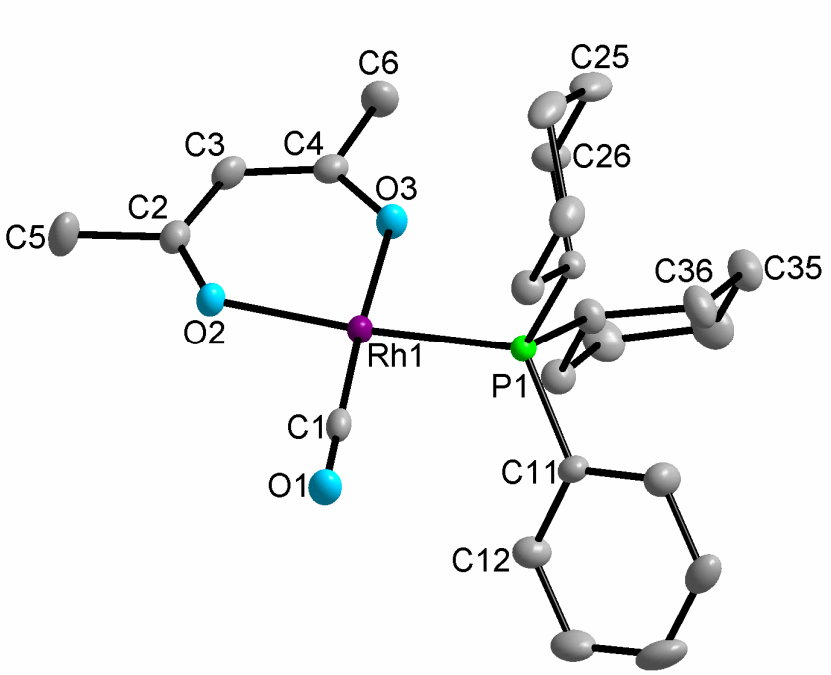

Figure 3.16: **Molecular structure of [Rh(acac)(CO)(PCy_2Ph)] showing atom numbering system. For the phenyl and cyclohexyl rings, the first digit refers to the ring number, while the second digit refers to the C-atom in the ring. H atoms have been omitted for clarity.**

The crystal structure of **(3)** is similar to the previously described crystal structures. The only difference is observed in the phosphine ligand which consists of two cyclohexyl rings and one phenyl ring. A horizontal plane through C1, P1, Rh1, O2, and O3 was constructed in Figure 3.17. Complex **(3)** shows essentially no distortion from the four-coordinate square-planar geometry as indicated in Table 3.9 and Figures 3.17. The torsion angle also indicates the planarity of the complex (C2-O2-O3-C4 = 0.3(2)º).

[40] A. Brink, A. Roodt, H.G. Visser, *Acta Cryst.*, E**63**, 2007, m48

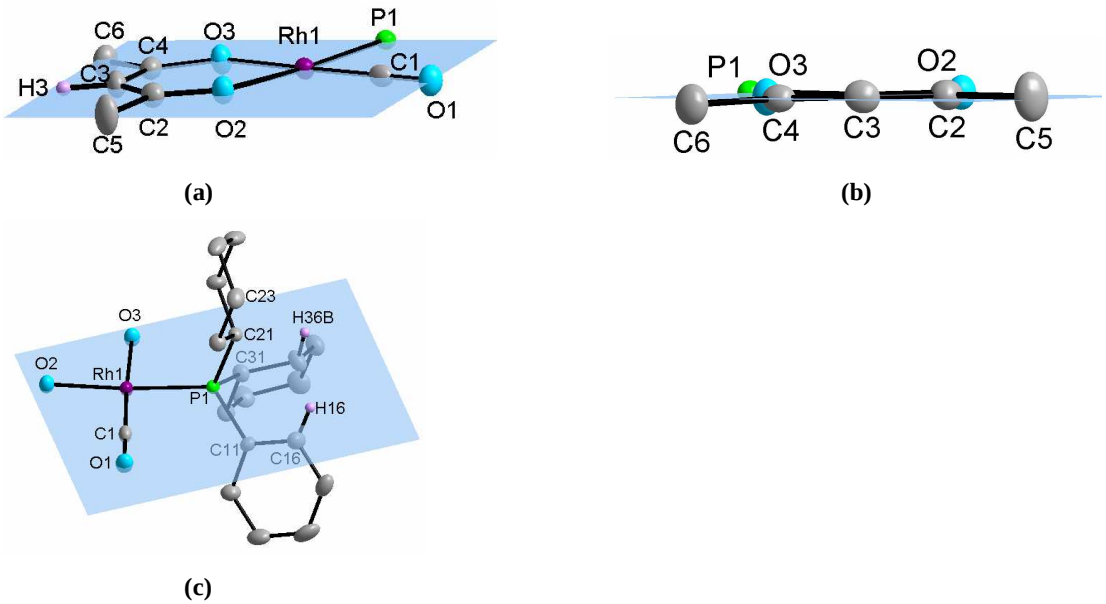

Figure 3.17: **Partial structure of [Rh(acac)(CO)(PCy_2Ph)]. (a) – Side view of ligands bonded to Rh(I) metal center. (b) – Front view of acac bidentate ligand. (c) – Position of the phosphine ligand with regards to the horizontal plane.**

The Rh-C1-O1 bond angle can be considered linear with a bond angle of 179.9(2)º. The O2-Rh-O3 and C1-Rh-P1 bite angles are of similar magnitude, 88.20(7) and 89.34(7)º respectively. The steric demand of the phosphine ligand is indicated by the smaller O3-Rh-P1 angle, 87.72(5)º, compared to the carbonyl ligand (O2-Rh-C1 = 94.74(8)º). The phosphine ligand is bent slightly above the plane with a O2-Rh-P1 angle of 175.32(5)º. The C2 cyclohexyl ring is positioned above the plane (Figure 3.17 (c)) with a Rh-P1-C21 angle of 111.58(7)º and a C21 – plane distance of -1.714(2) Å. As with the other two complexes, **(1)** and **(2)**, its horizontal face is twisted to face the Rh-acac ring. The other cyclohexyl ring, C3, is found below the plane in the position of least steric interaction, away from the carbonyl ligand. The angle between the cyclohexyl ring and the Rh atom is similar to the C2 ring, Rh-P1-C31 = 110.35(8)º and is partially twisted so that only the H36B atom appears above the plane, however the C31 – plane distance (0.838(2) Å) is shorter than expected (Figure 3.17 (c)). The C2 cyclohexyl ring has no ring distortion and has an average C-C bond length which agrees with the expected value[38] of 1.540 ± 0.015 Å. The C3 cyclohexyl ring has a shorter average C-C bond length (1.497 Å) than the accepted norm.

Table 3.9: Selected distances between specific atoms and the horizontal plane through atoms C1, P1, O3, O2 and Rh1

Atom	Distance (Å)	Atom	Distance (Å)
C1	0.004(2)	C6	0.085(3)
O1	0.007(2)	C4	0.007(2)
P1	-0.0079(6)	C2	-0.054(2)
Rh1	0.0029(2)	C5	-0.049(3)
C3	-0.036(3)	O2	-0.070(2)
H3	-0.0531(2)	O3	0.008(2)

The C1 phenyl ring is angled below the plane, on the carbonyl ligand side, and is bent at a greater angle away from the Rh atom with a Rh-P1-C11 angle of 119.88(8)º but has a similar C11 – plane distance (0.799(2) Å) as C31. It is twisted so that only the H16 atom is above the plane. The phenyl ring shows no distortion and is planar, within experimental error. The average C-C bond distance of 1.398 Å and bond angles of 120.0º are within the expected range for phenyl rings.[37]

Table 3.10: Selected bond lengths and angles for [Rh(acac)(CO)(PCy_2Ph)].

Bond	Distance (Å)	Bond Angle	Angle (º)
P(1)-Rh(1)	2.2424(9)	O(1)-C(1)-Rh(1)	179.9(2)
C(1)-Rh(1)	1.797(3)	C(1)-Rh(1)-P(1)	89.34(7)
C(1)-O(1)	1.152(3)	O(3)-Rh(1)-O(2)	88.20(7)
O(2)-Rh(1)	2.0783(17)	O(2)-Rh(1)-P(1)	175.32(5)
O(3)-Rh(1)	2.0411(18)	C(1)-Rh(1)-O(3)	177.06(8)
O(2)-C(2)	1.273(3)	C(2)-O(2)-Rh(1)	126.30(15)
O(3)-C(4)	1.279(3)	C(4)-O(3)-Rh(1)	127.74(15)
P(1)-C(11)	1.825(2)	C(4)-C(3)-C(2)	125.7(2)
P(1)-C(21)	1.833(2)	C(11)-P(1)-Rh(1)	119.88(8)
P(1)-C(31)	1.842(2)	C(21)-P(1)-Rh(1)	111.58(7)
C(4)-C(3)	1.384(3)	C(31)-P(1)-Rh(1)	110.35(8)
C(2)-C(3)	1.396(3)		
C(4)-C(6)	1.509(3)		
C(2)-C(5)	1.504(3)		

The C3 cyclohexyl ring experiences intermolecular and intramolecular hydrogen bond interactions which results in a “cage-like structure” with the molecules bonded in a head to tail fashion as indicated in Figure 3.18. The H31 atom experiences intramolecular H-bonding with

O3 with a donor-acceptor (**D-A**) bond distance of 2.974(3) Å, while the H33A atom experiences intermolecular H-bonding with O2' of the Rh' molecule (-x+1, -y, -z; **D-A** = 3.455(3) Å).

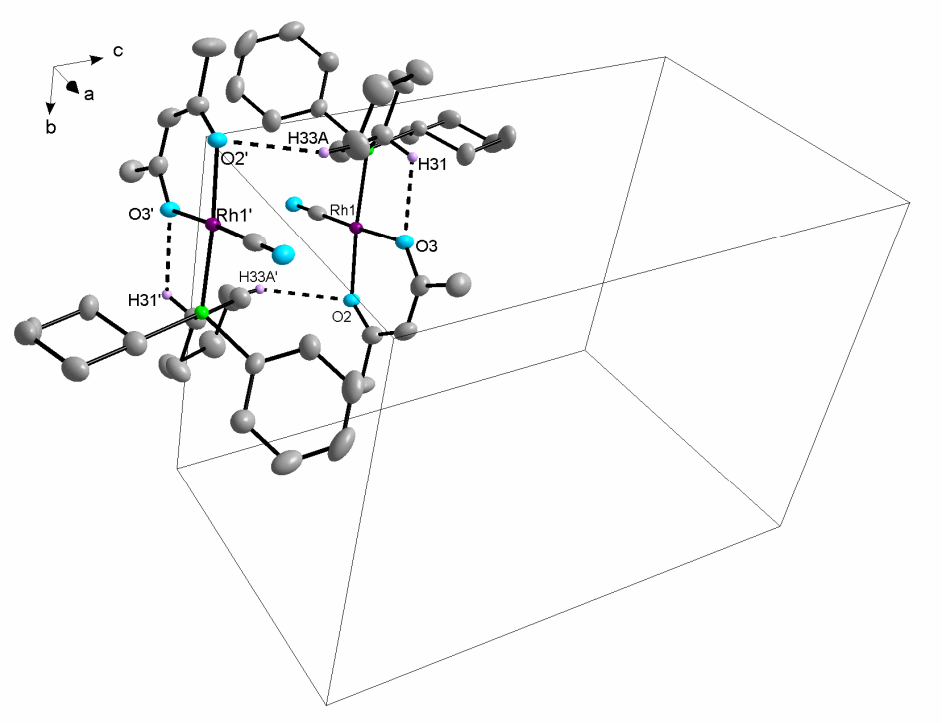

Figure 3.18: **Inter- and intramolecular H-bond interactions found between [Rh(acac)(CO)(PCy_2Ph)] molecules. Only applicable H atoms with relevance to H-bond interaction are indicated.**

A complete list of H-bond interactions can be found in Table 3.11 below. The "cage-like structure" of the molecules can be reproduced to form four-sided tunnels when viewed along the a-axis, as indicated in Figure 3.19.

Table 3.11: **Hydrogen bonds for [Rh(acac)(CO)(PCy_2Ph)] [Å and °].**

D-H...A	d(D-H)	d(H...A)	d(D...A)	<(DHA)
C(31)-H(31)...O(3)#1	1.00	2.40	2.974(3)	116.1
C(33)-H(33A)...O(2)#2	0.99	2.60	3.455(3)	144.7

Symmetry transformations used to generate equivalent atoms:
#1 x,y,z #2 -x+1,-y,-z

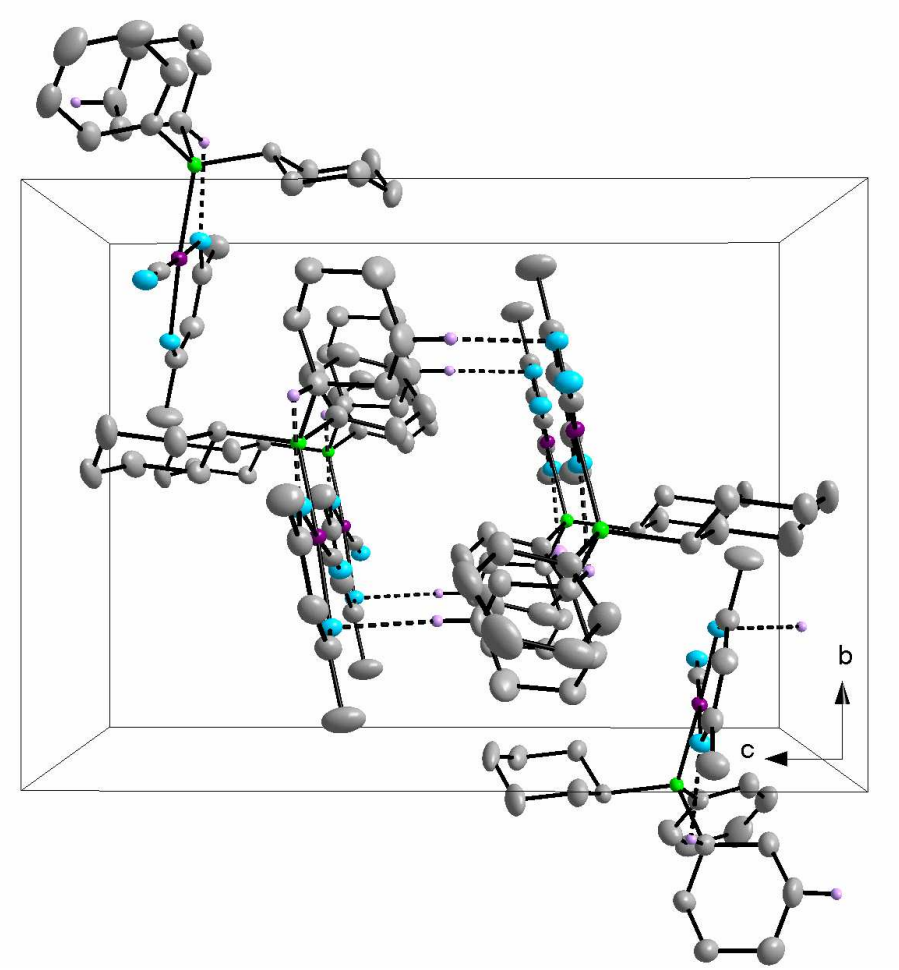

Figure 3.19: **Crystal packing of [Rh(acac)(CO)(PCy_2Ph)] complexes which form "cage-like" tunnels when viewed along the a-axis due to intramolecular and intermolecular H-bond interactions. Only applicable H atoms with relevance to H-bond interaction are indicated.**

3.5.5 Crystal Structure of [Rh(acac)(CO)(PCy_3)]

The crystal structure of [Rh(acac)(CO)(PCy_3)], **(4)**, was first investigated by Trzeciak *et al.*[23] in 2004, who synthesized the [Rh(acac)$(CO)_2$] complex according to the method described by Varshavskii *et al.*[36] For the purpose of this study, the [Rh(acac)(CO)(PCy_3)] complex, **(4)**, was resynthesised and analysed at low temperature. The redetermination compares well with the original values published by Trzeciak *et al.* A comparison between the values is found in Table 3.15.

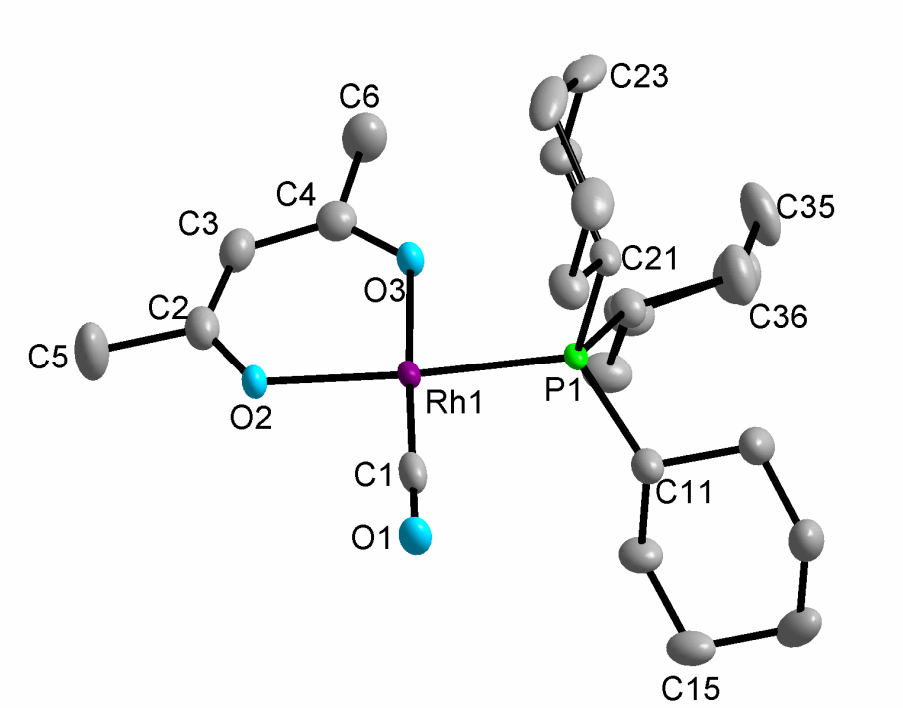

Figure 3.20: **Molecular structure of [Rh(acac)(CO)(PCy_3)] showing atom numbering system. For the cyclohexyl rings, the first digit refers to the ring number, while the second digit refers to the C-atom in the ring. H atoms have been omitted for clarity.**

Yellow crystals of the title compound were prepared according to the experimental procedure described in Section 3.4.2.3 (D). [Rh(acac)(CO)(PCy_3)] crystallized in the monoclinic space group, $P2_1/n$, with four molecules in the unit cell and is isomorphic to the [Rh(acac)(CO)(PCy_2Ph)] complex. The molecular structure of **(4)** is illustrated in Figure 3.20 along with the atom numbering system. Selected bond distances and angles are given in Table 3.12. The positional and thermal parameters for the atoms can be found in Table D of the Appendix.

Table 3.12: Selected bond lengths and angles for [Rh(acac)(CO)(PCy_3)].

Bond	Distance (Å)	Bond Angle	Angle (º)
O(1)-C(1)	1.157(2)	O(3)-Rh(1)-O(2)	87.77(4)
C(1)-Rh(1)	1.7914(17)	C(1)-Rh(1)-P	89.11(5)
P-Rh(1)	2.2537(4)	O(1)-C(1)-Rh(1)	179.37(14)
O(2)-Rh(1)	2.0880(10)	C(1)-Rh(1)-O(3)	177.40(6)
O(3)-Rh(1)	2.0464(11)	O(2)-Rh(1)-P	176.23(3)
O(2)-C(2)	1.270(2)	C(1)-Rh(1)-O(2)	94.47(6)
O(3)-C(4)	1.272(2)	O(3)-Rh(1)-P	88.62(3)
C(4)-C(3)	1.387(2)	C(2)-O(2)-Rh(1)	126.49(10)
C(2)-C(3)	1.396(2)	C(4)-O(3)-Rh(1)	127.94(10)
P-C(31)	1.8427(16)	C(4)-C(3)-C(2)	125.39(16)
P-C(21)	1.8452(15)	C(31)-P-Rh(1)	109.24(5)
P-C(11)	1.8528(16)	C(21)-P-Rh(1)	110.81(5)
		C(11)-P-Rh(1)	117.30(5)

The four-coordinated Rh(I) complex shows little deviation from the square-planar geometry as indicated in Figures 3.21 and Table 3.13. The torsion angle confirms the planarity of the complex (C2-O2-O3-C4 = 0.5(1)º). The carbonyl ligand is planar with respect to the plane with a Rh-C1-O1 angle of 179.36(13)º whereas the phosphine ligand is slightly elevated above the plane with a O2-Rh-P angle of 176.23(3)º. The steric demand of the phosphine ligand results in a larger bite angle for C1-Rh-P = 89.11(5)º, than for the acac bidentate ligand (O2-Rh-O3 = 87.77(4)º).

Table 3.13: Selected distances between specific atoms and the horizontal plane through atoms C1, P1, O3, O2 and Rh1

Atom	Distance (Å)	Atom	Distance (Å)
C1	-0.028(1)	C6	-0.001(2)
O1	-0.059(1)	C4	-0.028(1)
P1	-0.0034(3)	C2	-0.040(1)
Rh1	0.0010(1)	C5	-0.032(2)
C3	-0.049(2)	O2	-0.037(1)
H3	-0.0705(0)	O3	-0.011(1)

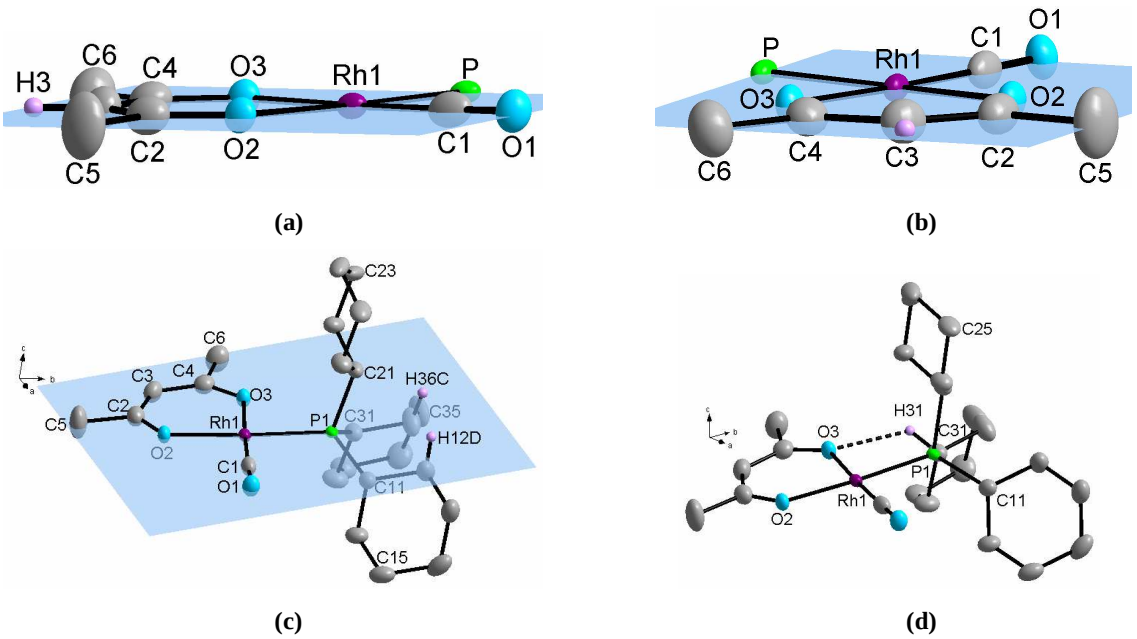

Figure 3.21: **Partial structure of [Rh(acac)(CO)(PCy_3)]. (a) – Side view of ligands bonded to Rh(I) metal center. (b) – Front view of acac bidentate ligand. (c) – Position of the phosphine ligand with respect to the horizontal plane. (d) – Intramolecular hydrogen bond interaction.**

The average C-C bond distance of all the cyclohexyl rings on the PCy_3 ligand, are consistent with the expected value of 1.540 Å.[38] The C2 cyclohexyl ring is positioned above the plane in the position of least steric hindrance (Figure 3.21) with a Rh-P-C21 angle of 110.81(5)º whereas the C3 cyclohexyl ring is completely submerged below the plane except for the H36C atom (Rh-P-C31 = 109.26(5)º). The C1 cyclohexyl ring, positioned below the plane on the same side as the carbonyl ligand, has a larger Rh-P-C11 angle, 117.31(5)º, than expected. This may be due to steric interference with the carbonyl ligand.

Intramolecular hydrogen bonding (Figure 3.21 (d)) is found between H31 and O3 of the same molecule with a donor-acceptor (**D-A**) bond distance of 2.984 Å. The complete list of H-bond distances is given in Table 3.14. The intramolecular interaction may be the cause for the "zig-zag" sheet-like crystal packing of the molecules as indicated in Figure 3.22. The molecules pack in horizontal sheets along the a-axis and each Rh-acac backbone is enclosed above, below, left and right by cyclohexyl rings. No intermolecular hydrogen bonding is found between the molecules.

Table 3.14: Hydrogen bonds for [Rh(acac)(CO)(PCy_3)] [Å and °].

D-H...A	d(D-H)	d(H...A)	d(D...A)	<(DHA)
C(31)-H(31)...O(3)#1	1.00	2.42	2.9841(18)	115.1

Symmetry transformations used to generate equivalent atoms:
#1 x,y,z

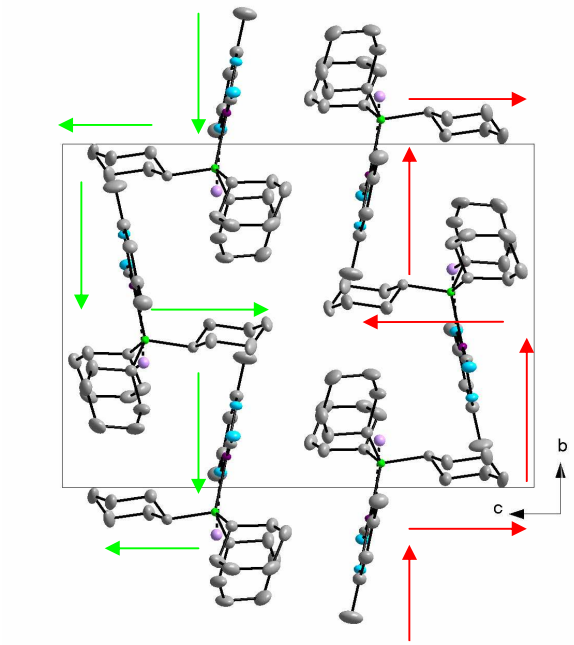

Figure 3.22: The sheet-like crystal packing of [Rh(acac)(CO)(PCy_3)] which forms a "zig-zag" pattern when viewed along the a-axis. The red and green arrows indicate the "zig-zag" pattern.

3.5.6 Comparison of the [Rh(acac)(CO)($PR_1R_2R_3$)] Crystal Structures where R_1, R_2 and R_3 = phenyl or cyclohexyl rings.

Table 3.15 presents a comparative summary of the crystal structures, **(1)** to **(4)**, as obtained in this study. Some crystallographic data for complexes [Rh(acac)(CO)(**PPh_3**)] and [Rh(acac)(CO)(**PCy_3**)], as previously published by Leipoldt *et al.*[21] and Trzeciak *et al.*[23] are included. Unit cell contents and selected interatomic bond distances and angles are illustrated in the table.

Table 3.15 (a): Summary of crystallographic data for the four complexes of [Rh(acac)(CO)($PR_1R_2R_3$)].

[Rh(acac)(CO)($PR_1R_2R_3$)]				
$PR_1R_2R_3$	**(1)** - PPh_3	**(2)** - $PCyPh_2$	**(3)** - PCy_2Ph	**(4)** - PCy_3
Crystal system	Triclinic	Orthorhombic	Monoclinic	Monoclinic
Space group	Pī	$P2_12_12_1$	$P2_1/n$	$P2_1/n$
Z	2 2	4	4	4 4
a (Å)	8.856(5) 8.90	9.4682(5)	10.076(5)	10.3418(5) 10.404(2)
b (Å)	10.314(5) 10.45	12.7534(6)	12.990(5)	13.0644(6) 13.091(3)
c (Å)	12.844(5) 13.20	18.4602(9)	17.937(5)	17.9301(8) 17.981(4)
α (º)	71.298(5) 97.05	90.00	90.000(5)	90.00 90.0
β (º)	70.143(5) 110.85	90.00	90.576(5)	90.612(2) 90.00(3)
γ (º)	82.775(5) 103.15	90.00	90.000(5)	90.00 90.0
Volume ($Å^3$)	1045.0(9) -	2229.10(19)	2347.6(16)	2422.39(19) 2449.0(9)
Vol. per molecule ($Å^3\ Z^{-1}$)	522.5	557.3	586.9	605.6
$Density_{calc.}$ ($g.cm^{-1}$)	1.565 -	1.485	1.427	1.400 1.384

* Values determined by Leipoldt *et al.*[21]; Values determined by Trzeciak *et al.*[23]

Table 3.15 (b): Summary of crystallographic bond distances and angles for the four complexes of [Rh(acac)(CO)($PR_1R_2R_3$)].

Bond distance (Å)				
Rh-C1	1.807(2) 1.801(8)	1.802(3)	1.798(2)	1.7910(17) 1.804(4)
C1-O1	1.153(3) 1.153(11)	1.149(4)	1.151(3)	1.157(2) 1.160(4)
Rh-P1	2.2418(9) 2.244(2)	2.2327(6)	2.2425(9)	2.2537(4) 2.2613(10)
Rh-O3	2.0331(15) 2.029(5)	2.0427(19)	2.0409(18)	2.0462(11) 2.052(2)
Rh-O2	2.0747(16) 2.087(4)	2.0764(17)	2.0788(16)	2.0879(10) 2.096(2)
P1-C11	1.827(2) 1.828(7)	1.835(3)	1.825(2)	1.8525(16)
P1-C21	1.823(2) 1.822(7)	1.821(3)	1.833(2)	1.8451(14)
P1-C31	1.823(2) 1.834(8)	1.819(3)	1.842(2)	1.8426(15)
Bond angles (º)				
C1-Rh-P1	87.18(7) 87.8(2)	88.50(8)	89.34(7)	89.12(5) 88.93(10)
O2-Rh-O3	88.02(7) 87.9(2)	88.72(7)	88.20(7)	87.77(4) 87.50(9)
Rh-C1-O1	176.0(2) 176.8(9)	179.2(3)	179.9(2)	179.36(13)
O3-Rh-C1	174.45(8)	177.27(9)	177.06(8)	177.41(5) 177.54(12)
O2-Rh-P1	179.01(5)	174.95(5)	175.32(5)	176.23(3) 176.299(7)
Rh-P1-C11	114.74(7) 114.7(2)	112.38(9)	119.88(8)	117.31(5)
Rh-P1-C21	114.81(7) 114.4(2)	109.85(8)	111.58(7)	110.81(5)
Rh-P1-C31	114.12(7) 114.8(2)	119.18(9)	110.35(8)	109.26(5)
Effective cone angle (θ_E)	149.3	151.2	163.5	169.5

* Values determined by Leipoldt *et al.*[21]; Values determined by Trzeciak *et al.*[23]

Only the [Rh(acac)(CO)(PPh_3)] complex crystallises with 2 molecules per unit cell. The other three complexes all contain 4 molecules per unit cell. Complex **(3)** and **(4)** both crystallise in the monoclinic space group, while complex **(1)** and **(2)** crystallise in the triclinic and orthorhombic space groups respectively.

The increasing spatial demand, as the series progresses from **(1)** to **(4),** is indicated by the volume required per molecule ($Å^3\ Z^{-1}$), which increases from 522.5 to 605.6 $Å^3\ Z^{-1}$. The ratio by

which the volume increases is 1 : 1.07 : 1.12 : 1.16. The spatial demand of the phosphine ligands is further illustrated by the reverse trend in density (Table 3.15).

The Tolman cone angle (θ_T) is the most widely used method for determining ligand steric behaviour at a metal center as described by Tolman (1977).[25] The steric demand of the phosphine ligands, in this study, was quantified by the effective Tolman cone angle (θ_E), using the actual Rh-P bond distance.[41] A van der Waals radius of 1.2 Å for hydrogen and C-H bond distances of 0.97 Å for CH_2 and 0.93 Å for CH were used. In solution, the ligand substituents orientation might differ, resulting in a variation in cone angle size.[42] The effective cone angles (θ_E), all indicate the increasing steric demand of the phosphine ligands from complex **(1)** to **(4)** (Table 3.15). The θ_E values of 149.3 and 169.5º for PPh_3 and PCy_3 ligands, correspond well to the published Tolman cone angles,[25] θ_T, of 145 and 170º determined according to definition using a Ni-P bond distance of 2.28 Å.

The Rh-P bond distance indicates a tendency to increase from **(1)** to **(4)**, which corresponds well to the determined coupling constants, $^1J_{Rh\text{-}P}$ (Table 3.1 and 3.16). The Rh-P bond distance for **(2)** is shorter than expected, which may be due to H-bond interaction. The decreasing carbonyl stretching frequency, ν(CO) as indicated in Table 3.1 and 3.16, suggests that the C≡O bond length would increase as the σ-donating ability of the phosphine ligands increases. From the crystallographic data (Table 3.15), the C≡O bond length does indicate a tendency to increase. Factors such as H-bond interaction and crystal packing may be the reason why the crystallographic data for complexes **(2)** and **(3)** does not always fit well into the proposed sequence.

The ratio of Rh-O2 bond distance relative to the Rh-O2 bond distance of complex **(1)** shows a rapid increase with the systematic substitution of phenyl with cyclohexyl rings as indicated in Figure 3.23. This gives an indication of the varying *trans* influence of the phosphine ligands as the steric demand of the ligands increase.

[41] S. Otto, A. Roodt, J. Smith, *Inorg. Chim. Acta*, 2000, 303, 295
[42] G. Ferguson, P.J. Roberts, E.C. Alyea, M. Khan, *Inorg. Chem.*, 1978, 17, 2965

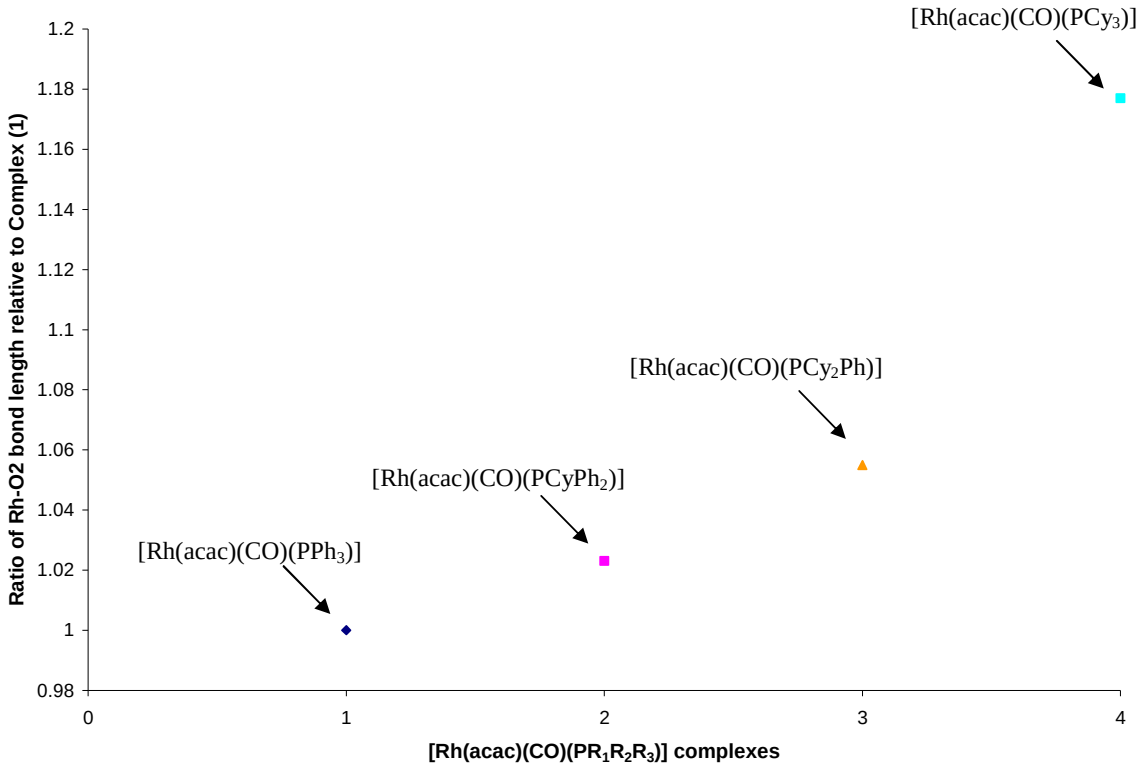

Figure 3.23: **The *trans* influence of the phosphine ligands as indicated by the ratio of Rh-O2 bond length relative to Complex (1).**

The C1-Rh-P1 and O2-Rh-O3 bite angles seem unaffected by changing phosphine ligand systems. Only the Rh-C1-O1 bond angle of complex **(1)**, is bent above the square-planar geometry of the Rh metal centre with an angle of 176.0(2)º. The other three complexes all have linear geometry. Complexes **(3)** and **(4)** both have ideal square-planar configuration with small torsion angles (C2-O2-O3-C4 = 0.3(2) and 0.5(1)º). Complex **(1)** is bent in an upside-down-boat shape (Figure 3.8 (a)) but with minimal twisting (C2-O2-O3-C4 = -0.3(2)º). Complex **(2)** is significantly twisted (C2-O2-O3-C4 = -3.2(2)º) due to intramolecular H-bond interaction between H11 and H16B with O3 (Figure 3.14).

The angles between the metal centre, phosphorous and carbon atom of the phenyl rings for **(1)** appear unaffected by the H-bond interaction experienced by the H24, H33 and H22 atoms (Table 3.3). However the Rh-P1-C11 bond angle of **(4)** is much larger than the angles for the other two cyclohexyl rings (117.31º versus 110.81º and 109.26º). The "zig-zag" sheet packing of the molecules may restrict the rotation of the C2 and C3 cyclohexyl rings (Figure 3.22).

Complexes of the type [Rh(L,L'-Bid)(CO)($PR_1R_2R_3$)] (L,L'-Bid = monoanionic bidentate ligand with donor atoms L and L') are formed when one CO ligand is replaced in [Rh(L,L'-Bid)$(CO)_2$]

complexes. The replacement of one CO ligand can lead to the formation of two isomeric monocarbonyl complexes if the donor capabilities of L and L' are similar, for example in the case of asymmetrical β-diketones [Rh(R_aCOCHCOR_b)(CO)($PR_1R_2R_3$)] with $R_a \neq R_b$.[22] However, if the difference in the donor/acceptor properties of the donor atoms L and L' are large enough then high selectivity for one of the isomers occurs.[24] Two isomers are formed for β-aminovinylketonate ligands in solution, with a well pronounced dominance for one isomer.[43,44,45] The predominant isomer in solution generally corresponds to the same isomer that was isolated in the solid state. The isomer ratio of some Rh(I)-aminovinylketonate complexes are sensitive to the type of solvent used and proved the existence of a dynamic equilibrium between the two isomers in solution. A unique case was noted where both isomers of the [Rh(ba)(CO)(PPh_3)] complex (ba = benzoylacetonate) crystallized in the same unit cell.[46] In complexes of the type [Rh(OX)$(CO)_2$] (OX = 8-hydroxyquinolate), substitution of the CO ligand only occurs *trans* to the strongest donor atom, i.e. the N atom. A number of similarities occur between the [Rh(OX)(CO)($PCyPh_2$)][47] and [Rh(acac)(CO)($PCyPh_2$)] complexes. Both have a slightly distorted square planar geometry, both pack with the phenyl and cyclohexyl rings directed towards the neighbouring bidentate ligand and both have intramolecular C-H···O contacts between two H-atoms on the cyclohexyl ring and the O-atom which lies *trans* to the CO ligand. The effective cone angle for both complexes are comparable with the value of 153º for the corresponding Vaska-type palladium complex *trans*-[$PdCl_2(PCyPh_2)_2$].[48]

A comparison of spectroscopic data has already been discussed in Section 3.4.3. The stronger π-acceptor properties of the $P(NC_4H_4)_3$ ligand are indicated by comparing the Rh-P bond distances as indicated in Table 3.16. It is by far the shortest distance, followed closely by $P(OPh)_3$ ligand. The best σ-donor ligand, according to Rh-P bond distances and carbonyl stretching frequency, is PCy_3. In general the $PR_1R_2R_3$ ligands can be arranged in the following order of decreasing π-acceptor and increasing σ-donor properties and *trans* influence:

$P(NC_4H_4)_3 > P(OPh)_3 > P(NC_4H_4)Ph_2 > PPh_3 > PCyPh_2 > PCy_2Ph > PCy_3$

[43] M.R. Galding, T.G. Cherkasova, L.V. Osetrova, Y.S. Varshavsky, *Rhodium Express*, 1993, 1, 14
[44] I.A. Poletaeva, T.G. Cherkasova, L.V. Osetrova, Y.S. Varshavsky, A. Roodt, J.G. Leipoldt, *Rhodium Express*, 1994, 3, 21
[45] T.G. Cherkasova, L.V. Osetrova, Y.S. Varshavsky, *Rhodium Express*, 1993, 1, 8
[46] W. Purcell, S.S. Basson, J.G. Leipoldt, A. Roodt, H. Preston, *Inorg. Chim. Acta*, 1995, 234, 153
[47] J.M. Janse van Rensburg, A. Roodt, A. Muller, *Acta Cryst.*, E**62**, 2006, m1040
[48] A.M.M. Meij, A. Muller, A. Roodt, *Acta Cryst.*, E**56**, 2003, m44

Table 3.16: Selected properties of [Rh(acac)(CO)($PR_1R_2R_3$)].

$PR_1R_2R_3$	*ν*(CO) (cm^{-1})	δ ^{31}P (ppm)	$^{1}J_{Rh-P}$ (Hz)	Cone angle (°)	Rh-P (Å)	Rh-O (Å) (*trans* to P)
PPh_3 [a]	1977.6	48.6	176.95	149.3	2.2418(9)	2.0747(16)
$PCyPh_2$ [a]	1959.3	53.3	171.25	151.2	2.2327(6)	2.0764(17)
PCy_2Ph [a]	1948.8	58.8	168.28	163.5	2.2425(9)	2.0788(16)
PCy_3 [a]	1945.3	59.3	164.27	169.5	2.2537(4)	2.0879(10)
$P(NC_4H_4)_3$ [b,e]	2012	102.5	251	141	2.166(1)	2.054(2)
$P(NC_4H_4)_2Ph$ [b]	2002	104.7	218	150	-	-
$P(NC_4H_4)Ph_2$ [b]	1990	90.0	194	154	2.223(1)	2.078(2)
$P(OPh)_3$ [b,c,d]	2006	212.1	293	136	2.170(1)	2.063(2)

[a] This MSc. Study; [b] Ref [27]; [c] Ref [25]; [d] Ref [22]; [e] Ref [26];

3.6 CONCLUSION

In this chapter, a range of relevant complexes consisting of [Rh(acac)(CO)(PPh_3)], [Rh(acac)(CO)($PCyPh_2$)], [Rh(acac)(CO)(PCy_2Ph)] and [Rh(acac)(CO)(PCy_3)] have been successfully synthesized and characterized with the use of infrared and nuclear magnetic resonance spectroscopy as well as X-ray crystallography.

It was possible to determine the manner in which the phosphine ligand coordination varies from [Rh(acac)(CO)(PPh_3)] to [Rh(acac)(CO)(PCy_3)] with the use of X-ray crystallography. The crystallographic geometric parameters, IR and NMR spectroscopy were successfully used to determine the variation of electron density on the metal centre.

An understanding of the electronic and steric properties of the [Rh(acac)(CO)($PR_1R_2R_3$)] complexes will contribute to solving the mechanistic pathway of the oxidative addition of iodomethane to the rhodium metal centre. These aspects will be addressed again in Chapter 4, where the actual kinetic reactivity of the four coordinated complexes will be discussed.

4 KINETIC STUDY OF THE IODOMETHANE OXIDATIVE ADDITION TO [Rh(acac)(CO)($PR_1R_2R_2$)] COMPLEXES

4.1 INTRODUCTION

Kinetics is the study of motion. Chemical kinetics is chiefly concerned with the observed characteristics of a chemical reaction, the manner in which a specific system changes from one state to another and the time required for the transition. It deals with the rate of chemical reactions and considers all the factors which affect the reaction rate, as well as how the rate can be described by a reaction mechanism.

On the other hand, thermodynamics gives little information about the mechanism of chemical reactions. An important part of thermodynamics is the state of equilibrium which is concerned only with the initial and final states of a system. The reaction mechanism and the rate are of no real importance in thermodynamics. Hence time is not one of the variables taken into account.[1]

In chemical kinetics, the presence of time is of great importance and adds both interest and difficulty.[2] Factors such as homogeneity of the system, concentration, pressure and temperature variations, sensitivity to light and air etc., can all play a role and affect the reaction mechanism and rate. Furthermore chemical kinetics only reflects a statistical average state of the molecules participating in the chemical reaction.[1] In order to study a chemical reaction and make a useful interpretation of the results, the system can be simplified by using a closed constant-volume,

[1] J.W. Moore, R.G. Pearson, *Kinetics and Mechanism*, 3rd Ed., New York: John Wiley & Sons, Inc., 1981
[2] K.A. Connors, *Chemical Kinetics: The Study of Reaction Rates in Solution*, New York: VCH Publishers, 1990

isothermal system. The rate of a chemical reaction can now be simply defined as the rate of change with time of the concentration of any of the reactants or products.[3]

With regards to the context of this study, kinetic investigations were considered very important and necessary in the investigation of possible catalytic behaviour of the chemical reaction systems. The experiments assisted in further understanding the inherent properties of the [Rh(acac)(CO)($PR_1R_2R_3$)] complexes and the rate of oxidative addition of iodomethane to these complexes which is the first step in the carbonylation of methanol *via* the well-known Monsanto process.

This chapter will discuss some selected theoretical principles of chemical kinetics followed by a summary of the experimental procedures as well as the results and discussion of the oxidative addition of iodomethane to [Rh(acac)(CO)(PPh_3)], [Rh(acac)(CO)($PCyPh_2$)], [Rh(acac)(CO)(PCy_2Ph)] and [Rh(acac)(CO)(PCy_3)] complexes.

4.2 THEORETICAL PRINCIPLES OF CHEMICAL KINETICS

4.2.1 Reaction Rates and Rate Laws

In a closed system, the rate of a chemical reaction can be defined as the rate of change with time *t* of the concentration of one of the reactants or of one of the products of the reaction. The rate is defined as a positive quantity, which is unaffected by the component whose concentration change is being measured.

For a generalised chemical reaction:

$$a\mathrm{A} + b\mathrm{B} \rightarrow f\,\mathrm{F} + j\mathrm{J} \qquad \textbf{... 4.1}$$

The rate can be expressed as a derivative because the rate almost invariably changes as time passes as illustrated in Eq. 4.2,

$$\mathrm{R} = -\frac{d[A]}{dt} = -\frac{d[B]}{dt} = \frac{d[F]}{dt} = \frac{d[J]}{dt} \qquad \textbf{... 4.2}$$

[3] G.G. Hammes, *Principles of Chemical Kinetics*, New York: Academic Press, Inc., 1978

Where t = time and the brackets indicate concentration of the species.

In general, the rate of reaction can be a function of the concentration of all the species present in a reaction mixture. Therefore

$$R = f(c_1, c_2, \ldots\ldots, c_j) \quad \textbf{... 4.3}$$

Equation 4.3 is called the rate law of a given reaction and cannot be predicted from the stoichiometric equation for the overall reaction. It is defined as *the experimentally determined dependence of the reaction rate on the reagent concentrations.*[4] The general form of the rate law is,

$$\text{Rate} = k[A]^m[B]^n\ldots. \quad \textbf{... 4.4}$$

where k is the proportionality constant called the *rate constant*. The exponents m and n are determined experimentally from the kinetic study. The rate constant is independent of the concentrations of A, B, …, but it may depend on environmental factors such as temperature and solvent. The magnitude of k will naturally depend on the particular reaction being studied.

An important objective of experimental kinetics is to propose a reasonable mechanism that will predict a rate law that is consistent with the experimentally observed rate law. The rate law can be uncomplicated as illustrated by the base hydrolysis of ethyl acetate,[2]

$$CH_3COOC_2H_5 + OH^- \rightarrow CH_3COO^- + C_2H_5OH$$

which has a rate law of,

$$R = k[CH_3COOC_2H_5][OH^-] \quad \textbf{... 4.5}$$

For other reactions, the rate law is far from simple:[3,5]

$$H_2 + Br_2 \rightarrow 2HBr$$

The rate law for this reaction can be written as,

$$R = \frac{1}{2}\frac{d}{dt}[HBr] = \frac{k[H_2][Br_2]^{1/2}}{1 + k'[HBr]/[Br_2]} \quad \textbf{... 4.6}$$

The rate law does not always depend on the concentrations of the reactants/products found in the overall reaction. It can also depend on the concentration of catalysts or inhibitors that assist the

[4] R.B. Jordan, *Reaction Mechanisms of Inorganic and Organometallic Systems*, Oxford: Oxford University Press, Inc., 1991

[5] M. Bodenstein, S.C. Lind, *Z. Phys. Chem.(Leipzig)*, 57, 168

reaction but which do not undergo any permanent change. The rate equation of imidazole-catalyzed hydrolysis of ethyl acetate[2] illustrates this aspect,

$$R = k[CH_3COOC_2H_5][\text{imidazole}] \quad \text{... 4.7}$$

however imidazole is not part of the balanced stoichiometric equation.

$$CH_3COOC_2H_5 + H_2O \rightarrow CH_3COOH + C_2H_5OH$$

4.2.2 Reaction Order

The rate law as indicated in Eq 4.4 has experimentally determined exponents. The sum of the exponents in the rate law is called the *order* of the rate law. For example if m = -2 and n = 1 in Eq 4.4, then the overall order of the rate law is -1. The reaction order with respect to any one component is simply the exponent associated with the particular component in question. In this example,[4] it will be the inverse second order in [A] and first order in [B]. The reaction order need not necessarily be an integer. The units of the rate constant, k, is dependant on the overall reaction order.[2] If the reaction conditions for a specific reaction are such that the concentration of one or more of the active species remain constant or nearly constant during a "run" then these concentrations may be included in the rate constant. The reaction is then said to be *pseudo-n^{th} order* where *n* is the sum of the exponents of the concentrations that change during the run. This occurs in catalytic reactions, when the catalyst concentration remains constant during the run, or if one reactant is in excess over another so that during the run there is only a minute change in the concentration of the former.[1]

4.2.3 Reaction Rates in Practice

The determination of reaction rates can be simplified to a study of concentrations as a function of time. The reaction rate is rarely obtained directly from experiment. Normally one or more concentrations, or one or more physical properties that are related to concentration, are measured as a function of time in an isothermal system. A number of kinetic runs of this type, analysed under changing conditions, provide the data needed to determine the rate expression and perhaps the variation of the rate constant with temperature.

CHAPTER 4

The concentration of specific species can be determined by numerous methods and can generally be divided into two broad categories, namely chemical and physical. Chemical analysis implies a direct determination of one of the species by volumetric or gravimetric procedures, the former is preferred because of their rapidity. Any chemical method used must be more rapid with respect to the reaction being studied. The advantage of chemical analysis is that it gives an absolute value of the concentration.

Physical methods are usually more convenient than chemical methods. A physical method measures some physical property of the reaction mixture that changes substantially as the reaction proceeds. Ideally the physical property that is measured must vary in a simple manner with the concentrations of reactants and products. The best manner is a linear relationship with regards to the concentration. Common physical methods include optical methods such as polarimetry, refractometry, colourimetry and spectrophotometry; pressure measurements in gaseous reactions; nuclear magnetic resonance, conductivity, potentiometry, etc. Physical methods have the general advantage of being rapid so that more experimental points are available in a given time.[1] The data received from whatever method is used, can be used to determine the reaction by plotting the species concentration change with time.

A typical result for a kinetic run is illustrated in Fig. 4.1, where the concentration c of a reactant starts at zero time at an initial value c_o and decreases more and more slowly, approaching zero or some equilibrium value c_∞ asymptotically. At any time, the rate would be the negative of the slope of the curve expressed in the appropriate units.

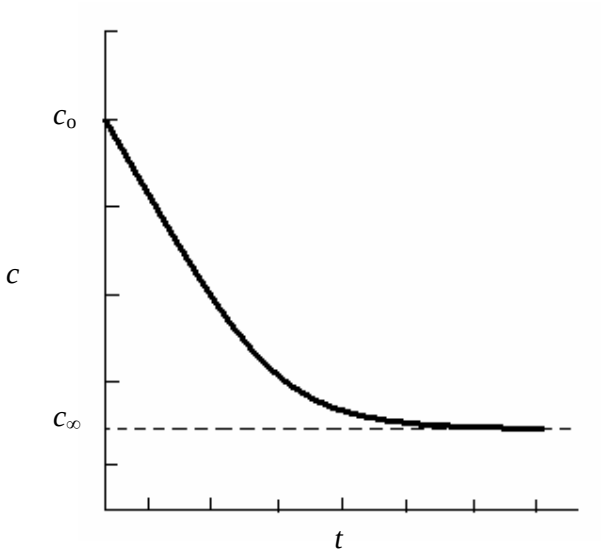

Figure 4.1: Concentration versus time for a typical reaction.[1]

A general rate equation can be determined for an n[th]-order reaction of a single component system. The stoichiometric equation for a single component[1] is indicated in Eq 4.8 below.

$$A \xrightarrow{k} Z.. \quad \text{... 4.8}$$

where Z.. = the concentration of the other reaction components which have been grouped together.

The form of the rate expression becomes,

$$\frac{-d[A]}{dt} = k[A]^n \quad \text{... 4.9}$$

Which can be integrated. The limits of integration are taken as $[A_0]$ = initial concentration at t = 0 and [A] = concentration at time t, respectively.

$$-\int_{[A_0]}^{[A]} \frac{d[A]}{[A]^n} = k\int_0^t dt \quad \text{... 4.10}$$

For a single component rate expression, there are several possible reaction orders, such as zero, first and second order. The integrated form of the common rate expression for zero, 1[st] and 2[nd] order reactions can be determined from Eq. 4.10 and are illustrated below:

For zero order in A: $[A] = [A_0] - kt$ **... 4.11**

For first order in A: $\ln[A] = -kt + \ln[A_0]$ **... 4.12**

or can be rewritten in the exponential form, $[A] = [A_0]e^{-kt}$ **... 4.13**

For second order in A: $\frac{1}{[A]} = kt + \frac{1}{[A_0]}$ **... 4.14**

In order to determine an acceptable rate equation, the experimentally determined concentration-time data is fitted to each of the integrated expressions in turn. A linear plot is obtained only when the integrated form of the correct rate law is used. The rate constant, k, can then be determined from the slope of the line.[4]

A very useful technique which can be used to simplify rate equations is *pseudo-order reactions.* Suppose a reaction has a second order rate equation:

$$R = k[A][D] \quad \text{... 4.15}$$

If the concentration of D is held essentially constant, then the rate equation becomes

$$R = k_{obs}[A] \quad \textbf{... 4.16}$$

The second order reaction has been transformed into a pseudo order reaction, where k_{obs} is the pseudo first-order rate constant and $k_{obs} = k[D]$. As mentioned previously, there are several methods by which this reaction equation can be achieved,[2] such as:

- By having a excess concentration of D ([D] >>>[A]) so that its concentration remains essentially constant.
- Using a buffer. If the reaction medium is water and D is either a hydronium ion or hydroxide ion, the use of a buffer could hold the concentration of D reasonably constant.
- The third method is illustrated by a first order solution reaction of a substance in the presence of its solid phase. If the dissolution rate of the solid is greater than the reaction rate of the dissolved solute, the solute concentration is maintained constant by the solubility equilibrium and the reaction becomes a pseudo zero order reaction.

Spectrophotometry is very useful in kinetic measurements because each molecule has a characteristic absorption spectrum. The Beer-Lambert law[6] provides a direct linear relationship between the concentration of a species; the intensity of the incident, I_0, and transmitted, I_t, monochromatic light and the electromagnetic radiation which the species absorbs.

$$Abs = -\log (I_0/I_t) = \varepsilon l c \quad \textbf{... 4.17}$$

where l = path length, ε = extinction coefficient, c = concentration and Abs = absorbance. The total absorbance of a solution containing more than one kind of absorbing substance is simply the sum of the individual absorbances.[7] The absorption of electromagnetic radiation can occur at any wavelength but particular interest with regards to this study is the absorption in the infrared, ultraviolet and visible region.

For the purpose of this study, the relationship between concentration and absorbance was used in order to determine the rate equation. All reactions were performed under pseudo first-order conditions. The change in absorbance, of a solution consisting of the reaction components, was plotted as a function of time after the components were mixed together. The plot obtained from

[6] P.W. Atkins, *Physical Chemistry*, London: Oxford University Press, 1994
[7] D.A. Skoog, D.M. West, F.J. Holler, S.R. Crouch, *Fundamentals of Analytical Chemistry*, 8th Ed., London: Brooks/Cole, 2004

the kinetic runs can be viewed as increasing or decreasing absorbance which represents the changing concentration of one of the reaction components. The observed first-order rate constants for the reactions were determined from Equation 4.18:

$$A_{obs} = A_f - (A_f - A_i)e^{-kt} \quad \textbf{... 4.18}$$

where A_{obs} = observed absorbance, A_f = final absorbance, A_i = inital absorbance, k = k_{obs} = pseudo first-order rate constant and t = time. The solid lines in the kinetic curves (Section 4.3.4) represent the fitted functions, with the points indicating experimental observations.

4.2.4 Reaction Half-Life

The reaction *half-life* ($t_{1/2}$) is defined as the time required for the reactant concentration to decay to one-half its initial value. The term is used to convey a qualitative idea of the time scale and has a quantitative relationship to the rate constant in simple cases.[4]

To determine the half-life of a reaction, the following substitutions are made: $[A] = \frac{[A_0]}{2}$ and $t = t_{1/2}$. Equation 4.12 for a first order equation now becomes,

$$t_{1/2} = \frac{\ln 2}{k} = \frac{0.693}{k} \quad \textbf{... 4.19}$$

The half-life for the other rate equations can be similarly defined.

4.2.5 Reaction Thermodynamics[3]

The rates of most chemical reactions are very sensitive to temperature fluctuations. Arrhenius[8] gave the first temperature dependent quantitative formulation of reaction rates. The following relationship between the specific rate constant, k, and the absolute temperature, T was determined to be:

$$k = Ae^{-Ea/RT} \quad \textbf{... 4.20}$$

where *A* and Ea are constants, which are called the pre-exponential factor and the activation energy respectively; R is the gas constant. Ea and *A* have different values for the forward and

[8] S. Arrhenius, *Z. Phys. Chem. (Leipzig)*, 1889, 4, 226

reverse reactions of a given chemical reaction. In practise, the reaction rate generally increases by a factor of 2 or 3 for each 10ºC rise in temperature.[1] The activation energy Ea and the constant *A* may be determined experimentally[9] from the values of k and T by applying the logarithmic form of Eq. 4.20.

$$\ln k = -Ea/RT + \ln A \quad \textbf{... 4.21}$$

A relationship between the parameters in Eq 4.20 and the equilibrium constant, K, has been determined to be,

$$K = \frac{k_f}{k_r} = \frac{A_f}{A_r}\exp\left[-\frac{(Ea_f - Ea_r)}{RT}\right] \quad \textbf{... 4.22}$$

where the subscript, *f* and *r*, indicate the values for the forward and reverse reaction.

At constant pressure and temperature, the thermodynamic equilibrium constant, K, can be written as

$$K = \exp(-\Delta G^o/RT)$$
$$= \exp(\Delta S^o/R)\exp(-\Delta H^o/RT) \quad \textbf{... 4.23}$$

where ΔG^o, ΔH^o and ΔS^o are the standard free-energy, standard enthalpy and standard entropy changes for the reaction.

4.2.6 Transition State Theory[4]

The parameters used in the transition state theory describe the temperature dependence of k_{exp}, the experimental rate constant, even for solution reactions that are much more complex than gas phases for which the original theory was formulated. Within the transition state theory, reactions are often illustrated in terms of "reaction coordinate diagrams". These are plots of the energy of the system versus the "reaction coordinate", which is an ambiguous measure of the extent to which the reactant has converted to product. The transition state, is the species at the highest energy point on the reaction coordinate diagram (Figure 4.2).

[9] A.E. Merbach, P. Moore, O.W. Howarth, C.H. McAteer, *Inorg. Chim. Acta*, 1980, 39, 129

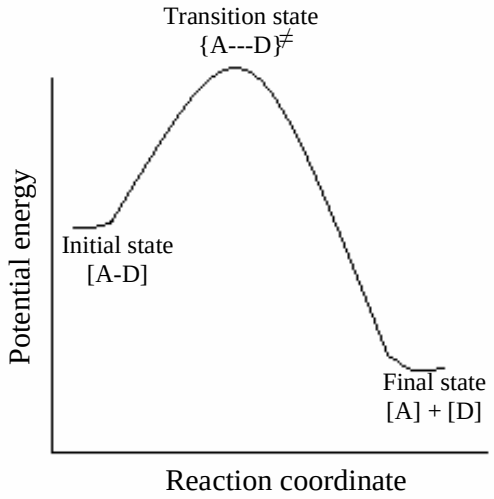

Figure 4.2: Reaction coordinate diagrams where the products are more stable than the initial reactants.

The transition state theory assumes that the reaction can be described by the following sequence:

$$A\text{-}D \underset{}{\overset{K^{\neq},\, k_1}{\rightleftharpoons}} \left\{A\text{----}D\right\}^{\neq} \xrightarrow{k_3} A + D$$

Activated complex
or transition state

... 4.24

The theory proposes that the activated complex will proceed to the products A and D, when the bond has sufficient thermal energy kT, so that the vibrational frequency $\nu = kT/h$ will equal the rate constant k_3 (k = Boltzmann's constant, h = Planck's constant). It is also assumed that the activated complex is always in equilibrium with the reactant, so that $K^{\neq} = \dfrac{[A\text{---}D]^{\neq}}{[A\text{-}D]}$. If $K^{\neq}$ is a normal equilibrium constant, then

$$\frac{d[D]}{dt} = k_3[A\text{---}D]^{\neq} = k_3K^{\neq}[A\text{-}D] = \frac{kT}{h}K^{\neq}[A\text{-}D] \qquad \textbf{... 4.25}$$

and

$$\ln K^{\neq} = -\frac{\Delta G^{\circ\neq}}{RT} = -\frac{\Delta H^{\circ\neq}}{RT} + \frac{\Delta S^{\circ\neq}}{R} \qquad \textbf{... 4.26}$$

where $\Delta G^{o\neq}$, $\Delta H^{o\neq}$ and $\Delta S^{o\neq}$ are the standard molar free energy, enthalpy and entropy differences between the activated complex and the reactants. If the first-order rate expression, $\frac{d[D]}{dt} = k_{exp}[A - D]$ is compared to Eq. 4.25, then substitution from Eq. 4.26 shows that

$$k_{exp} = \frac{kT}{h} K^{\neq} = \frac{kT}{h} \exp\left(\frac{-\Delta G^{o\neq}}{RT}\right) \quad \textbf{... 4.27}$$

An experimentally viable equation can be derived from substituting Eq. 4.26. The logarithmic form of the equation now becomes,

$$\ln\left(\frac{k_{exp}}{T}\right) = \ln\left(\frac{k}{h}\right) - \frac{\Delta H^{o\neq}}{RT} + \frac{\Delta S^{o\neq}}{R} \quad \textbf{... 4.28}$$

The value of $-\Delta H^{o\neq}/R$ can be determined from the slope of the graph of $\ln(k_{exp}/T)$ versus $1/T$. The value of $\Delta S^{o\neq}$ can be calculated from the intercept. The relationship in Eq. 4.28 is often called the Eyring equation.[10] An established Eyring plot can be used to calculate the rate constant at varying temperatures. Non-linear Arrhenius and Eyring plots are unusual. The deviations from a linear plot indicate reactions involving equilibria, parallel or consecutive reactions.[11]

[10] C.H. McAteer, P. Moore, *J. Chem. Soc., Dalton Trans.*, 1983, 353

[11] R.G. Wilkins, *Kinetics and Mechanism of Reactions of Transition Metal Complexes*, 2nd Ed., New York: VCH Publishers, Inc., 1991

4.3 IODOMETHANE OXIDATIVE ADDITION TO [Rh(acac)(CO)($PR_1R_2R_3$)] ($PR_1R_2R_3$ = PPh_3, $PCyPh_2$, PCy_2Ph and PCy_3).

4.3.1 Introduction

The oxidative addition of iodomethane to a number of rhodium(I) complexes, of the form [Rh(acac)(CO)($PR_1R_2R_3$)], is discussed in detail in this section. The kinetic data for these reactions were determined in order to obtain a reasonable reaction mechanism. Initial rates indicate that the reactions proceed *via* a second-order reaction to a rhodium(III) product with *trans*-iodomethane configuration.

4.3.2 Experimental

All reagents were of analytical grade. All organic solvents were pre-dried over alumina and then distilled before use. The [Rh(acac)(CO)($PR_1R_2R_3$)] complexes were prepared as described in Section 3.4.2.3

Kinetic measurements were conducted on an infrared Digilab FTS 2000 Fourier transform spectrometer utilizing a He-Ne laser at 632.6 nm, in the range of 3000 – 600 cm^{-1}. Solution infrared spectra were collected in the same range, in dry organic solvents, in a NaCl cell. The IR spectrometer was equipped with a temperature cell regulator (accurate within 0.3˚C). UV-Vis measurements were conducted on a Varian Carey 50 Conc. spectrometer equipped with a Julabo F12-mV temperature cell regulator (accurate within 0.1 ˚C) in a 1.00 cm quartz cuvette cell. The ^{31}P NMR spectra were obtained on a 300 MHz Bruker spectrometer. ^{31}P chemical shifts are reported relative to 85% H_3PO_4 (0 ppm) external standard; positive shifts are downfield. All kinetic measurement was conducted in dichloromethane unless otherwise indicated.

Data analysis was conducted by means of Microsoft Office Excel 2003[12] and MicroMath Scientist for Windows[13] Version 2.01.

4.3.3 Mechanistic Investigation

In order to construct a complete reaction mechanism, the following arguments were utilized as obtained from preliminary measurements, characterisation studies and literature:

1. The starting materials, [Rh(acac)(CO)(PPh_3)] **(1)**, [Rh(acac)(CO)($PCyPh_2$)] **(2)**, [Rh(acac)(CO)(PCy_2Ph)] **(3)** and [Rh(acac)(CO)(PCy_3)] **(4)** had been well characterised by IR, ^{31}P NMR and X-ray crystallography (Section 3.4.2 and 3.5). The data for complex **(1)** and **(4)** is in good agreement with data published by Leipoldt *et al.*[14] and Trzeciak *et al.*[15]

2. The oxidative addition reaction of iodomethane to the [Rh(acac)(CO)($PR_1R_2R_3$)] complexes was followed with the use of IR, ^{31}P NMR and UV-Vis spectroscopy. The use of IR, with regards to the carbonyl stretching frequency, and ^{31}P NMR was essential to determine the exact nature of the final product, whether alkyl or acyl. UV-Vis spectroscopy was used for quantitative determination of the rate constant, since this technique is more effective in utilising the minimal amount of starting material. The oxidative addition products Rh(III)-alkyl, [Rh(acac)(I)(CH_3)(CO)($PR_1R_2R_3$)], and Rh(III)-acyl, [Rh(acac)(I)($COCH_3$)($PR_1R_2R_3$)] (Fig. 4.3), of all four complexes were well characterised (IR and ^{31}P NMR, Section 4.3.3) and compare well with previously published reports.[16, 17, 18, 19, 20, 21, 22]

[12] Microsoft Office Professional Edition 2003 Copyright© 1985-2003 Microsoft Corporation
[13] MicroMath Scientist for Windows, Version 2.01, Copyright ©1986-1995, MicroMath, Inc.
[14] J.G. Leipoldt, S.S. Basson, L.D.C. Bok, T.I.A. Gerber, *Inorg. Chim. Acta*, 1978, 26, L35
[15] A.M. Trzeciak, B. Borak, Z. Ciunik, J.J. Ziółkowski, M.F.C. Guedes da Silva, A.J.L. Pombeiro, *Eur. J. Inorg. Chem.*, 2004, 1411
[16] J.G. Leipoldt, E.C. Steynberg, R. van Eldik, *Inorg. Chem.* 1987, 26, 3068
[17] S.S. Basson, J.G. Leipoldt, A. Roodt, J.A. Venter, *Inorg. Chim. Acta,* 1987, 128, 31
[18] A. Roodt, G.J. Steyn, *Recent Res. Devel. Inorganic Chem.*, 2000, 2, 1
[19] Y.S. Varshavsky, T.G Cherkasova, N.A. Buzina, L.S. Bresler, *J. Organometallic Chem.*, 1994, 464, 239
[20] G.J.J. Steyn, A. Roodt, J.G. Leipoldt, *Inorg. Chem.*, 1992, 31, 3477
[21] S.S. Basson, J.G. Leipoldt, A. Roodt, J.A. Venter, T.J. van der Walt, *Inorg. Chim. Acta,* 1986, 119, 35
[22] S.S. Basson, J.G. Leipoldt, J.T. Nell, *Inorg. Chim. Acta*, 1984, 84, 167

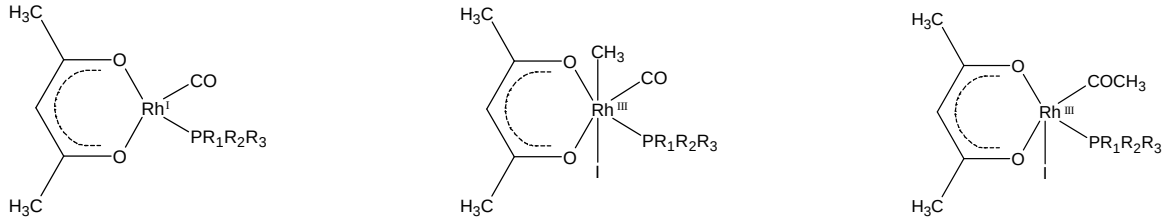

Figure 4.3: **General configuration of rhodium complexes (a) Rh(I) species, (b) Rh(III)-alkyl species and (c) Rh(III)-acyl species.**

3. A reaction mechanism was proposed by Basson *et al.*[21] for the oxidative addition of MeI to complexes of the form [Rh(acac)(CO)(PR_3)] (PR_3 = *p*-chlorophenyl, phenyl, *p*-methoxyphenyl) as illustrated in Scheme 4.1. In the case of [Rh(acac)(CO)(PPh_3)], evidence supporting an initial dissociative equilibrium of the Rh(I) complex was obtained. The oxidative addition proceeds through an equilibrium step K_1 to form an ionic intermediate, followed by the formation of the acyl intermediate **C** to yield the *trans*-addition alkyl product **D**. Although a k_2 value was previously reported,[22] Basson *et al*.[21] now believe the mechanism proceeds solely *via* **C.**

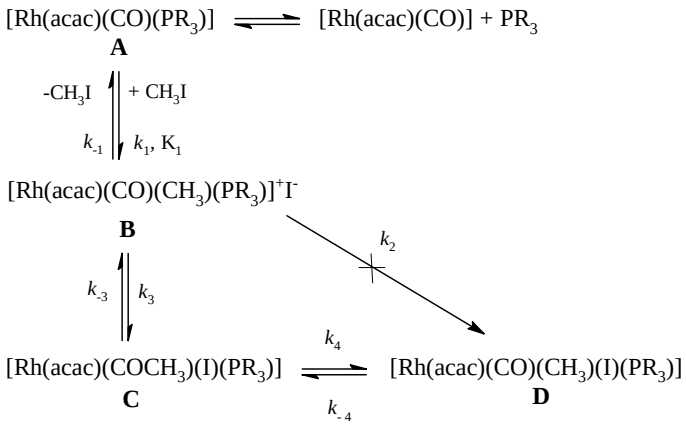

Scheme 4.1: **Reaction mechanism proposed by Basson *et al.*[21] for the oxidative addition of MeI to [Rh(acac)(CO)(PR_3)] (PR_3 = *p*-chlorophenyl, phenyl, *p*-methoxyphenyl).**

4. The oxidative addition of iodomethane to other [Rh(L,L'-Bid)(CO)(PR_3)] complexes (L,L'-Bid = mono anionic bidentate ligand, PR_3 = tertiary phosphine), have resulted in a different mechanism proposal. Oxidative addition reaction with complexes such as [Rh(OX)(CO)(PPh_3)] (OXH = 8-hydroxyquinoline) and [Rh(dmavk)(CO)(PPh_3)]

(dmavkH = dimethylaminovinylketone) first yield the *trans*-alkyl product,[23, 24] while [Rh(cupf)(CO)(PPh_3)] (cupfH = cupferron) gave the *cis*-alkyl complex.[17] Other complexes such as [Rh(Sacac)(CO)(PPh_3)][25] (SacacH = thioacetylacetone) also undergo oxidative addition reactions *via* the alkyl product before forming the acyl product. In the Sacac complex, a proposed mechanism, similar to Scheme 4.2 was suggested but without the reductive elimination step and the solvent pathway. The acyl formation (k_2) was assumed to be rapid relative to the alkyl formation[26] (k_1). Experimental results confirmed that the rate of disappearance of [Rh(Sacac)(CO)(PPh_3)] was equal to the rate of formation of the Rh(III) acyl species,[25] within experimental error. Studies of complexes consisting of N,S-bidentate ligands indicate that the complexes proceed *via* a mechanism[18] illustrated in Scheme 4.2. The reaction consists of a rapid oxidative addition equilibrium step to form the Rh(III) alkyl product, followed by a slower acyl formation. The solvent pathway does not observably contribute to the reaction rate.

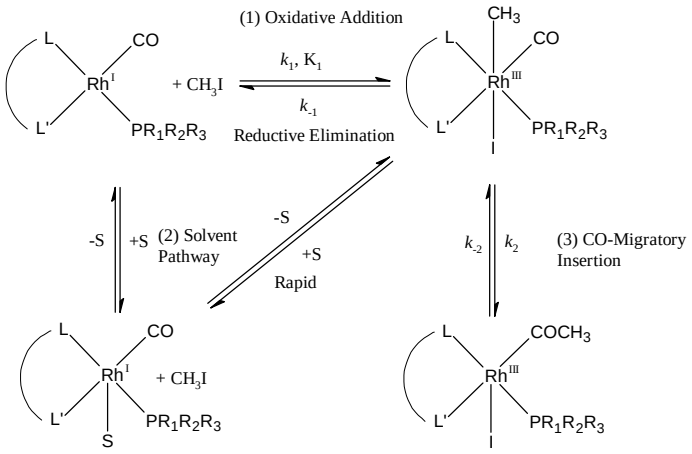

Scheme 4.2: The reaction scheme for the oxidative addition of iodomethane to [Rh^I(L,L'-Bid)(CO)(PR_3)] complexes and carbonyl migratory insertion. Two pathways for the oxidative addition reaction step are indicated, with the solvent indicated by S. The solvent path as well as the reductive elimination step is usually determined from the intercept.[18]

5. With regards to the reactions investigated in this study, initial runs of the oxidative addition reaction of iodomethane to [Rh(acac)(CO)($PR_1R_2R_3$)] complexes, resulted in the rapid formation of the Rh(III)-alkyl[1] species and then a slower formation of the Rh(III)-

[23] K.G. van Aswegen, J.G. Leipoldt, I.M. Potgieter, G.J. Lamprecht, A. Roodt, G.J. van Zyl, *Transition Met. Chem.*, 1991, 16, 369
[24] L.J. Damoense, W. Purcell, A. Roodt, *Rhodium Express*, 1995, 14, 6
[25] J.G. Leipoldt, S.S. Basson, L.J. Botha, *Inorg. Chim. Acta*, 1990, 168, 215
[26] C.H. Cheng, B.D. Spivack, R. Eisenberg, *J. Am. Chem. Soc.*, 1977, 99, 3003

acyl or Rh(III)-alkyl[2] isomer species (Fig. 4.4 – 4.12). The focus of this study was aimed at the oxidative addition step. A detailed study of the migratory insertion and isomerisation to Rh(III)-acyl and Rh(III)-alkyl[2] isomer was considered to be beyond the scope of this present study but will be investigated at a later stage.

6. The oxidative addition of iodomethane to [Rh(acac)(CO)(**PPh_3**)] (1977.6 cm^{-1}) resulted in a rapid alkyl[1] formation (2071.5 cm^{-1}), followed by a slower acyl formation (1720.5 cm^{-1}) as indicated by repetitive IR scans (Fig. 4.4). As the alkyl[1] started to disappear, the acyl was still increasing to a maximum absorbance.

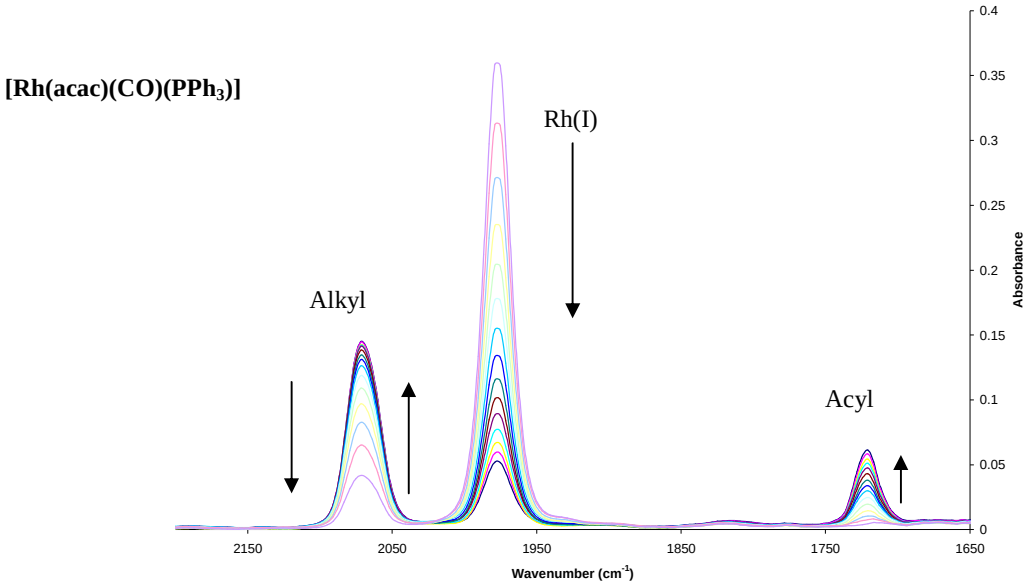

Figure 4.4: **Infrared spectra of oxidative addition of MeI to [Rh(acac)(CO)(PPh_3)] in dichloromethane at 25°C. Spectra indicates the disappearance of Rh(I) species with simultaneous increase of the alkyl[1] peak. The acyl peak formation corresponds to the disappearance of the alkyl[1] species. [Rh(acac)(CO)(PPh_3)] = 3.12 x 10^{-3} M, [CH_3I] = 0.165 M, Δt = 16.5 s, k_{obs} = 6.20(9) x 10^{-3} s^{-1}.**

7. Repetitive ^{31}P NMR scans (Fig. 4.5) of the same reaction indicated that after acyl formation (37.7 ppm), a Rh(III)-alkyl[2] (29.5 ppm) slowly began to form after 28 minutes which was not indicated by the IR spectra. Higher concentrations of **(1)** may be required to reveal the presence of the new alkyl[2] isomer by IR spectra, however the presence of the isomer was only reported by Basson *et al.*[21] and not by Varshavsky *et al.*[19]

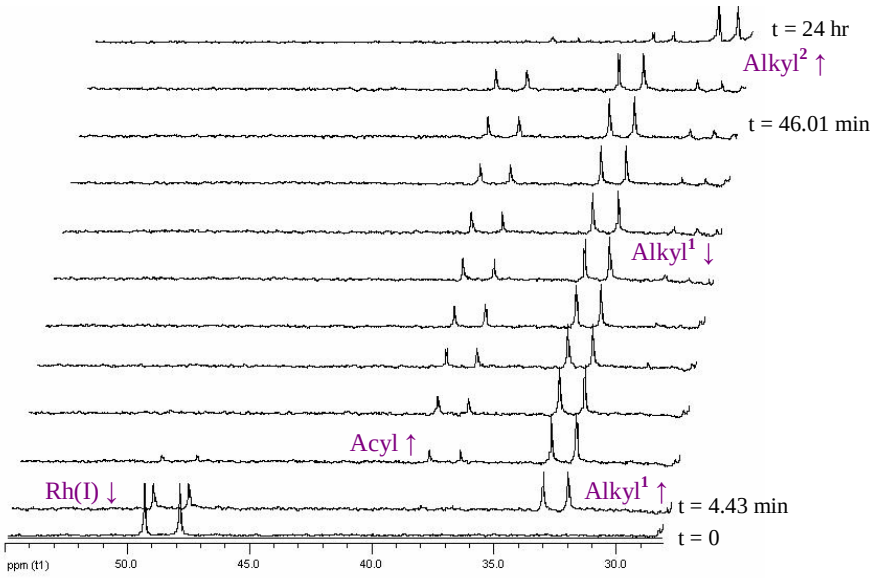

Figure 4.5: **Observed ^{31}P-NMR spectra for the disappearance of the four co-ordinated [Rh(acac)(CO)(PPh_3)] species and the formation of the alkyl^1, acyl and alkyl^2 intermediate products in dichloromethane at 25°C. [Rh(acac)(CO)(PPh_3)] = 3.583x10^{-2} M, [CH_3I] = 0.156 M, Δt = 3 min, k_{obs} = 5.3(8) x 10^{-3} s^{-1}.**

8. In the case of the $PCyPh_2$ complex, the IR data for the oxidative addition of CH_3I to [Rh(acac)(CO)(**$PCyPh_2$**)] indicated the formation of an alkyl^1 species (2067.7 cm^{-1}) which is not followed by acyl formation (Fig 4.6). An interesting observation, which cannot be explained currently, was that the breadth of the IR peak at 1975.1 cm^{-1} (starting complex) and the alkyl^1 at 2067.7 cm^{-1} for the $\underline{PCyPh_2}$ complex (Fig 4.6) are significantly broader (almost twice) compared to the corresponding peaks in the $\underline{PPh_3}$ complex (Fig 4.4). This might, in principle obscure other species. However ^{31}P NMR showed there was no other phosphine containing species present. ^{31}P NMR indicated the very rapid conversion of the Rh(I) complex to the alkyl^1 intermediate (35.8 ppm) followed by the formation of an alkyl^2 species (46.3 ppm) after 24 hours (Fig 4.7). No Rh(III)-acyl formation is indicated by NMR.

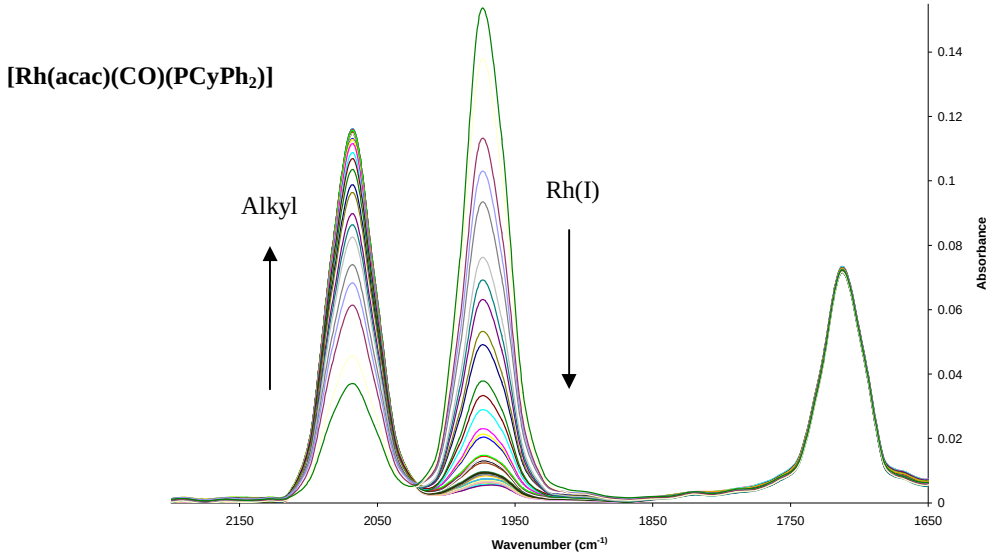

Figure 4.6: **Infrared spectra of the disappearance of [Rh(acac)(CO)($PCyPh_2$)] with the simultaneous appearance of the alkyl[1] species in dichloromethane at 25ºC. [Rh(acac)(CO)($PCyPh_2$)] = 3.26×10^{-3} M, [CH_3I] = 0.115 M, Δt = 16.5 s, $k_{obs} = 7.16(7) \times 10^{-3}$ s^{-1}.**

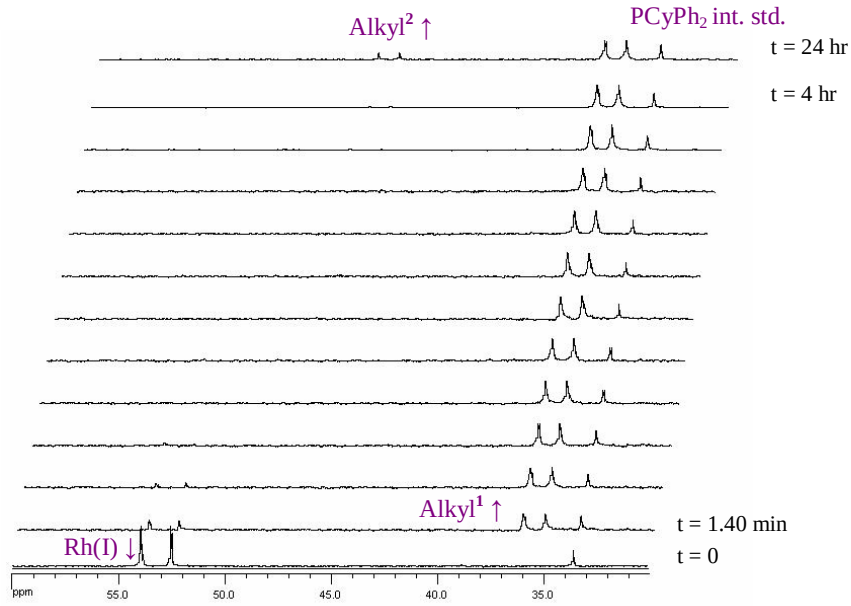

Figure 4.7: **Observed ^{31}P-NMR spectra for the disappearance of the four co-ordinated [Rh(acac)(CO)($PCyPh_2$)] species and the formation of the alkyl[1] and alkyl[2] products in dichloromethane at 25ºC. $PCyPh_2$ internal standard at 33.6 ppm. [Rh(acac)(CO)($PCyPh_2$)] = 3.44×10^{-2} M, [CH_3I]= 0.156 M, Δt = 0.9 min, $k_{obs} = 9.7(5) \times 10^{-3}$ s^{-1}.**

9. A trend similar to that for complex **(2)** is also found for [Rh(acac)(CO)(**PCy_2Ph**)]. Repetitive IR spectra (Fig. 4.8) shows the disappearance of the Rh(I) complex followed by the simultaneous increase of the alkyl[1] species (2052.3 cm^{-1}). The formation of the alkyl[1] species occurs at a much slower rate than for complexes **(1)** and **(2)**. No formation of the acyl species was indicated in the IR spectra. In this case, the IR peaks (Fig 4.8) had yet another interesting asymmetrical and broad shape. However repeated recrystallization yielded the same form of peaks every time. Repetitive NMR scans (Fig. 4.9) further showed that the alkyl[1] intermediate (43.0 ppm) is followed by a slower appearing acyl species after *ca* 37 minutes (38.1 ppm). The Rh(III)-alkyl[2] isomer (41.7 ppm) begins to form only after 3 hours.

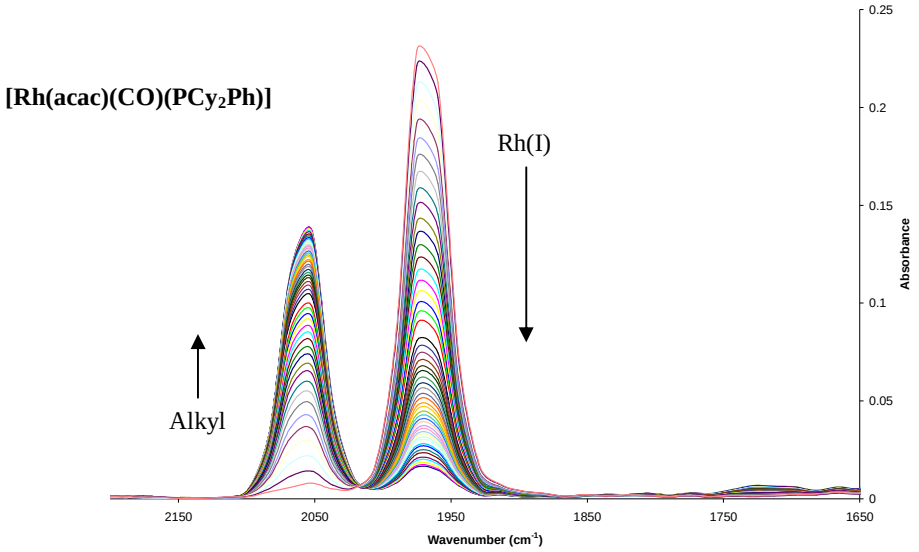

Figure 4.8: **Infrared spectra of the disappearance of [Rh(acac)(CO)(PCy_2Ph)] with the simultaneous appearance of the alkyl[1] species in dichloromethane at 25°C. [Rh(acac)(CO)(PCy_2Ph)] = 3.23×10^{-3} M, [CH_3I] = 0.134 M, Δt = 16.5 s, $k_{obs} = 1.014(2) \times 10^{-3}$ s^{-1}.**

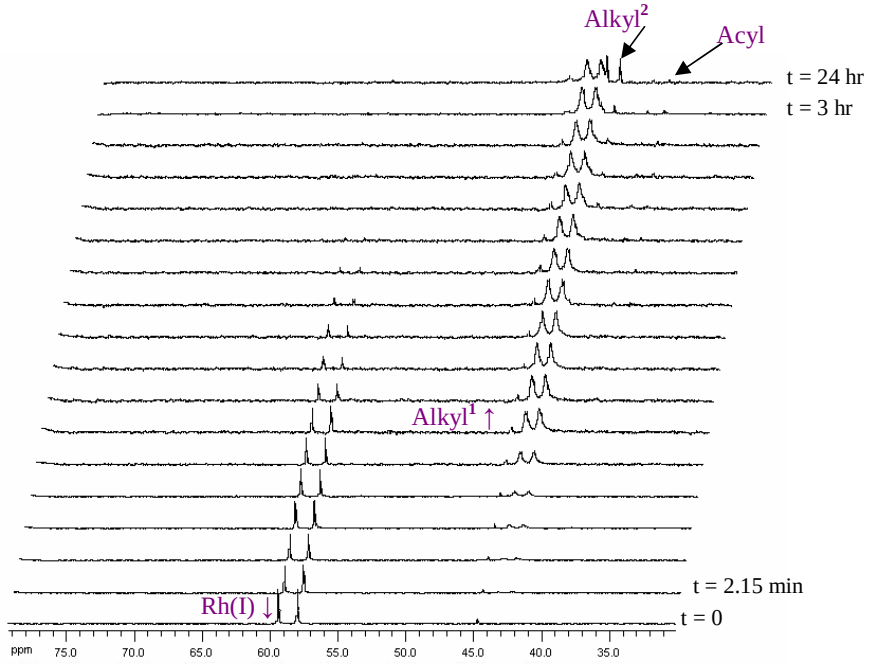

Figure 4.9: **Observed ^{31}P-NMR spectra for the disappearance of the four co-ordinated [Rh(acac)(CO)(PCy_2Ph)] species and the formation of the alkyl^1, acyl and alkyl^2 intermediate products in dichloromethane at 25°C. PCy_2Ph internal standard at 44.8 ppm. [Rh(acac)(CO)(PCy_2Ph)] = 3.58×10^{-2} M, [CH_3I] = 0.156M, Δt = 1.4min, $k_{obs} = 1.25(2)\times10^{-3}$ s^{-1}.**

10. In the case of the fourth tertiary phosphine PCy_3, the IR data for the oxidative addition of CH_3I to [Rh(acac)(CO)(**PCy_3**)] indicates rapid alkyl^1 formation (2052.3 cm^{-1}) and a small growth at 1720.5 cm^{-1} which could be assumed to be the acyl peak (Fig. 4.10). Repetitive ^{31}P NMR scans indicated that the alkyl^1 intermediate (50.2 ppm) is first followed by the formation of the alkyl^2 isomer (45.0 ppm) after 12 minutes and then by acyl formation (40.2 ppm) after 28 minutes (Fig. 4.11).

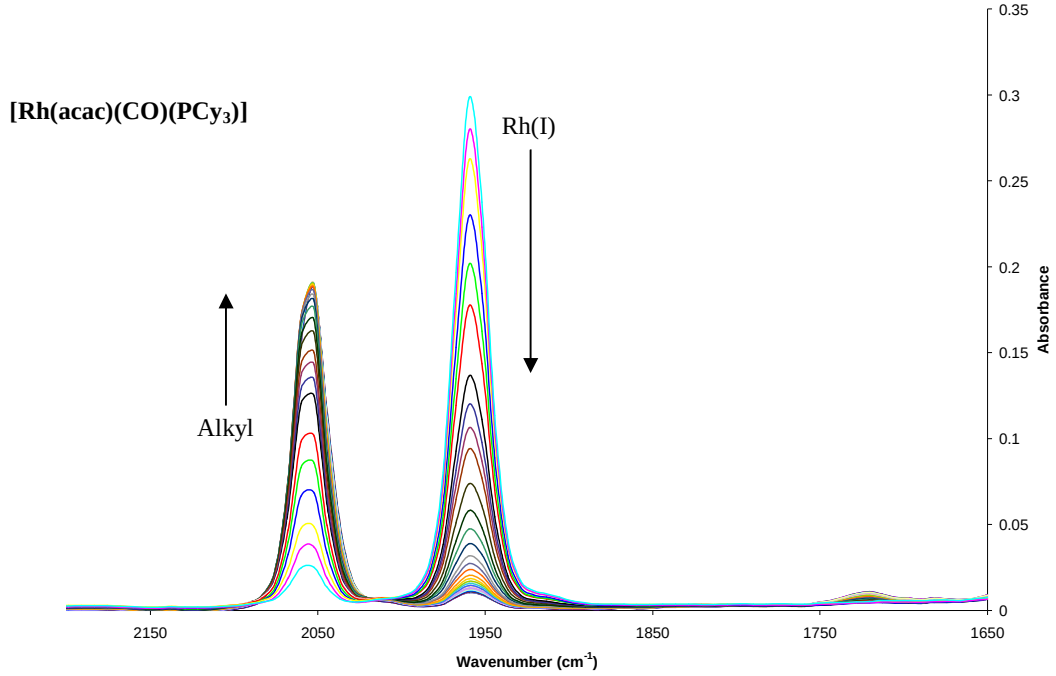

Figure 4.10: **Infrared spectra of the oxidative addition of MeI to [Rh(acac)(CO)(PCy_3)] in dichloromethane at 25°C. Rh(I) species disappears with simultaneous increase of alkyl[1] peak. [Rh(acac)(CO)(PCy_3)] = 3.21 x 10^{-3} M, [CH_3I] = 0.106 M, Δt = 24.8 s, k_{obs} = 3.06(1) x 10^{-3} s^{-1}.**

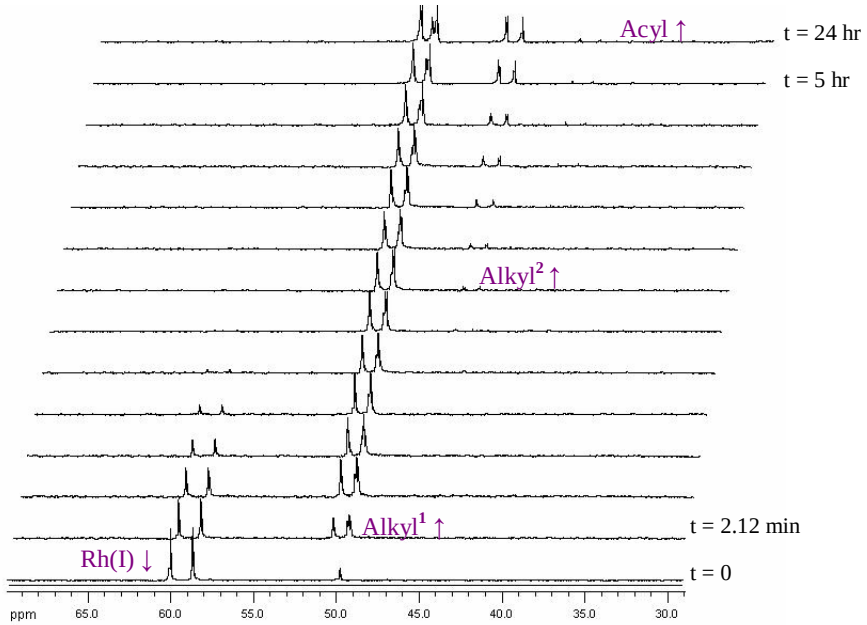

Figure 4.11: **Observed ^{31}P-NMR spectra for the disappearance of the four co-ordinated [Rh(acac)(CO)(PCy_3)] species and the formation of the alkyl[1], alkyl[2] and acyl intermediate products in dichloromethane at 25°C. PCy_3 internal standard at 49.8 ppm. [Rh(acac)(CO)(PCy_2Ph)] = 3.463x10^{-2} M, [CH_3I] = 0.156 M, Δt = 1.5 min, k_{obs} = 4.6(4)x10^{-3} s^{-1}**

11. The oxidative addition of iodomethane to the Rh(I) complexes is assumed to be an equilibrium reaction as suggested by Roodt *et al.*[18] At low iodomethane concentrations a small amount of alkyl[1] is formed from the Rh(I) reactant (Fig. 4.12(a)), while at higher [CH_3I], more of the alkyl[1] species is formed and at a much faster rate (Fig. 4.12(b)). In this specific example, [Rh(acac)(CO)($PCyPh_2$)], no acyl intermediate is indicated. The large yield of the alkyl[1] species suggests a reasonably large equilibrium constant (K_1).

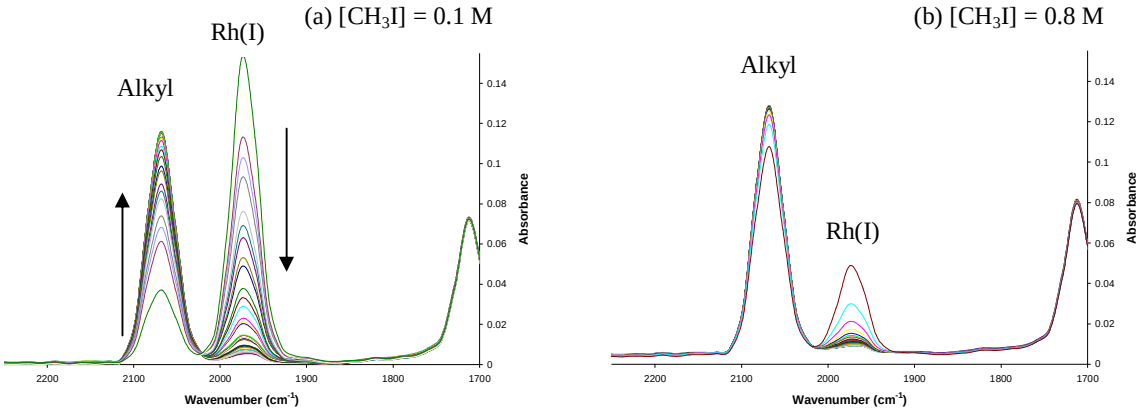

Figure 4.12: **Repetitive infrared scans of the disappearance of [Rh(acac)(CO)($PCyPh_2$)] with the simultaneous appearance of the alkyl[1] species in dichloromethane at 25°C. [Rh(acac)(CO)($PCyPh_2$)] = 3.26 x 10^{-3} M, Δt = 16.5 s, (a) k_{obs} = 7.16(7) x 10^{-3} s^{-1}, (b) k_{obs} = 4.54(5) x 10^{-2} s^{-1}**

12. In this study, no prominent solvent assisted pathway, as typically indicated by significant [CH_3I] independent reactions (large intercepts in graphical plots of k_{obs} vs [CH_3I]) was observed, however as future studies will consist of investigating various solvents, the pathway is still included in the reaction scheme (Scheme 4.3).

13. Based on all the above arguments, a proposed reaction scheme of the oxidative addition reaction for the complexes **(1)** to **(4)** representing the possible pathways are presented in Scheme 4.3.

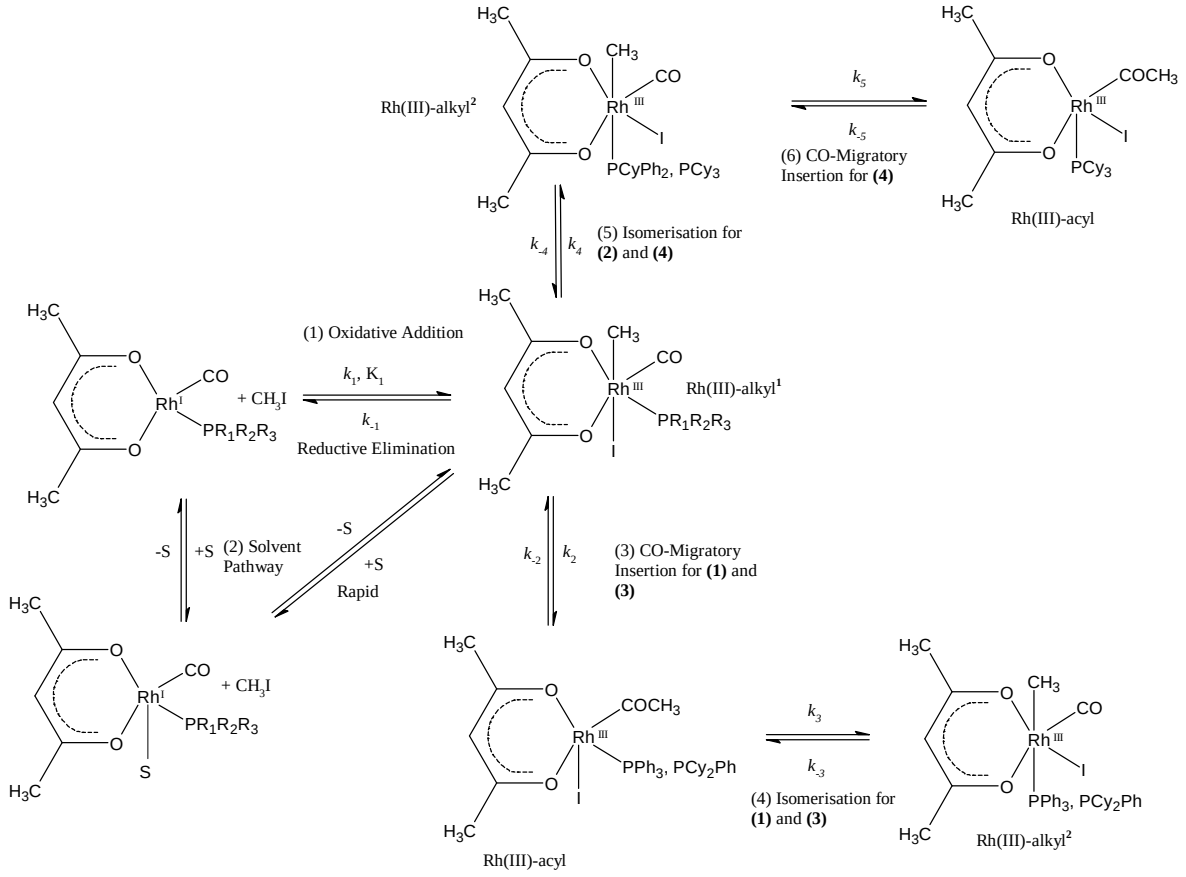

Scheme 4.3: **General reaction pathway for the reaction of [Rh(acac)(CO)($PR_1R_2R_3$)] complexes with iodomethane (CH_3I).**

Based on Scheme 4.3, the mechanism for the reaction of rhodium(I) acetylacetonato carbonyl phosphine complexes could be derived as given in the following paragraph.

The rate of formation of the Rh(III)-alkyl^{1} species is given by Eq. 4.29. The reaction from the Rh(III)-alkyl^{1} to Rh(III)-acyl species, in the case of complexes **(1)** and **(3)**, or to Rh(III)-alkyl^{2} isomer, in the case of complexes **(2)** and **(4)**, is considered to be very slow and is not included in the rate law for the oxidative addition.

$$R = \frac{d[Rh^{I}]}{dt} = - k_1[Rh^{I}][MeI] + k_{-1}[Rh^{III}\ alkyl] \qquad \textbf{... 4.29}$$

$[Rh^{III}\ alkyl] = [Rh^{I}]_0 - [Rh^{I}]$ *substitute in Eq. 4.29 gives,*

$$\frac{d[Rh^{I}]}{dt} = -[Rh^{I}]\{k_1[MeI] + k_{-1}\} + k_{-1}[Rh^{I}]_0$$

Call $k_1[MeI] + k_{-1} = k$ *and let* $k_{-1}[Rh^I]_0 = h$

The differential equation then becomes,

$$\frac{d[Rh^I]}{dt} = -k\,[Rh^I] + h \qquad \textbf{... 4.30}$$

To solve Eq. 4.30, first look at the homogenous part

$$\frac{d[Rh^I]}{dt} = -k\,[Rh^I]$$

Solution becomes $[Rh^I] = De^{-kt}$ **... 4.31**

To solve Eq. 4.30, let D *be thought of as a function of time* t

$[Rh^I] = D(t)e^{-kt}$ **... 4.32**

and substitute this assumption into Eq. 4.30

$$\frac{d[Rh^I]}{dt} = -k\,D(t)e^{-kt} + D'(t)e^{-kt} = -k\,D(t)e^{-kt} + h$$

$D'(t)e^{-kt} = h$

$D'(t) = h\,e^{kt}$

By integration the equation becomes, $D(t) = \frac{h}{k}e^{kt} + C_2$

By substituting into Eq. 4.32, will give the integrated rate form for a pseudo first order reaction

$$[Rh^I] = \frac{h}{k} + C_2\,e^{-kt} \qquad \textbf{... 4.33}$$

where $\frac{h}{k}$ *= constant term,* C_2 *= time dependent term*

and k = *the observed rate constant* $= k_1[MeI] + k_{-1}$ **... 4.34**

14. Typical IR and ^{31}P NMR spectra for the oxidative addition of CH_3I to complexes **(1)** to **(4)** were presented in Figures 4.4 – 4.12 and have already been discussed in detail in Section 4.3.3. The disappearance of the Rh(I) carbonyl peak and the formation of the Rh(III)-alkyl carbonyl peak as monitored by infrared directly reflects the results determined by ^{31}P NMR (Fig. 4.4 - 4.12). Both techniques yielded identical observed rate constants, within experimental error. Table 4.1 lists the ^{31}P NMR spectral parameters for the rhodium phosphine complexes.

Table 4.1: ^{31}P NMR spectral parameters of rhodium acetylacetonato phosphine complexes.

Complex		ν(CO) (cm^{-1})	δ ^{31}P NMR (ppm)	$^{1}J_{Rh-P}$ (Hz)
Rh(acac)(CO)(PPh_3)	Rh(I)	1977.6	48.6	176.9
	Rh(III)-alkyl[1]	2071.5	32.8	124.6
	Rh(III)-acyl	1720.5	37.7	153.3
	Rh(III)-alkyl[2]	-	29.5	118.3
Rh(acac)(CO)($PCyPh_2$)	Rh(I)	1959.3	53.3	171.3
	Rh(III)-alkyl[1]	2067.0	35.8	123.2
	Rh(III)-alkyl[2]	-	46.3	118.5
Rh(acac)(CO)(PCy_2Ph)	Rh(I)	1948.8	58.8	168.3
	Rh(III)-alkyl[1]	2052.3	43.0	122.1
	Rh(III)-acyl	-	38.1	146.3
	Rh(III)-alkyl[2]	-	41.7	117.9
Rh(acac)(CO)(PCy_3)	Rh(I)	1945.3	59.3	164.3
	Rh(III)-alkyl[1]	2052.3	50.2	118.1
	Rh(III)-alkyl[2]	-	45.0	116.4
	Rh(III)-acyl	1720.5	40.2	144.4

4.3.4 Results and Discussion

The oxidative addition reaction of [Rh(acac)(CO)($PR_1R_2R_3$)] with iodomethane was studied in dichloromethane and as the carbonyl migratory-insertion and alkyl isomerisation reactions were very slow, only the oxidative addition / reductive elimination reactions were investigated (Scheme 4.3, Reaction 1). A variable temperature study was also conducted to determine the activation parameters. All four complexes were investigated with the use of IR, ^{31}P NMR and UV-Vis spectroscopy. Typical kinetic data, as illustrated in Figure 4.13 below, was fitted to $A_{obs} = A_f - (A_f - A_i)e^{-kobs\ t}$ (Eq. 4.18) in order to determine the observed rate constant, k_{obs}.

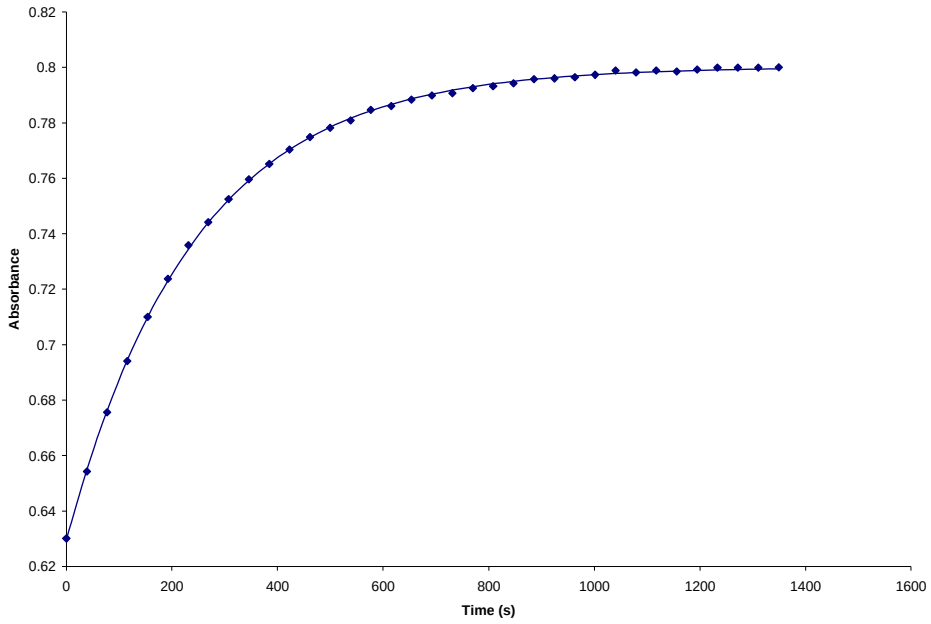

Figure 4.13: Typical UV-Vis absorbance versus time data for the oxidative addition reaction of [CH_3I] with [Rh(acac)(CO)($PCyPh_2$)] at 315 nm in dichloromethane at 25°C. [Rh] = 9.61 x 10^{-5} M, [CH_3I] = 0.0523 M.

(a) IR Studies

Graphs of the observed first-order rate constants, k_{obs} versus [CH_3I] were plotted from the infrared data and yielded a linear relationship with small intercepts (Fig. 4.14) for all four Rh(I) complexes. The fits are consistent with the first step in the reaction mechanism, as illustrated in Scheme 4.3, where the oxidative addition is an equilibrium reaction. The observed pseudo first order rate constant was fitted to Eq. 4.34, in order to determine the rate constant for the oxidative addition and reductive elimination steps, k_1 and k_{-1}, respectively.

$$k_{obs} = k_1[MeI] + k_{-1} \quad \textbf{… 4.34}$$

The results were surprising. Both the IR stretching frequencies and ^{31}P NMR coupling constants suggested that the electron density on the Rh(I) metal centre increases from complex **(1)** to **(4)** (Section 3.5.6). This suggested that [Rh(acac)(CO)(PCy_3)], with the highest electron density would have the fastest rate for the oxidative addition of iodomethane. The steric demand of the phosphine ligands, as indicated by the effective cone angle (Table 4.2), also increases from complex **(1)** to **(4)**. It was therefore expected that steric parameters would have a minimal effect with respect to electron density. From this assumption, it was thought the rate constant k_1 would increase systematically from **(1)** to **(4)**.

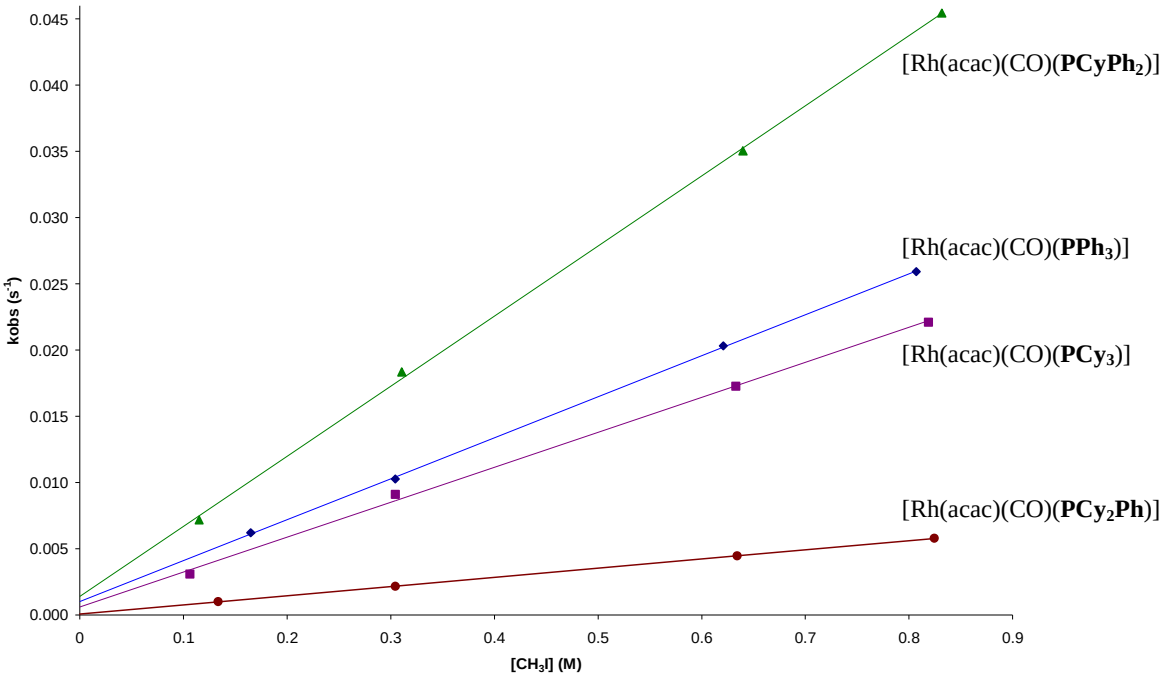

Figure 4.14: **The effect of various phosphine ligands on rhodium(I) acetylacetonato carbonyl complexes undergoing oxidative addition with [CH_3I] under pseudo first-order conditions for the formation of [Rh(acac)(I)(CH_3)(CO)($PR_1R_2R_3$)] in dichloromethane at 25°C, [Rh(acac)(CO)($PR_1R_2R_3$)] = 3 x 10^{-3}M. (Appendix, Table E.1)**

Table 4.2: **Infrared spectroscopic kinetic data obtained from Figure 4.14 for the oxidative addition of CH_3I to [Rh(acac)(CO)($PR_1R_2R_3$)] complexes in dichloromethane at 25°C.**

[Rh(acac)(CO)($PR_1R_2R_3$)]	Rate Constant		K_1 (M^{-1})	Effective cone angle (°)
	k_1 (x 10^{-3} $M^{-1}s^{-1}$)	k_{-1} (x 10^{-3} s^{-1})		
PPh_3	30.9(3)	1.0(2)	30(5)	149.3
$PCyPh_2$	52.9(8)	1.4(4)	38(12)	151.2
PCy_2Ph	6.92(4)	0.07(2)	95(27)[a]	163.5
PCy_3	26.4(8)	0.6(4)	44(30)[a]	169.5

[a]Since the intercept indicated a large esd, values should be treated as estimations.

The results, as indicated in Figure 4.14 and Table 4.2, with respect to the assumption made, is certainly surprising. The value of k_1 for **(1)** is 1.17 times larger than for **(4)** even though [Rh(acac)(CO)(**PCy_3**)] has the highest electron density. The steric demand of the PCy_3 ligand retards the ease with which the incoming iodomethane coordinates to the metal centre. The rate for [Rh(acac)(CO)(**$PCyPh_2$**)] was expected to be slightly faster than for **(1)**, however its k_1 value is 1.79 times larger than **(1)** and 7.64 times larger than **(3)**. The rate of [Rh(acac)(CO)(**PCy_2Ph**)] is the slowest at $k_1 = 6.92\ M^{-1}s^{-1}$. The large uncertainty in the k_{-1} value for complexes **(3)** and **(4)** prevented the more accurate determination of the equilibrium constant K_1.

(b) UV-Vis Studies

The kinetics were also monitored by UV-Vis spectroscopy and gave similar results, within experimental error, to that found by IR and NMR spectroscopy as described above. The systems were studied at different temperatures in order to determine the effect which the various phosphines may have on the oxidative addition reaction. The results are presented in Figures 4.15 – 4.18, and the rates determined by UV-Vis spectroscopy at the various temperatures, all follow the same trend as seen by IR spectroscopy (Fig. 4.14). The rates increase from complex **(3) → (4) → (1) → (2)**. Table 4.3 lists the rate constants determined for the oxidative addition of iodomethane to the [Rh(acac)(CO)($PR_1R_2R_3$)] complexes as determined by UV-Vis spectroscopy. As expected, the rate of each complex generally increases by a factor of two for each 10ºC increase of temperature. The near zero value of k_{-1} suggests that a solvent assisted pathway does not occur for these specific complexes in dichloromethane. The large equilibrium value for the oxidative addition reaction indicates the favourability towards the forward reaction. Table 4.3 shows a comparison between the rate constants determined by IR spectroscopy (25 ºC) and the rate constants determined by UV-Vis spectroscopy (*ca*. 25 ºC). The values are equivalent within experimental error.

Due to spectroscopic interference between the Rh(I), Rh(III)-alkyl and Rh(III)-acyl data readings, a combined effect was experienced at high iodomethane concentrations which led to lower absorbance readings at infinity (Abs_∞) than expected. As a result of this bi-phasic system the value of Abs_∞ was restricted to a higher value resulting in larger standard deviations than desired. The equilibrium constant, K_1, could not always be accurately determined due to the large uncertainties in some k_{-1} values. Future work will consist of more oxidative addition reactions at low iodomethane concentrations to increase the accuracy of all the K_1 values.

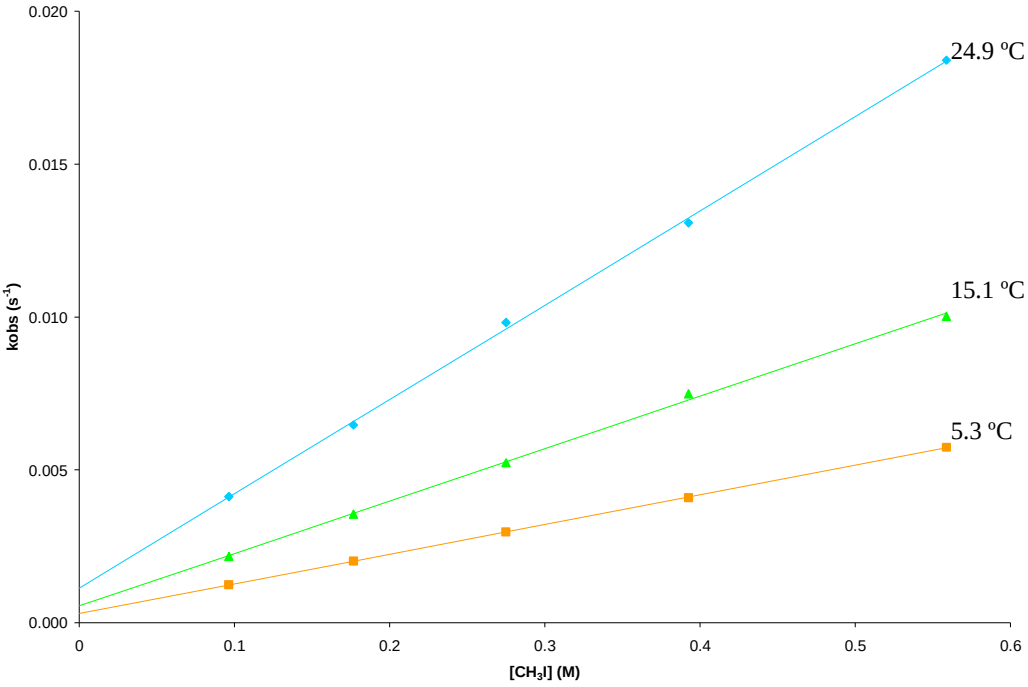

Figure 4.15: **Temperature and $[CH_3I]$ dependence of the pseudo-first order rate constant for the formation of $[Rh(acac)I(CH_3)(CO)(PPh_3)]$ in dichloromethane, (λ = 322 nm) $[Rh(acac)(CO)(PPh_3)] = 1.01 \times 10^{-4}$ M. (Appendix, Table E.2)**

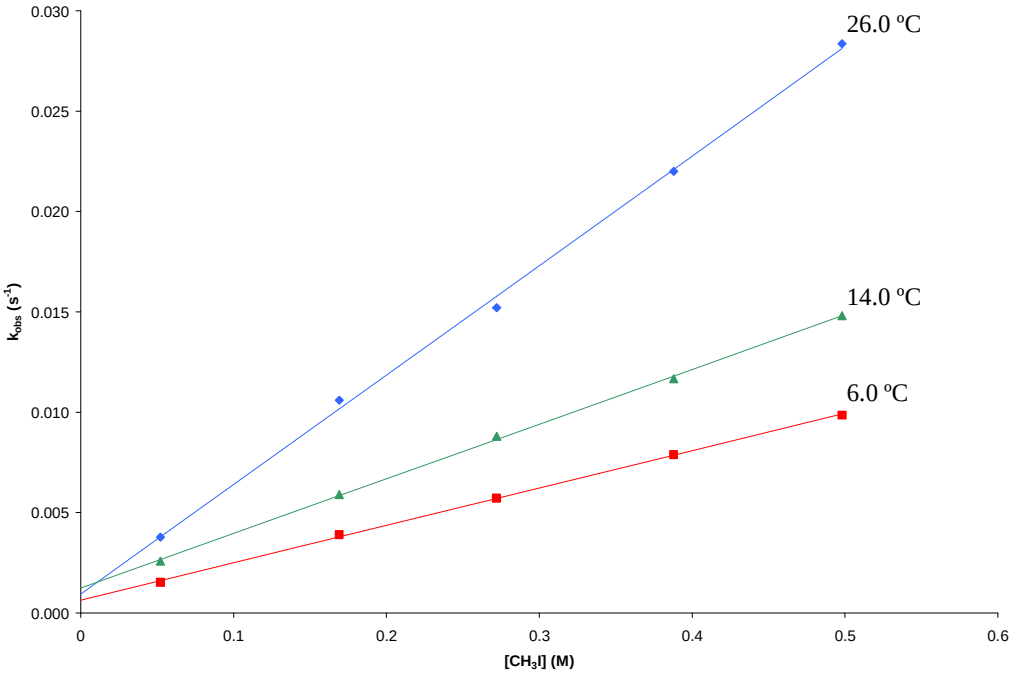

Figure 4.16: **Temperature and $[CH_3I]$ dependence of the pseudo-first order rate constant for the formation of $[Rh(acac)I(CH_3)(CO)(PCyPh_2)]$ in dichloromethane, (λ = 315 nm) $[Rh(acac)(CO)(PCyPh_2)] = 9.61 \times 10^{-5}$ M. (Appendix, Table E.3)**

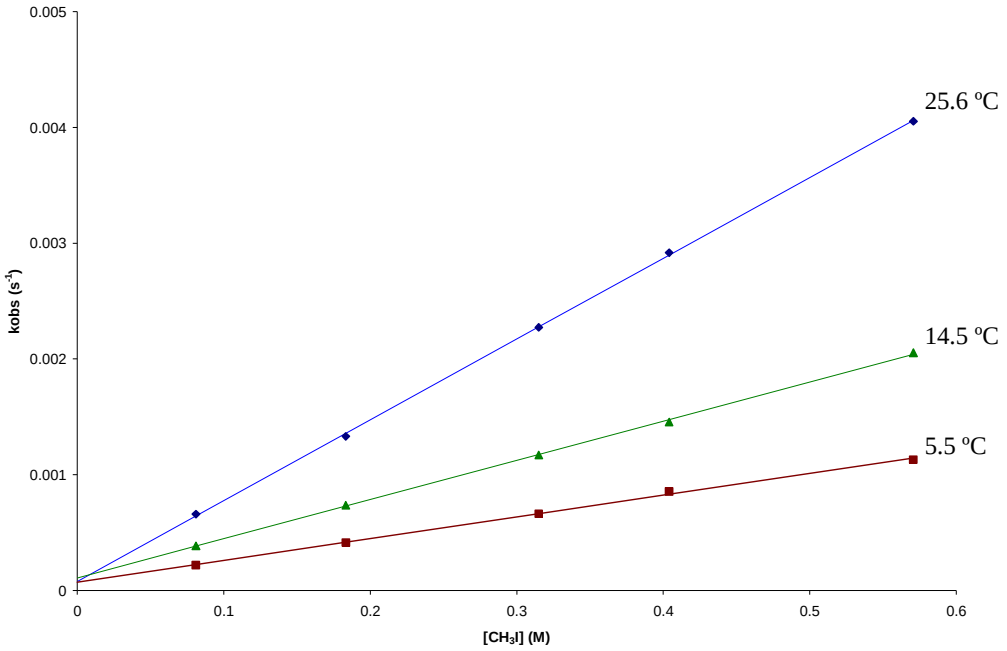

Figure 4.17: **Temperature and $[CH_3I]$ dependence of the pseudo-first order rate constant for the formation of $[Rh(acac)I(CH_3)(CO)(PCy_2Ph)]$ in dichloromethane, (λ = 323 nm) $[Rh(acac)(CO)(PCy_2Ph)] = 9.10 \times 10^{-5}$ M. (Appendix, Table E.4)**

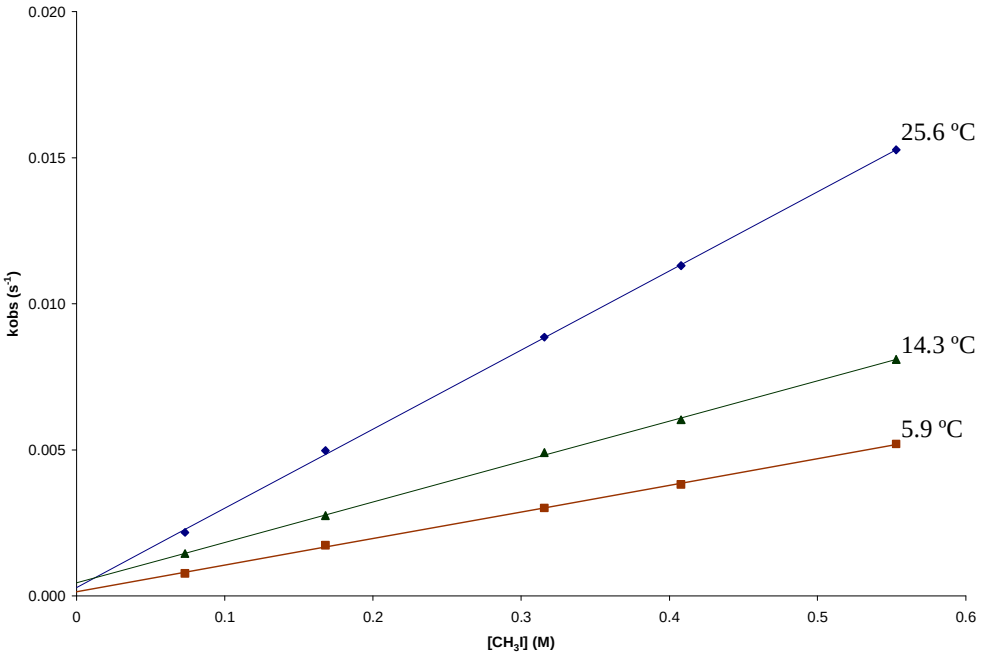

Figure 4.18: **Temperature and $[CH_3I]$ dependence of the pseudo-first order rate constant for the formation of $[Rh(acac)I(CH_3)(CO)(PCy_3)]$ in dichloromethane, (λ = 322 nm) $[Rh(acac)(CO)(PCy_3)] = 9.38 \times 10^{-5}$ M. (Appendix, Table E.5)**

Table 4.3: UV-Vis kinetic data obtained from Figure 4.15 – 4.18 for the oxidative addition of CH_3I to $[Rh(acac)(CO)(PR_1R_2R_3)]$ complexes at different temperatures in dichloromethane.

$[Rh(acac)(CO)(PR_1R_2R_3)]$	Temperature (°C)	Rate Constant				K_{eq} (M^{-1}) [b]
		k_1 (x 10^{-3} $M^{-1}s^{-1}$)		k_{-1} (x 10^{-3} s^{-1})		
		IR[a]	UV-Vis	IR[a]	UV-Vis	
PPh_3	24.9	30.9(3)	30.8(5)	1.0(2)	1.1(2)	27(4)
	15.1		17.2(4)		0.5(1)	31(7)
	5.3		9.71(4)		0.30(1)	33(1)
$PCyPh_2$	26.0	52.9(8)	55(1)	1.4(4)	0.9(4)	59(26)[c]
	14.0		27.2(4)		1.2(1)	22(2)
	6.0		18.6(2)		0.64(8)	29(4)
PCy_2Ph	25.6	6.92(4)	6.98(6)	0.07(2)	0.08(2)	90(24)[c]
	14.5		3.38(4)		0.11(2)	31(4)
	5.5		1.88(4)		0.07(2)	27(6)
PCy_3	25.6	26.4(8)	27.1(2)	0.6(4)	0.29(9)	92(29)[c]
	14.3		13.8(2)		0.45(6)	31(4)
	5.9		9.1(1)		0.15(5)	62(20)[c]

[a] IR kinetic data determined at 25°C (Table 4.2); [b] Values calculated for UV-Vis data; [c] Since the intercept indicated a large esd, values should be treated as estimations.

The activation entropy, ($\Delta S^{\neq}$) and activation enthalpy, ($\Delta H^{\neq}$) were determined from the temperature study by using the Eyring equation (Eq. 4.28).

$$\ln\left(\frac{k_{exp}}{T}\right) = \ln\left(\frac{k}{h}\right) - \frac{\Delta H^{\neq}}{RT} + \frac{\Delta S^{\neq}}{R} \qquad \textbf{… 4.28}$$

Eyring plots comparing the activation parameters for the k_1 step of the complexes described in Table 4.4 are shown in Figure 4.19. The Gibbs free energy for the first reaction was calculated by the following equation.

$$\Delta G^{\neq} = \Delta H^{\neq} - T\Delta S^{\neq} \qquad \textbf{... 4.35}$$

The activation parameters for the first reaction are typical of an associatively activated process, which are characterised by low, positive enthalpies and large negative entropies. The activation parameters indicate that very little bond breaking has occurred in the transition state. The electron acceptor ability of the phosphine ligands aids the stabilisation of the transition state. Rh(III) complexes also favour octahedral coordination which further aids in the stabilisation of the transition state.

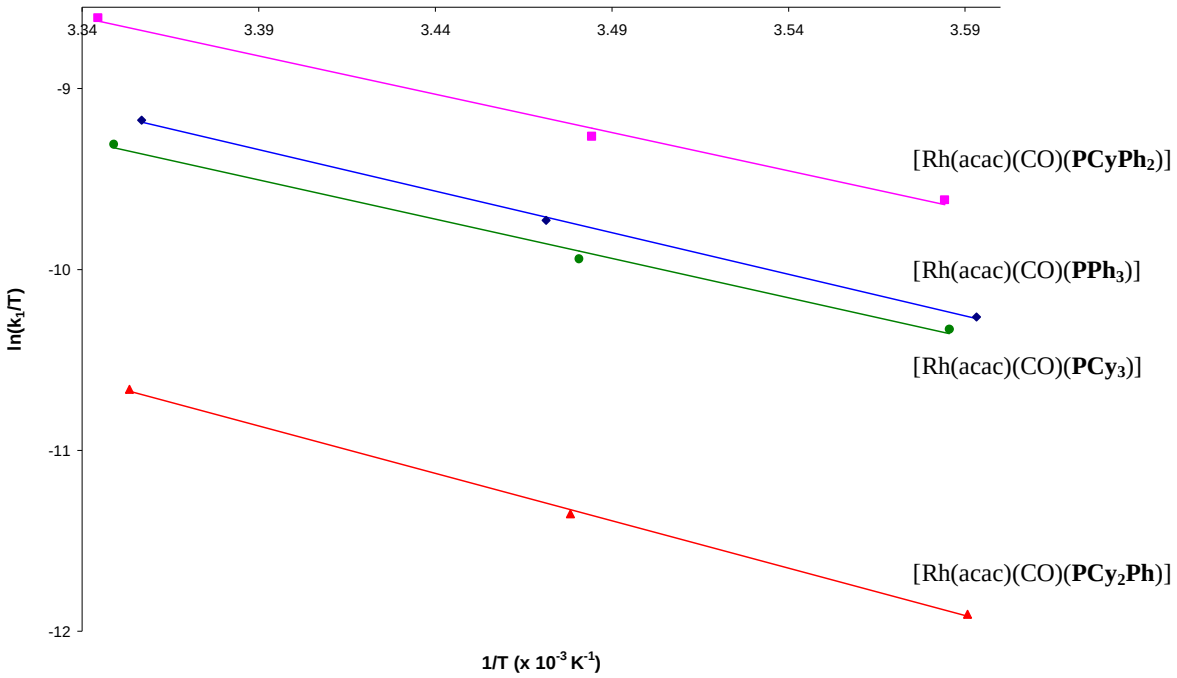

Figure 4.19: **Eyring plots of the k_1 rate constant for the formation of [Rh(acac)I(CH_3)(CO)($PR_1R_2R_3$)] in dichloromethane. (Appendix, Table E.6)**

Table 4.4: **Kinetic data obtained from the Eyring equation (Eq. 4.28, Fig 4.19). Also reported are the *ν*(CO) stretching frequency and ^{31}P NMR data of the four coordinated [Rh(acac)(CO)($PR_1R_2R_3$)] complexes in solution and associated k_1 ($M^{-1}s^{-1}$) values at 25°C in dichloromethane.**

[Rh(acac)(CO)($PR_1R_2R_3$)]	*ν*(CO) (cm^{-1})	δ ^{31}P NMR (ppm)	k_1 (x 10^{-3} $M^{-1}s^{-1}$)	$\Delta H^{\neq}(k_1)$ ($kJ.mol^{-1}$)	$\Delta S^{\neq}(k_1)$ ($J.K^{-1}mol^{-1}$)	$\Delta G^{\neq}(k_1)$ ($kJ.mol^{-1}$)
PPh_3	1977.6	48.6	30.8(5)	38(1)	-146(4)	82(4)
$PCyPh_2$	1959.3	53.3	55(1)	35(3)	-152(9)	81(9)
PCy_2Ph	1948.8	58.8	6.98(6)	44(1)	-140(5)	85(5)
PCy_3	1945.3	59.3	27.1(2)	36(3)	-154(9)	82(9)

As already mentioned, the trend observed from both the IR and ^{31}P chemical shift data regarding the electron density on the Rh(I) centres is: PCy_3 > PCy_2Ph > $PCyPh_2$ > PPh_3. This trend is not maintained in the kinetics, even when considering the steric effects of the $PR_1R_2R_3$ ligands. Further investigations into this phenomenon will therefore be conducted in the future.

4.4 PRELIMINARY CATALYTIC EVALUATIONS

4.4.1 Introduction

Preliminary catalytic experiments based on the Monsanto process, which produces acetic acid from methanol, is discussed in this chapter. *Mono* phosphine rhodium(I) complexes of the form [Rh(acac)(CO)($PR_1R_2R_3$)] and symmetrical diphosphine rhodium(I) complexes were the focus of this study.

4.4.2 Experimental

All reagents were of analytical grade. All organic solvents were pre-dried over alumina and then distilled before use. The [Rh(acac)(CO)($PR_1R_2R_3$)] complexes were prepared as described in Section 3.4.2.3. The following procedure was used for conducting the kinetic experiments. Under Schlenk conditions, the [Rh(acac)$(CO)_2$], methanol, iodomethane and respective phosphine ligand were mixed and transferred to a 300 ml Parr reactor. The reactions were carried out at 140ºC and 75 bar synthesis gas (2:1 H_2:CO) for *ca*. 20 hours. The reactions were monitored by gas uptake. The resultant solutions were analysed on a HP 6890 GC, using a FFAP column and standard FID detector.

4.4.3 Results and Discussion

A study by Moloy *et al.*[27] investigated the effect of diphosphine ligands on the rhodium catalyzed reductive carbonylation of methanol. Reaction rates (up to 6 M h^{-1}) were achieved at lower temperatures (130 – 150 ºC) and pressures (6 – 70 MPa) than generally used for the carbonylation of methanol. The use of the symmetrical diphosphine $Ph_2P(CH_2)_3PPh_2$ (Dppp) produced the formation of acetaldehyde with high selectivites approaching 90%. Ethanol was produced with the same selectivity and rate, due to *in situ* hydrogenation of acetaldehyde, if ruthenium was used as a co-catalyst. The stability of the rhodium diphosphine complexes was good, as the five-coordinate acyl complex [Rh(diphosphine)($COCH_3$)I_2] was detected at the end

[27] K.G. Moloy, R.W. Wegman, *Organometallics*, 1989, 8, 2883

of the catalysis experiments. Carraz *et al.*[28] reported rhodium complexes with asymmetrical ethylene diphosphines ligands which are efficient and longer-lived catalysts than their symmetrical anologues under the conditions of the industrial process. M*ono*-phosphine rhodium complexes, such as $[RhCl(CO)(PEt_3)_2]$ are 1.8 times faster than for $[RhI_2(CO)_2]^-$ for the carbonylation of methanol,[29] however the catalyst degrades to $[RhI_2(CO)_2]^-$ during the course of the reaction to yield $[Et_3PI]^+$ which is hydrolysed to give Et_3PO. Generally bidentate phosphines are better catalysts with regards to stability, because less free phosphine is present due to the high complex binding constants.[30]

Preliminary investigations conducted for the purpose of this study were based on the study done by Moloy *et al.*[27] and utilised a unmodified rhodium catalyst, $[Rh(acac)(CO)_2]$, two *mono*-phosphine modified catalysts, namely PPh_3 and PCy_2Ph, and one symmetrical diphosphine modified catalyst (Dppp). A ratio of 3:1 phosphine ligand to Rh was used for the *mono*-phosphine and for the diphosphine, a ratio of 1.5:1 phosphine ligand to Rh was used (Table 4.5). It was assumed that the rate would be the same for all ligands if the reaction proceeded *via* the unmodified Rh catalyst $[RhI_2(CO)_2]^-$.

Table 4.5 Experimental conditions for the carbonylation of methanol by various rhodium phosphine complexes.

	Reference[27]				
Phosphine	Dppp	PPh_3	PCy_2Ph	Unmodified	Dppp
Mass of Phosphine (mg)	2.0 mmol	314.1 (1.198 mmol)	329.3 1.200 mmol)		247.7 (0.601 mmol)
Vol MeOH (ml)	40	75	75	75	75
Vol Toluene (std) (ml)		5	5	5	5
Vol MeI (ml)	2.49 (40 mmol)	5 (80.3 mmol)	5 (80.3 mmol)	5 (80.3 mmol)	5 (80.3 mmol)
Mass $[Rh(acac)(CO)_2]$ (mg)	2.0 mmol	103.0 (0.399 mmol)	103.1 (0.399 mmol)	102.6 (0.398 mmol)	102.7 (0.398 mmol)
Total vol (ml)	40.3	85	85	85	85
Autoclave used	100 ml	300 ml			

*Note: all experiments were conducted at 70 bar of 2:1 H_2-CO and 140˚C, time ~ 20 h.

The maximum conversion of methanol with the corresponding maximum TOF and STY were observed for the unmodified Rh complex for a 393 minute reaction period. The data in Table 4.6 reveals the order of efficiency of the catalytic activity: Rh unmodified > Rh-PPh_3 complex >

[28] C.A. Carraz, E.J. Ditzel, A.G. Orpen, D.D. Ellis, P.G. Pringle, G.J. Sunley, *Chem. Commun.*, 2000, 1277
[29] J. Rankin, A.C. Benyei, A.D. Poole, D.J. Cole-Hamilton, *J. Chem. Soc., Dalton Trans.*, 1999, 3771
[30] P.W.N.M. van Leeuwen, *Homogeneous Catalysis: Understanding the Art*, Dordrecht: Kluwer Academic Publishers, 2004

Rh-PCy_2Ph complex > Rh-Dppp complex. The modified *mono*-phosphine catalyst degraded at some point during the reaction period, as the phosphine was only present in $[CH_3(PR_1R_2R_3)I]^+$ at the end of the reaction as determined by ^{31}P NMR for the Rh-PPh_3 and Rh-PCy_2Ph complexes. It appears that the presence of the phosphine ligand still influences the reaction rate (Fig. 4.20). As with the oxidative addition reactions, the Rh-PCy_2Ph complex has a slower reaction rate, conversion and TOF as compared with the Rh-PPh_3 complex. The results of batch carbonylation of methanol to acetic acid, acetaldehyde and side products in the presence of $[Rh(acac)(CO)_2]$ and various phosphine ligands are shown in Table 4.6 as determined by GC analysis. The Rh-PCy_2Ph complex resulted in a 100% conversion to methyl acetate, while the Rh-PPh_3 complex yielded 53.5% methyl acetate. As expected only the rhodium complex bonded to the Dppp ligand yielded any acetaldehyde. Due to the number of volatiles, the quantification studies were difficult and some uncertainties are present. Future work will consist of doing high pressure IR and completing the batch carbonylation with the other two phosphine ligands of the series.

Table 4.6 Results of the carbonylation of methanol.

	Mol % of product						
Phosphine	MeOAc	Acetic acid	DMA	AcH	TOF[a]	STY[b]	CONV[c]
PPh_3	53.5	46.5	-	-	102.9	0.48	14.5
PCy_2Ph	100	-	-	-	72.1	0.34	10.2
Unmodified	31.6	68	-	-	114.6	0.54	16.2
Dppp	22.3	-	11.9	65.8	24.3	0.11	3.4

***** MeOAc = Methyl acetate, DMA = dimethyl acetyl, AcH = acetaldehyde.
[a]Conversion = [mol syngas consumed / mol syngas charged] x 100, [b]STY = mol product per volume per hour,
[c]TOF = [mol syngas consumed] / [mol catalyst] per hour.

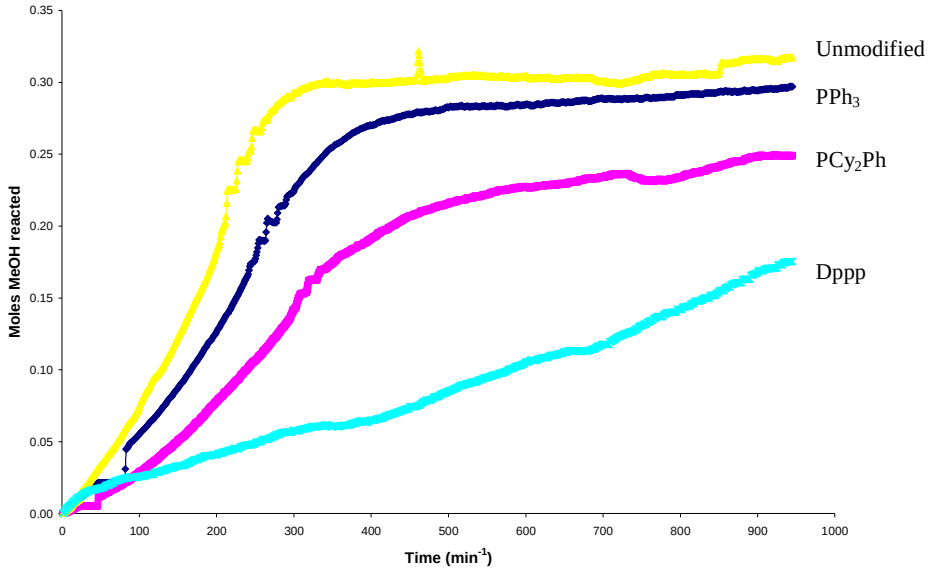

Figure 4.20: Figure of gas uptake by the rhodium phosphine complexes for the carbonylation of methanol to acetic acid and acetaldehyde.

4.5 CONCLUSION

Numerous studies have been undertaken over the years, of the formation of different products in the reactions between iodomethane and [Rh(L,L'-Bid)(CO)(PX_3)]. Both the *cis* and *trans* addition products of iodomethane on the Rh metal centre has been isolated. [RhI(cupf)(CO)(CH_3)(PPh_3)][17] formed the *cis* addition product while [RhI(OX)(CO)(CH_3)(PPh_3)][23] formed the *trans* alkyl species. When the bidentate ligand contained a sulphur atom as in the case of [Rh(Sacac)(CO)(PPh_3)],[25,26] the primary product formed was the acyl species. The rate of Rh(I) complex disappearance of the [Rh(Sacac)(CO)(PPh_3)] complex was the same as the formation of the Rh(III)-acyl species. Only a small amount of the intermediate Rh(III)-alkyl species was detected.

The oxidative addition of rhodium acetylacetonato carbonyl phosphine complexes have been carefully investigated in the context of this study. The phosphine series from PPh_3 to PCy_3 was used in order to improve the understanding of electronic versus steric effects. The kinetic pathways and the intermediate products of MeI oxidative addition to [Rh(acac)(CO)($PR_1R_2R_3$)] were positively identified.

The reaction pathway for all the Rh(I) complexes were expected to proceed *via* an Rh(III)-alkyl intermediate to a Rh(III)-acyl species. Oxidative addition of iodomethane to the Rh(I) complex, as indicated by detailed IR and NMR studies, revealed the formation of a Rh(III)-alkyl$^{\mathbf{1}}$ species for all four [Rh(acac)(CO)($PR_1R_2R_3$)] complexes. After this first step, the systems proceed *via* slightly different pathways. The [Rh(acac)(CO)(**PPh_3**)] complex indicates the conversion of the Rh(III)-alkyl$^{\mathbf{1}}$ species to an acyl species and then finally to a Rh(III)-alkyl$^{\mathbf{2}}$ species. The [Rh(acac)(CO)(**$PCyPh_2$**)] complex proceeds directly from the Rh(III)-alkyl$^{\mathbf{1}}$ species to the Rh(III)-alkyl$^{\mathbf{2}}$ species. No Rh(III) acyl formation was detected. For the [Rh(acac)(CO)(**PCy_2Ph**)] complex, Rh(III)-alkyl$^{\mathbf{1}}$ is followed by Rh(III)-acyl formation and then by the appearance of the Rh(III)-alkyl$^{\mathbf{2}}$ species. [Rh(acac)(CO)(**PCy_3**)] proceeds *via* the Rh(III)-alkyl$^{\mathbf{1}}$ to a Rh(III)-alkyl$^{\mathbf{2}}$ species before converting to the Rh(III)-acyl product. Future studies of theoretical computation calculations and crystal structure determinations of the Rh(III) products is needed in order to determine the absolute confirmation of the final products.

A solvent assisted pathway for all four complexes does not seem to occur as suggested by the small value of k_{-1}. The large equilibrium constant for the oxidative addition reaction indicates the

favourability towards the forward reaction. No solvent assisted pathways have been found in related studies of oxidative addition of iodomethane to [Rh(L,L'-Bid)(CO)(PPh_3)][18] complexes. However, the reaction with [Rh(cupf)(CO)(PPh_3)][17] had a definite solvent pathway with significant solvent interaction. The cupf is however a much weaker electron donor, coupled with the formation of a 5-membered chelate, which is expected to allow more solvent interaction at the metal center, compared to the acac systems (6-membered chelates). Studies related to complexes containing N,S-Bid ligands[18] indicates a negligible reversed reaction for the formation of the acyl species and do not indicate any solvent pathway.

From the initial IR and NMR data as reported in Chapter 3, it was postulated that as the electron density on the Rh(I) metal centre increased with gradual substitution of phenyl by cyclohexyl rings, as indicated by *ν*(CO) stretching frequency, ^{31}P chemical shift and $^{1}J_{Rh-P}$ (Table 4.1 and 4.4), so would the oxidative addition rate systematically increase from [Rh(acac)(CO)(**PPh_3**)] to [Rh(acac)(CO)(**PCy_3**)]. The steric interaction also increases systematically from **(1)** to **(4)** and is best indicated by the effective cone angle (θ_E) whose values vary accordingly 149.3º < 151.2º < 163.5º < 169.5º. It was assumed that the steric bulk of the phosphine ligands, would only play a minor role. Kinetic data however indicated that no systematic change occurred. The rates increased in the following order:

[Rh(acac)(CO)(**PCy_2Ph**)], **(3)** < [Rh(acac)(CO)(**PCy_3**)], **(4)** < [Rh(acac)(CO)(**PPh_3**)], **(1)** < [Rh(acac)(CO)(**$PCyPh_2$**)], **(2).**

The value of k_1 for complex **(3)** is approximately 8 times slower than complex **(2)**.

The reason for these reaction rates is still under investigation. It is thought that although [Rh(acac)(CO)(**PCy_3**)] has the highest electron density on the Rh(I) centre, its steric demand may inhibit the ease of the CH_3I moiety entering the rhodium co-ordination sphere, which causes the rate to be slower than for [Rh(acac)(CO)(**PPh_3**)]. Although complex **(1)** has the lowest electron density, its low steric demand may be in its favour. [Rh(acac)(CO)(**$PCyPh_2$**)] is only slightly more sterically demanding than **(1)** but the increase in electron density due to the Cy ring may result in the optimum balance between steric and electronic parameters. [Rh(acac)(CO)(**PCy_2Ph**)] is spatially smaller than **(4)** but the lower electron density due to only two Cy rings lowers the catalysts activity.

Another possible reason for this behaviour, may be due to intra- and intermolecular hydrogen bonding as indicated by the crystal structure determination (Section 3.5). Hydrogen bonding in complex **(3)** causes the formation of cage-like structures which may effectively block the

coordination sites on the Rh(I) metal centre. Complex **(1)** and **(4)** both pack in sheets due to H-bonding whereas complex **(2)** has no specific packing feature besides intramolecular H-bonding.

The manipulation of electron density and steric interaction has previously been studied for $[Rh(cacsm)(CO)(PX_3)]$[18] complexes (cacsmH = cyclohexyl 2-(methylamino)-1-cyclopentene-1-dithiocarboxylato) with different *mono*-dentate phosphine ligands where X = phenyl (Ph), *para*-chlorophenyl (*p*-cPh), *para*-methoxyphenyl (*p*-mPh) and cyclohexyl (Cy). The three phosphines $P(p\text{-cPh})_3$, PPh_3 and $P(p\text{-mPh})_3$ are sterically identical with the same cone angle[31] of 145º. However the respective Brønsted pK_a values[32] (1.03, 2.73 and 4.57) indicate an increase in their σ-donating ability. The second-order rate constants[18] for the oxidative addition (k_1) show a corresponding order of magnitude increase from $P(p\text{-cPh})_3$ to $P(p\text{-mPh})_3$ as expected for the increasing nucleophilicity of the Rh(I) complexes. The greater nucleophilicity of the PCy_3 ligand (pK_a = 9.7) suggests that its k_1 value should be significantly larger than the other three complexes. However its second-order rate constant is *ca*. three-four orders of magnitude smaller than the other three complexes. The larger steric demand of the PCy_3 ligand (cone angle = 170º) completely overshadows the electronic effect.

A similar study was conducted using $[Rh(acac)(CO)(PX_3)]$[21] complexes (where X = phenyl (Ph), *para*-chlorophenyl (*p*-cPh), *para*-methoxyphenyl (*p*-mPh)). The oxidative addition reaction was suggested to proceed *via* an equilibrium step to form a postulated ionic intermediate which converted to a Rh(III)-acyl species followed by a Rh(III)-alkyl^{2} isomer species. The value of k_1 increased with increasing σ-donator ability of the phosphine ligands as mention in the above paragraph. With regards to this M.Sc. study, the value of the second-order rate constant for $[Rh(acac)(CO)(PPh_3)]$ is of a similar order to that reported by Basson *et al.*[21] (k_1 =30.8 (5) x 10^{-3} $M^{-1}s^{-1}$ (dichloromethane) vs 24(3) x 10^{-3} $M^{-1}s^{-1}$ (1,2-dichloroethane)). Basson *et al.* reported the presence of the Rh(III)-alkyl^{2} isomer, by IR spectra for $[Rh(acac)(I)(CH_3)(CO)(PPh_3)]$ (ν(CO) = 2060 cm^{-1}). The IR spectra of this M.Sc. study, did not indicate the formation of the Rh(III)-alkyl^{2} species for any of the four complexes, only the ^{31}P NMR indicated the presence of this species. Studies by Varshavsky *et al.*[33] indicated the presence of the $[Rh(acac)(I)(CH_3)(CO)(PPh_3)]^{2}$ isomer in ^{13}C, ^{31}P and ^{1}H NMR but not in the IR spectra.

[31] C.A. Tolman, *Chem. Reviews*, 1977, 77, 313
[32] C.A. McAuliffe, *Comprehensive Coordination Chemistry*, G. Wilkinson (Ed.), New York: Pergamon Press, 1987, 989
[33] Y.S. Varshavsky, T.G Cherkasova, N.A. Buzina, L.S. Bresler, *J. Organometallic Chem.*, 1994, 464, 239

For the iodomethane reaction on the $[Rh(macsm)(CO)(PPh_3)]$[20] complex (macsmH = methyl 2-(methylamino)-1-cyclopentene-1-dithiocarboxylato), the disappearance of the Rh(I) complex is similarly followed by rapid formation of the Rh(III)-alkyl species and then slower appearance of the Rh(III)-acyl species. The activation parameters ($\Delta H^{\neq}$ = 23(3) kJ mol^{-1}, $\Delta S^{\neq}$ = -195(11) $J.K.mol^{-1}$) for the forward rate constant indicated to an expected associative pathway for the first step.

The activation parameters of the $[Rh(acac)(CO)(PR_1R_2R_3)]$ complexes of this study, are indicative of an associative mechanism for the oxidative addition step, which consist of low, positive enthalpies and large, negative entropies. This mechanism is typical of these types of reactions.[18]

The kinetic investigation has provided valuable insights into the effect that rhodium phosphine complexes experience by changing a single phenyl or cyclohexyl ring. However this study should indicate that more research is necessary to better understand the complex's system. Future investigations will be conducted to better understand all the different and important parameters.

5 STUDY EVALUTION

5.1 INTRODUCTION

This chapter includes a summary of the successes, results obtained and scientific importance of this M.Sc. study, as well as a discussion of some future research possibilities.

5.2 SCIENTIFIC RELEVANCE OF THE STUDY

One of the original motivations for this M.Sc. study was to gain further insight into the chemistry and intrinsic properties of phosphine ligands. Phosphine rhodium complexes have received a large amount of attention due to their potential in catalyst complexes. Particular interest has been aimed at their application in carbonylation catalysts.

The focus of the study was to understand the effects that occur when the phenyl ring in triphenylphosphine was systematically substituted by cyclohexyl rings to eventually produce tricyclohexylphosphine. These two phosphines are often used when comparing electronic and steric parameters.

Four model complexes of the type [Rh(acac)(CO)($PR_1R_2R_3$)] were successfully synthesized and characterized in the solution state by infrared and nuclear magnetic spectroscopy. The IR spectra indicated the conversion of two carbonyl stretching frequencies for the [Rh(acac)$(CO)_2$] changing to a single stretching frequency as the phosphine was added. The IR spectra indicated an increase in electron density on the Rh(I) metal centre in the [Rh(acac)(CO)($PR_1R_2R_3$)] complex as follows: PCy_3 > PCy_2Ph > $PCyPh_2$ > PPh_3. ^{31}P NMR indicated a doublet, as a result of the Rh-P coupling and also indicated a similar trend with regards to the electron density on the Rh(I) metal centre. From these observations it was concluded that the desired complexes were obtained. The four complexes were also crystallographically characterized to verify the four-

coordinated complex's formation and to determine the coordination mode of the ligands. The bond distances and angles compared well with those of similar complexes.

Kinetic investigation into the oxidative addition of iodomethane to the Rh(I) complexes, yielded interesting and unexpected results. The systematic increase of the rate constants for the reactions did not occur as the electron donating ability increased. Instead, a more insightful understanding into the alternating affects of steric and electronic parameters was gained. It also indicated the order of reactivity of $PCyPh_2$ > PPh_3 > PCy_3 > PCy_2Ph, which does not agree with the electron density trend as indicated by the IR data. This suggests a subtle steric effect of a combination of the cyclohexyl/phenyl substituents. The kinetic results indicated that the reaction proceeds *via* an associative reaction mechanism and a six-coordinate transition state. A possible mechanism was proposed for the model complexes.

The unpredicted range of reactivity for the oxidative addition of iodomethane to the Rh(I) complexes was unexpected and is not yet fully understood. Difficulty was experienced in the synthesis of bulk amounts of the Rh(I) complexes, as decomposition to an oil product rapidly occurred, particularly in the case of the [Rh(acac)(CO)($PCyPh_2$)] complex. Several experimental attempts were conducted in order to crystallize the Rh(III) alkyl and acyl oxidative addition products. Unfortunately only oil formation occurred. Other experimental procedures will be conducted in the future.

5.3 FUTURE RESEARCH

In this study an interesting (not as predicted) tendency in the reactivity of these four $PR_1R_2R_3$ ligands was observed during the iodomethane oxidative addition reactions. To further understand this, additional future experiments, as listed below, should be conducted.

- An extended kinetic investigation to study the second and third reaction steps for the reaction of [Rh(acac)(CO)($PR_1R_2R_3$)] with iodomethane. A study with different solvents would gain further insight into a possible solvent effect in these reaction steps.

- Theoretical computational calculations would assist in understanding which parameter, steric or electronic, is the dominant factor.

- Synthesis of the remaining Rh(III) complexes and isolation of single crystals thereof for further crystallographic investigation to confirm the complex conformation, especially the confirmation of the various isomers.

- Modification of the bidentate ligand through either the donor atoms to the rhodium metal centre or substituents on the ring to enhance electron donating and withdrawing effects.

- Synthesis of similar *bis*-phosphine Rh(I) and Rh(III) complexes and the kinetic investigation of oxidative addition.

- Synthesis of similar *mono*-phosphite, stibine and arsine Rh(I) and Rh(III) complexes and a comparison with respect to the phosphine systems in terms of structure and reaction mechanisms.

- Evaluate the catalytic activity of these systems in carbonylation reactions.

APPENDIX

Table A.1: Atomic coordinates (x 10^4) and equivalent isotropic displacement parameters ($Å^2$ x 10^3) for [Rh(acac)(CO)(PPh_3)]. U(eq) is defined as one third of the trace of the orthogonalized U^{ij} tensor.

	x	y	z	U(eq)
Rh(1)	3344(1)	5082(1)	7364(1)	11(1)
P(1)	4040(1)	3052(1)	8420(1)	10(1)
O(3)	3100(2)	4244(1)	6198(1)	15(1)
O(2)	2741(2)	6965(1)	6368(1)	16(1)
O(1)	3293(2)	6181(2)	9239(1)	26(1)
C(1)	3371(3)	5764(2)	8489(2)	16(1)
C(11)	6194(2)	2790(2)	8191(2)	11(1)
C(36)	4030(3)	2173(2)	10742(2)	15(1)
C(26)	2484(2)	566(2)	9034(2)	15(1)
C(22)	4054(3)	1464(2)	7030(2)	15(1)
C(14)	9503(3)	2464(2)	7781(2)	17(1)
C(21)	3486(2)	1570(2)	8157(2)	12(1)
C(3)	2108(3)	6198(2)	5008(2)	17(1)
C(5)	1811(3)	8655(2)	4983(2)	22(1)
C(32)	1546(3)	3128(2)	10421(2)	16(1)
C(13)	8612(3)	1390(2)	7890(2)	16(1)
C(12)	6967(2)	1547(2)	8097(2)	14(1)
C(24)	2611(3)	-625(2)	7673(2)	20(1)
C(31)	3151(2)	2736(2)	9982(2)	12(1)
C(2)	2247(2)	7179(2)	5504(2)	14(1)
C(25)	2049(3)	-535(2)	8791(2)	19(1)
C(6)	2419(3)	3880(2)	4703(2)	21(1)
C(16)	7098(2)	3862(2)	8097(2)	14(1)
C(34)	1739(3)	2416(2)	12343(2)	21(1)
C(23)	3611(3)	370(2)	6795(2)	18(1)
C(15)	8744(3)	3694(2)	7897(2)	17(1)
C(4)	2549(2)	4818(2)	5358(2)	15(1)
C(35)	3323(3)	2023(2)	11919(2)	20(1)
C(33)	848(3)	2960(2)	11594(2)	19(1)

Table A.2: Bond distances (Å) and angles (º) for [Rh(acac)(CO)(PPh_3)].

Bond	Distance (Å)	Bond Angle	Angle (º)
Rh(1)-C(1)	1.807(2)	C(1)-Rh(1)-O(3)	174.45(8)
Rh(1)-O(3)	2.0332(15)	C(1)-Rh(1)-O(2)	93.01(8)
Rh(1)-O(2)	2.0748(16)	O(3)-Rh(1)-O(2)	88.02(7)
Rh(1)-P(1)	2.2418(9)	C(1)-Rh(1)-P(1)	87.17(7)
P(1)-C(21)	1.823(2)	O(3)-Rh(1)-P(1)	91.88(5)
P(1)-C(31)	1.823(2)	O(2)-Rh(1)-P(1)	179.01(5)
P(1)-C(11)	1.827(2)	C(21)-P(1)-C(31)	104.21(9)
O(3)-C(4)	1.275(3)	C(21)-P(1)-C(11)	103.39(9)

O(2)-C(2)	1.273(3)	C(31)-P(1)-C(11)	104.23(9)
O(1)-C(1)	1.153(3)	C(21)-P(1)-Rh(1)	114.81(7)
C(11)-C(16)	1.396(3)	C(31)-P(1)-Rh(1)	114.12(7)
C(11)-C(12)	1.397(3)	C(11)-P(1)-Rh(1)	114.74(7)
C(36)-C(35)	1.390(3)	C(4)-O(3)-Rh(1)	127.75(13)
C(36)-C(31)	1.391(3)	C(2)-O(2)-Rh(1)	126.46(13)
C(36)-H(36)	0.95	O(1)-C(1)-Rh(1)	175.9(2)
C(26)-C(21)	1.390(3)	C(16)-C(11)-C(12)	118.92(19)
C(26)-C(25)	1.397(3)	C(16)-C(11)-P(1)	119.36(15)
C(26)-H(26)	0.95	C(12)-C(11)-P(1)	121.71(15)
C(22)-C(23)	1.389(3)	C(35)-C(36)-C(31)	120.1(2)
C(22)-C(21)	1.398(3)	C(35)-C(36)-H(36)	119.9
C(22)-H(22)	0.95	C(31)-C(36)-H(36)	119.9
C(14)-C(13)	1.383(3)	C(21)-C(26)-C(25)	120.4(2)
C(14)-C(15)	1.387(3)	C(21)-C(26)-H(26)	119.8
C(14)-H(14)	0.95	C(25)-C(26)-H(26)	119.8
C(3)-C(2)	1.394(3)	C(23)-C(22)-C(21)	120.1(2)
C(3)-C(4)	1.396(3)	C(23)-C(22)-H(22)	120
C(3)-H(3)	0.95	C(21)-C(22)-H(22)	120
C(5)-C(2)	1.513(3)	C(13)-C(14)-C(15)	119.8(2)
C(5)-H(5A)	0.98	C(13)-C(14)-H(14)	120.1
C(5)-H(5B)	0.98	C(15)-C(14)-H(14)	120.1
C(5)-H(5C)	0.98	C(26)-C(21)-C(22)	119.21(19)
C(32)-C(33)	1.382(3)	C(26)-C(21)-P(1)	122.05(16)
C(32)-C(31)	1.400(3)	C(22)-C(21)-P(1)	118.72(15)
C(32)-H(32)	0.95	C(2)-C(3)-C(4)	125.1(2)
C(13)-C(12)	1.387(3)	C(2)-C(3)-H(3)	117.5
C(13)-H(13)	0.95	C(4)-C(3)-H(3)	117.5
C(12)-H(12)	0.95	C(2)-C(5)-H(5A)	109.5
C(24)-C(25)	1.382(3)	C(2)-C(5)-H(5B)	109.5
C(24)-C(23)	1.385(3)	H(5A)-C(5)-H(5B)	109.5
C(24)-H(24)	0.95	C(2)-C(5)-H(5C)	109.5
C(25)-H(25)	0.95	H(5A)-C(5)-H(5C)	109.5
C(6)-C(4)	1.507(3)	H(5B)-C(5)-H(5C)	109.5
C(6)-H(6A)	0.98	C(33)-C(32)-C(31)	120.2(2)
C(6)-H(6B)	0.98	C(33)-C(32)-H(32)	119.9
C(6)-H(6C)	0.98	C(31)-C(32)-H(32)	119.9
C(16)-C(15)	1.390(3)	C(14)-C(13)-C(12)	120.3(2)
C(16)-H(16)	0.95	C(14)-C(13)-H(13)	119.9
C(34)-C(35)	1.382(3)	C(12)-C(13)-H(13)	119.9
C(34)-C(33)	1.385(3)	C(13)-C(12)-C(11)	120.43(19)
C(34)-H(34)	0.95	C(13)-C(12)-H(12)	119.8
C(23)-H(23)	0.95	C(11)-C(12)-H(12)	119.8
C(15)-H(15)	0.95	C(25)-C(24)-C(23)	120.0(2)
C(35)-H(35)	0.95	C(25)-C(24)-H(24)	120
C(33)-H(33)	0.95	C(23)-C(24)-H(24)	120
		C(36)-C(31)-C(32)	119.2(2)
		C(36)-C(31)-P(1)	122.30(16)
		C(32)-C(31)-P(1)	118.47(16)
		O(2)-C(2)-C(3)	126.1(2)
		O(2)-C(2)-C(5)	114.82(19)
		C(3)-C(2)-C(5)	119.0(2)

		C(24)-C(25)-C(26)	119.9(2)
		C(24)-C(25)-H(25)	120
		C(26)-C(25)-H(25)	120
		C(4)-C(6)-H(6A)	109.5
		C(4)-C(6)-H(6B)	109.5
		H(6A)-C(6)-H(6B)	109.5
		C(4)-C(6)-H(6C)	109.5
		H(6A)-C(6)-H(6C)	109.5
		H(6B)-C(6)-H(6C)	109.5
		C(15)-C(16)-C(11)	120.25(19)
		C(15)-C(16)-H(16)	119.9
		C(11)-C(16)-H(16)	119.9
		C(35)-C(34)-C(33)	120.0(2)
		C(35)-C(34)-H(34)	120
		C(33)-C(34)-H(34)	120
		C(24)-C(23)-C(22)	120.4(2)
		C(24)-C(23)-H(23)	119.8
		C(22)-C(23)-H(23)	119.8
		C(14)-C(15)-C(16)	120.3(2)
		C(14)-C(15)-H(15)	119.9
		C(16)-C(15)-H(15)	119.9
		O(3)-C(4)-C(3)	125.83(19)
		O(3)-C(4)-C(6)	114.48(19)
		C(3)-C(4)-C(6)	119.67(19)
		C(34)-C(35)-C(36)	120.2(2)
		C(34)-C(35)-H(35)	119.9
		C(36)-C(35)-H(35)	119.9
		C(32)-C(33)-C(34)	120.2(2)
		C(32)-C(33)-H(33)	119.9
		C(34)-C(33)-H(33)	119.9

Table A.3: Anisotropic displacement parameters ($Å^2 x\ 10^3$) for [Rh(acac)(CO)(PPh_3)].

	U11	U22	U33	U23	U13	U12
Rh(1)	11(1)	11(1)	11(1)	-3(1)	-4(1)	1(1)
P(1)	9(1)	11(1)	11(1)	-3(1)	-4(1)	0(1)
O(3)	19(1)	15(1)	13(1)	-4(1)	-7(1)	1(1)
O(2)	18(1)	15(1)	13(1)	-3(1)	-6(1)	3(1)
O(1)	44(1)	18(1)	22(1)	-9(1)	-15(1)	-2(1)
C(1)	18(1)	10(1)	19(1)	-1(1)	-9(1)	1(1)
C(11)	8(1)	17(1)	7(1)	-2(1)	-2(1)	-1(1)
C(36)	14(1)	15(1)	16(1)	-4(1)	-4(1)	1(1)
C(26)	15(1)	15(1)	15(1)	-3(1)	-7(1)	2(1)
C(22)	15(1)	15(1)	16(1)	-6(1)	-7(1)	3(1)
C(14)	10(1)	28(1)	12(1)	-2(1)	-5(1)	-1(1)
C(21)	9(1)	12(1)	16(1)	-4(1)	-7(1)	3(1)
C(3)	16(1)	21(1)	12(1)	-2(1)	-5(1)	0(1)
C(5)	24(1)	18(1)	17(1)	-1(1)	-6(1)	6(1)
C(32)	14(1)	17(1)	16(1)	-5(1)	-4(1)	-2(1)
C(13)	15(1)	18(1)	14(1)	-3(1)	-5(1)	4(1)
C(12)	15(1)	14(1)	13(1)	-2(1)	-6(1)	-1(1)
C(24)	24(1)	14(1)	32(1)	-9(1)	-18(1)	3(1)
C(31)	12(1)	10(1)	13(1)	-3(1)	-2(1)	-2(1)

C(2)	10(1)	19(1)	9(1)	-1(1)	2(1)	0(1)
C(25)	16(1)	14(1)	26(1)	-3(1)	-10(1)	-2(1)
C(6)	26(1)	23(1)	16(1)	-5(1)	-9(1)	-4(1)
C(16)	15(1)	15(1)	14(1)	-5(1)	-5(1)	1(1)
C(34)	25(1)	20(1)	13(1)	-6(1)	1(1)	-8(1)
C(23)	20(1)	19(1)	21(1)	-12(1)	-12(1)	6(1)
C(15)	15(1)	22(1)	14(1)	-2(1)	-6(1)	-6(1)
C(4)	12(1)	20(1)	11(1)	-3(1)	-2(1)	-4(1)
C(35)	25(1)	21(1)	14(1)	-3(1)	-9(1)	-1(1)
C(33)	12(1)	21(1)	21(1)	-9(1)	2(1)	-3(1)

Table B.1: Atomic coordinates (x 10^4) and equivalent isotropic displacement parameters ($Å^2$ x 10^3) for [Rh(acac)(CO)($PCyPh_2$)]. U(eq) is defined as one third of the trace of the orthogonalized U^{ij} tensor.

	x	y	z	U(eq)
Rh(1)	621(1)	5228(1)	1010(1)	14(1)
C(1)	2395(3)	5479(2)	702(1)	21(1)
O(1)	3520(2)	5647(2)	500(1)	32(1)
P(1)	795(1)	6636(1)	1722(1)	15(1)
O(2)	442(2)	3840(1)	429(1)	19(1)
O(3)	-1403(2)	5019(1)	1364(1)	20(1)
C(2)	-620(4)	3231(2)	425(1)	19(1)
C(4)	-2233(3)	4268(2)	1198(1)	19(1)
C(3)	-1889(3)	3390(2)	785(1)	21(1)
C(5)	-466(4)	2259(2)	-37(2)	29(1)
C(6)	-3723(3)	4383(2)	1464(2)	26(1)
C(31)	1616(4)	7820(2)	1368(2)	27(1)
C(21)	1789(3)	6309(2)	2536(1)	19(1)
C(11)	-932(3)	7093(2)	2045(2)	27(1)
C(16)	-1869(3)	7418(2)	1449(1)	24(1)
C(12)	-1015(3)	7766(2)	2700(2)	26(1)
C(14)	-3460(4)	8273(3)	2347(2)	37(1)
C(15)	-3322(4)	7656(3)	1673(2)	43(1)
C(13)	-2472(4)	7981(3)	2938(2)	47(1)
C(22)	1108(3)	5768(2)	3095(1)	26(1)
C(23)	1871(5)	5447(2)	3707(2)	37(1)
C(26)	3232(3)	6485(2)	2588(2)	26(1)
C(24)	3294(5)	5646(3)	3756(2)	47(1)
C(25)	3979(4)	6172(2)	3202(2)	39(1)
C(32)	1992(3)	8650(2)	1839(1)	22(1)
C(34)	2447(4)	9782(3)	806(2)	39(1)
C(36)	1472(4)	8046(2)	619(2)	28(1)
C(33)	2578(4)	9576(2)	1554(2)	35(1)
C(35)	2080(5)	8970(3)	339(2)	43(1)

Table B.2: Bond distances (Å) and angles (º) for [Rh(acac)(CO)($PCyPh_2$)].

Bond	Distance (Å)	Bond Angle	Angle (º)
C(1)-O(1)	1.149(4)	O(1)-C(1)-Rh(1)	179.1(3)
C(1)-Rh(1)	1.802(3)	C(1)-Rh(1)-O(3)	177.27(9)
P(1)-C(31)	1.819(3)	C(1)-Rh(1)-O(2)	93.70(10)
P(1)-C(21)	1.821(3)	O(3)-Rh(1)-O(2)	88.72(7)
P(1)-C(11)	1.835(3)	C(1)-Rh(1)-P(1)	88.51(8)
P(1)-Rh(1)	2.2328(6)	O(3)-Rh(1)-P(1)	89.17(5)
O(2)-C(2)	1.270(3)	O(2)-Rh(1)-P(1)	174.96(5)
O(2)-Rh(1)	2.0763(17)	C(31)-P(1)-C(21)	105.43(13)
O(3)-C(4)	1.276(3)	C(31)-P(1)-C(11)	103.55(15)
O(3)-Rh(1)	2.0428(19)	C(21)-P(1)-C(11)	105.38(13)
C(2)-C(3)	1.388(4)	C(31)-P(1)-Rh(1)	119.18(9)
C(2)-C(5)	1.513(3)	C(21)-P(1)-Rh(1)	109.85(8)

C(4)-C(3)	1.393(4)	C(11)-P(1)-Rh(1)	112.37(9)
C(4)-C(6)	1.502(4)	C(2)-O(2)-Rh(1)	126.04(17)
C(3)-H(3)	0.95	C(4)-O(3)-Rh(1)	126.75(17)
C(5)-H(5A)	0.98	O(2)-C(2)-C(3)	126.4(2)
C(5)-H(5B)	0.98	O(2)-C(2)-C(5)	115.3(3)
C(5)-H(5C)	0.98	C(3)-C(2)-C(5)	118.2(3)
C(6)-H(6A)	0.98	O(3)-C(4)-C(3)	126.2(3)
C(6)-H(6B)	0.98	O(3)-C(4)-C(6)	115.2(2)
C(6)-H(6C)	0.98	C(3)-C(4)-C(6)	118.5(3)
C(31)-C(32)	1.415(4)	C(2)-C(3)-C(4)	125.6(3)
C(31)-C(36)	1.419(4)	C(2)-C(3)-H(3)	117.2
C(21)-C(26)	1.388(4)	C(4)-C(3)-H(3)	117.2
C(21)-C(22)	1.399(4)	C(2)-C(5)-H(5A)	109.5
C(11)-C(16)	1.473(4)	C(2)-C(5)-H(5B)	109.5
C(11)-C(12)	1.485(4)	H(5A)-C(5)-H(5B)	109.5
C(11)-H(11)	1	C(2)-C(5)-H(5C)	109.5
C(16)-C(15)	1.468(5)	H(5A)-C(5)-H(5C)	109.5
C(16)-H(16A)	0.99	H(5B)-C(5)-H(5C)	109.5
C(16)-H(16B)	0.99	C(4)-C(6)-H(6A)	109.5
C(12)-C(13)	1.474(4)	C(4)-C(6)-H(6B)	109.5
C(12)-H(12A)	0.99	H(6A)-C(6)-H(6B)	109.5
C(12)-H(12B)	0.99	C(4)-C(6)-H(6C)	109.5
C(14)-C(15)	1.479(4)	H(6A)-C(6)-H(6C)	109.5
C(14)-C(13)	1.483(5)	H(6B)-C(6)-H(6C)	109.5
C(14)-H(14A)	0.99	C(32)-C(31)-C(36)	118.0(3)
C(14)-H(14B)	0.99	C(32)-C(31)-P(1)	120.5(2)
C(15)-H(15A)	0.99	C(36)-C(31)-P(1)	118.5(2)
C(15)-H(15B)	0.99	C(26)-C(21)-C(22)	118.8(3)
C(13)-H(13A)	0.99	C(26)-C(21)-P(1)	121.9(2)
C(13)-H(13B)	0.99	C(22)-C(21)-P(1)	118.9(2)
C(22)-C(23)	1.401(4)	C(16)-C(11)-C(12)	114.4(2)
C(22)-H(22)	0.95	C(16)-C(11)-P(1)	112.5(2)
C(23)-C(24)	1.374(6)	C(12)-C(11)-P(1)	119.7(2)
C(23)-H(23)	0.95	C(16)-C(11)-H(11)	102.4
C(26)-C(25)	1.393(4)	C(12)-C(11)-H(11)	102.4
C(26)-H(26)	0.95	P(1)-C(11)-H(11)	102.4
C(24)-C(25)	1.386(5)	C(15)-C(16)-C(11)	114.4(3)
C(24)-H(24)	0.95	C(15)-C(16)-H(16A)	108.7
C(25)-H(25)	0.95	C(11)-C(16)-H(16A)	108.7
C(32)-C(33)	1.406(4)	C(15)-C(16)-H(16B)	108.7
C(32)-H(32)	0.95	C(11)-C(16)-H(16B)	108.7
C(34)-C(35)	1.392(5)	H(16A)-C(16)-H(16B)	107.6
C(34)-C(33)	1.411(4)	C(13)-C(12)-C(11)	113.5(3)
C(34)-H(34)	0.95	C(13)-C(12)-H(12A)	108.9
C(36)-C(35)	1.410(5)	C(11)-C(12)-H(12A)	108.9
C(36)-H(36)	0.95	C(13)-C(12)-H(12B)	108.9
C(33)-H(33)	0.95	C(11)-C(12)-H(12B)	108.9
C(35)-H(35)	0.95	H(12A)-C(12)-H(12B)	107.7
		C(15)-C(14)-C(13)	115.4(3)
		C(15)-C(14)-H(14A)	108.4
		C(13)-C(14)-H(14A)	108.4
		C(15)-C(14)-H(14B)	108.4
		C(13)-C(14)-H(14B)	108.4
		H(14A)-C(14)-H(14B)	107.5
		C(16)-C(15)-C(14)	115.4(3)
		C(16)-C(15)-H(15A)	108.4

		C(14)-C(15)-H(15A)	108.4
		C(16)-C(15)-H(15B)	108.4
		C(14)-C(15)-H(15B)	108.4
		H(15A)-C(15)-H(15B)	107.5
		C(12)-C(13)-C(14)	114.7(3)
		C(12)-C(13)-H(13A)	108.6
		C(14)-C(13)-H(13A)	108.6
		C(12)-C(13)-H(13B)	108.6
		C(14)-C(13)-H(13B)	108.6
		H(13A)-C(13)-H(13B)	107.6
		C(21)-C(22)-C(23)	120.1(3)
		C(21)-C(22)-H(22)	120
		C(23)-C(22)-H(22)	120
		C(24)-C(23)-C(22)	120.3(3)
		C(24)-C(23)-H(23)	119.8
		C(22)-C(23)-H(23)	119.8
		C(21)-C(26)-C(25)	120.7(3)
		C(21)-C(26)-H(26)	119.7
		C(25)-C(26)-H(26)	119.7
		C(23)-C(24)-C(25)	120.0(3)
		C(23)-C(24)-H(24)	120
		C(25)-C(24)-H(24)	120
		C(24)-C(25)-C(26)	120.1(3)
		C(24)-C(25)-H(25)	119.9
		C(26)-C(25)-H(25)	119.9
		C(33)-C(32)-C(31)	119.9(2)
		C(33)-C(32)-H(32)	120.1
		C(31)-C(32)-H(32)	120.1
		C(35)-C(34)-C(33)	119.3(3)
		C(35)-C(34)-H(34)	120.3
		C(33)-C(34)-H(34)	120.3
		C(35)-C(36)-C(31)	119.3(3)
		C(35)-C(36)-H(36)	120.4
		C(31)-C(36)-H(36)	120.4
		C(32)-C(33)-C(34)	119.2(3)
		C(32)-C(33)-H(33)	120.4
		C(34)-C(33)-H(33)	120.4
		C(34)-C(35)-C(36)	119.7(3)
		C(34)-C(35)-H(35)	120.1
		C(36)-C(35)-H(35)	120.1

Table B.3: Anisotropic displacement parameters ($Å^2 x\ 10^3$) for [Rh(acac)(CO)($PCyPh_2$)].

	U11	U22	U33	U23	U13	U12
Rh(1)	18(1)	14(1)	11(1)	-1(1)	0(1)	0(1)
C(1)	24(2)	18(1)	20(1)	-3(1)	-2(1)	2(1)
O(1)	22(1)	37(1)	37(1)	-5(1)	7(1)	-1(1)
P(1)	20(1)	14(1)	11(1)	-1(1)	-1(1)	0(1)
O(2)	26(1)	16(1)	15(1)	-2(1)	4(1)	-1(1)
O(3)	22(1)	18(1)	20(1)	-2(1)	4(1)	0(1)
C(2)	29(1)	17(1)	12(1)	2(1)	-3(1)	-2(1)
C(4)	22(1)	19(1)	15(1)	5(1)	0(1)	0(1)
C(3)	26(2)	17(1)	20(1)	0(1)	-2(1)	-5(1)

C(5)	43(2)	18(1)	25(1)	-7(1)	5(1)	-4(1)
C(6)	24(2)	28(2)	26(1)	3(1)	4(1)	-1(1)
C(31)	46(2)	16(1)	18(1)	4(1)	-3(1)	-5(1)
C(21)	29(2)	15(1)	11(1)	0(1)	-4(1)	-1(1)
C(11)	22(2)	34(2)	26(1)	-16(1)	-4(1)	5(1)
C(16)	22(2)	27(1)	22(1)	0(1)	0(1)	4(1)
C(12)	29(2)	23(1)	26(1)	-1(1)	8(1)	-2(1)
C(14)	27(2)	26(2)	57(2)	0(2)	10(2)	-2(1)
C(15)	34(2)	41(2)	53(2)	-22(2)	-14(2)	13(2)
C(13)	36(2)	40(2)	65(2)	-35(2)	0(2)	5(2)
C(22)	42(2)	18(1)	18(1)	0(1)	-2(1)	-2(1)
C(23)	78(3)	18(1)	15(1)	1(1)	-6(2)	4(2)
C(26)	29(2)	17(1)	34(2)	-2(1)	-7(1)	-1(1)
C(24)	83(3)	23(2)	35(2)	-4(1)	-38(2)	13(2)
C(25)	43(2)	22(1)	53(2)	-8(1)	-32(2)	5(1)
C(32)	24(2)	23(1)	20(1)	3(1)	-1(1)	-4(1)
C(34)	46(2)	36(2)	34(2)	14(2)	9(1)	-13(2)
C(36)	38(2)	29(2)	17(1)	-1(1)	3(1)	-2(1)
C(33)	53(2)	19(2)	33(2)	5(1)	3(2)	-1(1)
C(35)	79(3)	31(2)	19(1)	10(1)	9(2)	14(2)

Table C.1: Atomic coordinates (x 10^4) and equivalent isotropic displacement parameters ($Å^2$ x 10^3) for [Rh(acac)(CO)(PCy_2Ph)]. U(eq) is defined as one third of the trace of the orthogonalized U^{ij} tensor.

	x	y	z	U(eq)
Rh(1)	4224(1)	880(1)	1521(1)	15(1)
O(2)	4995(2)	2341(1)	1335(1)	21(1)
O(3)	6123(2)	362(1)	1657(1)	22(1)
P(1)	3536(1)	-721(1)	1782(1)	14(1)
C(1)	2522(2)	1270(2)	1409(1)	19(1)
O(1)	1431(2)	1520(1)	1336(1)	25(1)
C(4)	7199(2)	877(2)	1599(1)	21(1)
C(2)	6219(2)	2581(2)	1317(1)	22(1)
C(3)	7288(2)	1919(2)	1448(1)	23(1)
C(6)	8438(2)	236(2)	1696(2)	29(1)
C(5)	6497(3)	3689(2)	1133(2)	35(1)
C(21)	3354(2)	-916(2)	2788(1)	15(1)
C(11)	2004(2)	-1209(2)	1363(1)	19(1)
C(31)	4788(2)	-1669(2)	1492(1)	19(1)
C(25)	4533(3)	-877(2)	4034(1)	30(1)
C(26)	4681(2)	-723(2)	3195(1)	23(1)
C(22)	2270(2)	-219(2)	3104(1)	21(1)
C(24)	3456(3)	-190(2)	4343(1)	30(1)
C(23)	2136(3)	-373(2)	3943(1)	26(1)
C(12)	1731(3)	-960(2)	614(1)	24(1)
C(15)	136(2)	-2400(2)	1341(2)	28(1)
C(16)	1244(3)	-1973(2)	1710(2)	28(1)
C(13)	625(3)	-1388(2)	254(2)	31(1)
C(14)	-101(3)	-2150(2)	599(2)	37(1)
C(36)	4602(3)	-2751(2)	1754(1)	26(1)
C(32)	5089(2)	-1614(2)	670(1)	22(1)
C(35)	5748(3)	-3434(2)	1552(1)	27(1)
C(33)	6229(3)	-2291(2)	471(1)	30(1)
C(34)	6103(3)	-3365(2)	744(2)	32(1)

Table C.2: Bond distances (Å) and angles (°) for [Rh(acac)(CO)(PCy_2Ph)].

Bond	Distance (Å)	Bond Angle	Angle (°)
O(2)-C(2)	1.273(3)	C(1)-Rh(1)-O(3)	177.06(8)
O(2)-Rh(1)	2.0783(17)	C(1)-Rh(1)-O(2)	94.74(8)
O(3)-C(4)	1.279(3)	O(3)-Rh(1)-O(2)	88.20(7)
O(3)-Rh(1)	2.0411(18)	C(1)-Rh(1)-P(1)	89.34(7)
P(1)-C(11)	1.825(2)	O(3)-Rh(1)-P(1)	87.72(5)
P(1)-C(21)	1.833(2)	O(2)-Rh(1)-P(1)	175.32(5)
P(1)-C(31)	1.842(2)	C(2)-O(2)-Rh(1)	126.30(15)
P(1)-Rh(1)	2.2424(9)	C(4)-O(3)-Rh(1)	127.74(15)
C(1)-O(1)	1.152(3)	C(11)-P(1)-C(21)	105.38(11)
C(1)-Rh(1)	1.797(3)	C(11)-P(1)-C(31)	103.28(11)
C(4)-C(3)	1.384(3)	C(21)-P(1)-C(31)	105.13(10)
C(4)-C(6)	1.509(3)	C(11)-P(1)-Rh(1)	119.88(8)
C(2)-C(3)	1.396(3)	C(21)-P(1)-Rh(1)	111.58(7)

C(2)-C(5)	1.504(3)	C(31)-P(1)-Rh(1)	110.35(8)
C(3)-H(3)	0.95	O(1)-C(1)-Rh(1)	179.9(2)
C(6)-H(6A)	0.98	O(3)-C(4)-C(3)	125.8(2)
C(6)-H(6B)	0.98	O(3)-C(4)-C(6)	113.8(2)
C(6)-H(6C)	0.98	C(3)-C(4)-C(6)	120.5(2)
C(5)-H(5A)	0.98	O(2)-C(2)-C(3)	126.2(2)
C(5)-H(5B)	0.98	O(2)-C(2)-C(5)	115.0(2)
C(5)-H(5C)	0.98	C(3)-C(2)-C(5)	118.7(2)
C(21)-C(22)	1.532(3)	C(4)-C(3)-C(2)	125.7(2)
C(21)-C(26)	1.537(3)	C(4)-C(3)-H(3)	117.1
C(21)-H(21)	1	C(2)-C(3)-H(3)	117.1
C(11)-C(16)	1.404(3)	C(4)-C(6)-H(6A)	109.5
C(11)-C(12)	1.406(3)	C(4)-C(6)-H(6B)	109.5
C(31)-C(36)	1.495(3)	H(6A)-C(6)-H(6B)	109.5
C(31)-C(32)	1.510(3)	C(4)-C(6)-H(6C)	109.5
C(31)-H(31)	1	H(6A)-C(6)-H(6C)	109.5
C(25)-C(24)	1.514(4)	H(6B)-C(6)-H(6C)	109.5
C(25)-C(26)	1.526(3)	C(2)-C(5)-H(5A)	109.5
C(25)-H(25A)	0.99	C(2)-C(5)-H(5B)	109.5
C(25)-H(25B)	0.99	H(5A)-C(5)-H(5B)	109.5
C(26)-H(26A)	0.99	C(2)-C(5)-H(5C)	109.5
C(26)-H(26B)	0.99	H(5A)-C(5)-H(5C)	109.5
C(22)-C(23)	1.524(3)	H(5B)-C(5)-H(5C)	109.5
C(22)-H(22A)	0.99	C(22)-C(21)-C(26)	110.38(19)
C(22)-H(22B)	0.99	C(22)-C(21)-P(1)	111.20(15)
C(24)-C(23)	1.524(4)	C(26)-C(21)-P(1)	110.45(16)
C(24)-H(24A)	0.99	C(22)-C(21)-H(21)	108.2
C(24)-H(24B)	0.99	C(26)-C(21)-H(21)	108.2
C(23)-H(23A)	0.99	P(1)-C(21)-H(21)	108.2
C(23)-H(23B)	0.99	C(16)-C(11)-C(12)	119.0(2)
C(12)-C(13)	1.398(4)	C(16)-C(11)-P(1)	121.72(18)
C(12)-H(12)	0.95	C(12)-C(11)-P(1)	118.09(18)
C(15)-C(14)	1.389(4)	C(36)-C(31)-C(32)	112.24(19)
C(15)-C(16)	1.407(3)	C(36)-C(31)-P(1)	116.90(17)
C(15)-H(15)	0.95	C(32)-C(31)-P(1)	112.87(16)
C(16)-H(16)	0.95	C(36)-C(31)-H(31)	104.4
C(13)-C(14)	1.381(4)	C(32)-C(31)-H(31)	104.4
C(13)-H(13)	0.95	P(1)-C(31)-H(31)	104.4
C(14)-H(14)	0.95	C(24)-C(25)-C(26)	111.2(2)
C(36)-C(35)	1.503(3)	C(24)-C(25)-H(25A)	109.4
C(36)-H(36A)	0.99	C(26)-C(25)-H(25A)	109.4
C(36)-H(36B)	0.99	C(24)-C(25)-H(25B)	109.4
C(32)-C(33)	1.493(3)	C(26)-C(25)-H(25B)	109.4
C(32)-H(32A)	0.99	H(25A)-C(25)-H(25B)	108
C(32)-H(32B)	0.99	C(25)-C(26)-C(21)	110.7(2)
C(35)-C(34)	1.498(4)	C(25)-C(26)-H(26A)	109.5
C(35)-H(35A)	0.99	C(21)-C(26)-H(26A)	109.5
C(35)-H(35B)	0.99	C(25)-C(26)-H(26B)	109.5
C(33)-C(34)	1.485(4)	C(21)-C(26)-H(26B)	109.5
C(33)-H(33A)	0.99	H(26A)-C(26)-H(26B)	108.1
C(33)-H(33B)	0.99	C(23)-C(22)-C(21)	111.01(19)
C(34)-H(34A)	0.99	C(23)-C(22)-H(22A)	109.4
C(34)-H(34B)	0.99	C(21)-C(22)-H(22A)	109.4
		C(23)-C(22)-H(22B)	109.4
		C(21)-C(22)-H(22B)	109.4
		H(22A)-C(22)-H(22B)	108

		C(25)-C(24)-C(23)	111.2(2)
		C(25)-C(24)-H(24A)	109.4
		C(23)-C(24)-H(24A)	109.4
		C(25)-C(24)-H(24B)	109.4
		C(23)-C(24)-H(24B)	109.4
		H(24A)-C(24)-H(24B)	108
		C(22)-C(23)-C(24)	111.0(2)
		C(22)-C(23)-H(23A)	109.4
		C(24)-C(23)-H(23A)	109.4
		C(22)-C(23)-H(23B)	109.4
		C(24)-C(23)-H(23B)	109.4
		H(23A)-C(23)-H(23B)	108
		C(13)-C(12)-C(11)	119.8(2)
		C(13)-C(12)-H(12)	120.1
		C(11)-C(12)-H(12)	120.1
		C(14)-C(15)-C(16)	119.2(2)
		C(14)-C(15)-H(15)	120.4
		C(16)-C(15)-H(15)	120.4
		C(11)-C(16)-C(15)	120.2(2)
		C(11)-C(16)-H(16)	119.9
		C(15)-C(16)-H(16)	119.9
		C(14)-C(13)-C(12)	120.1(3)
		C(14)-C(13)-H(13)	119.9
		C(12)-C(13)-H(13)	119.9
		C(13)-C(14)-C(15)	120.7(2)
		C(13)-C(14)-H(14)	119.7
		C(15)-C(14)-H(14)	119.7
		C(31)-C(36)-C(35)	112.4(2)
		C(31)-C(36)-H(36A)	109.1
		C(35)-C(36)-H(36A)	109.1
		C(31)-C(36)-H(36B)	109.1
		C(35)-C(36)-H(36B)	109.1
		H(36A)-C(36)-H(36B)	107.9
		C(33)-C(32)-C(31)	111.6(2)
		C(33)-C(32)-H(32A)	109.3
		C(31)-C(32)-H(32A)	109.3
		C(33)-C(32)-H(32B)	109.3
		C(31)-C(32)-H(32B)	109.3
		H(32A)-C(32)-H(32B)	108
		C(34)-C(35)-C(36)	112.9(2)
		C(34)-C(35)-H(35A)	109
		C(36)-C(35)-H(35A)	109
		C(34)-C(35)-H(35B)	109
		C(36)-C(35)-H(35B)	109
		H(35A)-C(35)-H(35B)	107.8
		C(34)-C(33)-C(32)	114.0(2)
		C(34)-C(33)-H(33A)	108.8
		C(32)-C(33)-H(33A)	108.8
		C(34)-C(33)-H(33B)	108.8
		C(32)-C(33)-H(33B)	108.8
		H(33A)-C(33)-H(33B)	107.7
		C(33)-C(34)-C(35)	113.4(2)
		C(33)-C(34)-H(34A)	108.9
		C(35)-C(34)-H(34A)	108.9
		C(33)-C(34)-H(34B)	108.9
		C(35)-C(34)-H(34B)	108.9

		H(34A)-C(34)-H(34B)	107.7

Table C.3: Anisotropic displacement parameters ($Å^2 x\ 10^3$) for [Rh(acac)(CO)(PCy_2Ph)].

	U_{11}	U_{22}	U_{33}	U_{23}	U_{13}	U_{12}
Rh(1)	15(1)	14(1)	17(1)	2(1)	0(1)	-1(1)
O(2)	19(1)	18(1)	28(1)	2(1)	0(1)	-2(1)
O(3)	16(1)	20(1)	31(1)	3(1)	1(1)	-1(1)
P(1)	16(1)	14(1)	13(1)	0(1)	0(1)	-1(1)
C(1)	26(2)	13(1)	18(1)	0(1)	2(1)	-3(1)
O(1)	19(1)	21(1)	34(1)	1(1)	-1(1)	2(1)
C(4)	18(1)	25(1)	19(1)	-2(1)	-1(1)	-2(1)
C(2)	24(1)	20(1)	22(1)	-1(1)	0(1)	-5(1)
C(3)	17(1)	25(1)	27(1)	-2(1)	1(1)	-7(1)
C(6)	20(1)	28(1)	38(2)	2(1)	-3(1)	1(1)
C(5)	25(2)	22(1)	57(2)	5(1)	-1(1)	-7(1)
C(21)	18(1)	15(1)	13(1)	1(1)	1(1)	-1(1)
C(11)	20(1)	19(1)	19(1)	-2(1)	-4(1)	-2(1)
C(31)	20(1)	20(1)	19(1)	0(1)	5(1)	4(1)
C(25)	34(2)	39(2)	17(1)	1(1)	-7(1)	-8(1)
C(26)	21(1)	31(1)	18(1)	-1(1)	-2(1)	-1(1)
C(22)	23(1)	21(1)	19(1)	-2(1)	4(1)	1(1)
C(24)	42(2)	34(1)	14(1)	-4(1)	3(1)	-16(1)
C(23)	33(2)	27(1)	19(1)	-3(1)	9(1)	-6(1)
C(12)	23(1)	30(1)	19(1)	-1(1)	0(1)	0(1)
C(15)	19(1)	24(1)	43(2)	-6(1)	0(1)	-2(1)
C(16)	25(2)	30(1)	28(1)	4(1)	-3(1)	-6(1)
C(13)	33(2)	36(1)	22(1)	-8(1)	-7(1)	5(1)
C(14)	23(2)	48(2)	40(2)	-14(1)	-11(1)	-3(1)
C(36)	35(2)	22(1)	23(1)	4(1)	8(1)	7(1)
C(32)	22(1)	25(1)	19(1)	0(1)	4(1)	-1(1)
C(35)	33(2)	23(1)	25(1)	0(1)	6(1)	7(1)
C(33)	36(2)	36(1)	19(1)	0(1)	10(1)	6(1)
C(34)	31(2)	34(1)	32(2)	-2(1)	10(1)	11(1)

Table D.1: Atomic coordinates (x 10^4) and equivalent isotropic displacement parameters ($Å^2$ x 10^3) for [Rh(acac)(CO)(PCy_3)]. U(eq) is defined as one third of the trace of the orthogonalized U^{ij} tensor.

	x	y	z	U(eq)
Rh(1)	5850(1)	4093(1)	1513(1)	15(1)
P	6483(1)	5709(1)	1762(1)	15(1)
O(2)	5146(1)	2619(1)	1314(1)	21(1)
O(3)	3974(1)	4552(1)	1646(1)	22(1)
O(1)	8589(1)	3503(1)	1378(1)	27(1)
C(1)	7513(2)	3735(1)	1427(1)	19(1)
C(4)	2954(2)	4011(1)	1595(1)	21(1)
C(2)	3967(2)	2345(1)	1304(1)	22(1)
C(6)	1724(2)	4604(1)	1709(1)	30(1)
C(3)	2901(2)	2972(1)	1439(1)	22(1)
C(21)	6612(2)	5924(1)	2777(1)	17(1)
C(31)	5201(2)	6603(1)	1462(1)	18(1)
C(11)	8077(2)	6116(1)	1405(1)	18(1)
C(5)	3732(2)	1232(1)	1124(1)	36(1)
C(23)	5431(2)	5901(1)	4001(1)	29(1)
C(26)	7673(2)	5249(1)	3124(1)	22(1)
C(22)	5315(2)	5733(1)	3159(1)	23(1)
C(25)	7775(2)	5418(1)	3968(1)	27(1)
C(24)	6483(2)	5233(1)	4341(1)	31(1)
C(13)	9949(2)	7362(1)	1416(1)	27(1)
C(12)	8592(2)	7138(1)	1707(1)	26(1)
C(16)	8118(2)	6092(1)	549(1)	22(1)
C(32)	4813(2)	6527(1)	634(1)	24(1)
C(15)	9477(2)	6321(1)	270(1)	24(1)
C(36)	5347(2)	7732(1)	1687(1)	28(1)
C(14)	9968(2)	7338(1)	567(1)	27(1)
C(33)	3538(2)	7086(1)	502(1)	25(1)
C(34)	3622(2)	8203(1)	746(1)	30(1)
C(35)	4065(2)	8290(1)	1556(1)	32(1)

Table D.2: Bond distances (Å) and angles (º) for [Rh(acac)(CO)(PCy_3)].

Bond	Distance (Å)	Bond Angle	Angle (º)
O(2)-C(2)	1.270(2)	C(1)-Rh(1)-O(3)	177.40(6)
O(2)-Rh(1)	2.0880(10)	C(1)-Rh(1)-O(2)	94.47(6)
O(3)-C(4)	1.272(2)	O(3)-Rh(1)-O(2)	87.77(4)
O(3)-Rh(1)	2.0464(11)	C(1)-Rh(1)-P	89.11(5)
O(1)-C(1)	1.157(2)	O(3)-Rh(1)-P	88.62(3)
C(1)-Rh(1)	1.7914(17)	O(2)-Rh(1)-P	176.23(3)
P-C(31)	1.8427(16)	C(2)-O(2)-Rh(1)	126.49(10)
P-C(21)	1.8452(15)	C(4)-O(3)-Rh(1)	127.94(10)
P-C(11)	1.8528(16)	O(1)-C(1)-Rh(1)	179.37(14)
P-Rh(1)	2.2537(4)	O(3)-C(4)-C(3)	126.08(16)
C(4)-C(3)	1.387(2)	O(3)-C(4)-C(6)	113.94(14)
C(4)-C(6)	1.505(2)	C(3)-C(4)-C(6)	119.97(16)

C(2)-C(3)	1.396(2)	O(2)-C(2)-C(3)	126.31(15)
C(2)-C(5)	1.509(2)	O(2)-C(2)-C(5)	115.24(15)
C(6)-H(6A)	0.98	C(3)-C(2)-C(5)	118.45(15)
C(6)-H(6B)	0.98	C(4)-C(6)-H(6A)	109.5
C(6)-H(6C)	0.98	C(4)-C(6)-H(6B)	109.5
C(3)-H(3)	0.95	H(6A)-C(6)-H(6B)	109.5
C(21)-C(22)	1.533(2)	C(4)-C(6)-H(6C)	109.5
C(21)-C(26)	1.534(2)	H(6A)-C(6)-H(6C)	109.5
C(21)-H(21)	1	H(6B)-C(6)-H(6C)	109.5
C(31)-C(36)	1.536(2)	C(4)-C(3)-C(2)	125.39(16)
C(31)-C(32)	1.537(2)	C(4)-C(3)-H(3)	117.3
C(31)-H(31)	1	C(2)-C(3)-H(3)	117.3
C(11)-C(12)	1.534(2)	C(31)-P-C(21)	103.64(7)
C(11)-C(16)	1.537(2)	C(31)-P-C(11)	110.93(7)
C(11)-H(11)	1	C(21)-P-C(11)	103.97(7)
C(5)-H(5A)	0.98	C(31)-P-Rh(1)	109.24(5)
C(5)-H(5B)	0.98	C(21)-P-Rh(1)	110.81(5)
C(5)-H(5C)	0.98	C(11)-P-Rh(1)	117.30(5)
C(23)-C(24)	1.517(3)	C(22)-C(21)-C(26)	110.56(13)
C(23)-C(22)	1.529(2)	C(22)-C(21)-P	111.18(11)
C(23)-H(23A)	0.99	C(26)-C(21)-P	110.91(10)
C(23)-H(23B)	0.99	C(22)-C(21)-H(21)	108
C(26)-C(25)	1.531(2)	C(26)-C(21)-H(21)	108
C(26)-H(26C)	0.99	P-C(21)-H(21)	108
C(26)-H(26D)	0.99	C(36)-C(31)-C(32)	109.85(13)
C(22)-H(22E)	0.99	C(36)-C(31)-P	117.62(11)
C(22)-H(22F)	0.99	C(32)-C(31)-P	114.85(11)
C(25)-C(24)	1.521(3)	C(36)-C(31)-H(31)	104.3
C(25)-H(25G)	0.99	C(32)-C(31)-H(31)	104.3
C(25)-H(25H)	0.99	P-C(31)-H(31)	104.3
C(24)-H(24I)	0.99	C(12)-C(11)-C(16)	110.92(13)
C(24)-H(24J)	0.99	C(12)-C(11)-P	115.81(11)
C(13)-C(14)	1.524(2)	C(16)-C(11)-P	111.94(11)
C(13)-C(12)	1.530(2)	C(12)-C(11)-H(11)	105.8
C(13)-H(13A)	0.99	C(16)-C(11)-H(11)	105.8
C(13)-H(13B)	0.99	P-C(11)-H(11)	105.8
C(12)-H(12C)	0.99	C(2)-C(5)-H(5A)	109.5
C(12)-H(12D)	0.99	C(2)-C(5)-H(5B)	109.5
C(16)-C(15)	1.526(2)	H(5A)-C(5)-H(5B)	109.5
C(16)-H(16E)	0.99	C(2)-C(5)-H(5C)	109.5
C(16)-H(16F)	0.99	H(5A)-C(5)-H(5C)	109.5
C(32)-C(33)	1.524(2)	H(5B)-C(5)-H(5C)	109.5
C(32)-H(32A)	0.99	C(24)-C(23)-C(22)	111.34(14)
C(32)-H(32B)	0.99	C(24)-C(23)-H(23A)	109.4
C(15)-C(14)	1.516(2)	C(22)-C(23)-H(23A)	109.4
C(15)-H(15G)	0.99	C(24)-C(23)-H(23B)	109.4
C(15)-H(15H)	0.99	C(22)-C(23)-H(23B)	109.4
C(36)-C(35)	1.529(2)	H(23A)-C(23)-H(23B)	108
C(36)-H(36C)	0.99	C(25)-C(26)-C(21)	111.05(13)
C(36)-H(36D)	0.99	C(25)-C(26)-H(26C)	109.4
C(14)-H(14I)	0.99	C(21)-C(26)-H(26C)	109.4
C(14)-H(14J)	0.99	C(25)-C(26)-H(26D)	109.4
C(33)-C(34)	1.526(2)	C(21)-C(26)-H(26D)	109.4
C(33)-H(33E)	0.99	H(26C)-C(26)-H(26D)	108
C(33)-H(33F)	0.99	C(23)-C(22)-C(21)	110.97(14)
C(34)-C(35)	1.523(2)	C(23)-C(22)-H(22E)	109.4

C(34)-H(34G)	0.99	C(21)-C(22)-H(22E)	109.4
C(34)-H(34H)	0.99	C(23)-C(22)-H(22F)	109.4
C(35)-H(35I)	0.99	C(21)-C(22)-H(22F)	109.4
C(35)-H(35J)	0.99	H(22E)-C(22)-H(22F)	108
		C(24)-C(25)-C(26)	111.14(14)
		C(24)-C(25)-H(25G)	109.4
		C(26)-C(25)-H(25G)	109.4
		C(24)-C(25)-H(25H)	109.4
		C(26)-C(25)-H(25H)	109.4
		H(25G)-C(25)-H(25H)	108
		C(23)-C(24)-C(25)	111.16(13)
		C(23)-C(24)-H(24I)	109.4
		C(25)-C(24)-H(24I)	109.4
		C(23)-C(24)-H(24J)	109.4
		C(25)-C(24)-H(24J)	109.4
		H(24I)-C(24)-H(24J)	108
		C(14)-C(13)-C(12)	110.99(15)
		C(14)-C(13)-H(13A)	109.4
		C(12)-C(13)-H(13A)	109.4
		C(14)-C(13)-H(13B)	109.4
		C(12)-C(13)-H(13B)	109.4
		H(13A)-C(13)-H(13B)	108
		C(13)-C(12)-C(11)	111.26(13)
		C(13)-C(12)-H(12C)	109.4
		C(11)-C(12)-H(12C)	109.4
		C(13)-C(12)-H(12D)	109.4
		C(11)-C(12)-H(12D)	109.4
		H(12C)-C(12)-H(12D)	108
		C(15)-C(16)-C(11)	110.99(14)
		C(15)-C(16)-H(16E)	109.4
		C(11)-C(16)-H(16E)	109.4
		C(15)-C(16)-H(16F)	109.4
		C(11)-C(16)-H(16F)	109.4
		H(16E)-C(16)-H(16F)	108
		C(33)-C(32)-C(31)	109.61(13)
		C(33)-C(32)-H(32A)	109.7
		C(31)-C(32)-H(32A)	109.7
		C(33)-C(32)-H(32B)	109.7
		C(31)-C(32)-H(32B)	109.7
		H(32A)-C(32)-H(32B)	108.2
		C(14)-C(15)-C(16)	111.33(13)
		C(14)-C(15)-H(15G)	109.4
		C(16)-C(15)-H(15G)	109.4
		C(14)-C(15)-H(15H)	109.4
		C(16)-C(15)-H(15H)	109.4
		H(15G)-C(15)-H(15H)	108
		C(35)-C(36)-C(31)	109.58(14)
		C(35)-C(36)-H(36C)	109.8
		C(31)-C(36)-H(36C)	109.8
		C(35)-C(36)-H(36D)	109.8
		C(31)-C(36)-H(36D)	109.8
		H(36C)-C(36)-H(36D)	108.2
		C(15)-C(14)-C(13)	111.11(13)
		C(15)-C(14)-H(14I)	109.4
		C(13)-C(14)-H(14I)	109.4
		C(15)-C(14)-H(14J)	109.4

		C(13)-C(14)-H(14J)	109.4
		H(14I)-C(14)-H(14J)	108
		C(32)-C(33)-C(34)	111.58(15)
		C(32)-C(33)-H(33E)	109.3
		C(34)-C(33)-H(33E)	109.3
		C(32)-C(33)-H(33F)	109.3
		C(34)-C(33)-H(33F)	109.3
		H(33E)-C(33)-H(33F)	108
		C(35)-C(34)-C(33)	111.15(13)
		C(35)-C(34)-H(34G)	109.4
		C(33)-C(34)-H(34G)	109.4
		C(35)-C(34)-H(34H)	109.4
		C(33)-C(34)-H(34H)	109.4
		H(34G)-C(34)-H(34H)	108
		C(34)-C(35)-C(36)	111.23(15)
		C(34)-C(35)-H(35I)	109.4
		C(36)-C(35)-H(35I)	109.4
		C(34)-C(35)-H(35J)	109.4
		C(36)-C(35)-H(35J)	109.4
		H(35I)-C(35)-H(35J)	108

Table D.3: Anisotropic displacement parameters ($Å^2 x\ 10^3$) for [Rh(acac)(CO)(PCy_3)].

	U_{11}	U_{22}	U_{33}	U_{23}	U_{13}	U_{12}
Rh(1)	21(1)	10(1)	14(1)	-1(1)	1(1)	-1(1)
P	22(1)	11(1)	10(1)	0(1)	1(1)	-1(1)
O(2)	24(1)	13(1)	25(1)	-2(1)	2(1)	-2(1)
O(3)	23(1)	14(1)	28(1)	-2(1)	2(1)	0(1)
O(1)	25(1)	20(1)	37(1)	-1(1)	3(1)	2(1)
C(1)	30(1)	9(1)	17(1)	0(1)	1(1)	-2(1)
C(4)	25(1)	20(1)	18(1)	2(1)	1(1)	0(1)
C(2)	30(1)	16(1)	20(1)	0(1)	1(1)	-3(1)
C(6)	26(1)	24(1)	39(1)	2(1)	4(1)	1(1)
C(3)	24(1)	19(1)	24(1)	1(1)	1(1)	-5(1)
C(21)	27(1)	12(1)	12(1)	0(1)	1(1)	-2(1)
C(31)	24(1)	14(1)	15(1)	1(1)	-1(1)	1(1)
C(11)	25(1)	13(1)	16(1)	-1(1)	4(1)	-1(1)
C(5)	33(1)	18(1)	58(1)	-7(1)	4(1)	-7(1)
C(23)	40(1)	32(1)	15(1)	-3(1)	11(1)	-14(1)
C(26)	32(1)	19(1)	16(1)	1(1)	-3(1)	1(1)
C(22)	30(1)	25(1)	14(1)	-2(1)	4(1)	-6(1)
C(25)	42(1)	25(1)	15(1)	2(1)	-7(1)	-6(1)
C(24)	54(1)	27(1)	13(1)	4(1)	-1(1)	-19(1)
C(13)	29(1)	18(1)	34(1)	-4(1)	10(1)	-5(1)
C(12)	32(1)	19(1)	28(1)	-7(1)	12(1)	-7(1)
C(16)	28(1)	23(1)	15(1)	2(1)	4(1)	2(1)
C(32)	27(1)	30(1)	15(1)	0(1)	-1(1)	5(1)
C(15)	29(1)	26(1)	18(1)	4(1)	7(1)	6(1)
C(36)	39(1)	14(1)	29(1)	0(1)	-13(1)	1(1)
C(14)	26(1)	22(1)	33(1)	9(1)	12(1)	4(1)
C(33)	29(1)	30(1)	17(1)	0(1)	-4(1)	4(1)
C(34)	36(1)	24(1)	30(1)	9(1)	-7(1)	5(1)
C(35)	48(1)	14(1)	35(1)	-2(1)	-12(1)	8(1)

APPENDIX

E. Supplementary Data for the Oxidative Addition of Iodomethane to [Rh(acac)(CO)($PR_1R_2R_3$)] Complexes.

Table E.1: **(Figure 4.14) The effect of various phosphine ligands on rhodium(I) acetylacetonato carbonyl complexes undergoing oxidative addition with [CH_3I] under pseudo first-order conditions for the formation of [Rh(acac)(I)(CH_3)(CO)($PR_1R_2R_3$)] in dichloromethane at 25°C, [Rh(acac)(CO)($PR_1R_2R_3$)] = 3 x 10^{-3}M.**

PPh_3		$PCyPh_2$		PCy_2Ph		PCy_3	
[CH_3I] (M)	k_{obs} (x 10^{-3} s^{-1})	[CH_3I] (M)	k_{obs} (x 10^{-3} s^{-1})	[CH_3I] (M)	k_{obs} (x 10^{-3} s^{-1})	[CH_3I] (M)	k_{obs} (x 10^{-3} s^{-1})
0.165	6.2(1)	0.115	7.16(8)	0.134	1.014(2)	0.106	3.06(1)
0.304	10.3(6)	0.311	18(1)	0.304	2.159(6)	0.304	9.1(1)
0.621	20(1)	0.640	35.0(9)	0.634	4.46(2)	0.633	17.3(1)
0.807	26(3)	0.832	45(1)	0.825	5.79(1)	0.819	22.1(2)

Table E.2 **(Figure 4.15) Temperature and [CH_3I] dependence of the pseudo-first order rate constant for the formation of [Rh(acac)I(CH_3)(CO)(PPh_3)] in dichloromethane, (λ = 322 nm) [Rh(acac)(CO)(PPh_3)] = 1.01 x 10^{-4} M.**

[CH_3I] (M)	k_{obs} (x 10^{-3} s^{-1})	k_{obs} (x 10^{-3} s^{-1})	k_{obs} (x 10^{-3} s^{-1})
	24.9 °C	15.1 °C	5.3 °C
0.097	4.13(9)	2.17(4)	1.24(1)
0.177	6.5(3)	3.56(8)	2.01(2)
0.275	9.8(5)	5.2(2)	2.97(3)
0.393	13.1(9)	7.5(3)	4.09(4)
0.559	18(2)	10.0(6)	5.74(9)

Table E.3 **(Figure 4.16) Temperature and [CH_3I] dependence of the pseudo-first order rate constant for the formation of [Rh(acac)I(CH_3)(CO)($PCyPh_2$)] in dichloromethane, (λ = 315 nm) [Rh(acac)(CO)($PCyPh_2$)] = 9.61x 10^{-5} M.**

[CH_3I] (M)	k_{obs} (x 10^{-3} s^{-1})	k_{obs} (x 10^{-3} s^{-1})	k_{obs} (x 10^{-3} s^{-1})
	26.0 °C	14.0 °C	6.0 °C
0.052	3.78(6)	2.58(1)	1.523(7)
0.169	10.6(4)	5.9(3)	3.89(9)
0.272	15.2(9)	8.8(6)	5.7(2)
0.388	22(1)	11.7(5)	7.9(4)
0.498	29(6)	14.8(6)	9.9(5)

Table E.4 **(Figure 4.17) Temperature and [CH_3I] dependence of the pseudo-first order rate constant for the formation of [Rh(acac)I(CH_3)(CO)(PCy_2Ph)] in dichloromethane, (λ = 323 nm) [Rh(acac)(CO)(PCy_2Ph)] = 9.10 x 10^{-5} M.**

[CH_3I] (M)	k_{obs} (x 10^{-4} s^{-1})	k_{obs} (x 10^{-4} s^{-1})	k_{obs} (x 10^{-4} s^{-1})
	25.6 ºC	14.5 ºC	5.5 ºC
0.081	6.59(3)	3.86(1)	2.161(9)
0.183	13.3(1)	7.35(4)	4.13(3)
0.315	22.7(3)	11.70(9)	6.61(3)
0.404	29.2(3)	14.5(2)	8.54(5)
0.571	40.5(7)	20.5(3)	11.30(5)

Table E.5 **(Figure 4.18) Temperature and [CH_3I] dependence of the pseudo-first order rate constant for the formation of [Rh(acac)I(CH_3)(CO)(PCy_3)] in dichloromethane, (λ = 322 nm) [Rh(acac)(CO)(PCy_3)] = 9.38 x 10^{-5} M.**

[CH_3I] (M)	k_{obs} (x 10^{-3} s^{-1})	k_{obs} (x 10^{-3} s^{-1})	k_{obs} (x 10^{-3} s^{-1})
	25.6 ºC	14.3 ºC	5.9 ºC
0.0732	2.17(2)	1.45(7)	0.777(4)
0.1680	4.98(9)	2.75(4)	1.74(1)
0.3156	8.9(2)	4.9(1)	3.01(3)
0.4079	11.3(4)	6.0(2)	3.82(7)
0.5531	15.3(5)	8.1(2)	5.2(1)

Table E.6 **(Figure 4.19) Eyring plots of the k_1 rate constant for the formation of [Rh(acac)(I)(CH_3)(CO)($PR_1R_2R_3$)] in dichloromethane.**

PPh_3		$PCyPh_2$		PCy_2Ph		PCy_3	
1/T (x10^{-3} K^{-1})	ln(k_1/T)	1/T (x10^{-3} K^{-1})	ln(k_1/T)	1/T (x10^{-3} K^{-1})	ln(k_1/T)	1/T (x10^{-3} K^{-1})	ln(k_1/T)
3.357	-9.176	3.344	-8.608	3.353	-10.663	3.349	-9.308
3.471	-9.728	3.484	-9.263	3.478	-11.350	3.481	-9.941
3.593	-10.263	3.584	-9.615	3.591	-11.905	3.586	-10.330